Multiscale Processing of Multichannel Electrocardiogram Signals

A

Thesis submitted

for the award of the degree of

DOCTOR OF PHILOSOPHY

By

L. N. Sharma

DEPARTMENT OF ELECTRONICS AND ELECTRICAL ENGINEERING
INDIAN INSTITUTE OF TECHNOLOGY GUWAHATI
GUWAHATI - 781 039, INDIA

JANUARY 2012

TH-1102_06610204

To my **Parents**

for support and encouragement

and

To my Daughter **Anisha** and Wife **Indu**

for their love and support

TH-1102_06610204

TH-1102_06610204

Certificate

This is to certify that the thesis entitled "**Multiscale Processing of Multichannel Electrocardiogram Signals**", submitted by **L. N. Sharma** (06610204), a research scholar in the *Department of Electronics and Electrical Engineering, Indian Institute of Technology Guwahati*, for the award of the degree of **Doctor of Philosophy**, is a record of an original research work carried out by him under our supervision and guidance. The thesis has fulfilled all requirements as per the regulations of the Institute and in our opinion has reached the standard needed for submission. The results embodied in this thesis have not been submitted to any other University or Institute for the award of any degree or diploma.

Dr. S. Dandapat
Professor

Dr. A. Mahanta
Professor

Department of Electronics and Electrical Engineering
Indian Institute of Technology Guwahati
Guwahati - 781 039, India.

Dated:

Place: IIT Guwahati

TH-1102_06610204

TH-1102_06610204

Acknowledgements

At the outset, I would like to express my whole hearted and deep sense of gratitude to my guides Prof. Samarendra Dandapat and Prof. Anil Mahanta for their guidance, help and encouragement throughout my research work. I greatly admire their attitude towards research, creative thinking, hard work and dedication in work. These are the great source of inspiration for me in all my endeavours. I am highly grateful to them for patiently checking all my manuscripts and thesis. This thesis would not have been possible without their bounteous effort. More than guides, they are my mentors for shaping my personal and professional life, without whom I would not have been where I am today. As friends and guides their help are immeasurable. I owe my profound gratitude to Prof. Samarendra Dandapat and Prof. Anil Mahanta for their supports in all respects.

My sincere thanks are due to my doctoral committee members Dr. H. B. Nemade, Dr. C. Mahanta, Dr. Roy P. Paily, Dr. S. R. M. Prasanna and Dr J. S. Sahambi for their support, encouragement and suggestions rendered during my research work. Many faculty members of the department gave me suggestions and encouragement time to time. The kind support and valuable suggestions from faculty members of the department helped me a lot to improve myself academically and personally. I sincerely acknowledge and thanks the senior faculties, Prof. P. K. Bora, Prof. A. K. Gogoi, Prof. S. Majhi, Prof. R. Bhattacharjee and Prof. S. K. Bose in this regard. I would like to thank other faculties of the department who helped me directly or indirectly during my research work. My special thank to Prof. A. Srinivasan who encouraged me now and then.

I would like to acknowledge the support shown by my colleagues Mr. Sanjib Das, Mr. P. J. Goswami, Mr. Utpal Sarma, Ms Josephine S., Mr. M. P. Das, Mr. S. Sonowal, Ms J. Rhabha, Mr. N. J. Dutta, Mr. T. Kakati and Mr. Kumud Das, who were with me during tenure of my research. I would like to thanks Dr. M. Sabarimalai Manikandan and Ms S. R. Nirmala for valuable discussions that we had time to time. I would like to thank Mr. Malaya Nath for the help provided during my programming stage. My sincere gratitude to all the research scholars of Electro-medical and Speech Technology Laboratory who work with me and it is a great research support and help. I acknowledge the help and my thanks to Dr. P. Krishnamoorthy, Dr. H. S. Jayanna, Dr. Shweta Ghai, Dr. Debadatta Pati, Ms

TH-1102_06610204

Sumitra Shukla, Mr Govind D., Mr. Gayadhar Pradhan, Mr. Haris B.C., Mr. Syed Shahnawazuddin, Mr. Deepak K. T., Mr. Biswajit Dev Sarma, Mr. Kukil Khanikar, Mr. Sunil Y. and others. I would like to thank project staffs Ms. Pushpanjali Sharma, Ms. Bandita Sarma, Ms. Sagarika Das, Mr. Aniruddha Deka, Mr. G Siva Reddy who helped me in some related work.

Finally, it is the love, affection, moral support and sacrifice of my Wife “Indu” and Daughter “Anisha”, which has made this research a success. I sincerely acknowledge the help and support provided by them and I am extremely grateful. My greatest debt of gratitude is owed to my parents, whose hard work and sacrifices gave me the opportunities I have today. This dissertation is dedicated to my wife, daughter and my parents.

L. N. Sharma

TH-1102_06610204

Abstract

This thesis documents our investigations on processing of multichannel electrocardiogram signals using multiscale principal component analysis (MSPCA). There are three broad contributions. First, wavelet based denoising methods are proposed and evaluated for noise cancellation. The proposed denoising methods are based on relative subband energy of the signal and its Gaussianity from real data. Higher order statistics at different wavelet subbands provides significant information about the statistical nature of the data in time and frequency. The fourth order cumulant, Kurtosis, and the Energy Contribution Efficiency (ECE) of signal in a wavelet subband are combined to assess the noise content in the signal. The proposed methods show improved performance over soft threshold, hard threshold and SURE methods when applied to ECG signals.

Second, multiscale principal components analysis (MSPCA) is investigated for compression of multichannel electrocardiogram signals. If all the channels of a standard 12-lead ECG are subjected to wavelet transform with the same decomposition level and mother wavelet, it is expected that, at the same wavelet scale the inter-lead correlation may be much higher. The correlations across the ECG channels at the same wavelet scales are investigated using scatter plots and correlation coefficients. The higher correlations between multichannel ECG signal-components at similar wavelet scales help reduce dimension and remove redundant information present in signals. Using covariance method for PCA, it is found that the proposed method perform data dimension reduction without introducing distortion on clinical information. Multichannel compression is implemented using uniform quantizer and entropy coding of MSPCA coefficients. Third, clinical entropy (Centropy) is proposed based on an information theoretic approach to eigenvalue matrices resulted from MSPCA. It is shown that Centropy can effectively quantify the distortions in the clinical components in an ECG signal.

TH-1102_06610204

The major contributions of the work reported in this thesis includes,

1. Denoising using Higher Order Statistics in Wavelet Subbands.
2. Denoising based on Kurtosis based Noise Variance and Multiscale Energy.
3. Multiscale Principal Component Analysis (MSPCA) for multichannel ECG processing and ECG data compression.
4. Clinical Entropy based Principal Component Analysis (PCA) and MSPCA for multi-channel ECG Signals.

The other contributions are,

1. Multiscale multivariate energy contribution efficiency for multichannel ECG.
2. Denoising multichannel ECG using Multiscale PCA.
3. Quality controlled denoising of multichannel ECG signals using Multiscale PCA.
4. Multiscale Distortion Measure for Multichannel Electrocardiogram.

Keywords: Multichannel electrocardiogram, Denoising, Principal Component Analysis, Multiscale Principal Component Analysis, Distortion Measure, PRD, WWPRD, WEDD.

TH-1102_06610204

Synopsis

Introduction

This thesis work is an investigation of multichannel electrocardiogram (ECG) signal processing using wavelets. Cardiac signal processing aims at extracting significant information from ECG signals for diagnosis, therapy and monitoring. Multi-lead or Multichannel Electrocardiogram (MECG) signals are essential for a physician to make a critical diagnostic decision for a cardiac patient. In case of clinical evaluation, 12-lead standard ECG recording view the heart at different angles. This gives spatio-temporal distribution of electrical potential of heart. Due to its special nature, such signals need to be addressed with care during their processing. Processing of these signals should preserve the clinically important information and relevant diagnostics features. A good amount of temporal correlation exists in a single channel ECG. Also, the inter-lead correlation is high in a multichannel channel ECG signal. These correlation properties can be exploited for efficient implementation of algorithms for multichannel ECG signal processing.

This work consists of three major contributions. First, for preprocessing of ECG signals, wavelet based denoising methods are proposed and evaluated for noise cancellation. The proposed denoising methods are based on relative subband energy of the signal and its Gaussianity from real data. Higher order statistics at different wavelet subbands provides significant information about the statistical nature of the data in time and frequency. The fourth order cumulant, Kurtosis, and the Energy Contribution Efficiency (ECE) of signal in a wavelet subband are combined to assess the noise content in the signal. Second, Multiscale Principal Components Analysis (MSPCA) is investigated for compression of multichannel electrocardiogram signals. The higher correlations between multichannel ECG signal-components at similar wavelet scales help reduce dimension and remove redundant information present in signals. Using covariance method for PCA, it is found that the proposed method perform data dimension reduction without introducing distortion on clinical information. Multichannel compression is implemented using uniform quantizer and entropy coding of MSPCA coefficients. Third, Clinical Entropy (Centropy) is proposed based on an information theoretic approach to eigenvalue matrices resulted from MSPCA. It is shown that Centropy can effectively quantify the

TH-1102_06610204

distortions in the clinical components in an ECG signal.

Motivation

The cardiac potentials recorded using multiple leads on human body represent the same cardiac event at different spatial locations. The same electrical pulse originating from sinus node creates 'PQRST' morphologies and appears in different ECG channels. Thus, the signals at different leads are highly correlated. The individual components, P-wave, QRS-complex and T-wave, of an ECG do have different frequency contents. Multiresolution decomposition segments these components or information broadly in different frequency bands. It is expected that, at a wavelet scale, inter-lead correlation may be high.

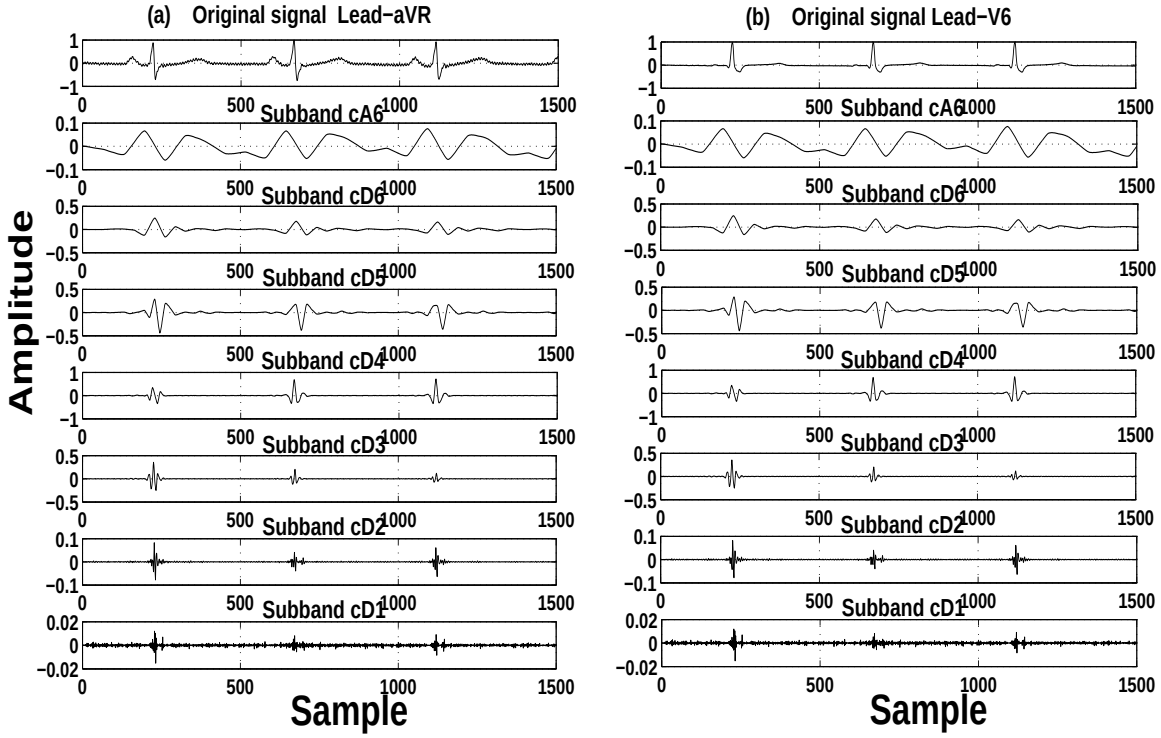

Figure: Original time domain Lead-aVR and V6 signals and their reconstructed subbands signals due to six level wavelet decomposition. In panels, (a) Original Lead-aVR signal with reconstructed subband signals and (b) Original Lead-V6 signal with reconstructed subband signals. Data base used is from CSE multilead measurement library, Data set: MO1-041

In Figure above, wavelet subband signals with original signals are shown for Lead-aVR and Lead-

V6. It is observed that cA6 subband reflects the parts of low frequency components such as P-wave and T-wave in leads (Figure (a) and (b)). The cD6 and the cD5 subbands show the lower frequency component of QRS-complex with higher frequency component of T-wave. The cD4 and the cD3 subbands show the significant higher frequency component of QRS-complex. The cD2 and the cD1 subbands contain some higher frequency component of QRS-complex and noise. It is seen that in same subband levels or scales, in both the cases, there are similarities between segmented signal components. So, it is expected to get higher correlation between different channels in the same subband level. If all the channels of a standard 12-lead ECG are subjected to wavelet transform with the same decomposition level and mother wavelet, it is expected that, at a wavelet scale, inter-lead correlation may be much higher.

So, there is a scope of applying multivariate data analysis method at a wavelet scale if the coefficients of all the channels are organized as multivariate data. These multivariate data are expected to show higher inter-channel redundancies at a wavelet scale. Also, it is expected to have similar pattern of multiscale energy for multivariate data. Based on these assumptions, dimensions can be reduced applying principal component analysis (PCA) at wavelet scales for non-significant multivariate data.

Preprocessing of Multichannel Electrocardiogram Signals

Preprocessing of an ECG signal consists of noise cancellation and amplitude and time normalization. In this work, noise cancellation of multichannel ECG data using wavelets is dealt as a preprocessing problem. Processing of ECG signals should preserve the clinically important information and relevant diagnostics features. Though the ECG signal denoising is an old problem, still there should be special consideration to ensure signal fidelity for retention of clinical information. In this work, two novel denoising methods are proposed. The first method is based on evaluation of higher order statistics at different wavelet subbands for an electrocardiogram (ECG) signal. Higher order statistics at different wavelet subbands provides significant information about the statistical nature of the data in time and frequency. The fourth order cumulant, Kurtosis, and the Energy Contribution Efficiency (ECE) of signal in a wavelet subband are combined to assess the noise content in the signal. Accordingly, four denoising factors are defined. Performance of the denoising factors are evaluated and compared with

the soft thresholding method. The filtered signal quality is assessed using Percentage Root Mean Square Difference (PRD), Wavelet Weighted Percentage Root Mean Square Difference (WWPRD), Wavelet Energy-based Diagnostic Distortion (WEDD) measures. It is observed that the proposed denoising scheme not only filters the signal effectively but also help retain the diagnostic information.

The second denoising method is based on a threshold which is derived by considering energy contribution of a wavelet subband, noise variance which is based on a Gaussian measure, Kurtosis, and number of samples. The robust noise estimator, median absolute deviation (MAD), is scaled by a normalized wavelet subband Kurtosis instead of conventional statistical quantile function for Gaussian distribution. The method is tested with spatially nonhomogeneous functions, Blocks, Bumps, HeaviSine and Doppler with noise. The performance of the proposed thresholding method is evaluated using synthetic ECG signal after adding noise and the recorded noisy ECG signal from database. Also, it is compared with the existing classical thresholding methods such as soft thresholding, hard threshoding and SURE. The lowest PRD, WWPRD and WEDD values are achieved as 9.523%, 17.743% and 4.000% for lead-V2, lead-V3 and lead-II signal respectively. Results show that the performance of the proposed method is better compared to the existing methods. The proposed denoising method not only filters ECG signal effectively but also can help retain the clinical information in the signal.

Multiscale PCA for Multichannel ECG Compression

Cardiac signal-components (P-wave, QRS-complex and T-wave) are grossly segmented to different wavelet subbands. In wavelet subbands, the correlation between multichannel ECG signal-components can be effectively captured. In this work, the correlations across the ECG channels at the same wavelet scales are investigated using scatter plots and correlation coefficients. Higher correlation of multichannel ECG data in wavelet subbands will help efficient implementation of PCA. If there are n number of ECG channels which are 'L' level wavelet decomposed and j^{th} subband of all channels are collected in a matrix, it forms '$L+1$' wavelet subband matrix. Multiscale wavelet subband matrix for approximation band is $\mathbf{A_L}$ and subband matrices for details are $\mathbf{D_j}$, where $j = 1, 2, \cdots, L$. In this, the number of columns is the number of ECG channels and number of rows is the number of

coefficients in that particular subband. The selection of principal components based on subband energy is proposed. It is based on average fractional energy contribution of eigenvalue in a data matrix. It is seen that the selected PC represent the clinical information while discarding redundant information associated with non-significant PC. For evaluation of clinical fidelity, quantitative measures such as percentage PRD, WWPRD and WEDD are evaluated. The dimension reduced signals fall under excellent category with lowest WEDD value of 1.67%. The dimension reduction at multiscale multivariate matrices gives an overall samples reduction of 50.37% for 12 channel ECG with an average PRD of 10.01%. These results motivated us for developing a compression scheme for multichannel electrocardiogram (MECG) data, using multiscale principal component analysis (MSPCA). Multichannel compression is implemented using uniform quantizer and entropy coding of PCA coefficients. Using data set from CSE mutlilead measurement library, multichannel compression ratio of 5.98:1 is found with PRD value 2.09% and the lowest WEDD value of 4.19%. Based on, gold standard subjective quality measure, the lowest mean opinion score (MOS) error value of 5.56% is found.

Clinical Entropy based MSPCA and Multiscale Distortion

A novel MSPCA based clinical entropy measure is proposed to evaluate the clinical information in the processed signal. Higher correlation between different channels in the same subband level help efficient implementation of PCA at the subband level. The eigenvalues at different wavelet scales capture the energy of the multichannel signal. Also, the gross segmentation of different ECG components in wavelet scales help capture of clinical information through these eigen values. Clinical entropy is investigated from the diagonal eigenvalue matrix. Centropy based PC selection may be applied in PCA and MSPCA based processing of multichannel ECG signals. Centropy based PCA is compared with conventional PCA qualitatively and quantitatively evaluated using distortion metrics, PRD, Root Mean Square Error (RMSE) and Cross Correlation (CC) for all 12 channel data. It is observed that the PRD and the RMSE values are lower for all the channels in case of the proposed Centropy based PCA method compared to the conventional PCA based method. Also, the compressed signals after Centropy based PCA and Centropy based MSPCA are compared. For Centropy based MSPCA method, the PRD, WWPRD and WEDD values for lead-III signal are 11.725% 29.124% and 5.274% respec-

tively. The Centropy based method shows the best performance over others. After reconstruction of MSPCA processed multichannel signals, Multiscale Multivariate Distortion (MMD) is evaluated. For Centropy based MSPCA (using same data set), if the threshold is decided at 80% of information, the MMD values for D_1, D_2, D_3 D_4, D_5, D_6 and A_6 are 79.92%, 45.48%, 63.89%, 2.14%, 2.08%, 1.93%, and 2.07% respectively. The average Multiscale Distortion (MD) value is found as 0.5268%.

Organization of the Thesis

The contents of the thesis are organized as: In **Chapter 1**, introduction to ECG signals and its processing in time, frequency and time-frequency domain are discussed with published literatures. In **Chapter 2**, a related reviews of wavelet transform based ECG signal processing is given. PCA based processing and the motivation for this thesis work is discussed. In **Chapter 3**, for preprocessing of multichannel ECG, two novel ECG denoising methods are presented and evaluated. In **Chapter 4**, multiscale PCA is introduced for multichannel ECG signal processing. A compression scheme for multichannel ECG using multiscale PCA is proposed. In **Chapter 5**, clinical entropy based multiscale PCA and multiscale distortion measure are introduced. Conclusion of the thesis is drawn in **Chapter 6** with major contributions from this thesis and scope for further research.

Contents

TH-1102_06610204

TH-1102_06610204

भारतीय प्रौद्योगिकी संस्थान गुवाहाटी
Indian Institute of Technology Guwahati

List of Figures

TH-1102_06610204

TH-1102_06610204

भारतीय प्रौद्योगिकी संस्थान गुवाहाटी • Indian Institute of Technology Guwahati •

List of Tables

TH-1102_06610204

List of Acronyms

ANN	Artificial Neural Networks
AV	Atrioventricular
AZTEC	Amplitude Zone Time Epoch Coding
AWGN	Additive White Gaussian Noise
AVQ	Adaptive Vector Quantization
AMSMPCA	Adaptive Multiscale Multiway PCA
AFEC	Average Fractional Energy Contribution
APRD	Average PRD
Centropy	Clinical Entropy
CC	Cross Correlation
CSE	Common Standard for Electrocardiography
CORTES	Coordinate Reduction Time Encoding System
CR	Compression Ratio
CSAPA	Combined SAPA
CUSAPA	Cubic Spline SAPA
CWD	ChoiWilliams Distribution
CDR	Compressed Data Rate
cuvt	Creighton University Ventricular Tachyarrhythmia
DCT	Discrete Cosine Transform
DFT	Discrete Fourier Transform
DLT	Discrete Legendre Transform
DWT	Discrete Wavelet Transform

TH-1102_06610204

DSM	Differencing Significance Map
DF	Denoising Factor
DECE	Details Energy Contribution Efficiency
dB	Decibel
DR	Dimension Reduction
ECG	Electrocardiogram
ECE	Energy Contribution Efficiency
EMG	Electromyogram
EZW	Embedded Zerotree Wavelet
EPF	Energy Packing Efficiency
EMD	Empirical Mode Decomposition
EEG	Electroencephalogram
FVQ	Fuzzy Vector Quantization
FFT	Fast Fourier Transform
FDC	Frequency Domain Compression
FD	Fourier Descriptor
FIR	Finite Impulse Response
GMM	Gaussian Mixture Models
HT	Haar Transform
HOPE	Higher-order Polynomial Expansions
HCM	Hybrid Compression Method
HE	Hilbert Envelope
HMM	Hidden Markov Models
HC	Hierarchical Combination
HHT	Hilbert-Huang Transform
HOS	Higher Order Statistics
ICA	Independent Component Analysis
IIR	Infinite Impulse Response
IT	Identity Transform

IDWT	Inverse Discrete Wavelet Transform transform
IMF	Intrinsic Mode Function
KLT	KarhunentLove Transform
Kurt	Kurtosis
LAE	Left Atrial Enlargement
LA	Left Arm
LL	Left Leg
LP	Linear Prediction
LPC	Linear Predictive Coefficients
MECG	Multichannel Electrocardiogram
MSPCA	Multiscale Principal Component Analysis
MAD	Median Absolute Deviation
MBC	Model based Compression
MSAPA	Modified SAPA
MAE	Maximum Absolute Error
MC-LTP	Multichannel Long-Term Prediction
MOS	Mean Opinion Score
MaxErr	Maximum Error
MAX	Maximum Amplitude Error
MMD	Multiscale Multivariate Distortion
MD	Multiscale Distortion
MRD	Multi-resolution Decomposition
MPCA	Multiway PCA
MRA	Multiresolution Analysis
mita	MIT-BIH Arrhythmia
mitsva	MIT-BIH Supraventricular Arrhythmia
MMECE	Multiscale Multivariate Energy Contribution Efficiency
MSE	Mean Square Error
RMSE	Root Mean Squared Error

NRMSE	Normalized Root Mean Squared Error
NN	Neural Network
NLPCA	Non-linear Principal Component Analysis
NMSE	Normalized MSE
NCC	Normalized Cross Correlation
NRDPWT	Nonrecursive Discrete Periodized Wavelet Transform
NMAE	Normalized MAE
NMAX	Normalized Maximum Amplitude Error
OWT	Optimally Warped Transform
OZWC	Optimal Zonal Wavelet Based Compression
PDF	Probability Density Function
PC	Principal Component
PCA	Principal Component Analysis
PE	Peak Error
PRD	Percentage Root Mean Square Difference
QMF	Quadrature Mirror Filter
QLV	Quad Level Vector
RLE	Right Atrial Enlargement
RL	Right Leg
RA	Right Arm
RMSE	Root Mean Square Error
RBFN	Radial Basis Function Network
SVM	Support Vector Machines
SNR	Signal-to-Noise Ratio
SBC	Subband Coding
StdErr	Standard Error
STFT	Short Time Fourier Transform
SPIHT	Set Partitioning in Hierarchical Trees
SKR	Signal-to-Kurtosis Ratio

SRR	Sample Reduction Ratio
TDC	Time Domain Compression
TP	Turning Point
TDL	Target Distortion Level
TDR	Target Data Rate
TWA	T-wave Alternans
USZZQ	Uniform Scalar Zero Zone Quantizer
VQ	Vector Quantization
WWPRD	Wavelet Weighted Percentage Root Mean Square Difference
WPRD	Weighted Percentage Root Mean Square Difference
WEDD	Wavelet Energy based Diagnostic Distortion Measure
WDD	Weighted Diagnostic Distortion
WT	Wavelet Transform
WP	Wavelet Packet
WVT	WignerVille Transform

TH-1102_06610204

भारतीय प्रौद्योगिकी संस्थान गुवाहाटी
Indian Institute of Technology Guwahati

List of Symbols

A_L	Subband Matrix at L^{th} wavelet level
$\widehat{A_L}$	Reconstructed Subband Matrix at L^{th} wavelet level
A	Symmetric Matrix
α_j	Ratio between ECE and DECE
B	Symmetric Matrix
β_j	Estimated Noise Variance
cAL	Approximation Subband at L^{th} Level
cDj	Details Subband at j^{th} Scale
C_{A_L}	Covariance Matrix at L^{th} Level
C_{A_j}	Covariance Matrix at j^{th} Scale
C	Constant Scale Factor
C_s	Covariance Matrix for S
ΔF_j	The bandwidth of j^{th} Subband
DF_j	Denoising Factor at $j^{th.}$ wavelet scale
D_j	Subband Matrix at j^{th} wavelet scale
$\widehat{D_j}$	Reconstructed Subband Matrix at j^{th} wavelet scale
D	Diagonal Eigenvalue Matrix
E_t	Total Energy of Wavelet Subbands
E_j	Energy at j^{th} Wavelet Scale
E_{A_L}	Energy at Approximation matrix at L^{th}Level
E_{D_j}	Energy at Detail matrices at j^{th} Scale
ϵ_j	ECE

TH-1102_06610204

$\widehat{\epsilon_j}$	DECE
ε_{AL}	MMD for Approximation
ε_j	MMD for Details
$f(x)$	Function of x
F_s	Sampling frequency
F_{A_L}	Feature Vector at L^{th} Approximation Matrix
F_{D_j}	Feature Vector at j^{th} Detail Matrices
γ_j	Threshold Factor based on Number of Samples
H_i	Entropy information by i^{th} Eigenvalue
I	Identity Matrix
I_i	Self Information by i^{th} Eigenvalue
K	Kurtosis
$\mathbf{\Lambda_{A_L}}$	Eigenvalue Matrix at L^{th} Approximation Level
$\mathbf{\Lambda_{D_j}}$	Eigenvalue Matrices at j^{th} Detail Scale
$\lambda_{A_{L_n}}$	Eigenvalue at L^{th} Approximation Level
$\lambda_{D_{jn}}$	Eogenvalue at j^{th} Detail Scale
μ^4	Fourth-order Central Moment
η_{A_L}	AFEC by eigenvalues of L^{th} Approximation Matrix
η_{D_j}	AFEC by eigenvalues of j^{th} Detail Matrices
P_i	Probability of i^{th} Eigenvalue
R_x	Correlation Matrix
R_{A_L}	Dimension reduced data set for Approximation Matrix
R_{D_j}	Dimension reduced data set for Detail Matrices
$\psi(x)$	Mother Wavelet
σ^4	Square of the Variance
σ	Variance
σ_n	Noise Variance
$\widehat{\sigma_n}$	Estimated Noise Variance
S	Multichannel ECG Signal Matrix

S_σ	Sum of Energies by all Multiscale Matrices
t	Threshold
T_s	Threshold in Conventional PCA
T_H	Centropy based Threshold
T_{A_L}	Threshold for Approximation in in Conventional PCA
T_{D_j}	Threshold for Details in Conventional PCA
U	Eigen Matrix
$\mathbf{V_{A_L}}$	Eigenvector Matrix at L^{th} Approximation Level
$\mathbf{V_{D_j}}$	Eigenvector Matrix at j^{th} Detail Scale
$w_{j,k}$	k^{th} wavelet coefficient at j^{the} scale
w_j	Weight based on Normalized Area
$w_j^{'}$	Weights based on Energy Feature
W_{A_L}	Weights for approximation subband matrix
W_{D_j}	Weights for Details subband Matrices
$x(n)$	Sequence of Samples
$\widehat{x(n)}$	Reconstructed Sequence of Samples
X	$N \times M$ Data Matrix

भारतीय प्रौद्योगिकी संस्थान गुवाहाटी • Indian Institute of Technology Guwahati •

1

Introduction

Contents

TH-1102_06610204

This thesis work is an investigation of multichannel electrocardiogram (ECG) signal processing using wavelets. Multi-lead or multichannel electrocardiogram signals (MECG) are clinically essential for a physician to make a critical diagnostic decision for a cardiac patient. In a clinical ECG, 12-lead standard recording view the heart at different angles [1]. This gives spatio-temporal distribution of electrical potential of heart. Due to its special nature, such signals need to be addressed with care during their processing. Cardiac signal processing aims at extracting significant information from signals for diagnosis, therapy and monitoring. Processing of these signals should preserve the clinically important information and relevant diagnostics features. A good amount of temporal correlation exists in a single channel ECG. Also the inter-lead correlation is high in a multichannel channel ECG signal. These correlation properties can be exploited for efficient implementation of algorithms for multichannel ECG signal processing. In this work, three problems of multichannel ECG signals are dealt.

The first problem deals with the denoising of the multichannel ECG signal. A novel denoising method is proposed. Higher order statistics at different wavelet subbands provides significant information about the statistical nature of the data in time and frequency. The fourth order cumulant, Kurtosis, and the Energy Contribution Efficiency (ECE) of signal in a wavelet subband are combined to assess the noise content in the signal. The robust noise estimator, median absolute deviation (MAD), is scaled by a normalized wavelet subband Kurtosis instead of conventional statistical quantile function for Gaussian distribution.

The second problem deals with multiscale principal component analysis (MSPCA) for multichannel ECG to reduce data dimension and multichannel ECG compression. Higher correlation is observed between standard 12 lead ECG signals in different wavelet scales. To apply MSPCA, wavelet subband matrices are formed with the wavelet transformed coefficients of all the 12 standard leads of multichannel ECG signals. The multiscale properties of wavelet transform and the correlations between data at wavelet scales in different channels are used for dimension reduction of multichannel ECG signals without introducing significant distortion of clinical information. A novel method for the selection of principal components is proposed by dividing the sum of eigenvalues at a wavelet scale by total cumulative sum of eigenvalues of all scales. Multichannel compression is implemented using uniform quantizer and entropy coding of PCA coefficients.

The third problem deals with information theoretic approach applied for multiscale principal component analysis (MPCA) for multichannel ECG signals. Clinical information (clinical entropy) is evaluated from the inverse of the diagonal eigenvalue matrix. Clinical entropy (Centropy) based MSPCA methods show improved performance compared to the conventional PCA. The proposed method exhibits superior signal quality with higher cross correlation (CC), lower percentage root mean square difference (PRD) and lower root mean square error. Also, a novel wavelet based multiscale distortion mesure is proposed and evaluated for multichannel ECG signals.

The main standard ECG database used for this work is CSE mutlilead measurement library [2]. For this work, the data set 3 of CSE multilead measurement library is considered. The data set 3 has 125 original ECG data sets with almost equal numbers of normal and various pathological cases.

1.1 Electrocardiogram (ECG) and Its Clinical Components

Human physiological activities recorded as signals or captured as an images give pathological or normal condition of a specific organ of human body. Among these, cardiac signal recorded as electrocardiogram (ECG), reflects nature and activities of human heart. In standard clinical electrocardiogram, signals are recorded with single lead or multiple lead configuration from the surface of human body. Each lead bears a good amount of clinically relevant diagnostic information.

In Figure 1.1, shows an ECG signal marked with their amplitudes and time intervals. Local waves P, Q, R, S and T are present in a typical ECG cycle. The physiological significance of these local waves [3–5] are presented in the following paragraphs

P wave: The electrical impulses initiated at sinoatrial node of right atrium starts atrial depolarization and produces the P wave on the electrocardiogram. P wave represents the composite electrical activation of right and left atria. The duration of the P wave is in the range of 80 to 100 ms. The maximum normal amplitude of P is 0.25 mV. Normal P wave is never pointed or peaked. A P wave with magnitude $>$0.25 mV signifies Right Atrial Enlargement (RLE) and a widened P wave indicates Left Atrial Enlargement (LAE). In case of hyperkalemia, P wave may be decreased in height.

PR interval: The time interval between the atrial depolarization and the beginning of ventricular depolarization is the PR interval. The PR interval is measured from P wave to the Q wave or the R wave if the Q wave is absent. The normal PR interval is 120-200 ms. A short PR intervals is observed

TH-1102_06610204

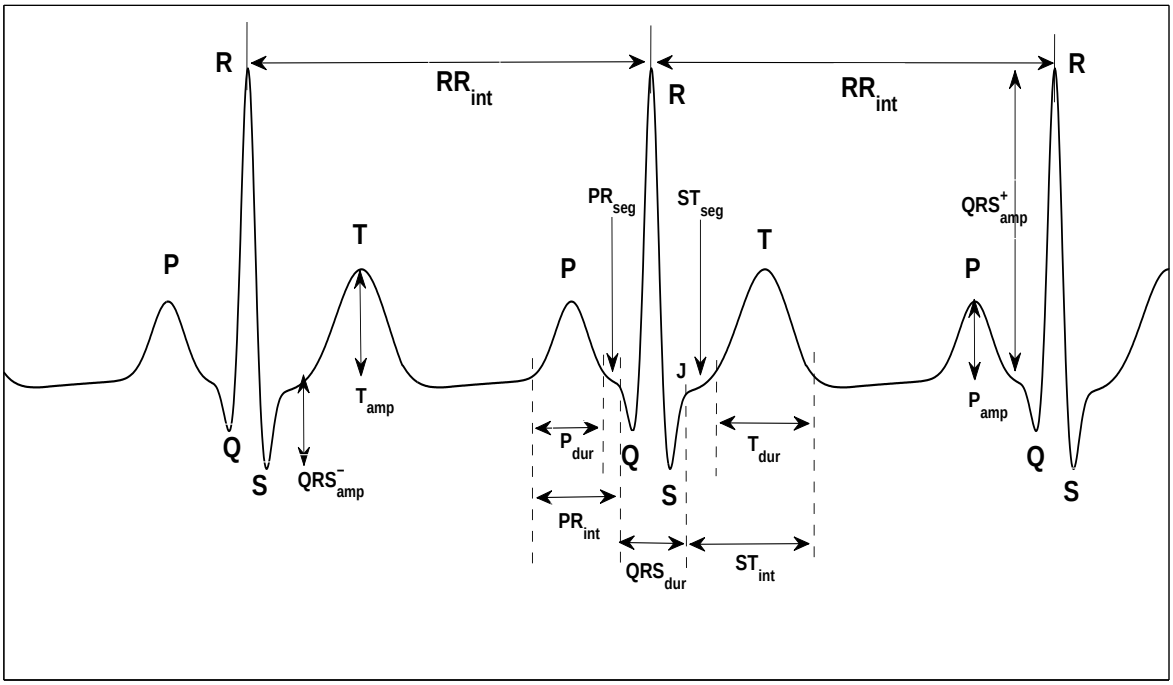

Figure 1.1: Clinical components of an ECG signal with their duration and amplitude

in patients with pheochromocytoma and Wolfe-Parkinson-White Syndrome. Prolonged PR intervals are observed in ECG signals from patients with 1st degree atrioventricular (AV) block, 2nd degree AV block and rheumatic heart diseases.

Q wave: First downward deflection of the QRS-complex is the Q-wave. Depolarization of the intraventricular septum is represented by the Q wave. A normal Q wave has a duration less than 40 ms and its amplitude is 25% of the amplitude of the R wave. Myocardial infarction shows a wide or deep Q wave.

R wave: First upward deflection of the QRS-complex is the R wave. A part of the ventricular depolarization cycle is represented by this wave. The presence of a bundle branch block is indicated by a reverse or greatly disturbed R-wave.

S wave: The downward deflection of QRS-complex is the S-wave. It represents the remaining part of time period for ventricular depolarization. In the presence of bundle branch blocks, S-waves have irregular shapes.

QRS complex: The QRS complex represents the depolarization of the myocardial cells of the ven-

tricles. Its duration is normally 60 ms to 100 ms. Abnormal intraventricular conduction velocity is reflected as a change in the duration of QRS-complex.

ST segment: ST-segment represents the period from the end of systole to the beginning of repolarization of the ventricles. It has a duration of 80 ms to 120 ms. It may appear as a flat line between the QRS complex and the T wave or it may appear with a up-slope from 0.1 mV to 2 mV. The ST segment will become depressed with a long duration and a large amplitude before it joins the T wave during ischemia. During an acute myocardial infarction, the ST segment is elevated. In the diagnoses of heart problems, the shape of the ST-segment plays an important role.

T wave: The ventricular repolarization is represented by the T-wave. Its duration is 100 ms to 250 ms and its amplitude is less than 0.5 mV. The normal T-wave has a more gradual slope than its second half. Cardiac ischemia or infarction are indicated by normally shaped T waves.

QT interval: The beginning of the QRS-complex to the end of the T wave is represented by the QT-interval. Its duration varies between 350 ms to 450 ms. In higher heart rate the duration of the QT interval is reduced. The ventricular tachyarrhythmias leading to sudden cardiac death can be diagnosed from prolonged QT-interval.

U wave: A small deflection that follows the T-wave is the U-wave. Repolarization of the mid-myocardial cells is represented by the U-wave. Many electrocardiograms do not show the U waves. The abnormal U wave is inverted or tall with an amplitude of 0.2 mV or more.

RR interval: The RR interval is the heart rate which represents the duration of cardiac cycle.

ECG signal has a bandwidth of 0.05 to 100 Hz. It has been found that notches and slurs may be superimposed on the slowly varying QRS complexes. They may contain additional information and they are located in the higher frequency bands of 100 Hz to 1000 Hz . In addition, the recording of the electrical field generated by the His and Purkinje activities produces a signal in the ECG with an amplitude range of about 1 to 10 μV which is useful in the identification of conduction abnormalities.

1.2 Multichannel Electrocardiogram

In a standard clinical ECG, 12 leads are used and they are known as leads I, II, III, aVR, aVL, aVF, V1, V2, V3, V4, V5 and V6. This 12-channel ECG is recorded using six limb leads and six chest leads in six positions. The simultaneous recording of these 12 channel ECG signals is called multichannel

TH-1102_06610204

electrocardiogram (MECG). The reference electrode is right leg (RL). Leads I, II and III are known

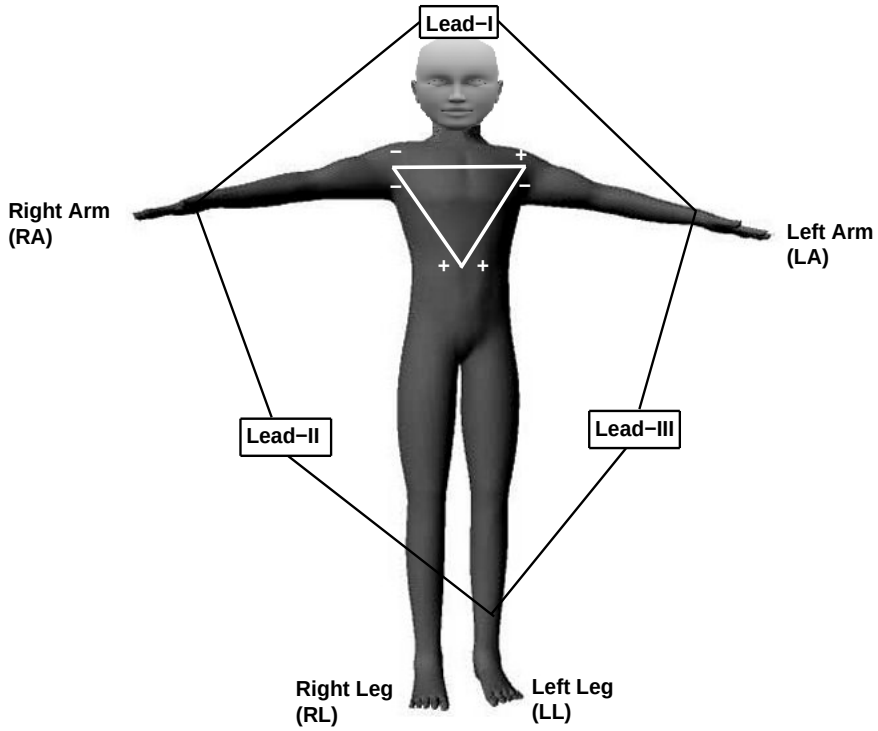

Figure 1.2: Bipolar limb leads configuration and Einthoven's triangle

as bipolar limb leads [6]. The lead configuration using left arm (LA), right arm (RA) and left leg (LL) during recording of ECG waveforms, is shown in Figure 1.2. The hypothetical triangle drawn around the area of the heart in Figure 1.2, is known as Einthoven's triangle. According to the Einthoven law, the potential at limb lead II is the summation of potential of limb lead-I and limb lead-III.

Leads aVR, aVL, and aVF are called augmented limb leads where Wilson's central terminal is the reference. Wilson's central terminal is formed by combining the left arm, right arm and left leg leads. Wilson's central terminal is also used as the reference for chest leads V1, V2, V3, V4, V5 and V6. In Figure 1.3, augmented limb leads and six chest leads are shown with Wilson's central terminal as reference.

These six chest leads are obtained from six standardized positions on the chest. Leads V1 and V2 are placed at the fourth intercostal space just to the right and left of the sternum respectively.

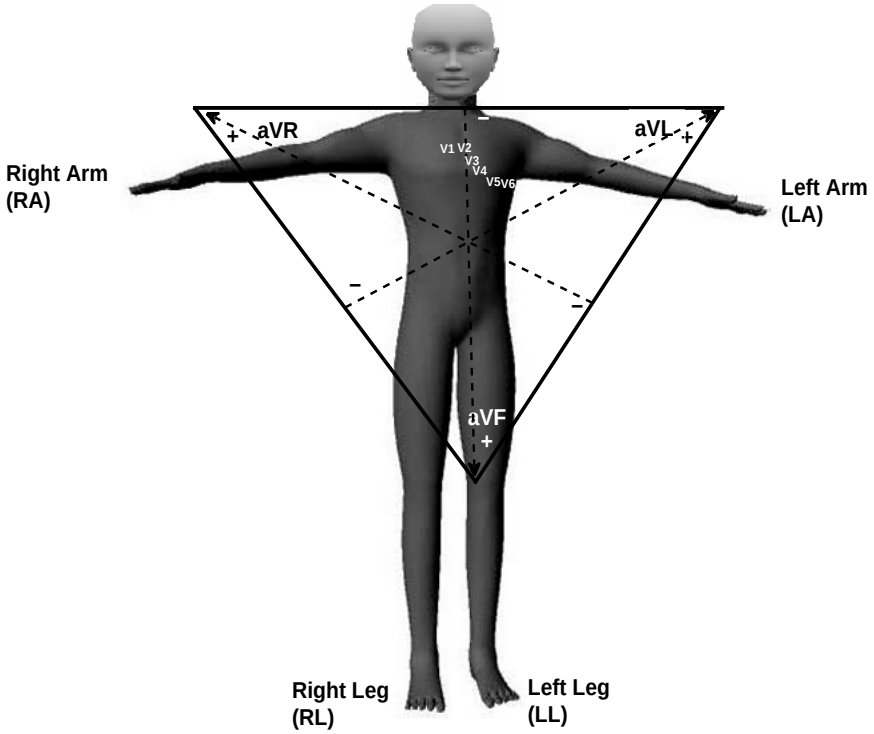

Figure 1.3: Unipolar leads: Augmented limb leads and chest leads

Signal at lead V4 is recorded at the fifth intercostal space at the left midclavicular line. Lead V3 is placed between the V2 and V4 leads. V5 and V6 leads are placed at the same level as the lead V4 at the anterior axillary line and the midaxillary line.

1.2.1 Correlations of Electrical Activities with Multichannel ECG

The standard ECG signals at six limb leads (3 bipolar and 3 augmented lead) and six chest leads, look" at the heart in frontal (vertical) and horizontal (transverse) planes. The six chest leads enable viewing the cardiac electrical vector in horizontal plane. In Figure 1.4, chest leads V1, V2, V3, V4, V5 and V6 are shown in the horizontal plane. Leads V5 and V6 are most sensitive to left ventricular activity whereas V3 and V4 depict septal activity. Leads V1 and V2 reflect electrical activity in the right-half of the heart.

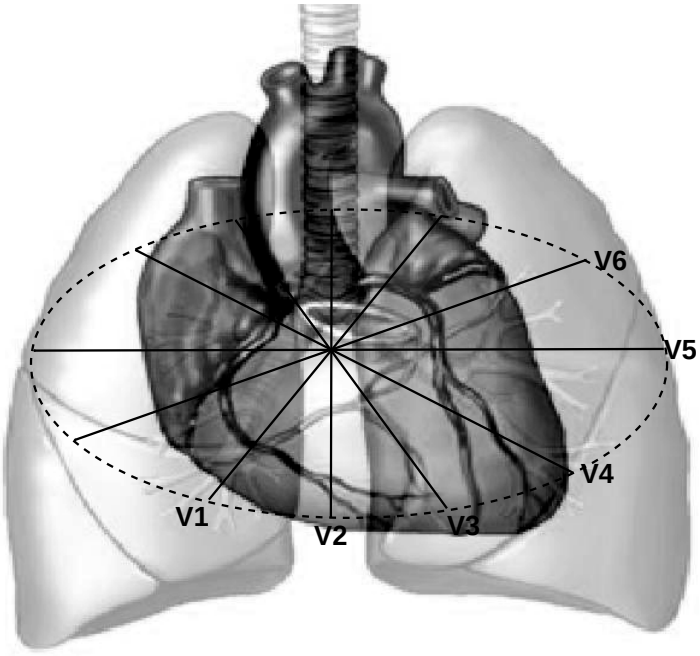

Figure 1.4: Viewing the heart in horizontal plane with chest leads

The bipolar limb leads (I, II, and III) and the augmented limb leads (aVR, aVL and aVF) depict the electrical activity of the heart from the edges of the frontal plane. The six limb leads measure projections of the three-dimensional cardiac electrical vector onto the axes illustrated in Figure 1.5. The six axes lie in the steps of 30^0. The vectors at specific angle facilitate viewing the electrical activity of the heart with the emphasis in the direction. This helps analyze the behaviors of cardiac chambers and muscles at frontal plane.

Looking to the anatomical relations of above lead system (Figure 1.4 and Figure 1.5) in standard 12-lead ECG, the inferior surface of the heart is viewed by leads II, III and aVF. Anterior surface is looked by leads V1, V2, V3 and V4. The lateral surface is electrically scanned by leads I, aVL, V5 and V6. Leads V1 and aVR view the right atrium and ventricle. So, these ECG leads may provide spatial information of electrical activity of the heart in three dimensional orthogonal space: left lateral to right lateral, inferior to superior and anterior to posterior. Each lead gives a specific orientation

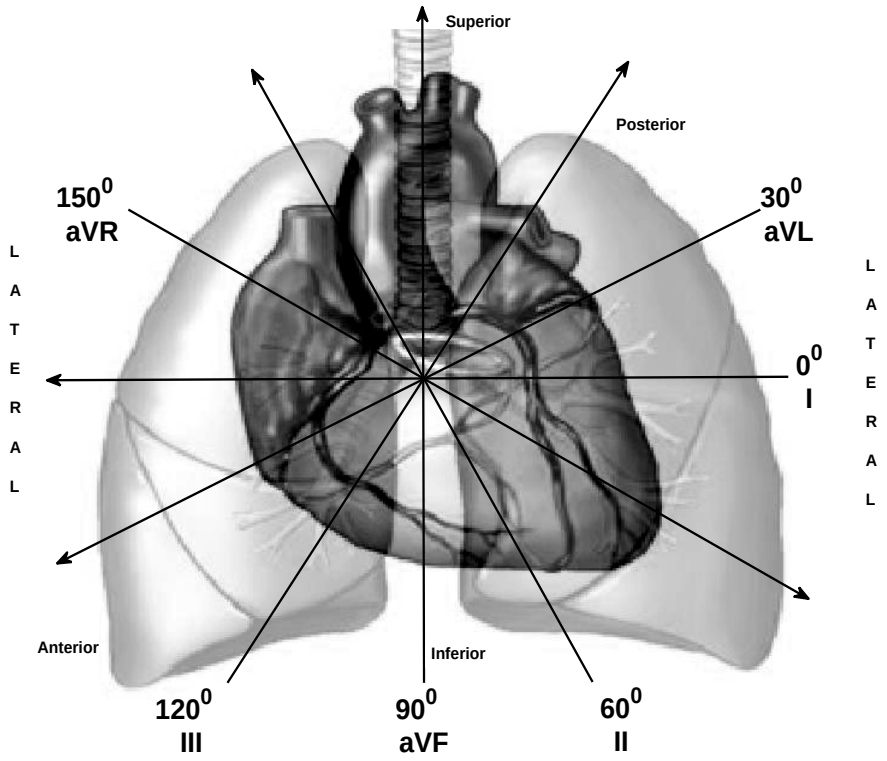

Figure 1.5: Electrical axes for vertical directional views of the heart for bipolar limb leads and augmented limb leads

in space. The direction of depolarization of heart chambers in 3-dimensional space can give better understanding of its electrical activities. The deviation of these cardiac vectors from the normal one in spatial domain captures the diagnostic information.

1.2.2 ECG Signal Components in Different Leads

The 12-lead ECG view the heart electrically from different angles. In each of these leads, the cardiac events, the depolarization and re-polarization, appear simultaneously during an ECG cycle. The depolarization spreading towards a lead causes an upward deflection. Similarly, depolarization spreading away from a lead shows downward deflection in electrocardiogram. Figure 1.6, shows a cycle of ECG waveform appearing at different leads when the signals are digitized by simultaneous sampling. Electrical impulse originating at the SA node travels from the direction of superior-to-inferior, and depolarizes the atria. So, P wave is upright in lead-I and lead-II. It is inverted in lead-aVR. It is most

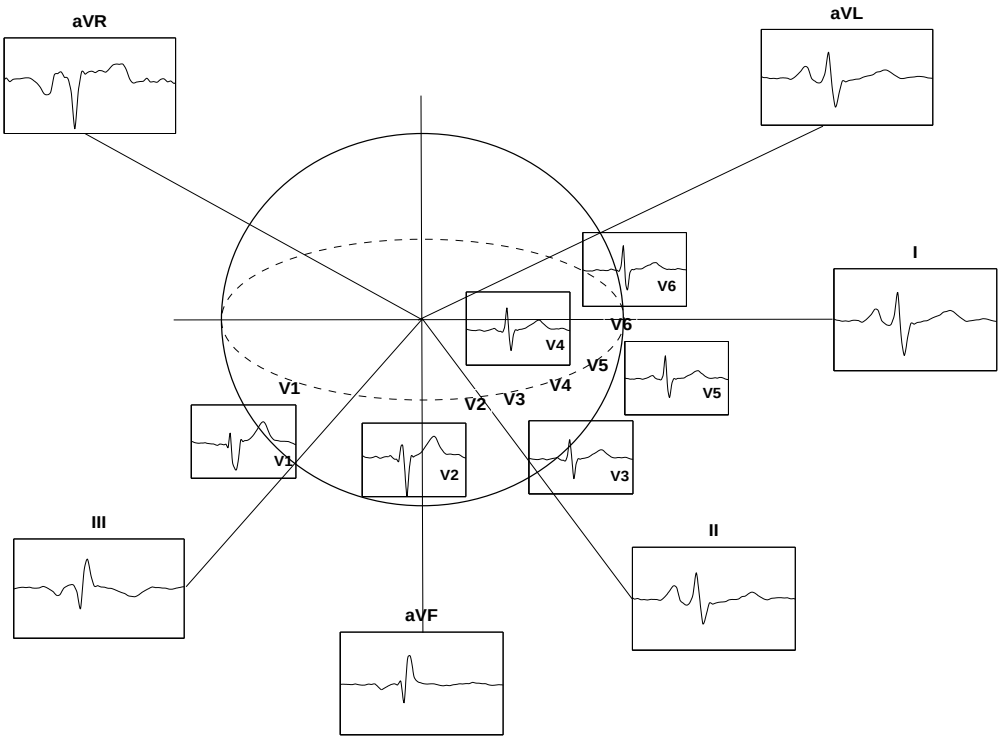

Figure 1.6: Signals in limb leads and chest leads due to activation sequence

prominently seen in leads-II. Due to dextrocardia or abnormal atrial rhythms, a negative P-wave may appear in the lead-I. An impulse originating other than the SA node depolarizes the atria in a different direction and disturbs the P wave morphology.

The QRS-complex is the most important and prominent trace in an ECG waveform. In normal condition, the depolarization wave travels through the interventricular septum via the bundle of His and bundle branches and reaches the ventricular myocardium through the purkinje fibre. The left side of the septum depolarizes first, and the impulse then spreads towards the right. QRS-complex is positive in leads-I and lead-V6 and negative in lead-aVR and lead-V1. QRS morphology in the precordial leads vary depending on the depolarization forces that move towards or away from a lead. Small septal Q-wave is often present in the leads-I, lead-aVL, lead-V5, and lead-V6. The forces generated by the left ventricle predominate, and therefore in lead V1 a small R-wave is followed by

a large negative deflection S-wave. The amplitude of R wave in the precordial leads increases in lead-V1 to lead-V6 with a corresponding decrease in S-wave depth culminating in a predominantly positive complex in V6. The height of the R wave is variable and increases progressively across the precordial leads (leads V5 and V6). The R wave in lead V6, however, is often smaller than the R wave in V5, since the V6 electrode is further from the left ventricle. The S wave is deepest in the right precordial leads; it decreases in amplitude across the precordium, and is often absent in leads V5 and V6.

T-wave orientation usually corresponds with that of the QRS complex, and thus is inverted in lead aVR, and may be inverted in lead III. T-wave inversion in lead V1 is also common. It is occasionally accompanied by T-wave inversion in lead V2, though isolated T-wave inversion in lead V2 is abnormal. The presence of symmetrical inverted T-waves is highly suggestive of myocardial ischaemia. Asymmetrical inverted T-waves are frequently a non-specific finding. The tallest T-waves are seen in leads V3 and V4. Tall T-wave may be seen in acute myocardial ischaemia and is a feature of hyperkalemia. The T-wave in most circumstances follows the same direction (polarity) as the predominant portion of the QRS complex. It is normally upright in leads I and V6 and inverted in lead aVR. However, the normal T-wave can be either upright or inverted in leads V1, aVL, and III. The Table 1.1 [3–5], shows

Table 1.1: Orientations of P-wave, QRS-complex and T-waves in different leads for a 12-lead ECG with view of the heart

Leads	P-wave	QRS-complex	T-wave	Views
I	upright	upright	upright	lateral
II	upright	upright	upright	inferior
III	upright	upright	upright	inferior
aVR	negative	negative	negative/upright	right atrium/left ventricle
aVL	upright	upright	upright	lateral
aVF	upright	upright	upright	inferior
V1	upright/biphasic	small R-wave/QS	upright	septum
V2	upright/biphasic	small R-wave/QS	upright	septum
V3	upright	equiphasic/QRS upright	upright	anterior
V4	upright	upright	upright	anterior
V5	upright	upright	upright	lateral
V6	upright	upright	upright	lateral

the ‘PQRST’ morphologies at different ECG leads. The last column gives the views of the heart as seen from each lead.

1.3 Processing of ECG Signals

The processing of single or multichannel ECG is preceded by the an important pre-processing stage. In Figure 1.7, a typical block diagram for ECG signal processing is shown. In the first pre-processing

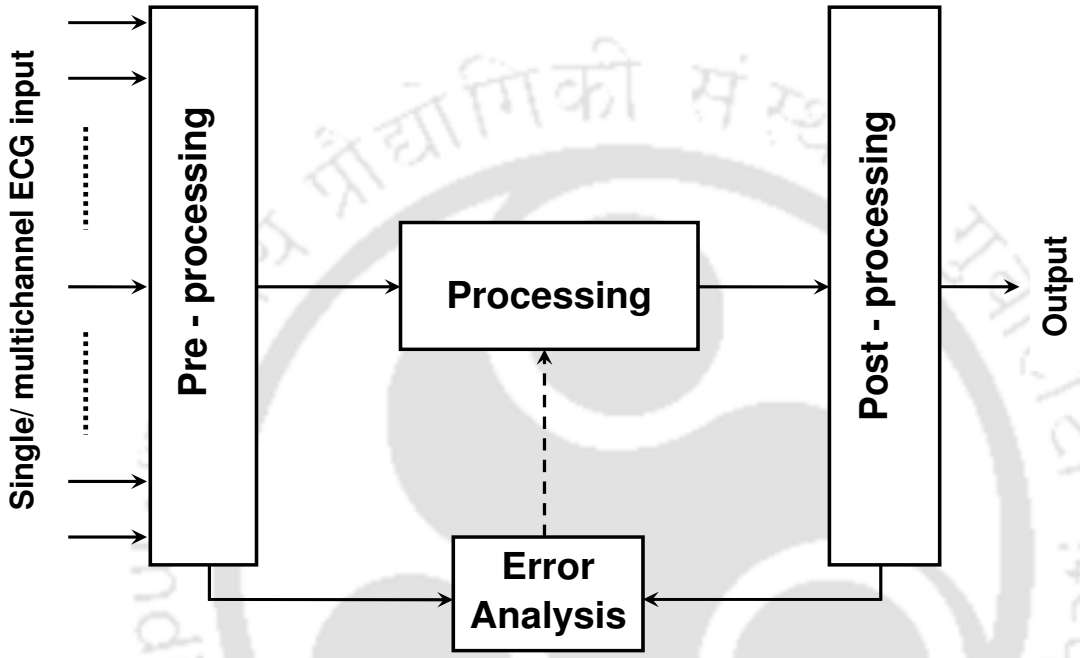

Figure 1.7: System block diagram

block, signal is amplitude and time normalized. Artifacts and noise is removed by applying suitable filter. In the processing block, signal is processed for feature extraction, time or frequency domain processing and analysis for specific task. Post-processing unit does the work for its diagnostic decision. The error introduced during the processing of ECG signal is evaluated in error analysis block using Percentage Root Mean Square Difference (PRD), Wavelet Weighted Percentage Root Mean Square Difference (WWPRD), Wavelet Energy based Diagnostic Distortion (WEDD) measure etc. .

In time domain, recorded ECG display 'PQRST' morphologies with P-wave, QRS-complex and T-wave. This helps a cardiologist to get first-hand information on signal shape, time and amplitudes. Any processing of ECG signal should preserve the shape, duration and amplitudes of its clinical components. One of the goals of research on ECG signal is to get noise free ECG with distinct

parameters. Similarly, many algorithms are developed for extraction of features for the purpose of diagnosis. The use of multilead ECG help cardiologist to analyze the cardiac events from different angles. To extract information which may not be readily available from the original time domain signal, transformed domain tools are applied on single or multiple lead ECG signals. The wavelet-based signal processing is extensively used for non-stationary ECG signal analysis and interpretation. Also, it is used for characterization of local waves (P, T and QRS complex morphologies).

Processing and analysis of multilead ECG is of great important due to its wide application in clinical diagnosis of cardiac rhythmicity. Generally, the signal processing algorithms are applied for pre-processing, denoising [7] and processing of signals for specific task. These may include beat detection, wave boundary measurement of P-wave, QRS-complex and T-wave, measurement of important features such as RR interval, PQ interval, QT interval, measurement of QRS duration, detection of ST segment [8, 9]. In addition to these, dimension reduction and data compression are the area to be addressed. Shen et al. [10] have reported multi-lead Electrocardiogram (ECG) classification and the feature extracting stage by an improved Independent Component Analysis (ICA) method. For each segment of an ECG, P wave, QRS interval and ST segment ICA is used to extract the features separately. These three feature vectors constructed from single lead are combined to generate a multi-lead feature vector. The Support Vector Machine (SVM) is used for multi-classification. The multilead ECG characteristic points detection is introduced [11] by an approach of lead optimization using the single lead result. In the process of global characteristic points determination, the similar methods are used such as the detection of the onset and the offset of QRS-complex, P-wave and T-wave.

For physiological signals, conventional PCA has been applied for data reduction, noise elimination, beat detection, classification, signal separation and feature extraction [12], [13]. Also, it is used to separate respiratory and non-respiratory segments in an ECG signal [14]. The rhythmical beats of the heart with proper PQRST morphologies and the normal shapes of waveform are more important. These features are most important for a physician for the diagnosis of pathological condition of human heart. So, the signal processing algorithm applied on recorded MECG should not alter or deform the original signals. That is, a small change in clinically important diagnostic features of PQRST may mislead a judgement for clinical trial. Thus, to check the distortion introduced on these features or

TH-1102_06610204

signals during the processing of the signals, certain error measures are essential.

1.3.1 Preprocessing

The raw ECG signal may contain a few undesired signals or other artifacts. Few of them are baseline wander or drift, high frequency slur and noises and artifacts. Preprocessing of single lead or multi-lead ECG emphasizes the signal and at the same time it deemphasizes the undesired and unwanted part or parts of the signal. Thus, it improves the signal quality for more accurate analysis and measurement.

Noise elimination is an important signal processing task for ECG signals. The ECG filtering techniques are used for preprocessing of the signal before applying other algorithms. The most common types of noise and artifacts presence in the ECG signal and different filtering schemes are presented below.

Baseline wander is a low-frequency artifact present in an ECG signal. Its spectral content is below 1 Hz [15]. It may appear due to a variety of noise sources such as perspiration, respiration, body movements, and poor electrode contact. Due to its presence in ECG waveform, the isoelectric line cannot be recognized. It affects the low frequency 'ST-T segment' and may create confusion in the diagnosis of ischemia. The determination of the QRS-complex becomes difficult when its amplitude is high. The baseline wander may be filtered out by applying linear filtering methods or polynomial fitting methods. The critical requirement for this filter is the linear phase. This is required to avoid any phase distortion which may affect the time and duration parameters in an ECG signal. Infinite impulse response (IIR) filter may not be suitable due to its nonlinear phase response.

Electrode motion artifacts appear due to skin stretching. This may change the impedance of the skin under the electrode. Electrode motion artifacts are problematic during ambulatory ECG monitoring. Motion artifacts is similar to the signal characteristics of baseline wander. Its spectral content is in the range of 1 to 10 Hz [16], [17] which overlaps with the spectrum of the PQRST complex.

Powerline interference [18] is caused by improper grounding of the ECG equipment and interference from nearby equipment. Such interference can be removed in many situations by means of linear or nonlinear filtering.

The electrical activity of skeletal muscles during periods of contraction causes **electromyographic (EMG) noise**, commonly seen in ECG signals recorded during ambulatory monitoring or exercise. EMG noise can either be intermittent in nature, due to a sudden body movement or have more stationary noise properties. The frequency components of EMG considerably overlap those of the QRS complex which may extend to higher frequencies (in the 0.01 Hz to 100 Hz range) [19], [20]. As a result, application of bandpass filtering fails to remove EMG noise from the ECG signal without introducing distortion. The influence of EMG noise can also be reduced by ensemble averaging when the recurrent property of the heartbeats can be exploited. Respiratory activity influences electrocardiographic measurements not only through heart rate but also through beat morphology [21]. Such beat-to-beat variations in morphology are caused by chest movements, changes in the position of the heart, and changes in lung conductivity. During the respiratory cycle, the vector describing the dominant direction of the electrical wave propagation changes so that variations in beat morphology arise. Thakor and Zhu [22] discussed different adaptive filtering methods to eliminate baseline wander, 60 Hz power line interference, muscle noise, and motion artifact. Spectral substraction method may introduce artificial noise and disturb the original signal [23]. Due to non-stationary nature of ECG and noise signals, Wiener filter may not yield good result [24]. Adaptive filtering is one of the popular methods for ECG filtering [25, 26] due to its ability to denoise signal with overlapping spectra. The wavelet based signal denoising using wavelet shrinkage and soft thresholding are proposed [27–29]. In general, wavelet based denoising can be accomplished by thresholding coefficients with an appropriate method. A comparison between Adaptive filtering and wavelet shrinkage on denoising of ECG signals is presented by Jianbo et al. [30].

1.4 Compression of ECG Signals

ECG signals recorded for longer duration require substantial volumes of data storage. If more ECG leads, higher sampling rate and finer amplitude resolution are needed, it demands even higher memory space. Thus, long-term recording accumulates huge data. To overcome this constraint, data reduction and compression of signal play important role. Data compression method reduces the number of bits to represent the information. The need for such compression system is to transmit ECG signals through public telephone network, cellular networks, intra-hospital networks, wireless

TH-1102_06610204

communication link and ambulance or a patient's home to the hospital [15]. So, ECG data compression is a method to reduce the bandwidth required to transmit a given amount of information in a given time or to reduce the time required to transmit a given amount of information in a given bandwidth. For physiological signals like ECG signal, the goal of compression is not only to achieve higher compression ratio but also to preserve the diagnostic or clinical features in the signal. It should enable to store or transmit digitized ECG signals without significant loss of signal quality.

The ECG signal can be compressed in time domain, frequency domain, or time-frequency domain. The compression method employed may be lossy or lossless.

1.4.1 Time Domain Compression

In time domain, direct methods, the ECG signal is compressed by keeping 'M' number of significant samples from 'N' number of samples from the original signal $x(n)$, provided $M < N$.

Original signal $(x(n), n)$; where $n = 0, 2, ...N - 1$

Compressed signal $(x(n_m), n_m)$; where $m = 0, 2, ...M - 1$

Reconstruction of the signal is achieved by employing prediction or interpolation algorithms. These techniques try to reduce redundancy in a data sequence by examining a successive number of neighboring samples. Interpolation method utilizes a priori knowledge of both previous and future samples whereas prediction algorithm employs a priori knowledge of some previous samples.

$$\widehat{x(n)} = \begin{cases} x(n) & \text{if } n = n_0, n_1, \cdots, n_{M-1}; \\ f_{n_0,n_1}(n), & \text{if } n = n_0 + 1, \cdots, n_1 - 1; \\ \vdots & \\ f_{n_{M-2},n_{M-1}}(n), & \text{if } n = n_{M-2} + 1, \cdots, n_M - 1; \end{cases}$$

Samples between the significant samples is achieved by above interpolation. The interpolating function has a polynomial form of low order, approximating the signal with zero-order or first-order polynomials. First-order (linear) interpolation has become especially popular since the signal can be completely reconstructed from the set of significant samples $x(n_M)$.

Time Domain Compression (TDC) methods are sensitive to noise level in the signal. Some of the methods use more than one variables to achieve the desired data reduction. But the selection and the tuning of these variables are difficult. In most of the methods, the reconstruction is achieved by linear interpolation. Four categories of data handling approaches are used in this method [31], 1) Statistical coding techniques, 2) Redundancy reduction techniques, 3) Adaptive sampling techniques, and 4) Model based compression (MBC) techniques.

In adaptive sampling, the sampling rate of the original waveform is varied while in redundancy reduction the waveform is initially sampled at a constant rate and nonessential samples are eliminated later.

Cox et al. developed the **Amplitude Zone Time Epoch Coding** (AZTEC), one of the earliest ECG coding methods [32] for preprocessing real-time ECG for rhythm analysis. Though, work claims high compression ratio, it introduces significant features distortion which is not acceptable to the cardiologists. It gives up to $20:1$ reduction by producing plateaus and slopes to encode the ECG signal. The **Turning Point** (TP)data reduction method [33] is basically an adaptive down sampling method developed for ECG compression. It reduces the sampling frequency of an ECG signal by a factor of two. So, the resulting compression ratio (CR) is $2:1$. A PRD of 5.3% is reported for an ECG signal sampled at 200 Hz with 12 bit/sample resolution. A hybrid of TP and AZTEC was developed [34] known as the **Coordinate Reduction Time Encoding System** (CORTES). The CORTES provides nearly as great data reduction as AZTEC with approximately the same small compression or reconstruction error as TP. The average percent RMS differences for CORTES is 7% with the average amount of data reduction of 78%. **Scan-along Polygonal Approximation** (SAPA) is an another data compression method [35]. In this, to avoid the plateau representation of AZTEC, the signal is represented by consecutive straight lines.

Some of the adaptive sampling techniques are reviewed by Jalaleddine et al. [36] for compression. **SLOPE algorithm** [37] by Tai uses the slope value of a linear segment to select the significant samples. He has also developed the corner detection algorithm for real time ECG compression and compared the results with the AZTEC algorithm [38]. The performance evaluation shows that a considerable improvement of the Signal-to-Noise Ratio (SNR) and Root Mean Square Error (RMSE) under the same bit rate. Huang et al. have proposed two algorithms named as **Modified SAPA**

TH-1102_06610204

(MSAPA) and **Combined SAPA** (CSAPA) [39]. These algorithms were tested using the 15 different ECG signals including ischaemic episodes, tachycardia, inverse QRS complexes and power-line noise. Results showed that the algorithms achieved a compression ratio of more than 5:l with a PRD value of less than 3.5%. Shahein and Abbas [40] have presented the **CUSAPA** algorithm based on the Cubic-Splines and the SAPA. An improved AZTEC reported by Vinod Kumar et al. [41], incorporates two steps to the previous reported adaptive AZTEC algorithm. Adaptive sampling techniques are widely used for the reduction of ECG data. It is seen that, for the selection of significant samples a threshold is applied.

1.4.2 Frequency Domain Compression

Transform or Frequency Domain Compression (FDC) method translates the ECG signal in frequency-domain and coding method is applied on significant samples. Transforms of ECG signal possess the features of energy preservation, energy compaction, and decorrelation. In FDC, the rationale is to efficiently represent a given data sequence by a set of transformation coefficients. These compression techniques include the KarhunenLove transform (KLT), the Fourier Transform, the Walsh transform, the Discrete Cosine Transform (DCT), the Discrete Legendre Transform (DLT), the Optimally Warped Transform (OWT), the Subband Coding (SBC) and the Wavelet Transform (WT). These compression methods generally consist of 1) Transformation of signal using the transform, 2) Thresholding of coefficients, 3) Quantization process, and 4) Encoding of the symbols. Sometimes, the quantization was performed after the transformation without applying the thresholding process. When transform coding is concerned, it is important to select the orthogonal transform that can represent the maximum amount of signal energy with minimum number of coefficients. Principal component analysis (PCA) uses an orthogonal transformation to convert a set of observations of possibly correlated variables into a set of values of uncorrelated variables (Principal Components).

Ahmed et al. [42] tested the performances of the **Karhunen-Loeve Transform** (KLT), the Di**screte Cosine Transform** (DCT), the **Haar Transform** (HT) and the **Identity Transform** (IT) using the variance criterion. It is shown that almost all of the signal energy is packed into nearly 45 DCT and KLT components. Dual application of the KLT to a vector lead ECG partitioned into a P wave and a QRST segment has given a CR greater than 12 with good reconstruction [43]. However, the quality

of the reconstructed P-wave is not good. Feasibility of using a fast Walsh Transform algorithm for real-time microprocessor based ECG data-compression system has been investigated [44]. Walsh spectrum of a typical ECG shows an exponentially decaying energy content with increasing spectral index. Therefore, Berti et al. [45] suggested the logarithmic quantization of the expansion-coefficient amplitudes in addition to an exponential decrement of the number of quantization levels. For a spectral reduction of 2:1, the method reached a CR of 3.05 with a very low MSE of 0.011 without the filter and 0.0025 with the filter. Reddy et al. [46] presented Fourier descriptors (FD's) for ECG data compression by segmenting two-lead ECG into QRS complexes and S-Q intervals. The magnitudes of Fourier descriptors decrease rapidly for higher harmonics. Though, compression ratios of 10:1 are feasible for the S-Q interval, the clinical information requirements limited to 3:1 for the QRS complex. Nashash [47] proposed a method that relied on modeling quasi-periodic ECG signals by a set of time-varying Fourier coefficients. A higher CR with lower heart rates and a lower CR with higher heart rates can be obtained.

Tai [48] presented a six-band **Sub-band Coder (SBC)** for encoding of the ECG signal. **Quadrature Mirror Filter**s (QMF) are used for the frequency band decomposition. It claims an average SNR of 29.97 dB and average bit rate of 0.81 bits per sample. In another work, the ECG signal is decomposed into four sub-signals using a QMF bank in a tree structured fashion and the resulting stages of the tree are decimated by a factor of two [49]. Compression ratios as high as 5.7 is obtained with a PRD = 7.0%. The performance is tested with filtered ECG signal. A low-pass filter with a cutoff frequency of 125 Hz is used which results in a CR and PRD of 5.3 and 2.9% respectively. It is observed that the PRD measure is sensitive to smoothing of background noise. Both finite impulse response (FIR) and **Infinite Impulse Response** (IIR) filter banks are considered as main components in a sub-band coding system [50]. This system can provide compression ratios between 5 and 15 without loss of clinical information. Balnco [51], [52], compared the performance of a nearly perfect reconstruction cosine-modulated filter bank with the Wavelet Packet (WP) technique. Both apply the same coding in order to establish suitability for use in ECG compression. The results show that the nearly perfect reconstruction cosine-modulated filter bank method superior to the WP technique in terms of both quality and efficiency.

Philips and Jonghe [53] have discussed a compression method based on the approximation of

TH-1102_06610204

the ECG signal by **Higher-order Polynomial Expansions** (HOPE). The variable coding method is applied to reduce the correlation between the coefficients of the two intervals. For same value of polynomial expansions, the compression ratio of the Discrete Cosine Transform (DCT) is only half. The signals reconstructed by the **Discrete Legendre Transform** (DLT) [54] often suffer from ringing or Gibbs-effects. Alberto and Antonio [55] proposed the use of variable-length discrete Legendre polynomials and a variable-rate fixed quality scheme. The use of nonuniform quantizers and entropy coding improves the performance of the basic coder. Philips [56] presented the adaptive compression for ECG signal using the **Optimally Warped Transform** (OWT). The DLT error is larger than the OWT error especially near the QRS complexes. The results presented in this paper demonstrated the benefits of the OWT for ECG compression. An average CR of 9.3:1 is achieved for a PRD value equal to 2.5% for an ECG compressor based on optimized quantization of DCT coefficients [57]. Borsali et al. [58] proposed an ECG compression method combining the ECG beat alignment and the polynomial modeling. The QRS complexes are first detected and then aligned in order to reduce high frequency changes from beat to beat. Allen and Belina [59] discussed the implementation of DCT based compression routines for ECG. The average value and the width of each band are calculated and the coefficients are approximated using uniform quantization. It is concluded that the overall suitability of the DCT in ECG signal compression method is enhanced by the basic algorithm which allows the dynamic allocation and subband thresholding. Madhukar and Murthy [60] presented a compression algorithm based on the parametric modeling of the discrete cosine transformed single lead ECG signal. A maximum compression ratio of 40:1 is achieved with **Normalized Root Mean Squared Error** (NRMSE) in the range of 5 to 8%.

1.5 Error Measures

In an ECG cycle, cardiac components appear in a regular sequence of ‘P-QRS-T’ and carry clinical information. There are many algorithms extract basic ECG measurements of wave amplitudes and durations. A delineation determines the boundaries of each wave within the PQRST complex. It can give time instants and so wave duration can be computed. Once the wave has been delineated, other measurement characterizing the wave, such as amplitude and morphology, can be easily computed. The delineation is mainly applied to beats originating from the sinus node, to produce measurements

for use in automated beat classification.

Most of the ECG analysis algorithms, need a QRS detector to monitor arrhythmia [61], [62], [63]. The algorithms for QRS detection methods are mainly based on approaches like derivatives, filter-banks, wavelets, mathematical morphology and correlation [64] [65]. In derivative based approach to filtered out the high frequency noise, moving average filter is used. Then, the signal is differentiated to emphasize higher slopes as well as to suppress ECG waves (P and T waves) and baseline wanders. Then squaring the magnitude of the derivative signal results further enhancement of the high derivatives of the QRS complex. And then, one can find out the local maxima, by applying a suitable threshold on this.

The heart rate may be determined by calculating the time period between the two consecutive R peaks on 'QRS-complex'. Also, using the R peak locations certain ECG parameters can be derived such as, ST segment. It is measured at a certain predefined time interval from the end of the QRS complex [15]. The corrected QT interval is derived by classical Bazzet's equation ($QT_c = \frac{QT}{\sqrt{RR}}$) putting the current QT and RR intervals [66]. So, the QRS detection in cardiac signal processing is an important step. Most of the QRS detection algorithms, take advantage of the relatively high energy contents of complex that lie in 5-25Hz band [65], [67], [63]. The complex QRS detection algorithms apply the Neural Network (NN) and Hidden Markov Model (HMM).

On a standard ECG dataset, the Hamilton-Tompkins algorithm had the highest detection accuracy of 99.68% with sensitivity and 99.63% but gives the largest time error [68]. This algorithm is an improved version of the Pan-Tompkins algorithm [67]. Benitez et. al. [69], proposed a Hilbert transform-based method. The ST segment is normally at or near the baseline. Stamkopoulos et. al. have proposed [70] a new method based on Non-linear Principal Component Analysis (NLPCA), implemented using Neural Network for ST segment feature extraction. Subsequently, Radial Basis Function Network (RBFN) is used for the classification of ischemic ECGs which is found to be quite reliable in the classification of normal and ischemic beats.

The performance of a signal processing method or compression scheme is evaluated based on few signal distortion measure. Such error analysis on ECG signal processing is carried out by measures like Normalized MSE (NMSE), Root MSE (RMSE), Normalized RMSE (NRMSE), **Percentage Root Mean Square Difference** (PRD) and **Signal-to-Noise Ratio** (SNR). Few method which are

proposed for local error are **Maximum Absolute Error** (MAE) or **Peak Error** (PE), Normalized MAE (NMAE) and Standard Error (StdErr). Signal similarity may be evaluated using Normalized Cross Correlation (NCC). Signal like ECG should be evaluated taking account of its clinical information on its components. Some error measure which give the information related to loss of diagnostic information are **Weighted PRD** (WPRD), **Weighted Diagnostic Distortion** (WDD), **Wavelet Weighted PRD** (WWPRD) and **Wavelet Energy based Diagnostic Distortion** (WEDD) [71]. The PRD is widely used and it gives normalized value of the error between original and processed signal.

1.6 Wavelet Transform and ECG Signal

Time-Frequency Domain Compression mainly focuses wavelet based compression algorithms. This method is given higher important because of its good localization properties in time and frequency domains, high energy compaction capability and easy implementation. Wavelet based methods outperform the traditional time domain and frequency domain ECG compression methods [72]. In time-frequency plane the main algorithmic steps are 1) Amplitude normalization, 2) Period normalization, 3) Wavelet transform, and 4) Encoding of wavelet coefficients.

The resulting wavelet coefficients are encoded to achieve the compression. In existing literature, encoding of the wavelet coefficients are found based on 1) Threshold Methods [72–85], 2) Embedded Coding Methods [86–90], 3) Vector Quantization (VQ) Methods [91–95].

For signal decomposition there are methods such as, **Short Time Fourier Transform** (STFT), **WignerVille Transform** (WVT), **ChoiWilliams Distribution** (CWD) and the Wavelet Transform (WT). The STFT uses a single analysis window of fixed length in both time and frequency domains. This is a major drawback of the STFT. For proper analysis, it requires a shorter window in time domain for the high frequency content of a signal and a longer window length for the low frequency content of the signal. This is like contractions and dilations of the basis wavelet. The **Discrete Wavelet Transform** (DWT) is become the most desirable tool for ECG analysis. It makes easy to interpret resulting transformed signal in time-frequency domain. This linear process performs decomposition of ECG signal separating it into components, that appear at different scales. The dilation of the mother wavelet gives the low frequency components whereas translation represents the high frequency components.

The efficiency of wavelet analysis is its fast pyramid algorithm. The algorithm has the forward

algorithm (decomposition structure) to compute the DWT and backward algorithm (reconstruction structure) to compute the Inverse Discrete Wavelet Transform (IDWT). The forward algorithm uses low-pass and high-pass linear filters to decompose the signal into low-frequency and high-frequency subbands. It has down-sampling operations which speed-up the algorithm. The reconstruction or inverse process performs the up-sampling operation with linear filtering.

The ECG signal under evaluation passes through two complementary filters which give low-pass and high-pass components. The decomposition process may be iterative with successive low frequency components. In the process, the signal is broken down into many lower-resolution components. To reach the desired decomposition level, the iteration is repeated.

The **Hybrid Compression Methods** (HCM's) for ECG signal are some combination of the coding algorithms [93, 94, 96–99]. Compression methods under this category result in good compression performance with the cost of increased time and space complexity. These methods are suitable for off-line processing for the acceptable distortion level provided by the clinician.

The wavelet transform is found suitable for compression of ECG signal which gives a good reconstruction [100]. Thakor et al. [101] presented a multiwave ECG compression method by preserving the coarse sub-signals and discarding the differential sub-signals decomposed by the orthonormal wavelet transform. Best reconstruction results are obtained with vector quantization (VQ) on scales with long duration and low dynamic range, and scalar quantization on scales of short duration and high dynamic range [91]. Nagarajan et al. [72] presented a constraint ECG compression by introducing a constraint on PRD and using adaptive wavelet packet decomposition. ECG coding by wavelet based linear prediction based on beat segmentation, and period normalization (PN) is proposed by Ramakrishnan and Saha [97]. A series of experiments are performed to evaluate the ability of the **Embedded Zerotree Wavelet** (EZW) algorithm to compress ECG data and to identify which wavelet performs the best using the ECG data taken from the `mitct` database [86]. However, the EZW algorithm yields worse performance than the DWT because the best basis decomposition often splits the signal into a number of smaller hierarchies that cannot be efficiently encoded [84].

Chen and Itoh [73] presented a new ECG compression method based on orthonormal wavelet transform along with an adaptive quantization strategy. It is shown a predetermined PRD can be guaranteed with high compression ratio and low implementation complexity. For a mobile telecar-

diogram system, an **Optimal Zonal Wavelet Based Compression** (OZWC) method successfully transmit the compressed ECG at a standard GSM data rate of 9.6 kbps [75].

The **Set Partitioning in Hierarchical Trees** (SPIHT) scheme has received widespread recognition for its notable success in image and audio coding. A wavelet ECG codec based on the set partitioning SPIHT) compression algorithm is proposed by Lu et al. [87]. Rajoub [77] proposed a wavelet based ECG data compression algorithm using the BiorSpline (bior4.4) wavelet. It shows better performance than SPIHT coder in terms of PRD. Benzid et al. [79] have reported an ECG compression method based on the pyramidal wavelet decomposition. The resultant coefficients are subjected to an iterative thresholding till a fixed percentage of wavelet coefficients are zeroed out. Ku et al. [81] have proposed an ECG compression method based on the one-dimensional **Nonrecursive Discrete Periodized Wavelet Transform** (NRDPWT). Kim et al. [80] presented a wavelet transform based ECG compression method with a low delay property for continuous ECG transmission suitable for telecardiology applications over a wireless network. It employs waveform partitioning, adaptive frame size adjustment, wavelet compression, flexible bit allocation and header compression to attain low delay and high quality. Blanco et al. [84] presented a Wavelet Packets (WP's) thresholding based ECG compression method. The number of WP layers is set to 4 and the Cohen-Daubechies-Feauveau 9/7 (bior9.7) is used for decomposition. The performance is compared with SPIHT coding scheme. Manikandan and Dandapat [83] have reported wavelet threshold based ECG signal compression technique using Uniform Scalar Zero Zone Quantizer (USZZQ) and Huffman coding on Differencing Significance Map (DSM). WT coefficients in each subband are thresholded based on the Energy Packing Efficiency (EPF) and quantized with uniform scalar zero zone quantizer. Indices of the significant coefficients (significance map) are encoded by applying Huffman coding on the differences between indices in the significance map. Another two novel wavelet threshold based ECG compression algorithms are proposed for real-time applications [102] which take account of Target Distortion Level (TDL) and Target Data Rate (TDR). In recent, Cheng et al. [103], have proposed wavelet-Based ECG data compression system with linear quality control scheme. Kim et. al. [104] have reported an ECG signal processing with Quad Level Vector (QLV) for holster system. The compression is achieved by using ECG skeleton and the Huffman coding.

1.7 Scope for the Present Work

The simultaneous data acquisition from different ECG leads depicts the conduction sequence or activation sequence of heart. It carries vital clinical clue for cardiologist to diagnose pathological condition. The standard 12-lead clinical ECG is a diagnosis or prognosis tool which demands clean signals with all clinically essential components and morphologies. The processing of ECG may be performed in time domain, frequency domain or in time-frequency domain. Before any processing task, it is required to pre-process the signal to improve its quality. The signal may be processed for feature extraction, data reduction or wave boundary measurement by various methods in time or frequency domain. In recent days, the wavelet transform based processing has become preferable over others. It is due to its energy compaction property within a few transform domain coefficients. Also, the multiresolution decomposition with dyadic wavelet structure, separates ECG signal into components that appear at different scales. There are scopes to develop automatic signal denoising and processing systems using wavelets.

Multichannel ECG signals may provide spatio-temporal information of electrical activity of the heart in three dimensional orthogonal space. In spatial domain the ECG channels can view the heart from left lateral to right lateral, inferior to superior and anterior to posterior directions. Each lead gives a specific orientation in space. The direction of depolarization of heart chambers in 3-dimensional space can give better understanding of its electrical activities. So, these multichannel recordings, carry intra and inter-lead correlations in temporal and spatial domain. Wavelet based ECG filtering are reported mainly based on soft or hard thresholding of coefficients [28, 29]. The preprocessing for multichannel signals can be investigated in wavelet domain to derive thresholds which depend on real data in wavelet scales. The need of such automatic denoising system is essential. The clinical information appearing at different scales help retain the vital clinical components with minimal distortion in time and amplitude. The other aspect of multichannel correlations in wavelet domain are not addressed extensively. There are possible ways to extract inter-lead correlations quantitatively for these multichannel ECG signals. In wavelet scales, inter-lead correlations can be evaluated. This will help preserve clinical components of multichannel ECG signals. So, there are scopes for the processing of these type of multichannel physiological data by using correlation properties. It may be

TH-1102_06610204

applied for signal enhancement, data dimension reduction and multichannel compression.

1.8 Organization of the Thesis

The contents of the thesis are organized as: In **Chapter 1**, introduction to ECG signals and its processing in time, frequency and time-frequency domain are discussed with published literatures. In **Chapter 2**, a related reviews of wavelet transform based ECG signal processing is given. PCA based processing and the motivation for this thesis work is discussed. In **Chapter 3**, for preprocessing of multichannel ECG, two novel ECG denoising method are presented and evaluated. In **Chapter 4**, multiscale PCA is introduced for multichannel ECG signal processing. A compression scheme for multichannel ECG using multiscale PCA is proposed. In **Chapter 5**, clinical entropy based multiscale PCA and multiscale distortion measure are introduced. Conclusion of the thesis is drawn in **Chapter 6** with major contributions from this thesis and scope for further research.

TH-1102_06610204

2

Multichannel Electrocardiogram Signal Processing - A review

Contents

TH-1102_06610204

The key motivation for researchers is the designing of signal processing algorithms and systems without degrading in-depth clinical quality of signals. For a cardiovascular system, the standard 12-lead electrocardiogram is a basis to assess cardiac electrophysiological state, event and function. This simple standard clinical ECG system caters the need of a diagnostic and prognostic tool for a physician at an instant time. The first-hand information on signal shape, time and amplitudes helps a cardiologist to ascertain condition of a patient. To extract information further, which may not be readily available from the time domain original signal, signal transformation tools are essential. A wavelet-based signal processing may be an effective tool for non-stationary ECG signal analysis. Also, it may be applied for characterization of local waves (P-wave, QRS-complex and T-wave morphologies). The recording of cardiac events with multiple leads on the body surface helps finding spatiotemporal distribution of cardiac potential.

This chapter reviews wavelet transform application to ECG signal, wavelet transform based noise elimination methods, wavelet transform based ECG compression schemes and principal component analysis based ECG signal processing. At the end of the chapter, motivation for the present work is written.

Database

In this thesis, most of the algorithms developed are evaluated using data set from common standards for quantitative electrocardiography (CSE) multilead measurement library [2]. The ECG data of CSE multilead data set 3 used in this work were sampled at 500 Hz with a resolution of 10 bits and a maximal quantization of 5 mV. The data set 3 has 125 original ECG data sets with almost equal numbers of normal and various pathological cases. The original ECGs of data set 3 from CSE multilead measurement library were created without filtering and preprocessing on ECG signal [2]. The listed RMS noise is found upto 20 microvolt [2] in original ECGs. The other data base used is 'PTB Diagnostic ECG Database' which is retrieved from http://physionet.org/physiobank/database/ptbdb/. This database has 549 records from 290 subjects. Each recording includes 15 simultaneously measured signals out of which 12 are standard clinical leads and 3 are Frank lead ECG (vx, vy, vz). Signal is digitized at the sampling rate of 1 KHz, with 16 bit resolution over a range of $\pm 16.384 mV$.

2.1 Wavelet Transform Application to ECG signal

Wavelet transform (WT) is a linear process that performs decomposition to a signal separating it into components that appear at different scales. Wavelets are families of functions $\psi_{j,k}(x)$ generated from a single base wavelet $\psi(x)$, called the mother wavelet, by dilation and translation-

$$\psi_{j,k}(x) = \frac{1}{\sqrt{j}}\psi(\frac{x-k}{j}) \tag{2.1}$$

where j is the dilation parameter (scale) and k is the translation parameter [105, 106].

The dilation of the wavelet function match the low frequency components whereas translation version represents the high frequency components. Thus, the multi-resolution decomposition of the ECG signal separates the signal into "details" at different scales and a coarser representation of the signal named "approximation" [107, 108]. A given signal is represented by a linear combination of dilated and shifted version of the "mother wavelet"

$$f(x) = \sum_j \sum_k w_{j,k}\psi_{j,k}(x) \tag{2.2}$$

where $f(x)$ is the signal to be decomposed, $\psi_{j,k}(x)$ is the dilated and shifted version of "mother wavelet" $\psi(x)$, $j, k, \epsilon Z$ and $w_{j,k}$ are the wavelet coefficients. In order to simplify the computation of the coefficients, the wavelet bases function must be orthonormal and from (2.2), the wavelet coefficients $w_{j,k}$ [97], is given as

$$w_{j,k} = \langle f(x), \psi_{j,k}(x)\rangle \tag{2.3}$$

The energy of the signal f from the above wavelet coefficients $w_{j,k}$ at level j can be written as-

$$E_j = \sum_j w_{j,k}^2 \tag{2.4}$$

If the total energy of all decomposition levels of f is $E_t = \sum_j E_j$, percentile energy of level j can be expressed as

$$\varepsilon_j = \frac{E_j}{E_t} \times 100 \tag{2.5}$$

TH-1102_06610204

2.1.1 Multiresolution Pyramidal Decomposition

The dyadic wavelet transform is implemented using a multiresolution pyramidal decomposition technique. Multiresolution structure leads to an efficient discrete-time algorithm based on a filter bank

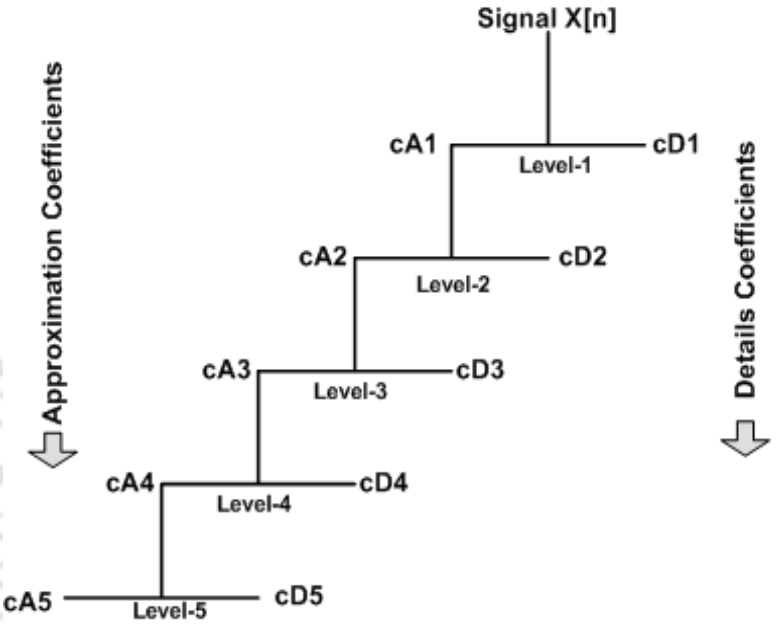

Figure 2.1: Wavelet decomposition (Analysis) structure.

implementation. Using the scaling function $\phi(t)$ and the wavelet function $\psi(t)$, it can defined the $\mathrm{cAL}(k)$ and $\mathrm{cDj}(k)$ coefficients as $\mathrm{cAL}(k) = \langle x(t), \phi_{j,k}(t) \rangle$ and $\mathrm{cDj}(k) = \langle x(t), \psi_{j,k}(t) \rangle$. The j^{th} scale coefficients (cAL) are filtered by two finite impulse responses of low-pass and high-pass digital filters respectively. After this operation, down-sampling gives the next coarser, $j+1$ scaling coefficients (cA_{j+1}) and wavelet coefficients (cD_{j+1}). The filters used in the synthesis or reconstruction structure are same. The fast pyramidal algorithm for wavelet analysis exhibits its efficiency in implementing the forward algorithm (decomposition structure) and the backward algorithm (reconstruction structure).

The forward algorithm uses linear low-pass and high-pass filters to decompose the signal into low and high frequency components, and also combines these filters with down-sampling operations. The backward algorithm simply inverts the process, by combining an up-sampling process with linear filtering operations.

The ECG signal passes through two complementary filters and emerges as two signals (low-pass and high-pass components). The decomposition process can be iterated, with successive low frequency components being decomposed in turn, so that one signal is broken down into many lower-resolution components. The Figure 2.1 illustrates the analysis part of a five-level decomposition scheme. Five level wavelet decomposition gives an approximation subband, cA5, and five details subbands, cD5, cD4, cD3, cD2 and cD1. In general, the details subbands are denoted as cDj, where decomposition level j=1,2, $\cdots$, L and the approximation subband is cAL. L is the order of Wavelet decomposition.

The bandwidth, ΔF_j, of j^{th} wavelet subband is given as [71]

$$2^{-j-1}.F_s \leq \Delta F_j \leq 2^{-j} \cdot F_s \tag{2.6}$$

where F_s is the sampling frequency of the signal. Accordingly, wavelet decomposition levels can be decided. For a sampling frequency of 360Hz, a five level wavelet decomposition, gives an approximation subband and five details subbands.

Clinical and diagnostic information or components of an ECG signal are decomposed to different wavelet subbands [83]. The choice of decomposition level, L, which satisfy the frequency range of the main features of an ECG is based on sampling frequency, F_s and is given as [109]

$$L = [\log_2(F_s) - 2.96] \tag{2.7}$$

Different physiological information of the ECG signal are present in a wavelet subband based upon their bandwidth or frequency content. It has been reported that the lower frequency subbands contain most of the diagnostically significant information of the ECG signal [71].

In Figure 2.2, original Lead-I signal from CSE multilead measurement library, Data set: MO1-041 is plotted along with its reconstructed subband signals due to six level wavelet decomposition. It is noticed cA6 subband reflects the parts of low frequency components such as P-wave and T-wave.

TH-1102_06610204

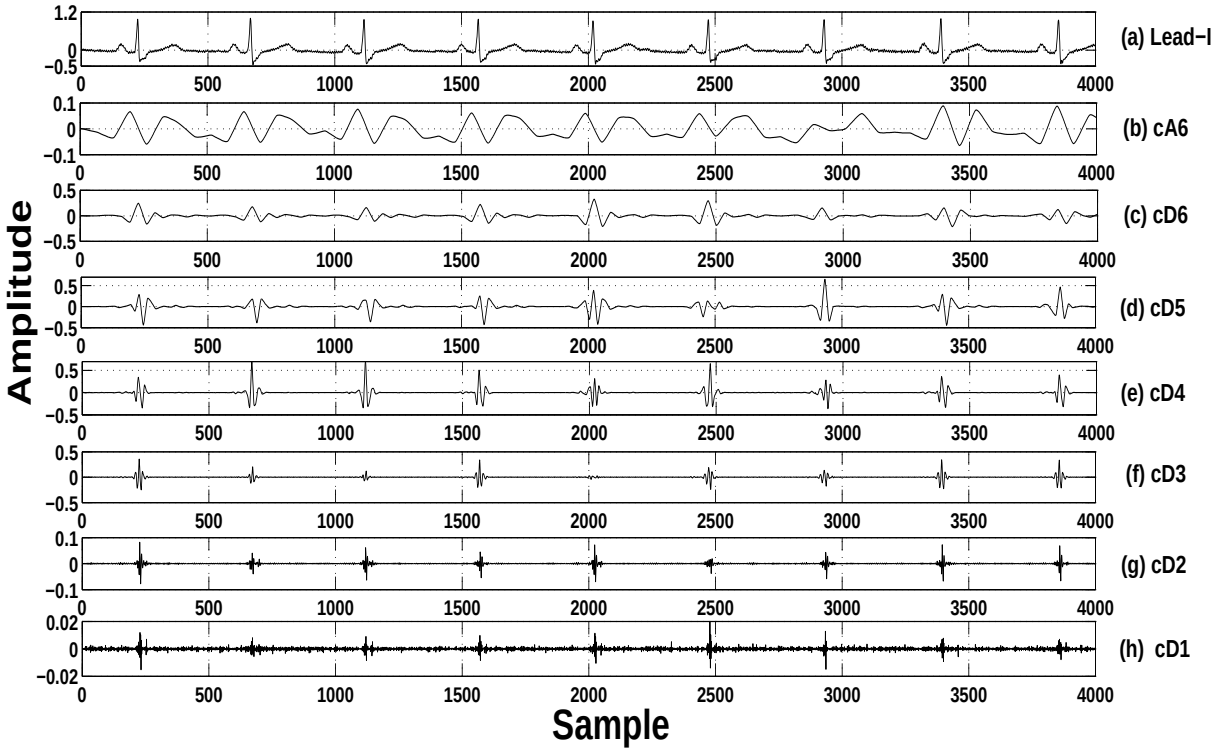

Figure 2.2: Original time domain Lead-I signal and reconstructed subbands signals due to six level wavelet decomposition. In panels, (a) Original Lead-I signal from CSE multilead measurement library, Data set: MO1-041 and reconstructed subband signals (b) cA6, (c) cD6, (d) cD5, (e) cD4, (f) cD3, (g) cD2, and (h) cD1.

cD6 and cD5 subbands show the lower frequency part of QRS-complexes with higher frequency part of T-wave. cD4 and cD3 subbands show the significant higher frequency part of QRS-complexes. cD2 and cD1 subbands contain some higher frequency part of QRS-complexes and noise.

2.2 Wavelet Transform based Noise Elimination

The recording of ECG signals are often contaminated with different sources of noise. This makes interpretation difficult and unstable. So, the signals acquired by means of multiple lead have to process for artifacts and noise elimination.Different techniques have been used to filter the ECG signal, in order to improve and optimize the Signal-to-Noise Ratio (SNR). The wavelet based signal denoising using wavelet shrinkage and soft thresholding are proposed [27–29]. In general, wavelet based denoising can be accomplished by thresholding coefficients with an appropriate method. Wavelet based denoising captures the energy of the original signal to a higher percentage by thresholding the

noisy coefficients whose magnitudes are all greater than a threshold [110]. The transform coefficients (assuming noise) whose magnitudes lie below the threshold are set equal to zero. It is shown that the threshold is optimum if power of discarded wavelet coefficients equals the noise power [111]. Another method of noise reduction based on energy features preserved by wavelet coefficients at conjunctive scales and their neighborhoods is proposed [112]. Wavelet based denoising method seems to be simple, but the signal and noise distribution in different subbands are important to find a suitable threshold. An effective threshold in wavelet domain was defined as

$$t = \sigma\sqrt{2\log(N)/N} \tag{2.8}$$

where t is threshold, σ is the variance of noise and N is the numbers of samples [28, 29]. The performance of this threshold depends on an efficient estimation of noise variance.

Charlotte Yuk-Fan-Ho et al. [113], have applied fuzzy multiwavelets to denoise ECG signal corrupted by an Additive White Gaussian Noise (AWGN). They proposed fuzzy rules on selecting and integrating different multiwavelets, pre- and post-filters together. A hard thresholding is applied on the multiwavelet coefficients.

Sameni et al. [19], proposed a nonlinear Bayesian filtering framework for single channel ECG signal denoising. It is reported to perform better over conventional bandpass filtering, adaptive filtering and wavelet denoising. But, denoising of abnormal ECG with cardiac arrythmia and over-filtering of signal are not addressed, which may result in loss of clinical and diagnostic information.

Xiao-Li Yang and Jing-Tian Tang [114] proposed **Hilbert-Huang Transform** (HHT) and wavelet transform based method to detect R-wave and denoise ECG signal. Using wavelet transform it denoise ECG signal and then it applied the **Empirical Mode Decomposition** (EMD) to electrocardiogram (ECG) decomposing into limited number of **Intrinsic Mode Functions** (IMF's). It uses a set of adaptive thresholds that are not limited to a strict range.

In recent, Jianbo et al. [30] proposed a nonlinear adaptive denoising algorithm for the Electrocardiogram (ECG) and other types of noise contaminated in electroencephalogram (EEG). It compares the nonlinear adaptive filtering with wavelet shrinkage with three different thresholding choices.

The motivation of this work is to find a more accurate threshold by estimating noise variance based on Kurtosis and considering the relative energy contribution efficiency of wavelet subbands.

TH-1102_06610204

2.3 Wavelet Transform based ECG Compression

The amplitude, shape and duration of these parameters at different leads helps in pathological findings. ECG signals recorded for longer duration creates substantial volumes of data for storage or transmission. Data compression method reduces the number of bits to represent the information. And it helps to store or transmit digitized ECG signals without significant loss of signal quality. The Discrete Wavelet Transform (DWT) has become one of the most desirable tool for ECG signal compression. It has received significant attention because of good localization properties in time and frequency domains, energy compaction ability and efficiency. It is due to its ability to transform the signal in time-frequency domain. This localizes the energy of the signal in few wavelet coefficients. Wavelet based ECG data compression In wavelet based methods, the compression is performed in time-frequency plane. Wavelet based methods outperform the traditional time domain and frequency domain ECG compression methods [72].

An application of multirate signal processing and transform domain coding of multichannel ECG signals is proposed by Cetin et al. [115]. Linear transforms such as KLT and DCT are applied to the standard ECG lead signals which give uncorrelated transform domain signals. Various coding methods are applied. It also demonstrate multirate signal processing and transform domain coding techniques. In this approach, at preprocessing stage redundant channels are removed from the standard 12 lead ECG signal resulting only 8 leads. Time domain signals $x_i, i = 0, 1, \cdots, 7$ are fed to the linear transforms like KLT and DCT, and 8 new transform domain signals $y_i, i = 0, 1, \cdots, 7$ are obtained. These transform domain signals are divided in to two classed based on energy. Higher energy content signals, y_0, y_1, y_2, y_3, y_4 are grouped in first class and lower energy content signals y_5, y_6, y_7 are grouped in second class. Class one signals are coded with subband coder while second class signals are coded with multirate transform coder.

Jie Chen and Shuichi Itoh [73] have applied orthonormal wavelet transform and an adaptive quantization on electrocardiogram (ECG) signal to compress it. This works on predetermined error in terms of percent root mean square difference (PRD) to maintain compression quality. The proposed algorithm yields high compression ratio and low implementation complexity. **Multichannel Long-Term Prediction** (MC-LTP) compression scheme proposed by Cohen and Zigel [116], is used to

compress 'PQRST' beats using a pattern code-book.

Ku et al. [81] have proposed an ECG compression method based on the one-dimensional **Non-recursive Discrete Periodized Wavelet Transform** (NRDPWT). Kim et al. [80] presented a wavelet transform based ECG compression method with a low delay property for continuous ECG transmission suitable for telecardiology applications over a wireless network. It employs waveform partitioning, adaptive frame size adjustment, wavelet compression, flexible bit allocation and header compression to attain low delay and high quality.

Manikandan and Dandapat [83] have reported wavelet threshold based ECG signal compression technique using **Uniform Scalar Zero Zone Quantizer** (USZZQ) and Huffman coding on **Differencing Significance Map** (DSM). WT coefficients in each subband are thresholed based on the energy packing efficiency (EPF) and quantized with uniform scalar zero zone quantizer. Indices of the significant coefficients (significance map) are encoded by applying Huffman coding on the differences between indices in the significance map. Another two novel wavelet threshold based ECG compression algorithms are proposed for real-time applications [102] which take account of target distortion level (TDL) and target data rate (TDR).

Blanco et al. [84] presented a wavelet packets (WP) thresholding based ECG compression method. The number of WP layers is set to 4 and the Cohen-Daubechies-Feauveau 9/7 (bior9.7) is used for decomposition. The performance is compared with SPIHT coding scheme.

Shaou-Gang Miaou and Heng-Lin Yen [117] have proposed an **Adaptive Vector Quantization** (AVQ) for electrocardiogram (ECG) compression. To exploit correlations across channels of multichannel ECG, a multichannel version of AVQ was reported. The AVQ index of each channel is collected to form a new input vector. The vector is quantized adaptively using one additional index code-book. The average compressed data rate/channel is 238.2 b/s using the MC-AVQ when used with MIT/BIH database.

In recent, Cheng et al. [103], have proposed wavelet-Based ECG data compression system with linear quality control scheme. Kim et. al. [104] have reported an ECG signal processing with Quad Level Vector (QLV) for holter system. The compression is achieved by using ECG skeleton and the Huffman coding.

TH-1102_06610204

2.4 Principal Component Analysis and ECG

In simultaneous signal acquisition, each leads record more or less information of the same cardiac events at the same time stamp. So, the surface ECG captured by multiple lead may provide vital clinical leads. This enables analyzing information captured by multiple leads in

- Temporal domain to reconstruct ECG morphologies
- Spatial domain to find the nature of cardiac electrical potential distribution

ECG signals may contain long or short isoelectric regions between two local events or waves. Redundancy exists whenever adjacent signal samples are statistically dependent. Many ECG compression methods are reported which exploit one or more of the correlations present in the signal. The multilead or multichannel long-term ECG signals have three correlations [15]

(i) inter-sample or intra-beat correlation,

(ii) inter-beat correlation and

(iii) inter-lead/channel correlation

The intra-beat correlation represents the correlation between the successive samples in a ECG cycle. The inter-beat correlation represents the correlation between successive beats in a single-channel ECG signal. The correlation that exists between the signals from different channels is termed as inter-lead correlation. This is due to fundamental fact that a heartbeat is ”viewed” concurrently in different leads. In ECG data compression methods, these three correlations are exploited using different methodology.

In temporal domain, many essential signal processing task can be performed. Few of them are noise elimination [118], beat detection, classification, signal separation [14] and feature extraction [12], [119], [13]. In spatial domain, multiple lead surface ECG signals are processed with advanced signal processing tools to get more spatial information such as cardiac mapping or body surface potential mapping [120], [121]. Principal components analysis (PCA) [122–124] is one the widely used multivariate signal analysis method. Since last couples of decades, PCA has been applied in different research area [125–134] to better penetrate into signal details . For physiological signals like

ECG signal enhancement, a robust extension of classical PCA by analyzing shorter signal segments is suggested [119]. It may be used in data reduction, beat detection, classification, signal separation and feature extraction [12,13]. PCA is used as a tool for separation of respiratory and non-respiratory segments in an ECG signal [14]. Castells et al. [12], reported an overview of PCA for ECG signal processing. It is proposed to extract signal segment of a beat as a column vector

$$\mathbf{x} = \begin{bmatrix} x(1) \\ x(2) \\ \vdots \\ x(N) \end{bmatrix}$$

N represents the number of samples. This segment is extracted from successive beats and one can have ensemble of M beats. The entire ensemble represented by $N \times M$ data matrix,

$$\mathbf{X} = \begin{bmatrix} x_1 x_2 \cdots x_M \end{bmatrix}$$

The beats $x_1, x_2, \cdots, x_M$ are M observations. Sample correlation matrix is defined as

$$R_x = \frac{1}{M} X X^T \tag{2.9}$$

From above, eigenvectors and eigenvalues are calculated. Eigenvalues are arranged in descending order. Significant eigenvalues gives Principal Component (PC). The resulting PCs characterize the intra-beat correlation. Since correlations between different ECG lead exist, this may be extended to and compression of multichannel ECG signals can be performed by inter-lead information.

Similarly, eigenvalue decomposition is used to process ECG signal. Sameni et al. [135] proposed the generalized eigenvalue decomposition for the decomposition of multichannel ECG signals using periodic component analysis. It is customized and improved extension of conventional source separation techniques. The method is used for the removal of maternal ECG artifacts from fetal ECG recordings. If $\mathbf{A}$ and $\mathbf{B}$ are $n \times n$ symmetric matrices, generalized eigenvalue decomposition for the pair $(\mathbf{A}, \mathbf{B})$ is to find the matrices $\mathbf{U}$ and $\mathbf{D}$ as

$$\mathbf{U^T A U} = \mathbf{D} \tag{2.10}$$

$$\mathbf{U^T B U} = \mathbf{I} \tag{2.11}$$

TH-1102_06610204

where, $\mathbf{D}$ and $\mathbf{U}$ are the diagonal eigenvalue matrix and the eigenmatrix. In this approach, $\mathbf{U}$ is a transformation that simultaneously diagonalizes A and B. If $X(t) = [x_1(t), x_2(t), \cdots, x_n(t)]^T$ is an n-dimensional observation vector and eigenvalues are sorted in descending order on its diagonal, the transformation $U^T X(t)$ gives the most periodic components in descending order of periodicity.

Langley et al. [14] proposed a principal component analysis (PCA) based algorithm to analyze changes in ECG morphology. It is applied to the derivation of surrogate respiratory signals from single-lead ECG. The variability features such as P waves, QRS complexes, and T waves due to respiration is analyzed by PCA. The derived respiratory signal was compared to the recorded breathing signal by magnitude squared coherence and cross-correlation.

The sudden cardiac death is associated with **T-wave Alternans** (TWA). TWA is a low amplitude activity. Although, there are various methods available to detect and estimate TWA. These methods suffers from their poor sensitivity to low-amplitude TWA. Monasterio et al. [136] reported a multilead analysis scheme to improve the detection and estimation of TWA using PCA. It applies PCA with a single-lead method based on the generalized likelihood ratio test. The method is evaluated to a single-lead scheme in which different types of simulated and physiological noise are considered under realistic conditions. It can detect TWA with an SNR 30 dB lower than the single-lead scheme. The multilead scheme claims a higher detection capability of TWA.

2.5 ECG Signal Distortion Measure

Performances of a signal processing system is assessed by evaluating quality of processed signal. There are mainly subjective and objective quality measures. The Mean Opinion Score (MOS) is the most widely accepted subjective measure. The signal quality is evaluated by visual inspection of diagnostic features such as amplitudes, durations and shapes of the ECG waves by cardiologists. The other class is objective quality measure which is further categorized by non-diagnostic distortion measure(e.g. MSE, RMSE, PRD, SNR, StdErr, Maximum Error (MaxErr), etc.) and diagnostic distortion measures (e.g. WDD [137], WPRD, WWPRD, WEDD, etc.).

Non-diagnostic Distortion Measure

The Mean Square Error (MSE) between the original and the processed ECG signals is used as a quality measure. If original signal sequence is $x(n) = \{x(1), x(2), x(3), ..., x(N)\}$, and processed signal sequence is $\widetilde{x}(n) = \{\widetilde{x}(1), \widetilde{x}(2), \widetilde{x}(3), ..., \widetilde{x}(N)\}$, the mean square error (MSE) is given as

$$\text{MSE} = \frac{1}{N}\sum_{n=1}^{N}[x(n) - \widetilde{x}(n)]^2 \tag{2.12}$$

where, N is the number of the samples. It is the mean of the square of Euclidean distance between the input and the output and distributes the error equally over all portions of the ECG signal. But each portion of the ECG cycle has a different diagnostic meaning. So, it is not acceptable in clinically.

Normalized Mean Square Error (NMSE) between the original and the processed ECG signals is defined as

$$\text{NMSE} = \frac{\sum_{n=1}^{N}[x(n) - \tilde{x}(n)]^2}{\sum_{n=1}^{N}[x(n)]^2} \tag{2.13}$$

The normalization is required to make the error measure independent of the amplitude scale of the original signals.

Root Mean Square Error (RMSE) is another measure employed to evaluate the distortion and is defined as

$$\text{RMSE} = \sqrt{\frac{1}{N}\sum_{n=1}^{N}[x(n) - \tilde{x}(n)]^2} \tag{2.14}$$

But root mean square distortion is not always considered as a good representation of ECG signal quality. To overcome this limitation a normalized version of RMSE is defined. The Normalized Root Mean Square Error (NRMSE), is defined as

$$\text{NRMSE} = \sqrt{\frac{\sum_{n=1}^{N}[x(n) - \tilde{x}(n)]^2}{\sum_{n=1}^{N}[x(n)]^2}} \tag{2.15}$$

Percentage Root Mean Square Difference (PRD) is widely used because of its simplicity [93, 138] and it is defined as

$$PRD = \sqrt{\frac{\sum_{n=1}^{N}(x(n) - \tilde{x}(n))^2}{\sum_{n=1}^{N} x(n)^2}} \times 100 \tag{2.16}$$

where, N is the number of the samples.

TH-1102_06610204

In addition to these some other measures are Signal-to-Noise Ratio (SNR), The Normalized Cross-Correlation (NCC), Maximum Amplitude Error (MAX) or Peak Error (PE), normalized maximum amplitude error (NMAX), Standard Error (StdErr) etc.

Diagnostic Distortion Measure

The error measures which consider the diagnostic features of ECG signal fall under this category. This class includes Weighted PRD (WPRD), Weighted Diagnostic Distortion (WDD), Wavelet based Weighted PRD (WWPRD) and WEDD.

In Wavelet based approach, Wavelet Weighted PRD (WWPRD) is introduced in [109] as

$$WWPRD = \sum_{j=0}^{M} w_j WPRD_j \tag{2.17}$$

where w_j is the weight for the subband j, M is the number of subbands or levels and $WPRD_j$ is the PRD of subband, j, and it is defined as

$$WPRD_j = \sqrt{\frac{\sum_{k=1}^{N_j}(w_{j,k} - \tilde{w}_{j,k})^2}{\sum_{k=1}^{N_j} w_{(j,k)}^2}} \tag{2.18}$$

where $w_{j,k}$ is an original coefficient, $\tilde{w}_{j,k}$ is a filtered coefficient and N_j is the number of coefficients within subband, j. The weight, (w_j), based on normalized area is estimated as [109]

$$w_j = \frac{\sum_{k=1}^{N_j} |w_{(j,k)}|}{\sum_{j=1}^{M+1}\sum_{k=1}^{N_j} |w_{(j,k)}|} \tag{2.19}$$

A wavelet energy-based approach is adopted in [71]. There, the Wavelet Energy-based Diagnostic Distortion (WEDD) measure is defined as

$$WEDD = \sum_{j=1}^{M+1} w_j' WPRD_j \tag{2.20}$$

where w_j' is the weight calculated based on energy as

$$w_j' = \frac{\sum_{k=1}^{N_j} w_{(j,k)}^2}{\sum_{j=1}^{M+1}\sum_{k=1}^{N_j} w_{(j,k)}^2} \tag{2.21}$$

2.6 Motivation for This Work

The cardiac potentials at multiple leads represent the same cardiac event at different spatial angles. The same electrical pulse originating from sinus node creates 'PQRST' morphologies and appears in different ECG channels. Thus, the signals at different leads are highly correlated. The individual components, P-wave, QRS-complex and T-wave, of an ECG have different frequency contents with different energy levels. Multiresolution decomposition of an ECG signal segments these components/information in different frequency bands [102]. The wavelet subbands contain different subband energies. When all the channels of a standard 12-lead ECG are subjected to wavelet transform with the same decomposition level and mother wavelet, it is expected that, at a wavelet scale, inter-lead correlation may be much higher.

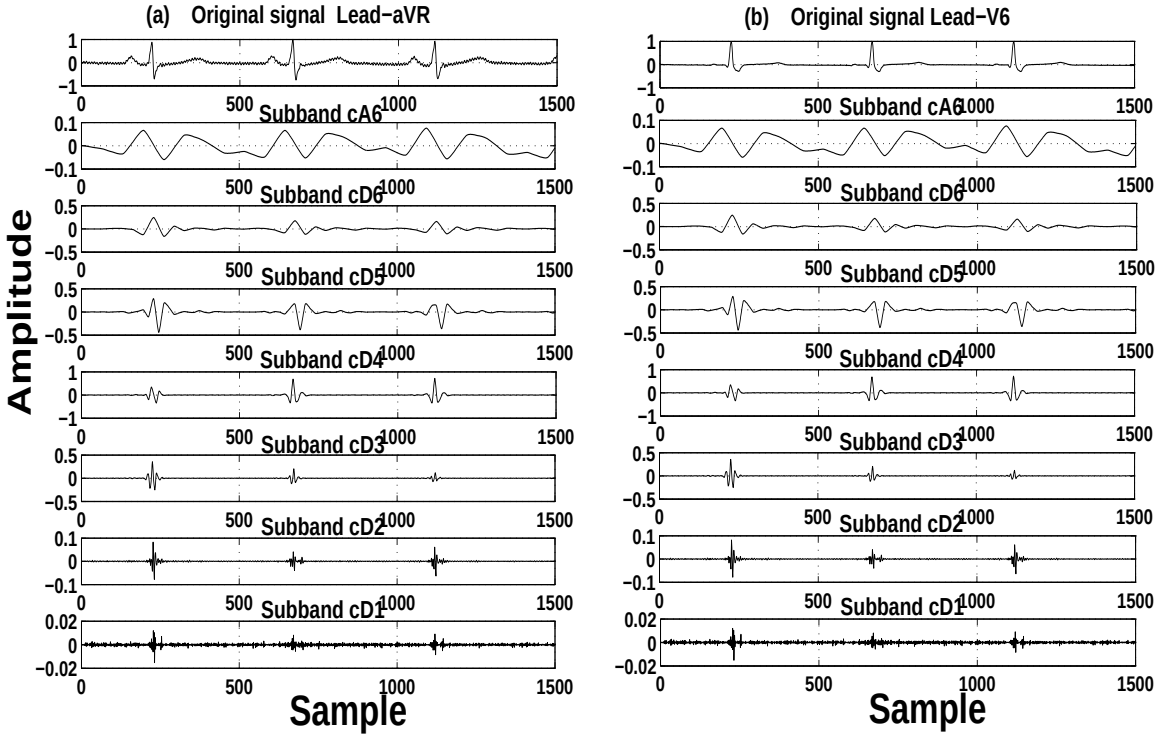

Figure 2.3: Original time domain Lead-aVR and V6 signals and their reconstructed subbands signals due to six level wavelet decomposition. In panels, (a) Original Lead-aVR signal with reconstructed subband signals and (b) Original Lead-V6 signal with reconstructed subband signals. Data base used is from CSE multilead measurement library, Data set: MO1-041

In Figure 2.3, wavelet subband signals with original signals are shown for Lead-aVR and Lead-V6.

TH-1102_06610204

It is observed that cA6 subband reflects the parts of low frequency components such as P-wave and T-wave in leads (Figure 2.3(a) and (b)). The cD6 and the cD5 subbands show the lower frequency component of QRS-complex with higher frequency component of T-wave. The cD4 and the cD3 subbands show the significant higher frequency component of QRS-complex. The cD2 and the cD1 subbands contain some higher frequency component of QRS-complex and noise. It is seen that in same subband levels of both the cases, there are similarities between segmented signal components. So, it is expected to get higher correlation between different channels in the same subband level.

The signals at a wavelet scale across different channels show similarity in terms of morphology, beat patterns, the frequency content and energy contribution. So, there is a scope of applying multivariate data analysis at a wavelet scale by arranging the coefficients of all the channels as multivariate data. These multivariate data are expected to show inter-channel redundancies at a wavelet scale. Also, it is expected to have similar pattern of multiscale energy for multivariate data. Based on these assumptions, dimensions can be reduced applying PCA at wavelet scales for non-significant multivariate data. Higher order wavelet scales may show higher correlations (Figure 2.3(a) and (b)), but they have vital clinical components. To avoid losing clinical details, data in three lower order scales can be considered for dimension reduction. Other data in higher scales may not be subjected to dimension reduction. This motivates to develop multiscale principal component analysis for multichannel electrocardiogram data. Multivariate analysis of multichannel ECG as multivariate data in wavelet domain may introduce distortion in signals. It is necessary to find the processing errors which may alter the clinical information. So, it may be necessary to develop distortion measure for MSPCA application.

The proposed investigations in this thesis are planned as

- To explore wavelet based preprocessing stage for multichannel ECG signals which rely on real data. Higher order statistics at different wavelet subbands is investigated for significant information of the data in time and frequency. The fourth order cumulant, **Kurtosis**, can be used as a measure of Gaussianity. Median absolute deviation (MAD), is scaled by a normalized wavelet subband Kurtosis instead of conventional statistical quantile function for Gaussian distribution. Combining these with the relative signal energy of wavelet subband, thresholds are derived for

removal of noise. The observations made in this preprocessing stage, motivates us for further analysis of multichannel signals in wavelet domain.

- To investigate multiscale principal component analysis of multichannel ECG. The multiscale properties of wavelet transform and the correlations between subband ECG data of different channels are evaluated. Also, the relative energy contribution of wavelet subbands for all multichannel ECG signals are investigated. The study of correlations and multiscale energies of subbands are exploited for efficient processing of multichannel data. The inter-lead correlations in wavelet domain may lead us to develop signal enhancement and data compression scheme.

- To compress multichannel ECG signals using multiscale PCA. In wavelet domain, if similar subbands of multichannel signals are arranged in matrix, principal components analysis (PCA) can be performed. This multiscale PCA for multiscale data helps reduce dimension and remove redundant information present in original data set. The proper selection of principal components (PC), gives fair representation of original data with reduced number of PCA coefficients. Multichannel compression is implemented using uniform quantizer and entropy coding of PCA coefficients. For data reduction application for signals like multichannel ECG, the method for selection of PC is an important step. The selected PC has to represent the clinical information while discarding non-significant PC has to remove redundant information.

- To develop a clinical entropy measure to better represent clinical information. Clinical entropy (Centropy) can be defined which is relevant to clinical information present in an ECG signal. The eigenvalues at different wavelet scales capture the energy of the signal and clinical information. Clinical entropy is investigated from the diagonal eigenvalue matrix. Centropy based PC selection may be applied in PCA and MSPCA based processing of multichannel ECG signal. Also, a signal distortion measure for multichannel ECG is investigated for MSPCA application. After reconstruction of MSPCA processed multichannel signals, Multiscale Multivariate Distortion (MMD) is evaluated for matrices at different wavelet scales. The average Multiscale Distortion (MD) is evaluated based on MMDs.

TH-1102_06610204

भारतीय प्रौद्योगिकी संस्थान गुवाहाटी
Indian Institute of Technology Guwahati

3

Preprocessing of Multichannel ECG

भारतीय प्रौद्योगिकी संस्थान गुवाहाटी • Indian Institute of Technology Guwahati •

Contents

TH-1102_06610204

The recorded ECG may contain undesired signals like high frequency slur and noises and artifacts. Preprocessing of ECG emphasizes the signal. It improves the signal quality for more accurate analysis, measurement and interpretation. The conventional bandpass filtering techniques may not be effective for ECG signal. The main challenge is to retain clinically relevant features of the P-wave, T-wave, ST-segment etc, having overlapping spectra with noise. Also, these methods require a priori knowledge of noise and signal distributions. Spectral substraction method may introduce artificial noise and disturb the original signal [23]. Due to non-stationary nature of ECG and noise signals, Wiener filter may not yield good result [24]. Adaptive filtering is one of the popular methods for ECG filtering [25, 26] due to its ability to denoise signal with overlapping spectra.

Wavelet based denoising method is simple, but to find a suitable threshold, a priori knowledge of signal and noise distributions in different subbands are required. Wavelet based denoising captures the energy of the original signal to a higher percentage by thresholding the noisy coefficients [110]. The performance of this threshold depends on an efficient estimation of noise variance. The motivation of the present work is to derive a more meaningful threshold which depends on noise variance, number of samples and higher order statistics.

In this Chapter, two denoising methods are proposed and evaluated. The first denoising method is based on evaluation of higher order statistics at different wavelet bands for an electrocardiogram (ECG) signal. Higher order statistics at different wavelet bands provides significant information about the statistical nature of the data in time and frequency. The fourth order cumulant, *Kurtosis*, and the Energy Contribution Efficiency (ECE) of signal in a wavelet subband are combined to assess the noise content in the signal. Accordingly, four denoising factors are proposed. In the second denoising method, a threshold is derived by considering energy contribution of a wavelet subband, noise variance which is based on a novel Gaussian measure, Kurtosis, and number of samples. The robust noise estimator, median absolute deviation (MAD), is scaled by a normalized wavelet subband Kurtosis instead of conventional statistical quantile function for Gaussian distribution. Signal distortion is evaluated using percentage root mean square difference (PRD), wavelet weighted percentage root mean square difference (WWPRD) and wavelet energy based diagnostic distortion (WEDD) measures. The results are compared with existing standard thresholding methods. The Section 3.1, discusses wavelet based denoising of multichannel ECG signals. In Section 3.2, two

proposed wavelet denoising methods are described. Section 3.3, and Section 3.3.3 give evaluations of proposed denoising methods and comparison of both the methods respectively.

3.1 Wavelet based Denoising of Multichannel ECG

The electrocardiogram (ECG) signal denoising in wavelet domain is based on the soft or the hard thresholding methods. Based on noise variance, the wavelet coefficients are thresholded at $t = \sigma\sqrt{2\log(N)/N}$, where t is threshold, σ is the variance of noise and N is the numbers of samples [28, 29]. It is claimed that the noise is better suppressed while the desirable features of the original signal remained unaltered. In this approach, the threshold value depends on noise variance, σ, and the length or number of samples, (N), of the data. The values of transform coefficients whose magnitudes lie below the threshold are set to zero. It is shown that the threshold is optimum if power of discarded wavelet coefficients equals the noise power [111]. Another method of noise reduction based on energy features of wavelet coefficients at conjunctive scales and their neighborhoods is proposed [112]. Wavelet based denoising method requires a priori knowledge of signal and noise distributions in different subbands are required. A nonlinear Bayesian filtering framework for single channel ECG signal denoising is demonstrated over conventional bandpass filtering, adaptive filtering and wavelet denoising [19]. In this, denoising of abnormal ECGs with cardiac arrythmia and over-filtering of signal which may result in loss of clinical and diagnostic information are not addressed. A comparison between adaptive filtering and wavelet shrinkage for denoising of nonlinear time series is carried out [30].

Higher order statistics is useful when dealing with non-Gaussian or possible nonlinear processes and many real world applications are truly non-Gaussian [139]. Higher order statistics-based methods are used by authors for evaluation of noise in the signals. Noise reduction in magnetocardiography by using the higher order statistics is reported [140]. In this paper, fourth order cumulant, is evaluated from the time domain signal for assessment of abrupt changes in the signal. Kurtosis in wavelet subband is used for spike detection in human muscle sympathetic nerve activity [141]. In this work, local Kurtosis is computed over N_k details coefficients at level j. Similarly, a mechanical fault signal denoising is proposed [142]. The denoising is based on a hybrid method where Kurtosis of the signal in wavelet domain is used. Kurtosis is used in engineering for detection of fault symptoms

TH-1102_06610204

because of its sensitivity to high amplitude events [143]. In this work, information in the form of higher order statistics at wavelet subbands are exploited to find an effective denoising method for ECG signals. Then denoising method is further investigated by estimating threshold which depends on noise variance, number of samples and higher order statistics.

3.2 Proposed Denoising Methods

In case of a five level wavelet decomposition of an ECG signal, the approximation band (cA5) contains most of the information related to P-wave and T-wave [71]. Significant information of the QRS-complex appear in the detail band, cD5, and the detail band, cD1, is dominated by the noise in an ECG signal. The noise is generally assumed as Gaussian in nature [28, 29]. The presence of ECG signal components, such as the 'PQRST' morphologies, will generate non-Gaussian coefficients at some frequency bands. On the other hand, significant presence of noise in wavelet subbands will produce Gaussian coefficients. A Gaussian measure, such as Kurtosis, can help form the perspicacity between the signal and the noise in a wavelet subband. This measure can give an idea of noise content of a signal in a subband.

3.2.1 Denoising using Higher Order Statistics in Wavelet Subbands

In this subsection, a novel denoising method based on evaluation of higher order statistics at different wavelet subbands for an electrocardiogram (ECG) signal is proposed. Higher order statistics at different wavelet subbands provides significant information about the statistical nature of the data in time and frequency. The fourth order cumulant, **Kurtosis**, and the Energy Contribution Efficiency (ECE) of signal in a wavelet subband are combined to assess the noise content in the signal. Accordingly, four denoising factors are proposed. Performance of the denoising factors are evaluated and compared with the soft thresholding method.

The k^{th} wavelet coefficient at j^{th} level, $w_{j,k}$, are estimated as inner product of signal and dilated and shifted version of wavelet which is given as, $w_{j,k} = \langle f(x), \psi_{j,k}(x) \rangle$, where $f(x)$ is the input signal and $\psi_{j,k}(x)$ is the dilated and shifted version of "mother wavelet", $\psi(x)$. The percentile energy, ε_j, of the signal at j^{th} level is

$$\varepsilon_j = \frac{E_j}{E_t} \times 100$$

where $E_j = \sum_k w_{j,k}^2$ is the energy of the signal at j^{th} level and $E_t = \sum_j E_j$ is the total energy of the signal. In case of ECG signals, the percentile energy of the signal at j^{th} level is referred as energy contribution efficiency (ECE) of j^{th} wavelet subband.

The bandwidth, ΔF_j, of j^{th} wavelet subband depends on the sampling frequency. Table-3.1 shows maximum frequency values of different subbands for three values of sampling frequency, i.e. $360Hz$, $500Hz$ and $1000Hz$. Maximum frequency of each subband depends on the decomposition levels, j, and the sampling frequency, F_s. Different physiological information of the ECG signal are present in a wavelet subband based upon their frequency content. It has been reported that the higher order subbands contain most of the diagnostically significant information of the ECG signal [71]. Figure-3.1 shows the spectra of an ECG signal (Dataset: MO1-003, Lead-aVL from CSE multilead measurement library) at different wavelet subbands. It is observed that most of the spectral energy lie in low frequency subbands whereas the noise content is significant in detail subbands such as cD1, cD2 and cD3. In order to avoid loosing clinically important components of the signal such as PQRST morphologies, coefficients in cD1, cD2 and cD3 wavelet subbands should be treated for denoising.

Table 3.1: Maximum frequency at different wavelet subbands for three sampling frequencies

$F_s = 1000$Hz	Subband	$F_s = 500$Hz	Subband	$F_s = 360$Hz	Subband
500	cD1	250	cD1	180	cD1
250	cD2	125	cD2	90	cD2
125	cD3	62.5	cD3	45	cD3
62.5	cD4	31.25	cD4	22.5	cD4
31.25	cD5	15.625	cD5	11.25	cD5
15.625	cD6	7.812	cD6	5.625	cA5
7.812	cD7	3.906	cA6	-	-
3.906	cA7	-	-	-	-

3.2.1.1 Proposed Threshold based on HOS and ECE

A Measure of deviation from Gaussianity will give an idea of noise content in a signal. Higher order statistics (HOS) can be effectively used to discriminate noise from the signal. If Gaussian noise is present in a wavelet subband, the coefficients will contain this noise. The fourth order statistics of a signal can be evaluated by estimating the Kurtosis value of the signal. Kurtosis is defined as the ratio between the fourth central moment and the square of the variance of the probability distribution [139, 144].

$$K = \frac{\kappa_4}{\kappa_2^2} = \frac{\mu^4}{\sigma^4} \tag{3.1}$$

TH-1102_06610204

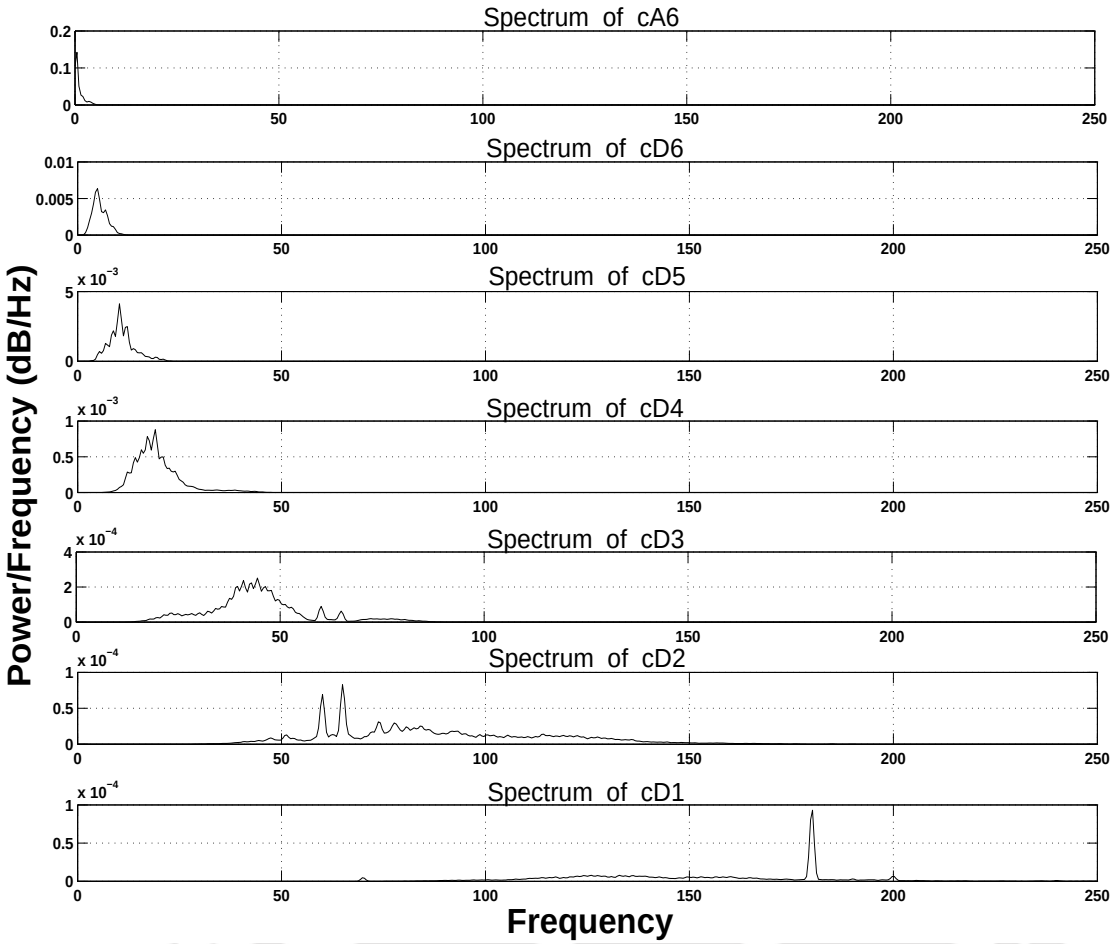

Figure 3.1: Spectrums (Weltch method) of wavelet sub-bands (Decompositions up to 6 level), CSE mutlilead measurement library database, Dataset: MO1-003, Lead-aVL

where K is the Kurtosis, μ^4 is the fourth-order central moment and σ^4 is the square of the variance. Kurtosis values higher than 3.0 indicate the presence of more extreme values than should be found in a Gaussian distribution [143]. If '3' is subtracted from above K, then it is known as excess Kurtosis. Excess Kurtosis can range from -2 to ∞. The fourth order cumulant, Kurtosis, is a measure of the peakedness of the probability distribution of a real-valued random variable. Kurtosis can be used as a measure of Gaussianity of a signal. Higher Kurtosis means more variance which is due to infrequent extreme deviations. On the basis of Kurtosis value [142], the signal can be classified as- a) sub-Gaussian ($K < 3$, i.e. the signal is not spiky), b) super-Gaussian ($K > 3$, signal become more spiky) and c) Gaussian ($K = 3$, the signal is dominated by noise). For discrete signal, the sample Kurtosis

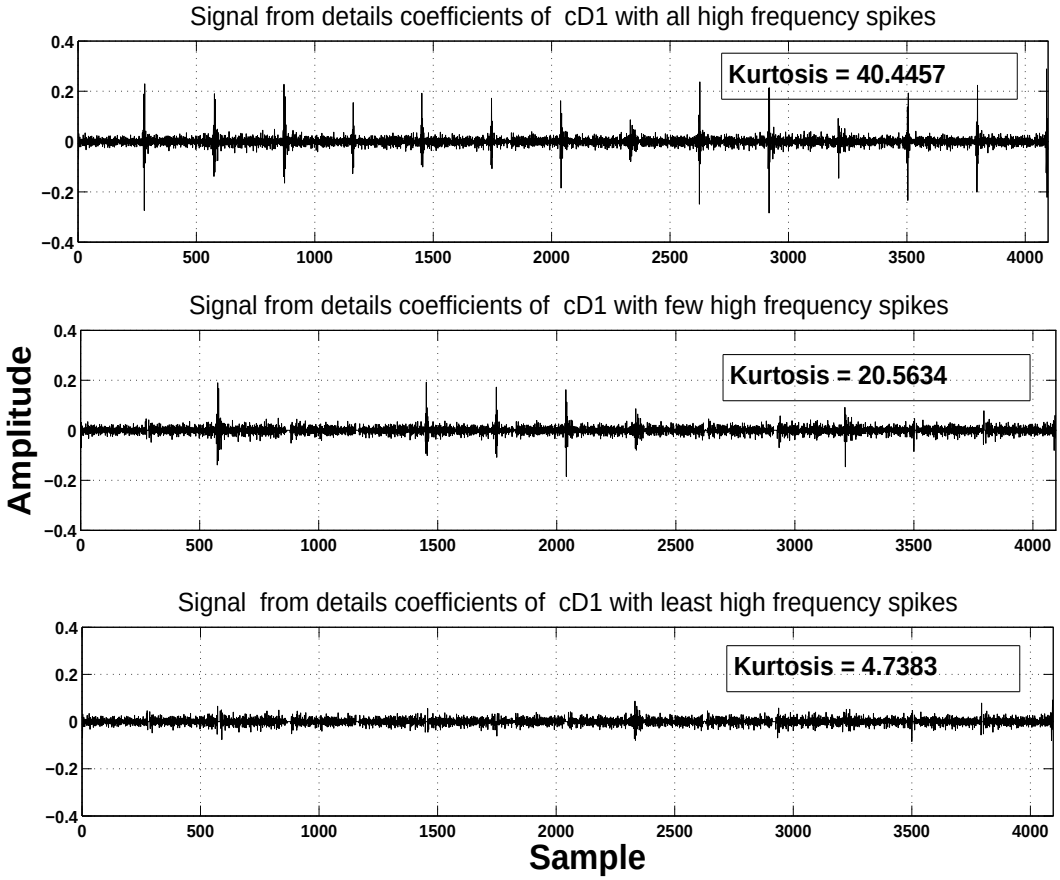

Figure 3.2: Kurtosis values of wavelet subband 'cD1' with reducing numbers of spikes (Decompositions up to 6 level), CSE mutlilead measurement library database, Dataset: MO1-003, Lead-aVL

is calculated over a sample-block (an N-point data), and it is defined as [144]

$$K' = \frac{m_4}{m_2^2} = \frac{\frac{1}{N}\sum_{i=1}^{N}(x_i - \overline{x})^4}{(\frac{1}{N}\sum_{i=1}^{N}(x_i - \overline{x})^2)^2} \tag{3.2}$$

where m_4 is the fourth sample moment about the mean, m_2 is the second sample moment about the mean (sample variance), x_i is the i^{th} sample and $\overline{x}$ is the sample mean. In case of ECG signal, the noise energy is higher compared to signal energy in higher frequency wavelet subbands. The QRS complex is one of the most important features of an ECG signal. Any information related to QRS complex is required to be preserved. Normally, QRS complex can be treated as a spike in the signal [145]. Figure-3.2 shows the Kurtosis values for three signals with different spike densities. The Kurtosis values are estimated from cD1 detail subbands of the signals. It is observed that higher

TH-1102_06610204

Kurtosis values are obtained for higher spike densities or more number of spikes in the signal. Signal with more number of spikes represent a super-Gaussian signal. A lower threshold value may be required to preserve the spikes such as QRS complexes in an ECG signal. Similarly, higher threshold value will be required to eliminate noise from the signal in a subband.

It is observed that the spectral energy is higher in a Wavelet subband where clinically significant information of ECG signal is present. The relative energy of a subband is measured as energy contribution efficiency (ECE) or percentile energy [83]. Any threshold for noise elimination should take into account both the Kurtosis and the ECE value of the subband. Accordingly, the denoising factor, (DF_{jM1}), for subband or level, j, is proposed as

$$DF_{jM1} = \frac{1}{\epsilon_j} \times \frac{max(w_{j,k})}{F_{jSN}} \tag{3.3}$$

where ϵ_j is the ECE value of the j^{th} subband, $max(w_{j,k})$ is the maximum value of wavelet coefficient, F_{jSN} is the ratio between the Kurtosis value of signal at j^{th} subband to Kurtosis value of Gaussian noise. The proposed denoising factor in equation (3.3) shows that it is inversely proportional to the ECE value. Higher the value of ECE as in lower frequency (higher order) subbands, lower is the threshold or denoising factor. Similarly, lower the ECE value in higher frequency (lower order) subbands, higher is the denoising factor.

The factor $\frac{max(w_{(j,k)})}{F_{jSN}}$, is the peak Signal-to-Kurtosis Ratio (SKR) [142]. In an ECG signal, QRS complex can be considered as an impulse-like component which has sharp rise and falling edges. The denoising factor (DF_{jM1}) is expected to be higher where SKR value is higher. A higher value of Kurtosis will be obtained in a subband which contains significant information of QRS complexes. The DF_{jM1} factor or the threshold value will be lower in this subband. This will help preserve the information related to QRS complexes.

It is seen that the noise is dominant in details wavelet subbands. In general, thresholding is performed in details subbands [146, 147]. So, a modified denoising factor $\widehat{DF}_{jM1}$ considering only details wavelet subbands is defined as

$$\widehat{DF}_{jM1} = \frac{1}{\widehat{\epsilon_j}} \times \frac{max(w_{j,k})}{F_{jSN}} \tag{3.4}$$

where $\widehat{\epsilon_j}$ is details energy contribution efficiency (DECE) of j^{th} detail subband. It is defined as

$$\widehat{\epsilon_j} = \frac{E_j}{\widehat{E_t}} \times 100 \tag{3.5}$$

where $\widehat{E_t}$ is the sum of energies in detail subbands. Instead of using signal-to-Kurtosis value, the denoising factor can be defined based on the ECE value and the Kurtosis. Alternatively, two denoising factors for j^{th} subband are defined as

$$\overline{DF}_{j1M1} = \frac{\widehat{\epsilon_j}}{K_j^{'}} \tag{3.6}$$

$$\overline{DF}_{j2M1} = \frac{\epsilon_j}{K_j^{'}} \tag{3.7}$$

where $K_j^{'}$ is the estimated Kurtosis value for the j^{th} subband.

3.2.2 Denoising based on Kurtosis, Variance and Energy

The motivation of this method is to derive a more meaningful threshold which depends on noise variance, number of samples and higher order statistics. Thus, a threshold is proposed based on noise variance which is computed using Kurtosis, relative energy of wavelet subbands and number of samples.

The previous method investigates the problem of ECG signal denoising using higher order statistics. The threshold is estimated based on ECE and peak signal-to-Kurtosis ratio. Accordingly, four thresholds were proposed. This gives the significance of higher order statistics for noise elimination. It has been established (by D. L. Donoho [28, 29]) that wavelet threshold depends on the noise variance and number of samples. A threshold which depends on noise variance, number of samples and higher order statistics would be more meaningful. In the following Section 3.2.2.1, a threshold is derived by considering energy contribution of a wavelet subband, noise variance which is based on a novel Gaussian measure, Kurtosis, and number of samples.

3.2.2.1 Proposed Thresholding Scheme

It is expected to achieve better denoising of signal by thresholding wavelet coefficients at different subbands. The proposed wavelet based ECG denoising is based on three factors. They are relative energy contribution efficiency (ECE) of all wavelet subbands to the details energy contribution effi-

TH-1102_06610204

ciency (DECE) of details subbands, the estimated noise variance of wavelet subbands and a factor based on number of samples, $\sqrt{2 \cdot \log(N_j)/N_j}$, similar to universal threshold [28]. The proposed threshold or denoising factor, DF_j, for each wavelet subband is defined as

$$\begin{aligned} DF_{jM2} &= \frac{1}{3} \cdot \left[\frac{\epsilon_j}{\widehat{\epsilon_j}} + \widehat{\sigma_{n_j}} + \sqrt{2 \cdot \log(N_j)/N_j} \right] \\ &= \frac{1}{3} \cdot \left[\alpha_j + \beta_j + \gamma_j \right] \end{aligned} \tag{3.8}$$

where ϵ_j is the energy contribution efficiency (ECE) of j^{th} wavelet subband considering all subbands or levels, $\widehat{\epsilon_j}$ is the details energy contribution efficiency (DECE) of j^{th} wavelet subband when only details subbands are considered. $\widehat{\sigma_{n_j}}$ is the estimated noise variance based on Kurtosis and N_j is the number of wavelet coefficients at j^{th} level. This threshold for j^{th} level is the average of α_j, β_j and γ_j. The wavelet coefficients below the threshold value are discarded. Wavelet decomposition using Daubechies 9/7 biorthogonal wavelet filters up to six levels are used [83].

The threshold factor, α_j, depends on the relative energy, ECE and DECE of the subband. The ECE, ϵ_j, of the signal at j^{th} level is $\epsilon_j = \frac{E_j}{E_t} \times 100$ where $E_j = \sum_k w_{j,k}^2$ is the energy of the signal at j^{th} level and $E_t = \sum_j E_j$ is the total energy of the signal, $j = 1, 2, \cdots, L+1$. Approximation subband is represented by $(L+1)^{th}$ subband. Similarly DECE, $\widehat{\epsilon_j}$, of j^{th} details subband is given as $\widehat{\epsilon_j} = \frac{E_j}{\widehat{E_t}} \times 100$, where $\widehat{E_t}$ is the sum of energies in detail subbands where $j = 1, 2, \cdots, L$.

In Figure 3.3, ECE and DECE values are shown for five level decomposition of an ECG signal. It is observed that the most of the signal energy remain in cA5, cD5 and cD4 subbands [102]. In other lower order subbands like cD1, cD2 and cD3 noise components become dominant and there may exist ECG components due to some pathological conditions. Details subbands show very less energy content. Relative energy of details subbands in terms of DECE will give an idea of noise content in the signal.

Table 3.2 shows ECE and DECE values for all 12 leads of a standard ECG database, dataset-M01-003 from CSE multilead measurement library. It is noticed that the higher order wavelet subbands have relatively more signal energies. ECE and DECE are observed to have higher values in cD5 subband compared to cD6 subband except for lead-II, aVR and aVL ECG signals. Similarly, ECE and DECE values in cD4 subband are higher compared to their values in cD6 subband in all chest lead except lead-V1 signal. cD1, cD2 and cD3 subbands have less than 10% of total ECE

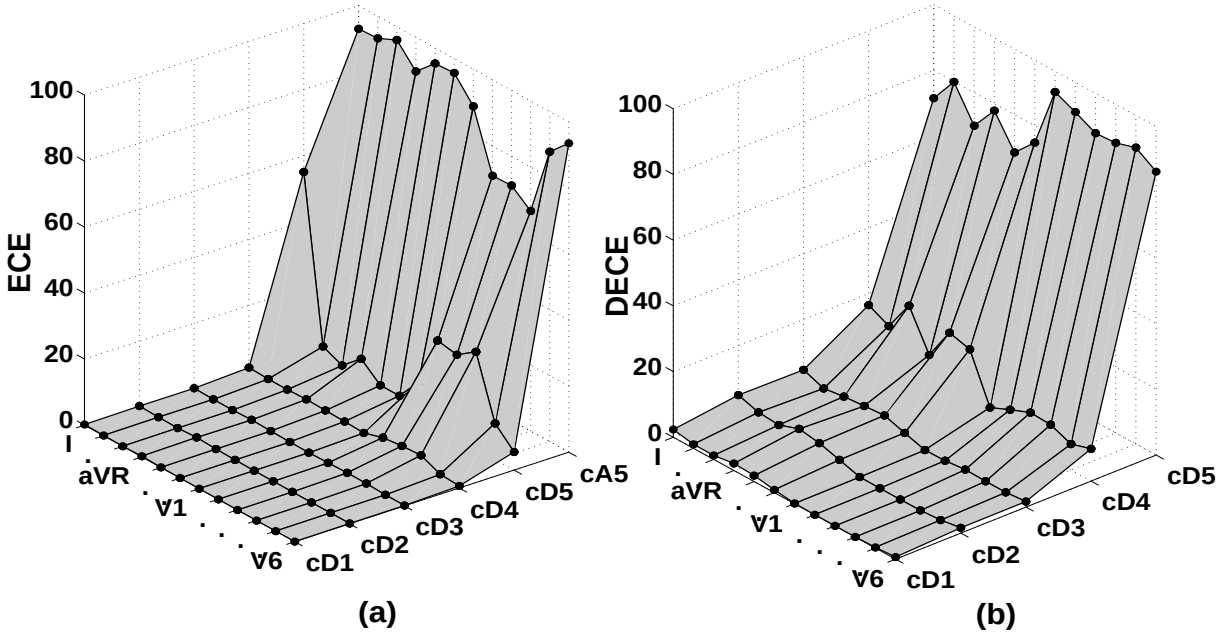

Figure 3.3: Relative energy distribution (a) when all the wavelet subbands are considered and expressed in terms of ECE, (b) when only details wavelet subbands are considered and expressed in terms of DECE. The ECE and DECE are based on 5-level wavelet decomposition of data set-patient001/(s0010re) from PTB diagnostic ECG database (PTBDB).

values. These results suggest that majority of the energies remain in cA6, cD6, cD5 and cD4 subbands. These subbands contain most of the clinical features of ECG signals [83]. To avoid the loss of diagnostic information, coefficients of lower order wavelet subbands are considered for denoising. In this work, coefficients of cD1, cD2 and cD3 subbands are considered for thresholding.

In Figure 3.4, the percentage relative energy distributions in wavelet subbands for real ECG signal and noise are shown. In case of noise, lower order subbands show higher ECE values compared to higher order subbands. In case of ECG signal, ECE values are higher for lower order subbands. This is because most of the signal energies of ECG remain in lower frequency region. The ECE values of noise are higher compared to those of ECG at cD1, cD2, cD3 and cD4 subbands. A threshold based on these relative signal energies is expected to be effective in filtering out the noise from the ECG signal which is the motivation for the factor, α_j, in equation 3.8.

TH-1102_06610204

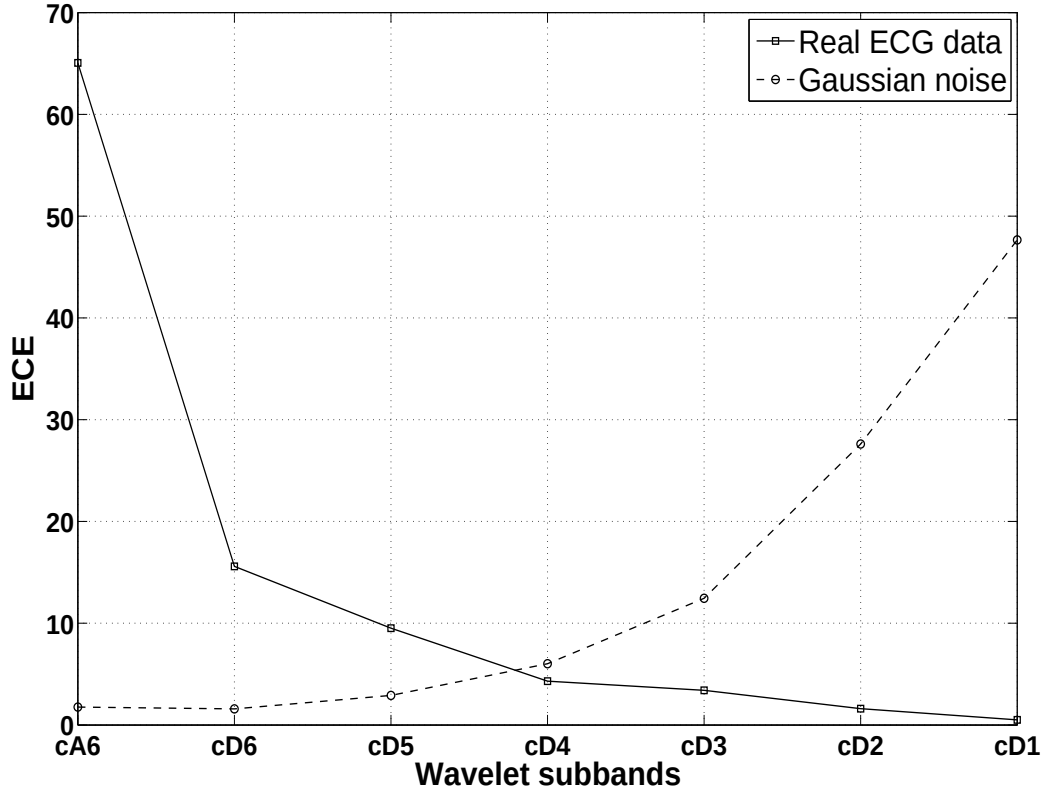

Figure 3.4: Distributions of ECE in wavelet subbands for real ECG signal (data set-MO1-003 from CSE multi-lead measurement library) and Gaussian noise. Wavelet decomposition up to 6-level is used.

The second factor, β_j, in the proposed threshold is based on an estimate of noise variance. The estimated noise variance, $\widehat{\sigma_{n_j}}$, in wavelet subband is estimated from median absolute deviation (MAD) as $\widehat{\sigma_{n_j}} = C.MAD_j$ where 'C' is a constant scale factor which depends on distribution of noise. For normally distributed data 'C=1.4826' is the 75^{th} percentile of the normal distribution with variance, $\sigma = 1$. The estimated noise variance can be written as [148]

$$\widehat{\sigma_{n_j}} = \frac{MAD_j}{0.6745} \tag{3.9}$$

where the constant term '0.6745' (i.e. $1/C$) does not include the real data. Also, when the signal contains stochastic components the MAD estimator tends to overestimate the true value of noise variance [149]. In this method, an estimator including real wavelet subband data is used. It is expected that the wavelet subband Kurtosis can give a better scale factor ($1/C$) on noise estimation.

Table 3.2: ECE and DECE values of data set-M01-003 from CSE multilead measurement library

(a) ECE							
Leads	cA6	cD6	cD5	cD4	cD3	cD2	cD1
I	47.55	14.35	21.47	9.57	5.10	1.32	0.65
II	65.06	15.58	9.51	4.31	3.41	1.61	0.51
III	32.46	11.88	28.80	18.45	6.05	1.37	0.96
aVR	60.22	13.68	9.53	10.61	3.33	1.86	0.77
aVL	58.69	15.51	14.660	5.05	4.16	1.43	0.50
aVF	44.90	14.47	21.04	13.59	3.97	1.75	0.28
V1	72.57	9.71	11.13	5.72	0.47	0.32	0.06
V2	29.94	11.73	30.41	22.84	4.58	0.37	0.10
V3	25.27	12.93	29.32	24.98	6.62	0.77	0.08
V4	24.43	13.06	28.89	25.35	7.11	1.06	0.07
V5	26.52	12.10	29.34	24.34	6.61	0.99	0.07
V6	22.83	12.40	30.08	27.47	6.18	0.88	0.13
(b) DECE							
I	-	27.40	40.90	18.20	9.70	2.50	1.20
II	-	44.60	27.20	12.30	9.80	4.60	1.50
III	-	17.60	42.70	27.30	9.00	2.00	1.40
aVR	-	34.40	24.00	26.70	8.40	4.70	1.90
aVL	-	37.60	35.50	12.20	10.10	3.50	1.20
aVF	-	26.30	38.20	24.70	7.20	3.20	0.50
V1	-	35.40	40.60	20.90	1.70	1.20	0.20
V2	-	16.70	43.40	32.60	6.50	0.50	0.10
V3	-	17.30	39.20	33.40	8.90	1.00	0.10
V4	-	17.30	38.20	33.60	9.40	1.40	0.10
V5	-	16.50	39.90	33.10	9.00	1.40	0.10
V6	-	16.10	39.00	35.60	8.00	1.10	0.20

ECE and Kurtosis values at different wavelet subbands for Laplace and Normal noise distributions are shown in Figure 3.5. Noise with unity variance and zero mean is wavelet decomposed which disseminates its content in different subbands. It is observed that ECE values (Figure 3.5.(b) and Figure 3.5. (e)) are similar for both the noise distributions. Same observations are also found for Kurtosis in Figure 3.5. (c) and Figure 3.5. (f). Experiments with other types of noise distribution show similar ECE and Kurtosis characteristics. On contrary, ECE values of ECG signal in wavelet subbands show reverse trend (Figure 3.4). For practical use, estimated noise variance in a wavelet subband is proposed as

$$\widehat{\sigma_{n_j}} = \frac{MAD_j}{\frac{K_N}{K_j}} \tag{3.10}$$

where K_N is the Kurtosis of a normal distribution and K_j is the Kurtosis of the j^{th} wavelet subband. For discrete signal, the sample Kurtosis is calculated over a sample-block (an N-point data), and it is defined as $K^{'} = m_4/m_2^2 = \frac{1}{N}\sum_{i=1}^{N}(x_i - \overline{x})^4/(\frac{1}{N}\sum_{i=1}^{N}(x_i - \overline{x})^2)^2$, where m_4 is the fourth sample moment about the mean, m_2 is the second sample moment about the mean (sample variance), x_i is the i^{th} sample and $\overline{x}$ is the sample mean [144, 150]. In wavelet domain, the x_i values are the wavelet

TH-1102_06610204

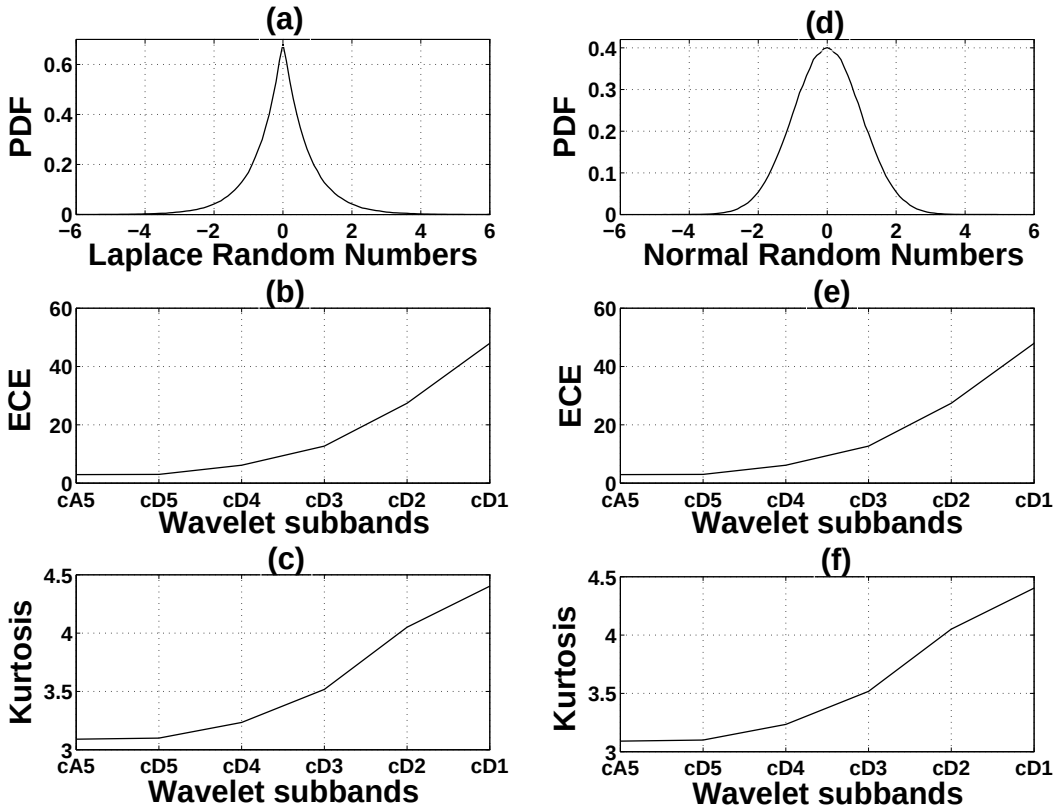

Figure 3.5: Probability density function (PDF), wavelet subband ECE and Kurtosis for Laplace and Gaussian noise with zero mean and unity variance, (a) PDF of Laplace noise, (b) ECE of different subbands for Laplace noise, (c) Kurtosis of different subbands for Gaussian noise, (d) PDF of Gaussian noise, (e) ECE of different subbands for Gaussian noise, (f) Kurtosis of different subbands for Gaussian noise (Wavelet Decompositions up to 5 levels)

coefficients in the subband.

In Figure 3.6, estimated noise variance based on Kurtosis measure (equation 3.10) and conventional MAD based (equation 3.9) estimators are plotted. Both the characteristics show a decreasing trend. This will result in a higher threshold value due to the variance term (second factor in equation 3.8) for lower order subbands. A higher value of threshold in lower order wavelet subbands is justified as the noise energy is higher in these subbands compared to those in higher order subbands. The proposed noise estimator shows higher values for lower order wavelet subbands. Approximation subband will have a lower noise variance due to lower value of Kurtosis for proposed method compared to the conventional method. This will help set a higher value of threshold for lower order subbands compared to conventional method. In approximation band it will result in a lower threshold. The third

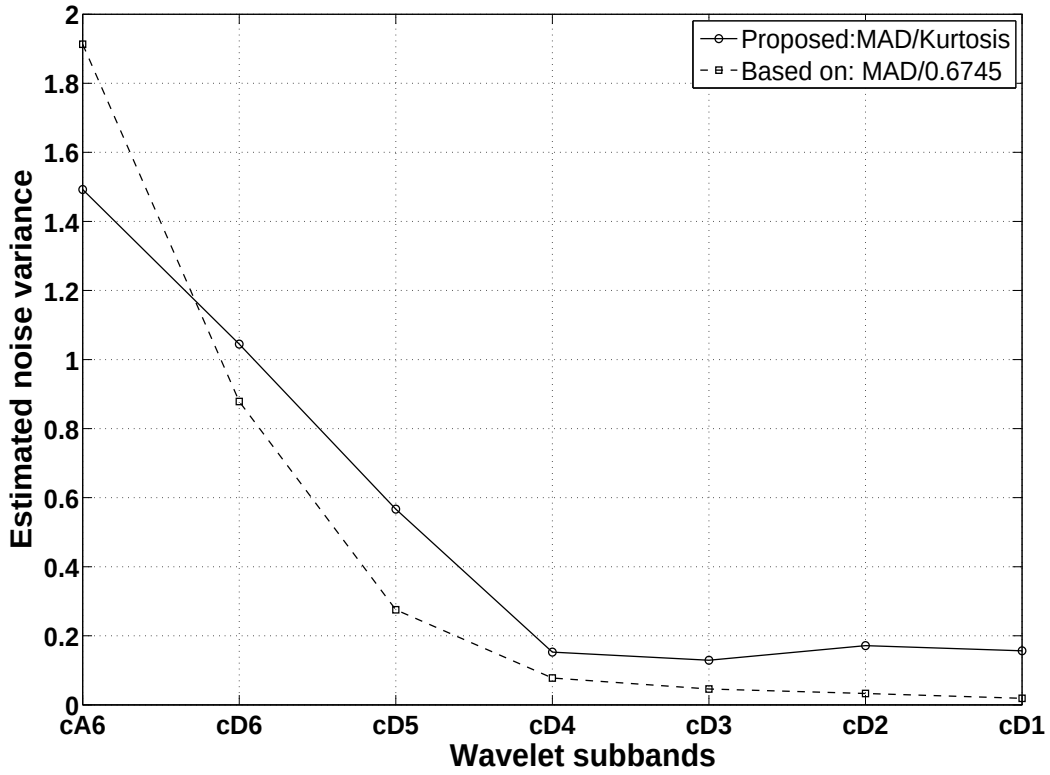

Figure 3.6: Proposed Kurtosis based estimated noise variance and existing MAD based estimator (Wavelet Decompositions up to 6 levels), CSE multilead measurement library, data set-(MO1-003)

factor, $\sqrt{2 \cdot \log(N_j)/N_j}$, is based on the length of the data and it is effectively used for filtering of the noise [28].

The proposed denoising threshold, DF_{jM2}, varies directly with estimated noise variance and percentile energy contribution efficiency of the subband. The first term (α_j), which is the ratio between ECE and DECE, is a constant term (invariant across the subbands), because it is equivalent to the ratio between sum of the energies at detail subbands and the total energy of the signal. A modified threshold, $\widehat{DF_{jM2}}$ for details j^{th} subband can be defined as

$$\begin{aligned} \widehat{DF_{jM2}} &= \frac{1}{3} \cdot \left[\frac{1}{\widehat{\epsilon_j}} + \widehat{\sigma_{n_j}} + \sqrt{2 \cdot \log(N_j)/N_j} \right] \\ &= \frac{1}{3} \cdot \left[\widehat{\alpha_j} + \beta_j + \gamma_j \right] \end{aligned} \tag{3.11}$$

As coefficients of details subbands, cD1, cD2 and cD3, are considered for thresholding, $\widehat{DF_{jM2}}$,

TH-1102_06610204

is defined only for details subbands. In the modified threshold, $\widehat{DF_{jM2}}$, the first term is the reciprocal of DECE. This term depends on the subband energy and thus yields a factor which varies across the subbands. It is observed that (Figure 3.4) lower order subbands have relatively higher noise energy compared to the signal energy. If noise energy is higher in a subband, it is expected to have a higher threshold value. Similarly, a lower threshold value is justified if signal energy is higher in a subband.

Table 3.3: Proposed denoising factors for three wavelet subbands using data set-M01-003 from CSE multilead measurement library, with six wavelet decomposition levels

Subbands	Lead-I		Lead-II		Lead-III		aVR		aVL		aVF	
	DF_{jM2}	$\widehat{DF_{jM2}}$	DF_{jM2}	$\widehat{DF_{jM2}}$	DF_{jM2}	$\widehat{DF_{jM2}}$	DF_{jM2}	$\widehat{DF_{jM2}}$	DF_{jM2}	$\widehat{DF_{jM2}}$	DF_{jM2}	$\widehat{DF_{jM2}}$
cD1	0.625	0.911	0.535	0.871	0.723	0.745	0.502	0.619	0.588	0.994	0.652	2.090
cD2	0.939	0.812	0.559	0.427	0.991	0.808	0.564	0.381	0.670	0.547	0.744	1.026
cD3	1.106	0.684	0.530	0.283	1.122	0.558	0.642	0.364	0.746	0.432	0.804	0.392

Both the thresholds (DF_{jM2} and $\widehat{DF_{jM2}}$) are based on energy contribution of wavelet subband, noise variance and number of samples. In Table 3.3, proposed denoising factors, DF_{jM2} and $\widehat{DF_{jM2}}$, for three subbands cD1, cD2 and cD3 are shown. It is observed that the values of denoising factor DF_{jM2} are maximum for cD3 subband for all signals except lead-II signal. In case of $\widehat{DF_{jM2}}$, maximum threshold values are found for cD1 subband and the threshold values are least in cD3 subband. Lower order subbands are expected to have relatively higher noise energy compared to the signal energy. Thus, it is expected that the threshold value should be higher for lower order subbands. The threshold factor, $\widehat{DF_{jM2}}$, follows the expected trend of maximum value for cD1 subband. In subsequent sections, results with $\widehat{DF_{jM2}}$ are shown.

3.3 Evaluation of Proposed Denoising Methods

It is important to measure any distortion of clinical or diagnostic information during the processing of ECG signal. Different error measures, which are commonly used, are applied for evaluation of quality of filtered ECG signal. Percentage root mean square difference (PRD) is widely used because of its simplicity [93, 138]. In wavelet based approach, Wavelet Weighted PRD (WWPRD) is introduced in [109]. A wavelet energy-based approach is adopted in [71] as Wavelet Energy-based Diagnostic Distortion (WEDD) measure

3.3.1 Results for Denoising using Higher Order Statistics

Noisy multichannel ECG (MECG) signals from 12 leads (Bipolar: Lead-I, II, III; Augmented Lead: aVR, aVL, aVF and Chest Lead: V1, V2, V3, V4, V5, V6) of standard ECG database, CSE mutlilead measurement library, dataset-M01-003, are subjected to amplitude normalization and mean removal. From each channel data, 4096 samples are chosen as a block. Data are arranged in a matrix form. Each column corresponds to one channel. This has resulted in a 4096×12 matrix. Wavelet decomposition using Daubechies 9/7 biorthogonal wavelet filters up to six levels are used for each column data and same has been applied for reconstruction filters also. The wavelet decomposition resulted in seven subband matrices. Each column in a subband matrix corresponds to subband of one channel.

After L level multi-resolution decomposition (MRD), wavelet coefficients, $w_{j,k}$, are found in '$L+1$' subbands. At each wavelet scale the number of wavelet coefficients are the same for all n number of ECG channels. So, this gives '$L+1$' subband matrices in wavelet domain. For multichannel representation, the approximation coefficients are denoted as $w^i_{L,k}$, where i is channel number ($i = 1, 2, ..., n$), L is the decomposition level or subband number and k is the numbers of coefficients at L^{th} scale. Similarly, the details coefficients are $w^i_{j,k}$. Therefore multiscale ECG wavelet subband matrix for approximations subband is given as

$$\mathbf{A_L} = \begin{bmatrix} w^1_{L,k} & . & . & w^n_{L,k} \\ . & . & . & . \\ . & . & . & . \\ w^1_{L,k} & . & . & w^n_{L,k} \end{bmatrix} \tag{3.12}$$

where number of columns is the number of ECG channels and number of rows is the number of coefficients in the subband. Similarly, wavelet subband matrices for details coefficients is given as

$$\mathbf{D_j} = \begin{bmatrix} w^1_{j,k} & . & . & w^n_{j,k} \\ . & . & . & . \\ . & . & . & . \\ w^1_{j,k} & . & . & w^n_{j,k} \end{bmatrix} \tag{3.13}$$

where $w^i_{j,k}$ is the k^{th} coefficient at j^{th} decomposition level of i^{th} channel. The wavelet subband

TH-1102_06610204

matrices A_L, D_j are used to determine signal statistics of channel in that subband. The ECE and the Kurtosis values are evaluated for all the subbands. The results are shown in Table-3.4 where columns show ECE and Kurtosis values for various leads with corresponding wavelet subbands.

Table 3.4: ECE and Kurtosis: Dataset-M01-003, CSE mutlilead measurement library

ECE and Kurtosis: Dataset-M01-003, CSE mutlilead measurement library												
Parameters	Lead-I	Lead-II	Lead-III	aVR	aVL	aVF	V1	V2	V3	V4	V5	V6
ECE - cA6	85.5819	88.1159	76.9139	76.2487	88.3448	88.2638	72.2600	69.1069	57.9469	50.6873	43.4555	47.0165
ECE - cD6	3.9472	5.3017	4.0635	8.1715	4.3790	3.0839	9.8209	5.1735	7.2787	8.5258	9.3184	8.5169
ECE - cD5	5.9002	3.2343	9.8464	5.6905	4.1338	4.4824	11.2605	13.4124	16.5031	18.8551	22.5831	20.6571
ECE - cD4	2.6283	1.4652	6.3067	6.3304	1.4239	2.8934	5.7896	10.0748	14.0572	16.5481	18.7293	18.8616
ECE - cD3	1.4016	1.1625	2.0693	1.9884	1.1736	0.8451	0.4774	2.0203	3.7288	4.6415	5.0887	4.2475
ECE - cD2	0.3630	0.5473	0.4690	1.1087	0.4027	0.3724	0.3275	0.1670	0.4381	0.6934	0.7671	0.6090
ECE - cD1	0.1778	0.1731	0.3313	0.4617	0.1422	0.0590	0.0641	0.0453	0.0473	0.0489	0.0579	0.0914
Kurt - cA6	2.9484	3.5464	2.6122	3.5827	3.2570	1.9344	3.4417	2.3932	4.0361	4.2925	2.9945	3.1688
Kurt - cD6	5.8796	5.2920	4.1624	3.9019	6.0562	3.0949	3.5615	4.3704	4.1881	4.1302	3.6340	3.9170
Kurt - cD5	10.2085	9.1479	9.6693	7.8912	10.8789	8.6683	9.1736	10.1024	10.1671	9.9963	9.7431	9.9810
Kurt - cD4	14.5639	8.7211	14.2460	12.5095	15.8173	13.7886	14.4952	15.4466	15.5672	15.4995	15.2510	15.1300
Kurt - cD3	16.6279	12.4473	14.9224	15.0107	14.4396	17.3184	16.0226	20.9392	24.1719	25.0462	24.0611	22.9798
Kurt - cD2	26.1219	23.1908	23.0539	18.3664	24.1067	25.9381	35.8326	59.0699	125.57	118.27	115.00	107.30
Kurt - cD1	6.4433	36.6372	2.1017	16.9055	22.7812	14.0943	37.4905	35.6119	65.46	95.97	49.5168	13.57

Note: **Kurt**: Kurtosis.

The energy contribution of cA6 subband is the highest whereas cD1 subband contributes the least. The difference in ECE values show the relative energy distribution of the subbands. The observed relative energy distributions are similar as mentioned in [83]. Kurtosis value for cD2 subband is found to be the highest (26.1219) and it is least (2.9484) for cA6 subband in case of Lead-I signal. This indicates that the cA6 subband signal has a distribution with lighter tails and it is relatively flatter. The Kurtosis value in cD2 subband exhibits some extreme deviation with Gaussian noise. Distribution with positive Kurtosis value has heavier tails and a higher peak than the normal. Other Leads show similar behavior. The positive Kurtosis values for cD3 and cD1 subbands across all the channels may contain Gaussian noise as well as higher peaks. For cD4, cD5 and cD6 subbands, the higher positive Kurtosis values are due to the presence of PQRST morphologies.

3.3.1.1 Evaluation of Proposed Denoising Factors

Four denoising factors (DF_{jM1}, $\widehat{DF}_{jM1}$, $\overline{DF}_{j1M1}$, $\overline{DF}_{j2M1}$) and soft threshold (ST) [28] are estimated for three subbands (cD1, cD2, cD3) using their ECE and Kurtosis values. These three subbands are normally thresholded for denoising applications [71].

Table-3.5 shows the results. The DF_{jM1} values for cD1, cD2 and cD3 subbands are dependent

Table 3.5: DF_{jM1}, $\widehat{DF_{jM1}}$, $\overline{DF}_{j2}$, $\overline{DF}_{j1}$ and ST: Dataset-M01-003, CSE mutlilead measurement library

Values of DF, $\widehat{DF}$, $\overline{DF}_{j2}$, $\overline{DF}_{j1}$ and ST: Dataset-M01-003, CSE mutlilead measurement library												
Parameters	Lead-I	Lead-II	Lead-III	aVR	aVL	aVF	V1	V2	V3	V4	V5	V6
DF_{jM1}-cD3	0.1149	0.2469	0.0670	0.0521	0.1766	0.1481	0.2328	0.0545	0.0284	0.0253	0.0242	0.0280
DF_{jM1}-cD2	0.1839	0.1466	0.0916	0.0505	0.2102	0.1538	0.1378	0.1096	0.0300	0.0239	0.0224	0.0268
DF_{jM1}-cD1	0.4227	0.1706	0.3526	0.0716	0.2563	0.3816	0.1869	0.1557	0.1066	0.0787	0.1221	0.2515
$\widehat{DF_{jM1}}$-cD3	1.6561	2.9339	1.5457	1.2366	2.0579	1.7376	6.4577	1.6849	1.1925	1.2456	1.3656	1.4816
$\widehat{DF_{jM1}}$-cD2	2.6509	1.7425	2.1147	1.2002	2.4503	1.8055	3.8230	3.3856	1.2635	1.1795	1.2645	1.4187
$\widehat{DF_{jM1}}$-cD1	6.0941	2.0278	8.1398	1.7005	2.9869	4.4787	5.1839	4.8087	4.4812	3.8803	6.9061	13.3254
$\overline{DF}_{j2M1}$-cD3	0.1805	0.1680	0.4427	0.5061	0.0900	0.2098	0.3994	0.6522	0.9030	1.0677	1.2281	1.2466
$\overline{DF}_{j2M1}$-cD2	0.0843	0.0934	0.1387	0.1325	0.0813	0.0488	0.0298	0.0965	0.1543	0.1853	0.2115	0.1848
$\overline{DF}_{j2M1}$-cD1	0.0139	0.0236	0.0203	0.0604	0.0167	0.0144	0.0091	0.0028	0.0035	0.0059	0.0067	0.0057
$\overline{DF}_{j1M1}$-cD3	1.2517	1.4137	1.9176	2.1306	0.7724	1.7880	1.4399	2.1112	2.1473	2.1651	2.1719	2.3529
$\overline{DF}_{j1M1}$-cD2	0.5846	0.7859	0.6007	0.5577	0.6974	0.4158	0.1074	0.3123	0.3668	0.3758	0.3740	0.3489
$\overline{DF}_{j1M1}$-cD1	0.0964	0.1986	0.0881	0.2542	0.1433	0.1223	0.0330	0.0092	0.0083	0.0119	0.0118	0.0107
ST-cD3	0.0139	0.0069	0.0135	0.0076	0.0118	0.0057	0.0042	0.0020	0.0011	0.0015	0.0028	0.0022
ST-cD2	0.0047	0.0037	0.0046	0.0031	0.0041	0.0022	0.0015	0.0008	0.0004	0.0005	0.0010	0.0012
ST-cD1	0.0027	0.0016	0.0026	0.0015	0.0022	0.0014	0.0008	0.0004	0.0002	0.0002	0.0005	0.0007

Note: **DF**: Denoising factor, **ST**: Soft thresholding.

on ECE values, Kurtosis values and maximum amplitudes of the coefficients in the subbands. The coefficients which have higher values compared to the value of the Denoising Factor (DF) or the threshold are retained. Normally, more threshold value is required for cD1 subband where noise content is more. For Lead-I signal, DF_{jM1} values for subbands cD1, cD2 and cD3 are found as 0.4227, 0.1839 and 0.1149 respectively. The higher frequency subbands contain more noise whereas lower frequency subbands have most of the ECG wave components. In other words, higher frequency subbands have lower SNR values compared to lower frequency subbands. Other three Denoising Factors $\widehat{DF_{jM1}}$, $\overline{DF}_{j1M1}$, $\overline{DF}_{j2M1}$ based on DECE and ECE are also computed. $\overline{DF}_{j1M1}$, $\overline{DF}_{j2M1}$ denoising factors have maximum values for cD3 subband and their values are lowest for cD1 subband. This shows an inverse trend for values of denoising factors compared to the DF_{jM1} values. The soft thresholding (ST) method as proposed in [28] has also been evaluated ($t = \sigma\sqrt{2\log(N)/N}$, where t is threshold, σ is variance of noise and N is the numbers of samples). The σ is calculated based on median absolute deviation (MAD) [148, 151, 152]. The estimated noise variance, σ, in a wavelet subband is given as $\sigma = C.MAD$ where 'C' is a constant scale factor which depends on distribution of noise. For a univariate data set with samples x_1, x_2, ..., x_n, the MAD is defined as [153]

$$MAD = median(|x_i - median(x_i)|) \tag{3.14}$$

TH-1102_06610204

where x_i is i^{th} data and $median(x_i)$ is the median. For normally distributed data '$C = 1.4826$' is the 75^{th} percentile of the normal distribution with unity variance. So, estimated noise variance can be written as $\sigma = \frac{MAD}{0.6745}$ [148]. MAD gives statistical dispersion of data and the basis of using it is higher breakdown point upto 50% that is better than interquartile range which has breakdown point 25% [151]. Also MAD is aim at symmetrical distribution and its Gaussian efficiency is about 37%. In Table-3.5, it is found the threshold set for cD3 is higher and cD1 is lower.

For qualitative comparison, four filtered signals using the four denoising factors are plotted with the original one in Figure-3.7. It is observed that DF_{jM1} performs better compared to the other three denoising factors. The filtered signal in Figure-3.7(b) has all the minute details of the original signal while removing the noise. It is observed in Figure-3.7(c), that the QRS complexes are smoothed out due to high values of denoising factors or threshold $\widehat{DF}_{jM1}$. In Figure-3.7(d), the filtered or denoised signal with $\overline{DF}_{j2M1}$ threshold, shows noise is not completely removed as marked at 1 and 2. This is due to the lower value of the denoising factor $\overline{DF}_{j2M1}$ as shown in fifth column corresponding to aVL channel, in Table-3.5. Similarly, the denoised signal in Figure-3.7(e) with $\overline{DF}_{j1M1}$ threshold fails at points marked 3 through 8. In Figure-3.8, original signal, wavelet filtered signal using soft threshold (ST) and wavelet filtered signal using proposed DF_{jM1} are shown. It is observed (Fig 3.8(b)) that ST-based method does not remove the noise effectively. This is the reason for the low PRD (1.1085) and WWPRD (1.6015) values shown in Fig 3.8(b) for the filtered signal with the soft threshold. The proposed DF_{jM1} is effective and denoising is distinctly visible in the filtered signal shown in Fig 3.8(c).

Table 3.6: Performance Analysis: CSE mutlilead measurement library database, dataset-M01-003

CSE mutlilead measurement library database, dataset-M01-003												
Parameters	Lead-I	Lead-II	Lead-III	aVR	aVL	aVF	V1	V2	V3	V4	V5	V6
PRD-DF_{jM1}	9.137	6.362	11.148	10.022	7.424	4.599	5.450	4.411	3.560	3.473	4.160	4.844
PRD-$\widehat{DF_{jM1}}$	17.202	17.369	20.909	24.566	16.269	12.304	11.229	18.338	26.518	28.646	27.939	26.053
PRD-$\overline{DF}_{j2M1}$	7.795	4.531	14.838	19.599	4.297	3.518	5.986	10.110	25.826	27.198	26.962	25.292
PRD-$\overline{DF}_{j1M1}$	17.006	16.816	20.909	24.566	12.951	12.086	8.931	18.114	26.101	28.171	27.510	25.578
PRD-ST	1.307	0.943	1.606	1.048	1.108	0.441	1.698	2.075	1.946	1.944	1.960	2.132
WWPRD-DF_{jM1}	21.710	11.367	26.054	18.096	15.716	12.165	10.604	8.547	5.381	5.190	8.506	11.343
WWPRD-$\widehat{DF_{jM1}}$	36.934	28.661	44.331	40.279	31.555	26.667	23.093	29.260	33.586	37.046	39.765	40.710
WWPRD-$\overline{DF}_{j2M1}$	12.099	7.344	25.846	30.669	7.330	7.059	7.237	11.716	26.370	28.400	31.269	30.475
WWPRD-$\overline{DF}_{j1M1}$	35.968	26.330	44.331	40.279	24.265	24.127	13.800	25.969	26.879	29.939	32.745	32.497
WWPRD-ST	1.748	1.378	1.818	1.521	1.604	0.776	1.755	1.968	1.751	1.827	1.924	1.940
WEDD-DF_{jM1}	3.061	1.992	3.799	2.252	1.871	2.825	2.998	2.871	2.147	1.928	2.843	3.2188
WEDD-$\widehat{DF_{jM1}}$	12.030	7.141	16.802	12.005	9.176	9.965	10.789	19.041	24.694	27.933	28.366	27.285
WEDD-$\overline{DF}_{j2M1}$	1.915	1.423	8.140	10.169	1.189	2.411	2.103	6.667	19.431	21.798	22.502	21.853
WEDD-$\overline{DF}_{j1M1}$	12.428	7.494	16.802	12.005	6.744	7.844	6.345	17.809	19.483	22.025	22.635	21.925
WEDD-ST	0.924	0.539	1.252	0.473	0.725	0.275	1.286	1.709	1.611	1.719	1.918	1.970

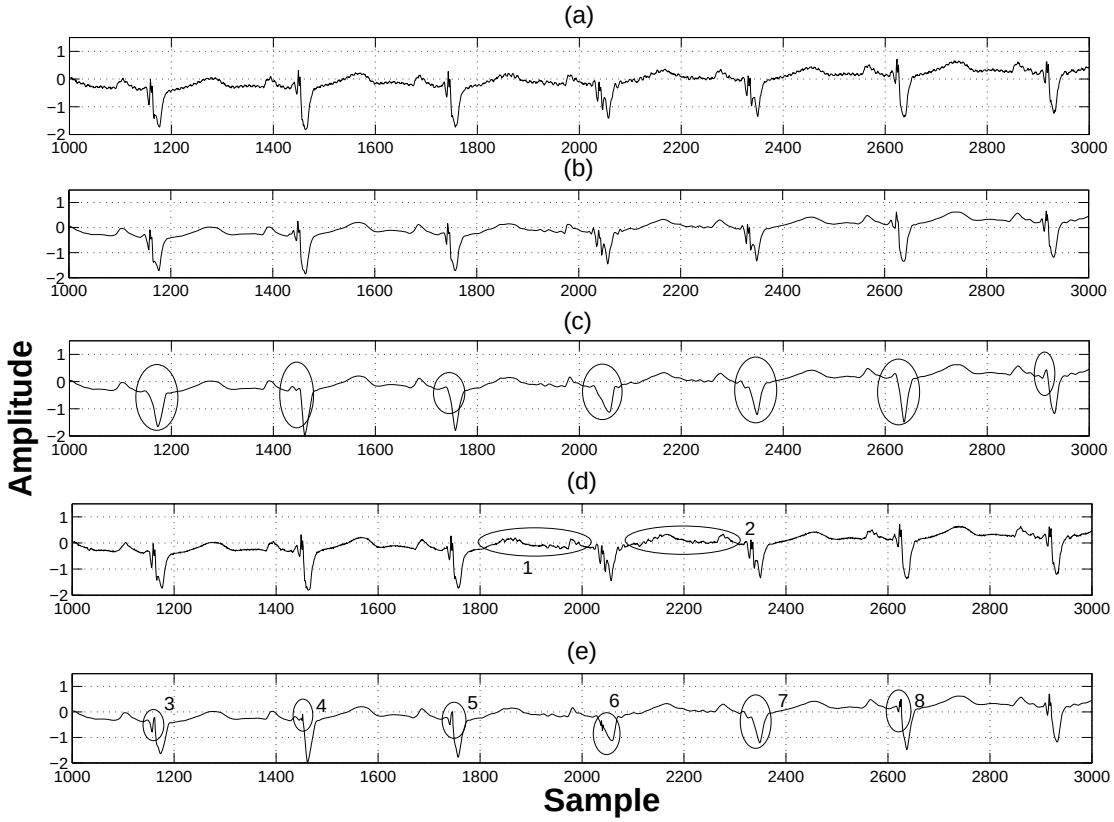

Figure 3.7: (a) Original signal and wavelet filtered signal using proposed denoising factors (b) DF_{jM1}, (c) $\widehat{DF_{jM1}}$, (d) $\overline{DF}_{j2M1}$ and (e) $\overline{DF}_{j1M1}$ (CSE mutlilead measurement library database, dataset: MO1-003, Lead-aVL)

Table-3.6 shows the different distortion values for four proposed denoising factors and for the soft threshold. All the 12-channel data are evaluated. It is observed that the distortion values for soft threshold are minimum in all cases. This is due to the very low soft threshold values shown in Table-3.5. Low distortion or error values appear as noise part of the signal is not filtered out. Among the four denoising factors, DF_{jM1} shows minimum PRD value for Lead-III, aVR, V1, V2, V3 and V4 channels. Minimum WWPRD values are obtained with the same denoising factor for aVR, V2, V3, V4, V5 and V6 channels. Similarly, minimum WEDD values are observed for Lead-III, aVR, aVL, V2, V3, V4, V5 and V6 channels. It is also found that minimum distortion values are obtained with $\overline{DF_{j2M1}}$ in all other channels. This has resulted due to low values of the denoising factor $\overline{DF_{j2M1}}$. It is shown in Figure-3.7(d) that the filtered signal with $\overline{DF_{j2M1}}$ denoising factor fails to remove the noise

TH-1102_06610204

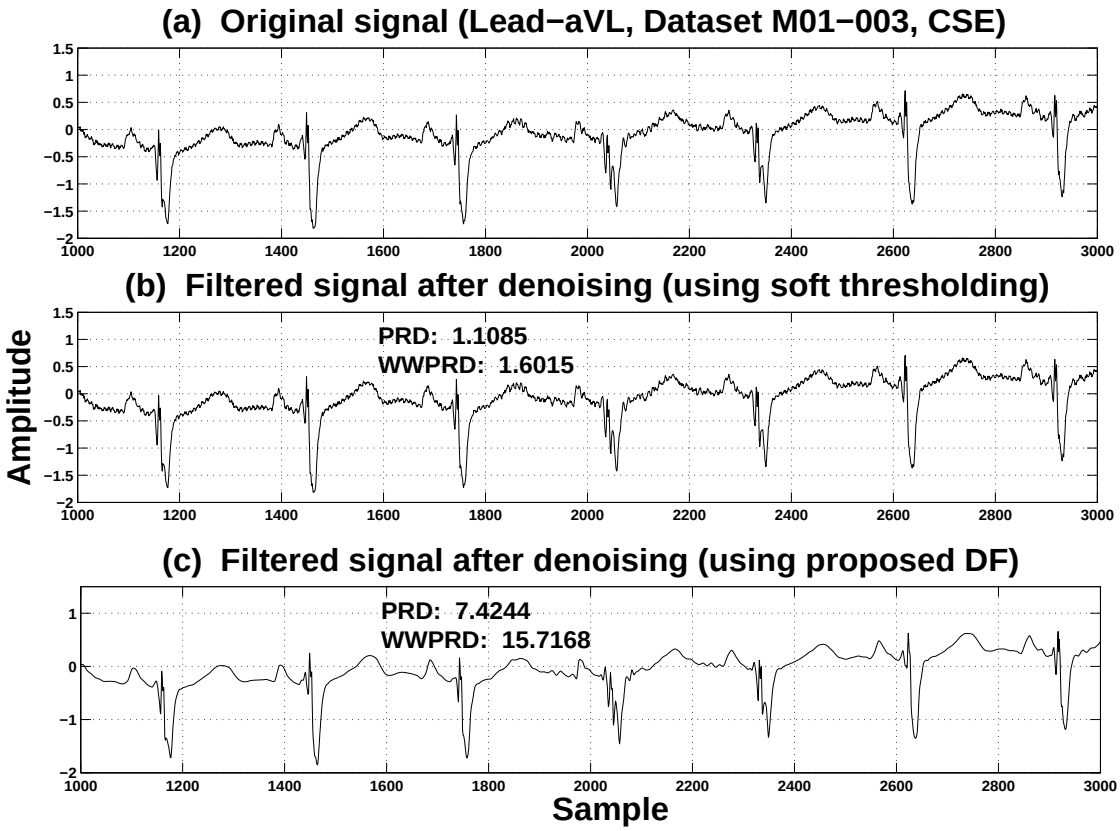

Figure 3.8: Original and filtered signals using soft thresholding and using proposed DF (a) original signal (Lead-aVL, Dataset M01-003, CSE), (b) filtered signal after denoising (using soft thresholding), (c) filtered signal after denoising (using proposed DF) (CSE mutlilead measurement library database, dataset: MO1-003, Lead-aVL)

efficiently. These results prove that the denoising factor DF_{jM1} will be the most effective not only from the point of view of effectively filtering the noise but also help retain the diagnostic information in the ECG signal.

It will be helpful to investigate if the values of the denoising factor DF_{jM1} for the three subbands, cD1, cD2 and cD3, are optimal from the point of view of the distortions in the signal. Figure-3.9 show the WEDD and WWPRD values when each of the three subbands are individually thresholded. For these results the signal in aVL channel is tested. It is observed that the maximum distortion value is attained when the threshold or denoising factor value exceeds certain value. For the signal in aVL channel the WEDD and WWPRD values (Table-3.6) with DF_{jM1} denoising factor are found as 1.8718 and 15.7168 respectively. The denoising factor, DF_{jM1}, has values (Table-3.5) in cD1, cD2

and cD3 subbands as 0.2563, 0.2102 and 0.1766 respectively. If these denoising factor values are

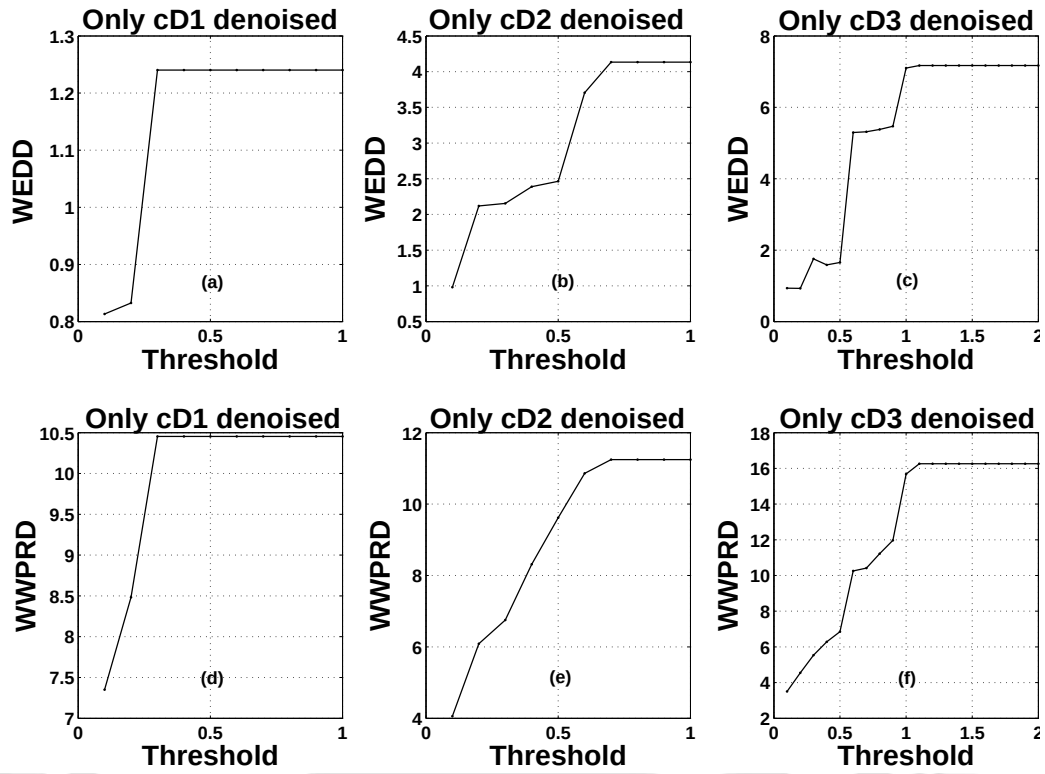

Figure 3.9: WEDD and WWPRD values using DF_{jM1},(a) and (d) only cD1 subband denoised, (b) and (e) only cD2 subband denoised (c) and (f) only cD3 subband denoised, Dataset: MO1-003, Lead-aVL, from CSE mutlilead measurement library.

used individually, as shown in Figure-3.9, for the three subbands, the WEDD values are 0.95, 1.2 and 1.0 for cD1, cD2 and cD3 subbands, this would have resulted in a total WEDD value of 3.15. But the observed WEDD value is 1.8718 when the three subbands are simultaneously thresholded. Similar results are observed with the WWPRD values. This shows that a proper choice of a set of optimal values for the denoising factor for the three subbands may results in an improved performance. To investigate further, two subbands, cD2 and cD3, are thresholded simultaneously. Table-3.7 shows

Table 3.7: WEDD values against thresholds of cD2 and cD3 subbands

Thresholds	cD3				
cD2	0.1	0.2	0.3	0.4	0.5
0.1	1.1895	0.9629	1.8755	1.7089	1.7771
0.2	2.3070	1.9412	3.0293	2.8843	2.9514
0.3	2.3423	1.9764	3.0648	2.9188	2.9869
0.4	2.5783	2.2669	3.4279	3.2727	3.3408
0.5	2.6530	2.3433	3.5061	3.3507	3.4187

TH-1102_06610204

the WEDD values for different threshold values in cD2 and cD3 subbands. It is observed that simultaneous thresholding has resulted in lower WEDD values. The WEDD value is 1.9412 for both the threshold values of cD2 and cD3 subbands as 0.2. Both threshold values as 0.2 is close to the values of the denoising factor for the both subbands which are 0.2102 and 0.1766. This value of WEDD is close to the observed value of WEDD (1.8718) as shown in Table-3.6. The lower WEDD value is due improved retention of diagnostic features in the signal when both the subbands are simultaneously thresholded. The results also indicate that the choice of a set of denoising factor values for the subbands based on Kurtosis and ECE values will result as an optimal set of threshold values for the subbands.

3.3.1.2 Evaluation of Proposed Method under Noise Conditions

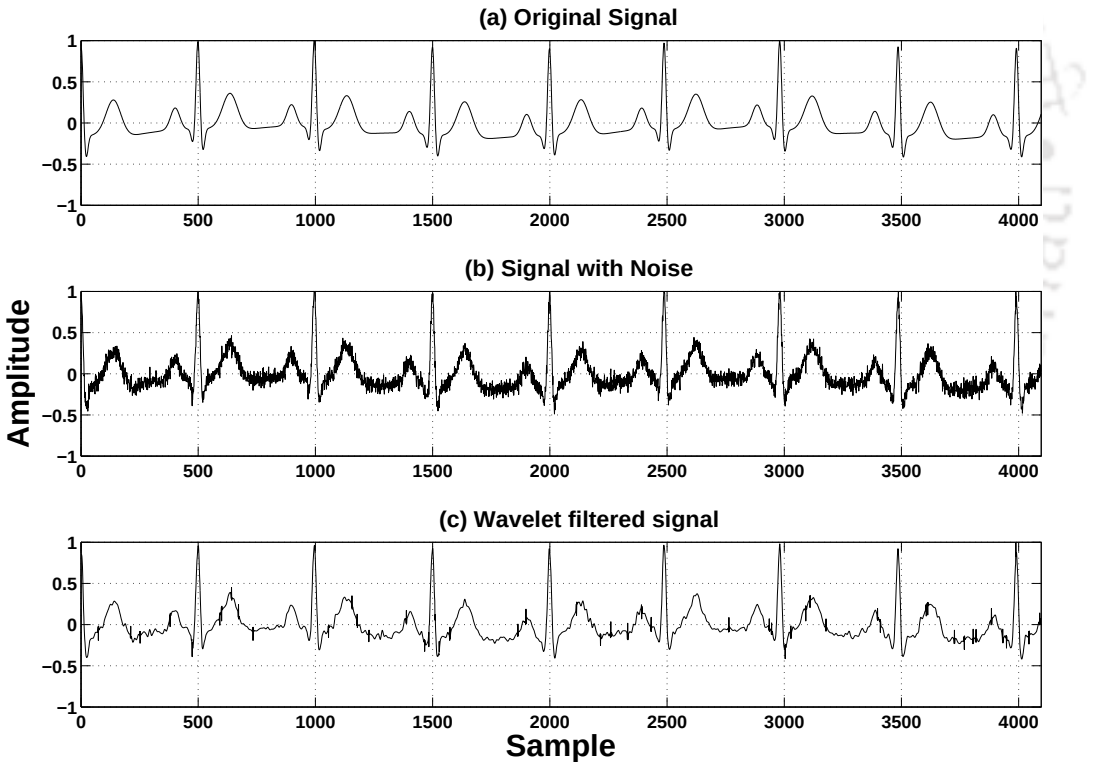

Figure 3.10: Wavelet filtered signal when corrupted with Gaussian Noise (Input SNR -2.476 dB),(a) Original Synthetic ECG signal, (b) Noisy ECG signal after addition of Gaussian Noise (Input SNR -2.476 dB) (c) Output filtered ECG signal using proposed denoising method.

In real application, an ECG signal may contain various types of noise and artifacts. It is essential to

evaluate the proposed method adding white Gaussian noise, Base line Wander and Power line Noise to an ECG signal. Noise corrupted signal is simulated by adding Gaussian noise, baseline wander and power line interference and is tested with the proposed method. Figure 3.10, shows the denoising

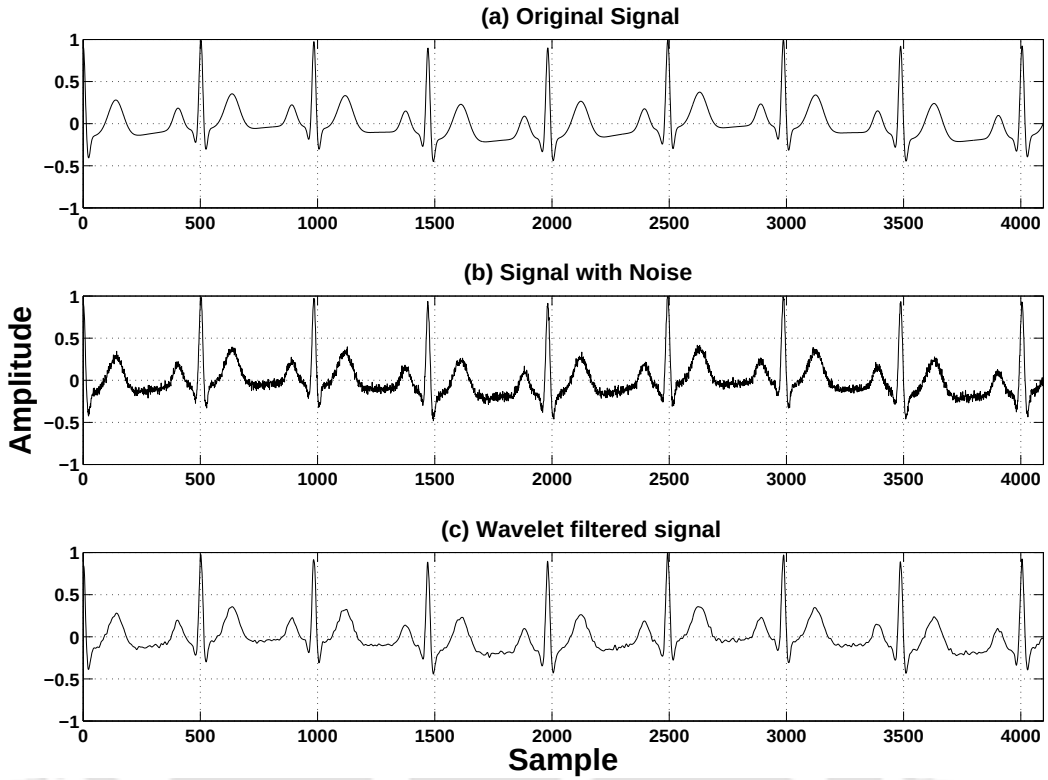

Figure 3.11: Wavelet filtered signal when corrupted with Gaussian Noise (Input SNR 4.7534 dB),(a) Original Synthetic ECG signal, (b) Noisy ECG signal after addition of Gaussian Noise (Input SNR 4.7534 dB) (c) Output filtered ECG signal using proposed denoising method.

of synthetic ECG signal when corrupted with Gaussian noise. The synthetic ECG signal is corrupted with white Gaussian noise at an input SNR of -2.476 dB. Then the signal is subjected to proposed denoising method. The method is able to filter out the noise and at the same time it has preserved the clinical components, P-wave, T-wave and QRS-complex. The filtered signal contains high frequency spikes which may be due to inclusion of Kurtosis in the proposed denoising factor. The quantitative performance of the method is accessed by output SNR, PRD, WWPRD and WEDD. The filtered signal has an output SNR value of 28.869dB, PRD value of 22.57%, WWPRD value of 47.067% and WEDD value of 6.308%. The WEDD value falls under very good category of reconstructed signal. In Figure 3.11, the input synthetic ECG signal is corrupted and the SNR value of the noisy signal is 4.7534

TH-1102_06610204

dB. The noisy ECG is filtered using the proposed denoising method. The filtered output signal is smooth and satisfactory. The output SNR improvement is good (41.3432 - 4.7534 = 36.5898dB). The filtered signal has a PRD value of 12.261% and a WWPRD value of 34.268%. The signal distortion measure WEDD has a value of 4.293% which falls in excellent category signal. This shows the better performance of the proposed method under relatively higher input SNR condition.

The method is also tested with the signals having higher input SNR values. Under high input SNR of 46.4458 dB, the filtered signal has output SNR value of 59.7176 dB and it shows smooth output. The PRD value is 5.11% whereas WWPRD value is 7.65%. The WEDD value is 2.83% which falls under excellent category.

3.3.2 Results for Denoising based on Kurtosis, Noise Variance and Multiscale Energy

For validation of proposed denoising factor, standard test functions, Blocks, Bumps, HeaviSine and Doppler [29] are used and shown in Figure 3.12. These functions show various spatially nonhomogeneous phenomena and represent complex signals which may appear in real world applications. Blocks represent sharp rise and fall in signal. Bumps may be encountered when handling spectra. HeaviSine may be considered as regular signal with sudden irregular notch. The doppler represents the variable frequency in the signal. It is desirous to check the adaptivity of the proposed wavelet denoising with these nonhomogeneous signals. The proposed wavelet denoising method is tested with these signals after addition of zero mean and unity variance Gaussian noise. The input SNRs for Blocks, Bumps, HeaviSine and Doppler are 30 dB, 20 dB, 30 dB and 30 dB respectively. The corresponding output SNRs are 49.68 dB, 29.36 dB, 61.38 dB and 55.53 dB. The output SNR is estimated as ratio between the energy of original signal (before addition of noise) and the energy of filtered noise signal. Output SNR values of 79.85 dB, 96.84 dB, 41.64 dB and 90.73 dB are obtained using Classical hard thresholding method [29]. It can be observed from Figure 3.12 that quantitatively better filtered signal is obtained for the proposed thresholding compared to the hard thresholding method. Higher output SNR values and better qualitative results suggests that the proposed method is more effective in filtering the noise. Standard 12-lead ECG (Bipolar: Lead-I, II, III; Augmented Lead: aVR, aVL, aVF and Chest Lead: V1, V2, V3, V4, V5, V6) of CSE multilead measurement library, data set-M01-003, are subjected to amplitude normalization and mean removal. From each channel data,

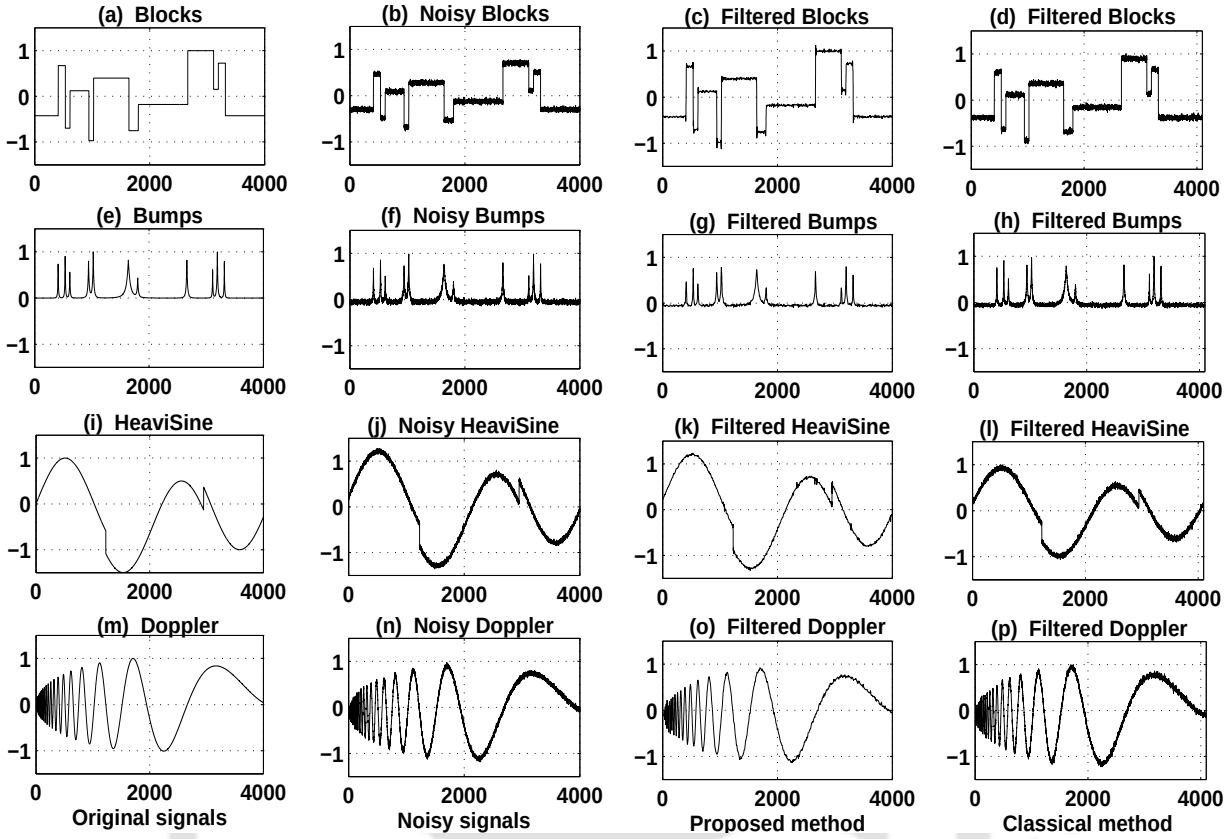

Figure 3.12: Clean, noisy and wavelet filtered test signals: Blocks, Bumps, HeaviSine and Doppler (a) Blocks, (b) noisy Blocks, (c) wavelet filtered noisy Blocks (proposed), (d) wavelet filtered noisy Blocks (Classical hard thresholding), (e) Bumps, (f) noisy Bumps, (g) wavelet filtered noisy Bumps (proposed), (h) wavelet filtered noisy Bumps (classical hard thresholding), (i) HeaviSine, (j) noisy HeaviSine, (k) wavelet filtered noisy HeaviSine (proposed), (l) wavelet filtered noisy HeaviSine (classical hard thresholding), (m) Doppler, (n) noisy Doppler, (o) wavelet filtered noisy Doppler (proposed) and (p) wavelet filtered noisy Doppler (classical hard thresholding). The x-axis represents samples and the y-axis represents amplitudes.

4096 samples are chosen as a block. Wavelet decomposition using Daubechies 9/7 biorthogonal wavelet filters up to six levels are used and same is applied for reconstruction filters also.

To see the performance of individual factors, $\widehat{\alpha_j}$ (factor-1), β_j (factor-2) and γ_j (factor-3), lead-II signal, data set-MO1-003 from CSE multilead measurement library, is used. The original signal and filtered signals by the individual factors or thresholds, $\widehat{\alpha_j}$, β_j and γ_j are shown in Figure 3.13(a-d). Filtered signal with threshold, $\widehat{DF_j}$, is shown in Figure 3.13(e). Individual factors fail to filter the signal cleanly in the R-wave region (marked with 'R'). Better filtering is observed at the region marked with 'R' using threshold $\widehat{DF_j}$. This shows that a threshold combining the three factors results in an

TH-1102_06610204

improved performance.

Table 3.8: PRD, WWPRD and WEDD for $\widehat{\alpha_j}$, β_j, γ_j and proposed denoising factors,$\widehat{DF_j}$ for lead-II signal using CSE multilead measurement library, data set-M01-003 with six levels wavelet decomposition

Metric	$\widehat{\alpha_j}$	β_j	γ_j	$\widehat{DF_j}$
PRD	10.05	7.63	16.32	13.04
$WWPRD$	17.51	13.46	11.46	21.31
$WEDD$	3.98	4.01	2.40	4.00

In Table 3.8, quantitative results are shown for three individual denoising factors, $\widehat{\alpha_j}$, β_j, γ_j and combined denoising factor or threshold $\widehat{DF_j}$. The diagnostic distortion is well captured by WEDD metric [71]. WEDD value (4.00) for $\widehat{DF_j}$ falls under excellent category [71] and the qualitative results (Figure 3.13) reveal better denoising effect. Though lower WEDD values are observed for individual denoising factors, $\widehat{\alpha_j}$ and γ_j, qualitative results shown in Figure 3.13(b) and Figure 3.13(d) do not show effective filtering in 'R' region. The thresholds set for factors $\widehat{\alpha_j}$ and γ_j remove lower numbers of wavelet coefficients than the combined denoising factor, $\widehat{DF_j}$, resulting in lower WEDD values.

In Figure 3.14, filtering of synthetic ECG signal, generated using 'ECGSYN' from 'Physionet Archive' [154], using proposed denoising factor, $\widehat{DF_j}$, is shown. Wavelet filtering of synthetic ECG corrupted with Gaussian noise at input SNR of 5 dB and output SNR of 13 dB, is plotted in Figure 3.14(a). In this case, WEDD value is 16.8. In Figure 3.14(b), result with input SNR of 10 dB is shown. The output SNR is 25 dB and WEDD value is 8.11. Wavelet filtering of synthetic signals at input SNRs of 15 dB and 20 dB with respective output SNRs of 36 dB and 46 dB are shown in Figure 3.14.c) and 3.14.d). The corresponding WEDD values are 3.53 and 2.64. The WEDD values of 8.11, 3.53 and 2.64 fall under very good and excellent category [71]. It is also seen that the filtering of noise contaminated signal preserve desired clinical components and 'PQRST' morphologies with improved output SNR.

Lead-III wavelet filtered signal with original signal and residual error is shown in Figure 3.15. It is observed that proposed method preserve all the diagnostic features. The noise present in the original signal is filtered out efficiently keeping 'PQRST' morphologies as in original.

The values for diagnostic distortion measures, PRD, WWPRD and WEDD for all the standard 12-leads are evaluated and shown in Table 3.9. The lowest PRD value 9.523, the lowest WWPRD value 17.743 and the lowest WEDD value 4.000 are found for chest leads V2, V3 and limb lead-II

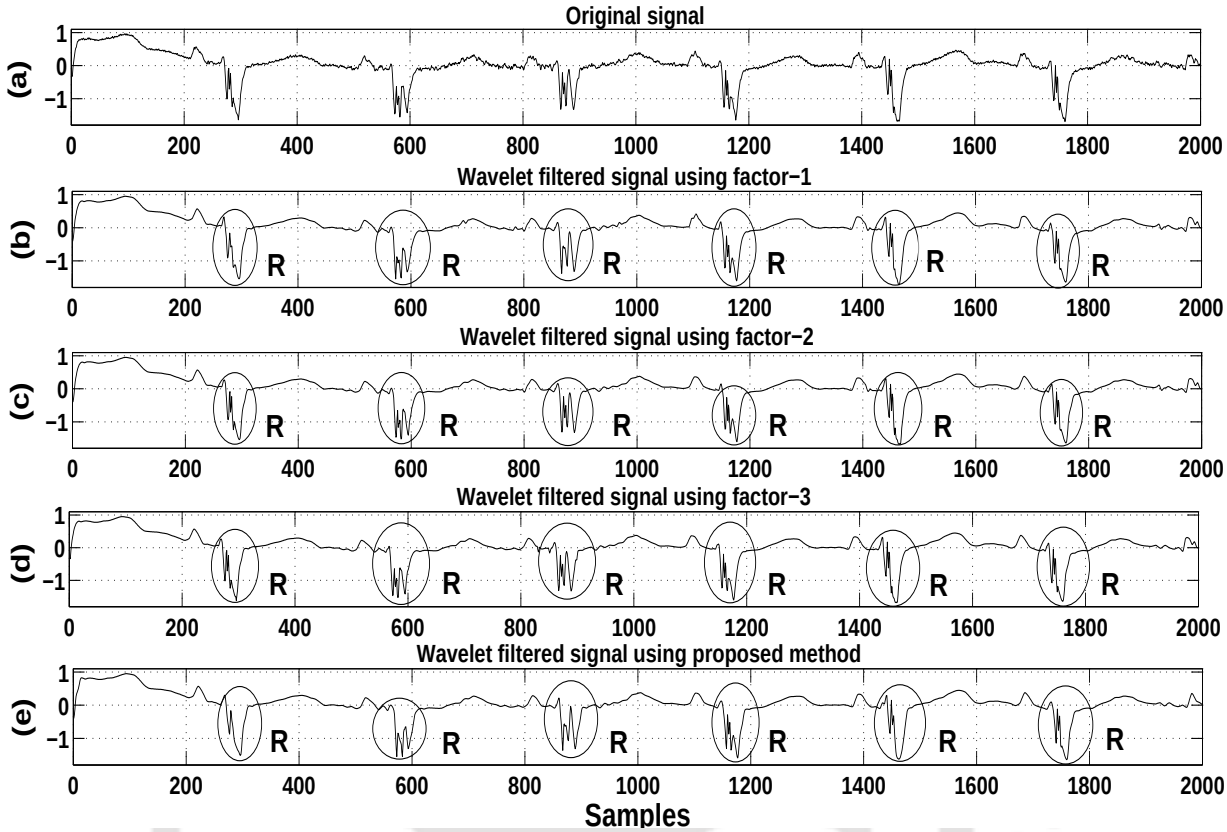

Figure 3.13: Wavelet filtered signal using proposed method compared with wavelet filtered signal using individual threshold factors α_j, β_j and γ_j. In panel (a) original lead-II ECG signal, (b) wavelet filtered signal using α_j (factor-1), (c) wavelet filtered signal using β_j (factor-2), (d) wavelet filtered signal using γ_j and (e) wavelet filtered signal using $\widehat{DF}_j$. Wavelet decomposition level is 6, CSE multilead measurement library, data set-(MO1-003)

Table 3.9: Distortion measures in terms of PRD, WWPRD and WEDD, CSE multilead measurement library, data set-M01-003

Metrics	Lead-I	Lead-II	Lead-III	aVR	aVL	aVF	V1	V2	V3	V4	V5	V6
PRD	18.041	13.042	22.329	24.204	15.768	15.665	12.065	9.523	10.345	11.020	11.925	11.717
WWPRD	39.115	21.313	47.110	41.216	29.064	23.361	20.006	20.454	17.743	18.321	20.669	23.955
WEDD	15.087	4.000	19.560	14.233	7.358	6.837	6.430	11.433	10.883	11.134	11.026	10.918

respectively. Among these measures, WEDD shows the lower values in most of the leads. The lead-III denoised ECG signal, in Figure 3.15, shows PRD, WWPRD and WEDD values 22.329, 47.110 and 19.560 respectively. Wavelet filtered signal shows that most of the diagnostic information remain intact.

The proposed wavelet denoising method is compared for qualitative and quantitative assessment

TH-1102_06610204

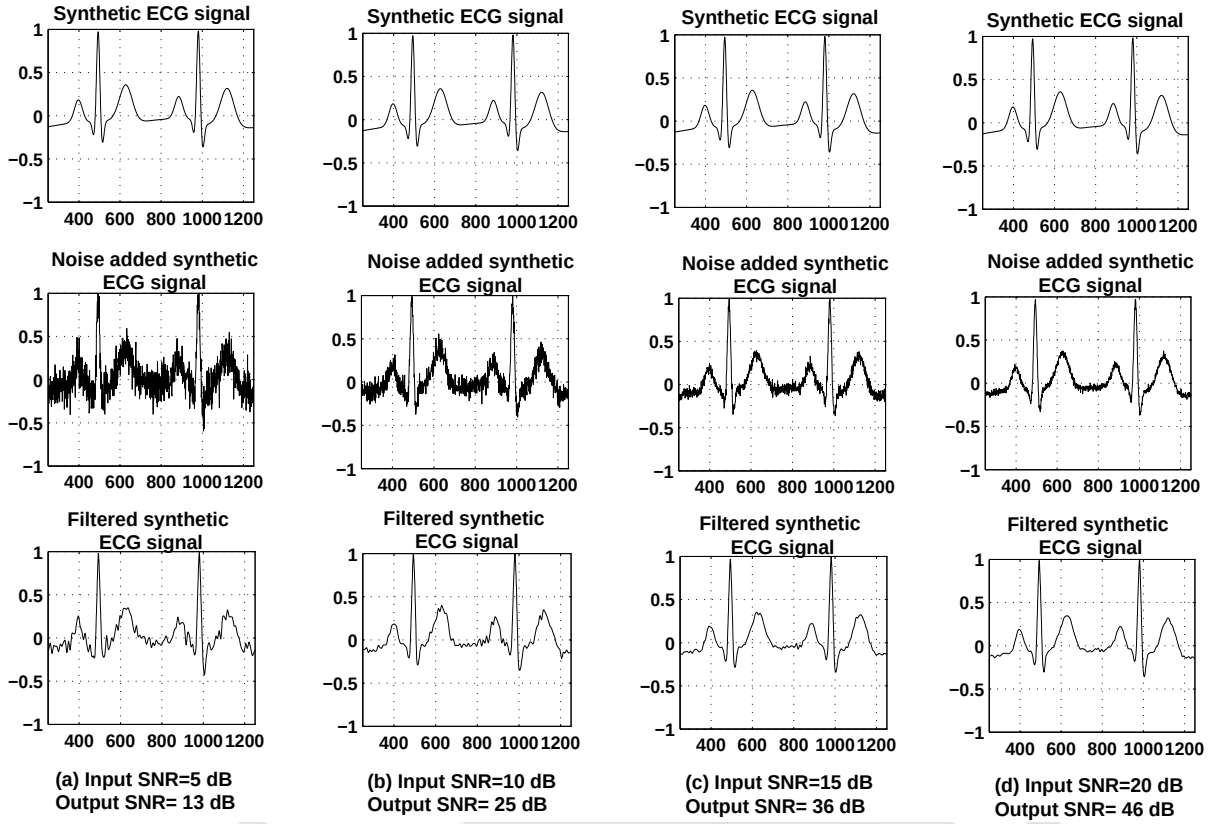

Figure 3.14: Wavelet filtered synthetic ECG signal using proposed $\widehat{DF_j}$: (a) original synthetic ECG signal, signal corrupted with Gaussian noise at input SNR of 5 dB and wavelet filtered synthetic ECG signal at output of SNR 13 dB , (b) original synthetic ECG signal, signal corrupted with Gaussian noise at input SNR of 10 dB and wavelet filtered synthetic ECG signal at output SNR of 25 dB (c) original synthetic ECG signal, signal corrupted with Gaussian noise at input SNR of 15 dB and wavelet filtered synthetic ECG signal at output SNR of 36 dB and (d) original synthetic ECG signal, signal corrupted with Gaussian noise at input SNR of 20 dB and wavelet filtered synthetic ECG signal at output SNR of 46 dB. Wavelet decomposition of synthetic ECG is six levels. The x-axis represents samples and the y-axis represents amplitudes.

with existing thresholding methods such as hard thresholding, soft thresholding [28] and thresholding based on principle of Stein's Unbiased Risk Estimate (SURE) [29]. Quantitative diagnostic distortion metrics are computed and denoised signals are plotted for qualitative analysis. In Figure 3.16, the wavelet filtered signals using above three methods are shown and are compared with the proposed denoising method. The signals shown in Figure 3.16(c) and Figure 3.16(e) are filtered nicely. But in Figure 3.16(c), denoising action has over-smoothed the signal (marked 1 though 6) whereas in Figure 3.16(e) all the diagnostic features are available. The filtering effect is less in other two methods as shown in Figure 3.16(b) and Figure 3.16(d). For this signal, filtering with the proposed threshold

TH-1102_06610204

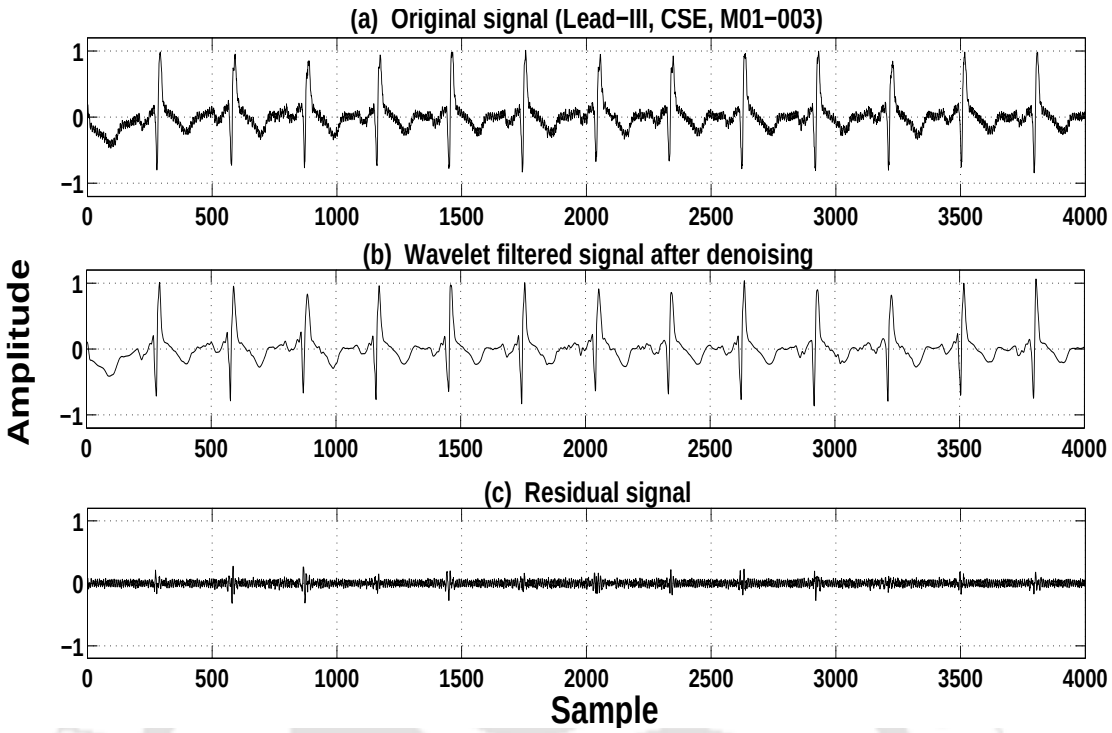

Figure 3.15: Wavelet filtered lead-III ECG signal using proposed $\widehat{DF_j}$: (a) original signal, (b) wavelet filtered signal using proposed denoising factor and (c) residual signal between original and filtered signal. CSE multi-lead measurement library, data set-M01-003 with six wavelet decomposition levels

.

results in PRD, WWPRD and WEDD values as 13.042, 21.313 and 4.000 respectively. PRD values, 1.4004, 1.5952 and 24.7621, WWPRD values, 1.8546, 2.3494 and 37.5364 and WEDD values, 1.2146, 1.2281 and 13.9818 are obtained with the other thresholding methods, hard thresholding, soft thresholding and SURE respectively (Table 3.10). Although hard and soft thresholding methods show lower

Table 3.10: PRD, WWPRD and WEDD for hard thresholding, soft thresholding, SURE and proposed method for lead-II signal using CSE multilead measurement library, data set-M01-003 with six wavelet decomposition levels

Method	PRD	WWPRD	WEDD
Hard thresholding	1.4001	1.8546	1.2146
Soft thresholding	1.5952	2.3494	1.2281
SURE	24.7621	37.5364	13.9818
Proposed method	13.042	21.313	4.000

values for distortion measures, the filtering of the signal is very less as shown in Figure 3.16. Thus, these two methods remove very less wavelet coefficients from subbands cD1, cD2 and cD3 and result in less denoising effect. However, the proposed denoising method and threshoding based on

TH-1102_06610204

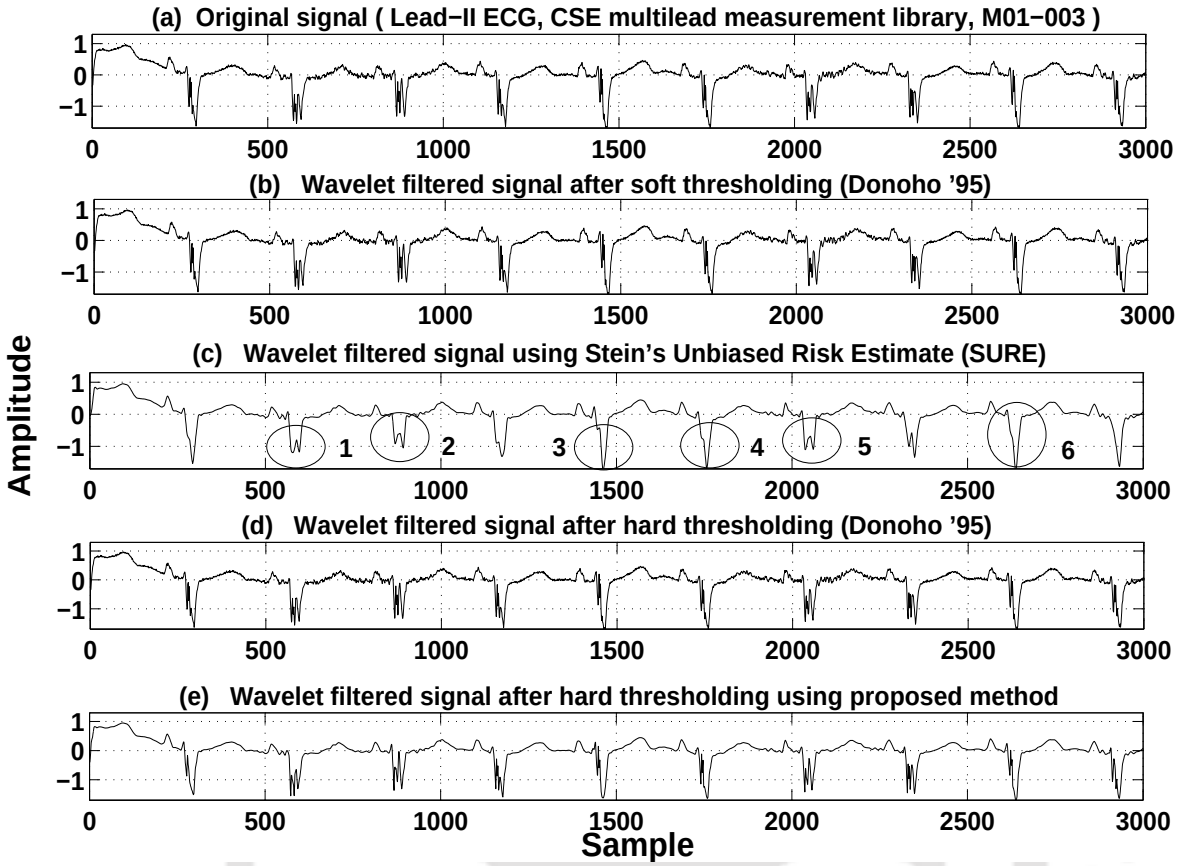

Figure 3.16: Wavelet filtered lead-II ECG signal: (a) original signal, (b) wavelet filtered signal using soft threshold method (Donoho'95), (c) wavelet filtered signal based on principle of Stein's Unbiased Risk Estimate (SURE), (d) wavelet filtered signal using hard threshold method (Donoho'95) and (e) wavelet filtered signal using proposed denoising method. CSE multilead measurement library, data set-M01-003.

SURE filter the signal but the later one over-smooth the signal as shown (marked at 1 to 6) in Figure 3.16(c). This is due to the higher threshold value set in SURE. The proposed method preserves all the clinical components and shows acceptable distortion values. This proves that the proposed denoising method is superior compared to the other three methods.

3.3.3 Comparison of Proposed Methods

In this section, the performances of the denoising methods are compared quantitatively and qualitatively. The PRD, WWPRD and WEDD are evaluated and are shown in Table 3.11. The first method is denoted with extention 'M1' after each distortion matrics and similarly, extention 'M2' is used for the second method. The lowest PRD value of 3.4736 is found for lead-V4 for the first denoising method

Table 3.11: Comparative Performance Analysis for proposed two methods, CSE mutlilead measurement library database, dataset-M01-003

CSE mutlilead measurement library database, dataset-M01-003												
Metrics	**Lead-I**	**Lead-II**	**Lead-III**	**aVR**	**aVL**	**aVF**	**V1**	**V2**	**V3**	**V4**	**V5**	**V6**
PRD-M1	9.1377	6.3625	11.1483	10.0227	7.4244	4.5998	5.4508	4.4116	3.5608	3.4736	4.1602	4.8440
PRD-M2	18.041	13.042	22.329	24.204	15.768	15.665	12.065	9.523	10.345	11.020	11.925	11.717
WWPRD-M1	21.7109	11.3672	26.0547	18.0969	15.7168	12.1657	10.6045	8.5475	5.3818	5.1903	8.5060	11.3438
WWPRD-M2	39.115	21.313	47.110	41.216	29.064	23.361	20.006	20.454	17.743	18.321	20.669	23.955
WEDD-M1	3.0614	1.9920	3.7993	2.2527	1.8718	2.8256	2.9981	2.8719	2.1474	1.9281	2.8439	3.2188
WEDD-M2	15.087	4.000	19.560	14.233	7.358	6.837	6.430	11.433	10.883	11.134	11.026	10.918

(M1) whereas for second method (M2) lead-V2 shows the lowest PRD value of 9.523. Similarly, the lowest WWPRD and WEDD values 5.1903 (lead-V4) and 1.8718 (lead-aVL) are found for the first method. The second method yields the lowest WWPRD and WEDD for lead-V3 (17.743) and lead-V2 (4.00) respectively. WEDD measure is more robust and it is claimed to represent the quality of the diagnostic features in a processed ECG signal [71]. As per this metric the filtered signals of all the leads by 'M1', fall under 'excellent' category whereas 'M2' gives excellent category signal only for leads Lead-II. Remaining filtered multichannel signals by means of 'M2' fall under 'very good' or 'good' categories. It may be due to higher thresholds for 'M2' filtering method which removes more wavelet coefficients giving higher WEDD values. Also, it is noticed that the non-diagnostic based error metric like PRD shows higher values for all the leads for second method. Computationally, 'M2' filtering method is more complex than 'M1' filtering method. In second method, to derive a threshold, it is required to calculate three terms and then perform the averaging operation whereas the first method is simple. The qualitative analysis for same data set for both the proposed filtering methods is performed.

In Figure 3.17, filtered lead-II ECG signals are compared using same dataset, CSE-M01-003. The second method (M2), slightly oversmooth the signal. It reduces the amplitude minimally keeping all the clinically essential components as in original. Higher thresholds derived by this method may have zeroed more wavelet coefficients in subbands. This may be the reason for getting higher distortion metrics for the second method compared to the first method (M1).

TH-1102_06610204

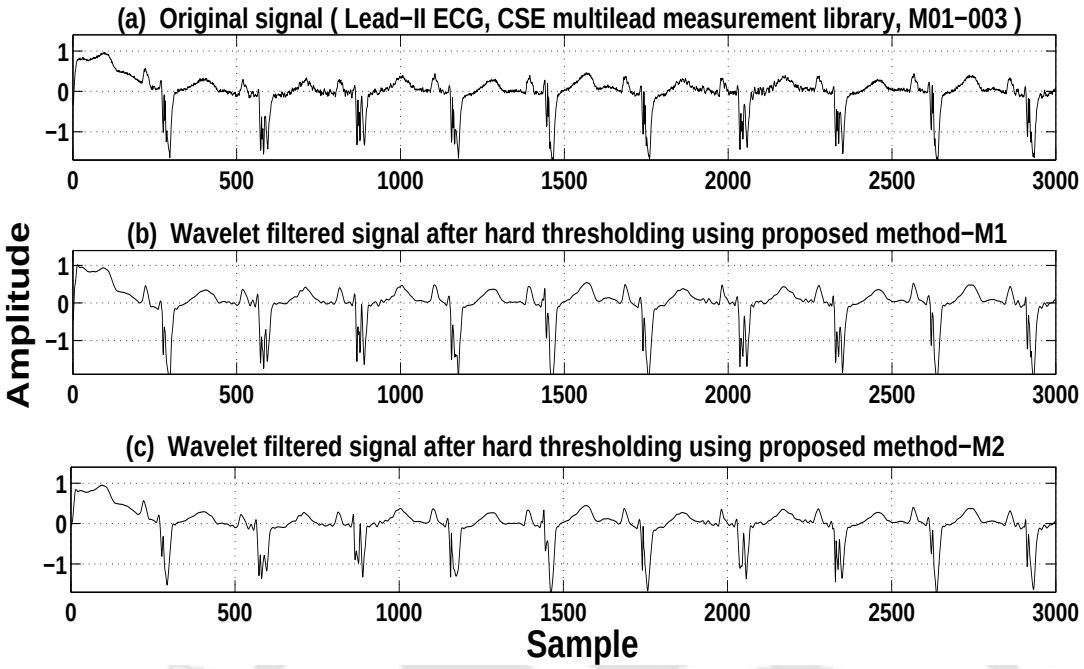

Figure 3.17: Wavelet filtered lead-II ECG signal using proposed methods (a) original signal, (b) wavelet filtered signal using proposed denoising method-M1 and (c) wavelet filtered signal using proposed denoising method-M2. CSE multilead measurement library, data set-M01-003 with six wavelet decomposition levels

.

3.4 Summary

In the first method based on HOS and ECE, four denoising factors are introduced for filtering of ECG signal. Best performance is observed with DF_j which is based on HOS and ECE of wavelet subband signal. Kurtosis employed in this work, discriminate signal and noise. It is observed that the spikes or sudden change in signal frequency along with noise gives a higher value of Kurtosis. Taking advantage of this property of Kurtosis, DF_j is scaled by ECE of MECG signal. Since it is established that the ECE value in higher level wavelet subband coefficients are more than lower ones, most of the energy of ECG signal remain in higher sub-bands such as cA6, cD6, cD5 and cD4. So, lower subbands, cD1, cD2 and cD3, are chosen for thresholding.

The second method, introduces a novel denoising method based on relative energy contribution of wavelet subbands and Kurtosis based Gaussian noise estimator for filtering of ECG signal. Estimated noise variance in wavelet subband is computed with a new approach which includes Gaussian-

ity measure in term of Kurtosis instead of conventional statistical approach. Lower order subbands are expected to have relatively higher noise energy compared to the signal energy. The proposed method gives higher threshold values for lower order subbands. It is the combination of three individual factors, α_j, β_j and γ_j. Combined denoising factor gives improved results. The method is tested with spatially nonhomogeneous functions, Blocks, Bumps, HeaviSine and Doppler with noise. The performance of the proposed thresholding method evaluated using synthetic ECG signal after adding noise and the recorded signal from database. Also, it is compared with the existing classical thresholding method such as soft thresholding, hard threshoding and SURE. Results show that the performance of the proposed method is better compared to the existing methods. The proposed denoising method not only filters ECG signal effectively but also can help retain the clinical information in the signal.

TH-1102_06610204

Indian Institute of Technology Guwahati

4

Multiscale Principal Component Analysis for Multichannel ECG Compression

Contents

TH-1102_06610204

In this Chapter, we introduce Multiscale Principal Component Analysis (MSPCA) for multichannel electrocardiogram (MECG) signals. In wavelet domain, principal components analysis (PCA) of multiscale multivariate matrices of multichannel signals may help reduce dimension and remove redundant information present in signals. Principal Component Analysis (PCA) is widely used for multivariate data analysis [124], [155]. Since last two decades, PCA is evolving with different extensions or modifications such as multiway PCA (MPCA) [125], multiblock PCA [156], non-linear PCA [126, 132], probabilistic principal component analysis [130] and weighted PCA [157]. PCA reduces data dimension by retaining an optimum number of Principal Components (PC). The data set is transformed to a new dimension with a reduced set of variables [124]. PCA transforms the data matrix in a statistically optimal manner by diagonalizing the covariance matrix. The first few significant components capture the correlations between the variables. Elimination of insignificant components reduces the redundant information in the data set [124].

The information at different wavelet scales can be effectively analyzed using PCA. MSPCA based analysis of multichannel ECG signals are not addressed in literature. Literature reviews in Chapter 2, show the classical PCA based applications in ECG signal processing. For physiological signals like ECG and EEG, conventional PCA has been applied for data reduction, noise elimination, beat detection, classification, signal separation and feature extraction [12], [119], [13]. PCA is used as a tool for separation of respiratory and non-respiratory segments in an ECG signal [14]. During processing of an ECG signal, it may not be advisable to distort the diagnostic information in the signal [102], [138]. Conventional PCA based methods have not considered the distortion of clinically important diagnostic features. Significant energies of cardiac signal-components or diagnostic components are present at different frequency bands in an ECG spectrum. Wavelet transform of an ECG signal reproduces them at different scales or subbands [102]. This grossly translates or segments 'PQRST' morphologies into different subbands. In wavelet subbands, the correlation between multichannel ECG signal components can be effectively captured. Correlation of multichannel ECG data in wavelet subbands may help implementation of PCA without affecting the clinical information. This motivates us to implement Multiscale Principal Component Analysis (MSPCA) at wavelet scales and coding the PCA coefficients to achieve multichannel compression.

The related review of literatures in Chapter 2, show that MSPCA based processing of multichan-

nel ECG and compression of these signals are not addressed. It is seen that MSPCA has higher potential to represent clinical signal components in few PCA coefficients. So, in this Chapter, we propose a compression scheme for multichannel electrocardiogram (MECG) data, using Multiscale PCA (MSPCA) and Huffman coding. In Section 4.1, conventional PCA for multichannel ECG signals is discussed. Section 4.2, presents the proposed multiscale PCA for Multichannel ECG. Section 4.3 contain proposed MSPCA based compression of MECG signals. Results are discussed in Section 4.4.

4.1 PCA for Multichannel Electrocardiogram

PCA is used for ECG signal processing using cut and align or lead piling process on the single channel signal [12] to form the multivariate data. This method uses the redundancies between ECG beats. For multichannel ECG signals, conventional PCA can be applied with appropriate multivariate matrix formation. The multichannel ECG signal, $\mathbf{S}$, can be represented as

$$\mathbf{S} = \begin{bmatrix} s_{11} & s_{12} & . & . & s_{1n} \\ s_{21} & s_{22} & . & . & s_{2n} \\ . & . & . & . & . \\ s_{N1} & s_{N2} & . & . & s_{Nn} \end{bmatrix} \tag{4.1}$$

where s_{pq} is the p^{th} sample of the q^{th} channel signal. There are n number of channels with N number of samples in each channel. In this, individual channel data are represented in separate columns.

To explore the correlations between the data in different channels or leads of MECG signals, scatter plots and correlation coefficients can be evaluated. The scatter plot provides a graphical display of correlation between variables in a cartesian co-ordinate system [158]. Fig.4.1 shows the scatter plots and the correlation values for a 12 channel ECG data. The scatter plots between data in different ECG leads are shown in lower half triangular plot matrix and the correlation values are shown at the upper half triangular table. The diagonal elements show correlation with same channel signal. Looking at the plots, the correlations and the redundancies between pairs of channels can be intuitively imagined. If dots of scatter plot are clustered from lower left to upper right it suggests

TH-1102_06610204

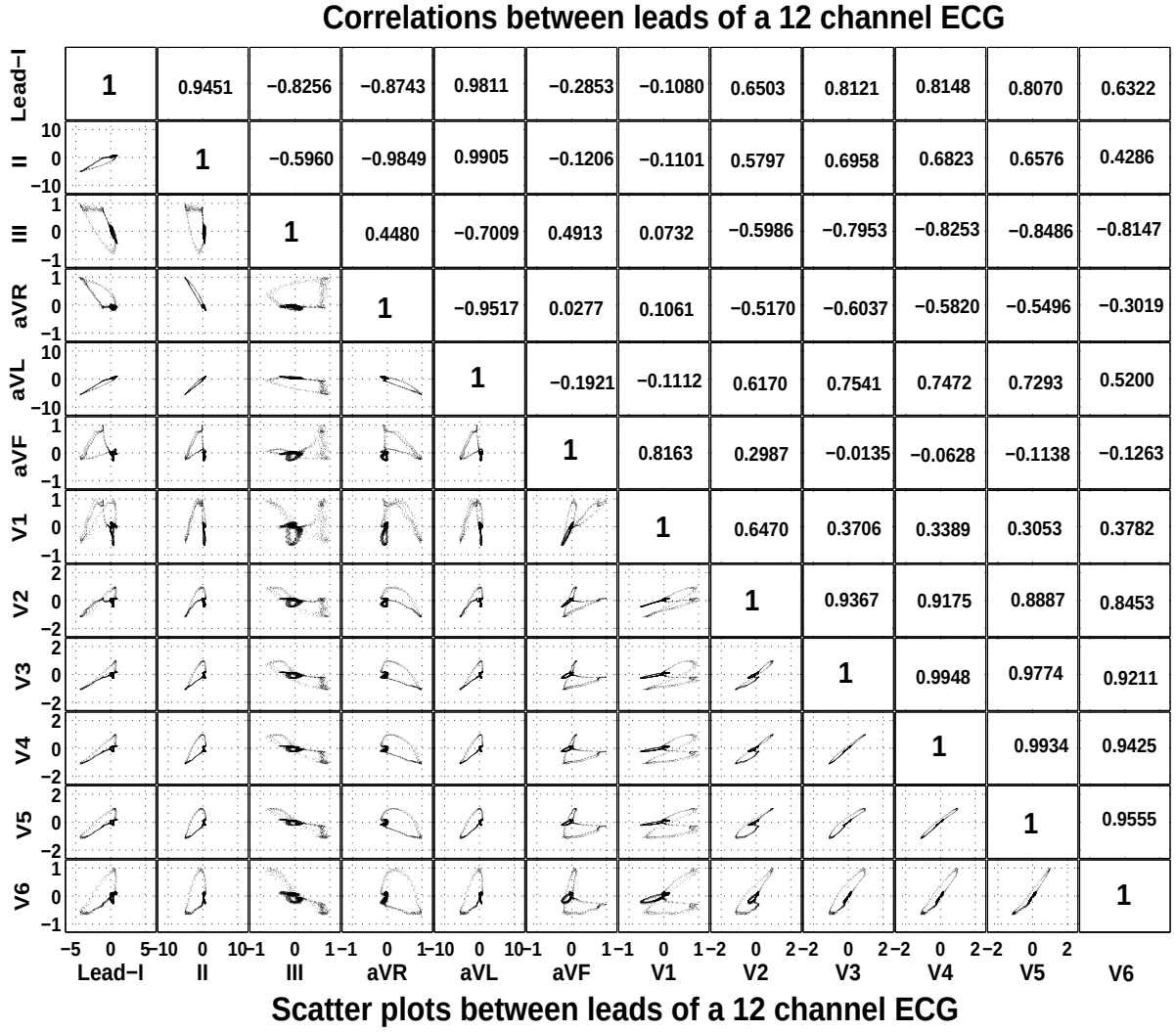

Figure 4.1: Scatter matrix plot for original signals. Signals in different ECG leads are scatter plotted. Database used is CSE multilead measurement library, data set M01-033.

.

positive correlation. Similarly dots from upper left to lower right indicate a negative correlation. If the data points are closer to form a straight line, it indicates higher correlation between the two variables. Between lead-I and lead-II the correlation value is high which is 0.9451. Lead-I signal is the potential difference between left arm (LA) and right arm (RA) and lead-II signal is the potential difference between left leg (LL) and right arm (RA). In both the cases, right arm is the common limb and this is the reason for high correlation value between Lead-I and Lead-II data. Likewise higher correlations are found between lead-II and lead-aVR ($-.9849$), between lead-II and lead-aVL (0.9905), between

TH-1102_06610204

lead-aVR and lead-aVL ($-.9517$) and among V2 to V6. Thus the plots between pairs of lead as in Fig.4.1 and correlations values indicate the redundancies present between leads. Thus there is possibility of dimension reduction by applying PCA on MECG signals.

4.2 Proposed Multiscale Principal Component Analysis

Multiscale wavelet decomposition of an ECG signal produces approximation coefficients and detail coefficients at different scales. Bandwidth of wavelet decomposition level j, ΔF_j, can be decided by Equation (2.6) provided the sampling frequency is given [111]. The wavelet coefficients, $w_{j,k}$, are estimated as inner product of signal and dilated and shifted version of wavelet which is given by Equation (2.3). After L level Multi-resolution Decomposition (MRD), wavelet coefficients, $w_{j,k}$, are found in '$L+1$' subbands. At each wavelet scale the number of wavelet coefficients are the same for all n number of ECG channels. So, this gives '$L+1$' subband matrices in wavelet domain. For multichannel representation, the approximation coefficients are denoted as $w^i_{L,k}$, where i is channel number ($i = 1, 2, ..., n$), L is the decomposition level or subband number and k is the number of coefficients at L^{th} scale. Similarly, the details coefficients are $w^i_{j,k}$. Therefore multiscale ECG wavelet subband matrix for approximations subband is given as $\mathbf{A_L}$ (Equation (3.12)). Similarly, for multichannel ECG wavelet subband matrices for details coefficients is given as $\mathbf{D_j}$ (Equation (3.13))

Fig.4.2 shows three ECG channels and their subband signals after 6 level wavelet decomposition by Daubechies 9/7 biorthogonal mother wavelet. In Fig.4.2(a), lead-I signal and signal components at different wavelet scales are produced. Similarly, in Fig.4.2(b) lead-aVR and Fig.4.2(c) lead-V6 signals are shown with subband signals. It is noticed that cA6 subband reflects the parts of low frequency components such as P-wave and T-wave. cD6 and cD5 subbands show the lower frequency part of QRS complexes with higher frequency part of T-wave. cD4 and cD3 subbands show the significant higher frequency part of QRS complexes. cD2 and cD1 Subbands contain some higher frequency part of QRS complexes and noise. It is observed that across the subbands there are similarities between segmented signal components. It is expected to get higher correlation between similar subbands of different channels. If multivariate matrices are formed at wavelet scales, it may help process subband signals more efficiently.

If relative energy contribution of wavelet subbands for an ECG signal is evaluated, it can show

TH-1102_06610204

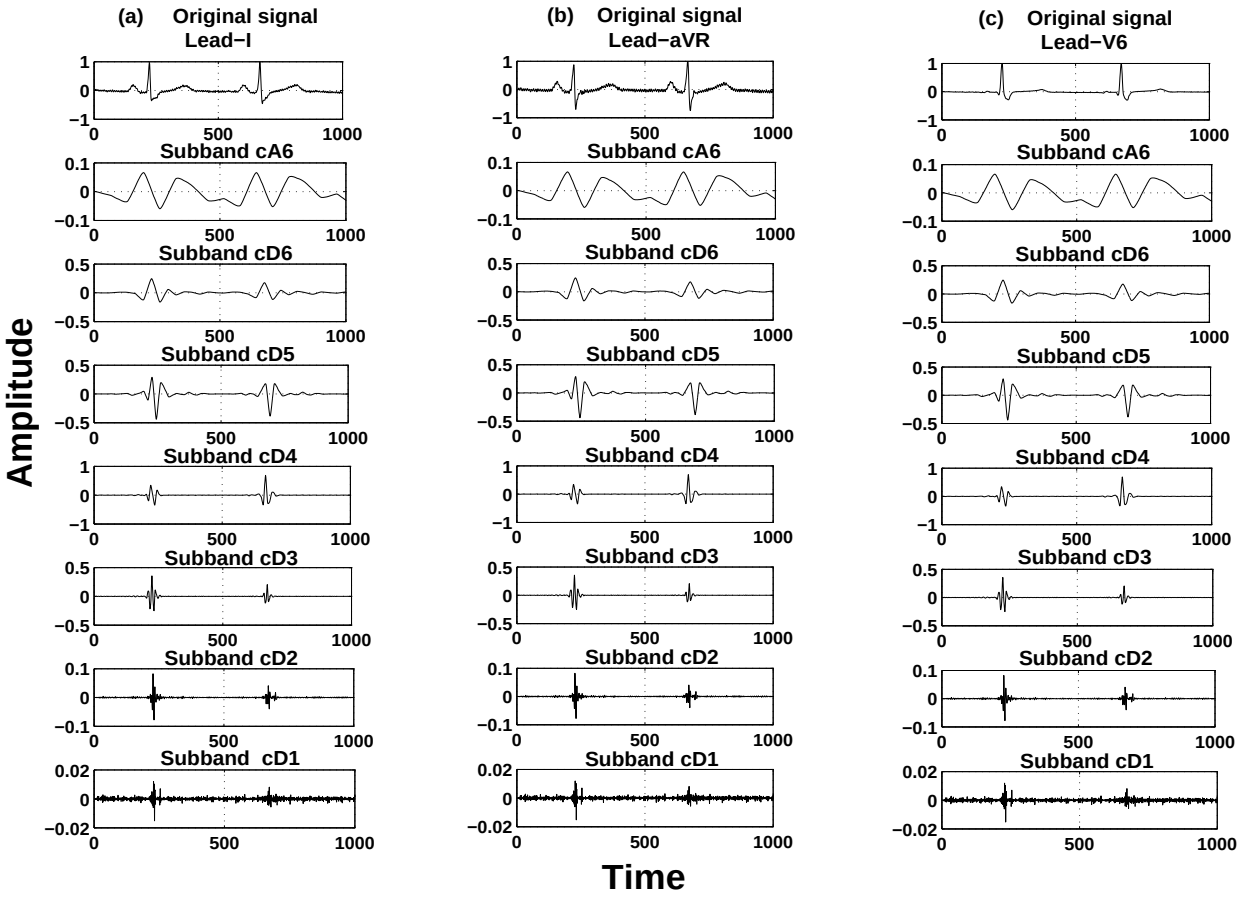

Figure 4.2: Multiscale time domain signals of 3 different leads (Lead-I, Lead-aVR and Lead-V6). Wavelet subband signals are reconstructed using 9/7 biorthogonal wavelet filter. In panel (a) original and reconstructed subband signals of Lead-I, (b) original and reconstructed subband signals of Lead-aVR and (c) original and reconstructed subband signals of Lead-V6 are reproduced. In this, CSE multilead measurement library, dataset-M01-041, with six wavelet decomposition levels is used.

us the relative importance of the subbands in terms of energy. Energy contribution efficiency (ECE) is defined as in Equation (3.1) [71, 102, 159]. In Fig.4.3, for standard 12 lead ECG signals, energy contributions of wavelet subband signals are shown. A typical MECG signal is decomposed with six level wavelet decomposition using 9/7 biorthogonal wavelet filters. It is noticed that for all the leads, ECE is higher for the higher order wavelet subbands. Energy contribution of the lowest order subbands are less. It shows that the 'PQRST' morphologies mainly exists in higher order subbands. The P-wave and T-wave are lowest frequency components.

TH-1102_06610204

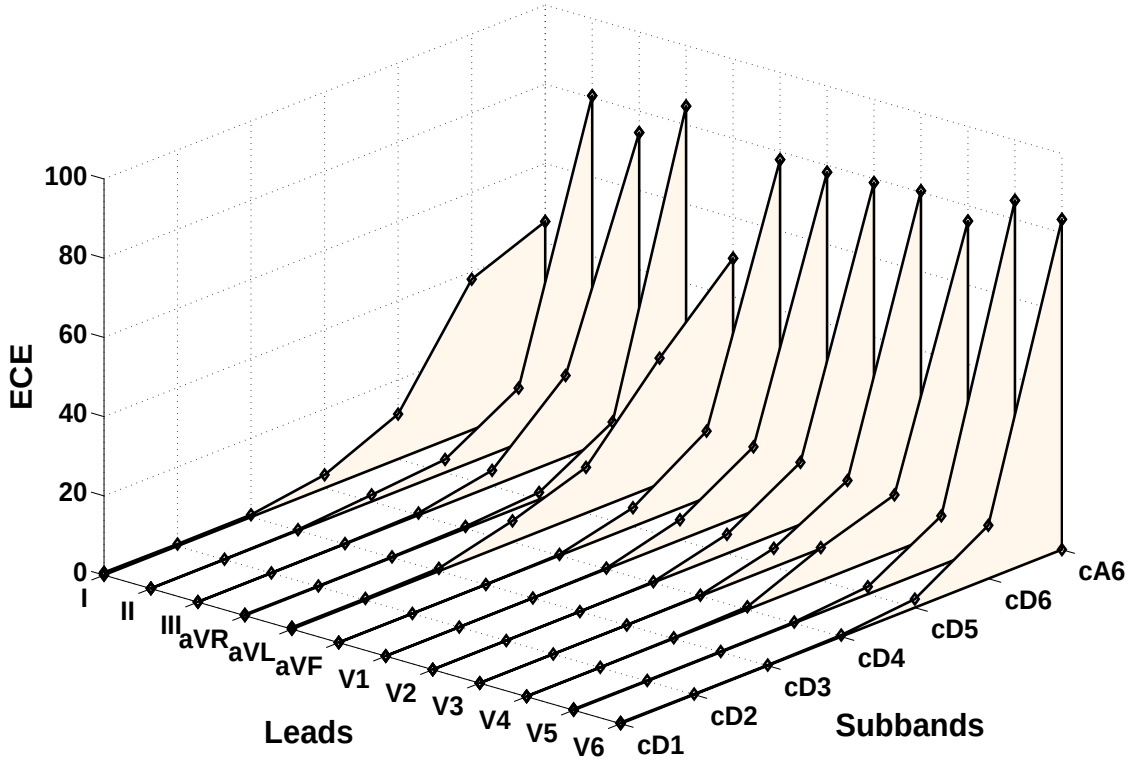

Figure 4.3: ECE for Multichannel ECG signals with six level wavelet decomposition.

.

4.2.1 Multiscale Multivariate Energy Contribution Efficiency

The analysis of ECE for 12 lead ECG [159], [160] for six level wavelet decomposition, suggests the relative importance of subbands. This analysis is based on single lead basis. It is seen that for all ECG leads, higher order wavelet subbands (cA6, cD6, cD5 and cD4) contribute significant amount of energies whereas lower order subbands (cD3, cD2 and cD1) have a very small fraction of total energy. For multiscale subband matrices relative energy contribution of individual matrix is proposed as multiscale multivariate energy contribution efficiency (MMECE). For approximation

TH-1102_06610204

band, $MMECE_{A_L}$, and details, $MMECE_{D_j}$, are defined as

$$MMECE_{A_L} = \frac{tr[\mathbf{C_{A_L}}]}{tr[\mathbf{C_{A_L}}] + \sum_{j=1}^{L} tr[\mathbf{C_{D_j}}]} \tag{4.2}$$

$$= \frac{E_{A_L}}{E_{A_L} + \sum_{j=1}^{L} E_{D_j}} \tag{4.3}$$

$$MMECE_{D_j} = \frac{tr[\mathbf{C_{D_j}}]}{tr[\mathbf{C_{A_L}}] + \sum_{j=1}^{L} tr[\mathbf{C_{D_j}}]} \tag{4.4}$$

$$= \frac{E_{D_j}}{E_{A_L} + \sum_{j=1}^{L} E_{D_j}} \tag{4.5}$$

where $\mathbf{C_{A_L}}$, E_{A_L} and $\mathbf{C_{D_j}}$, E_{D_j} represent covariance matrices and energies in approximation and details matrices respectively. The energy is derived from the trace of covariance matrix. Fig.4.4,

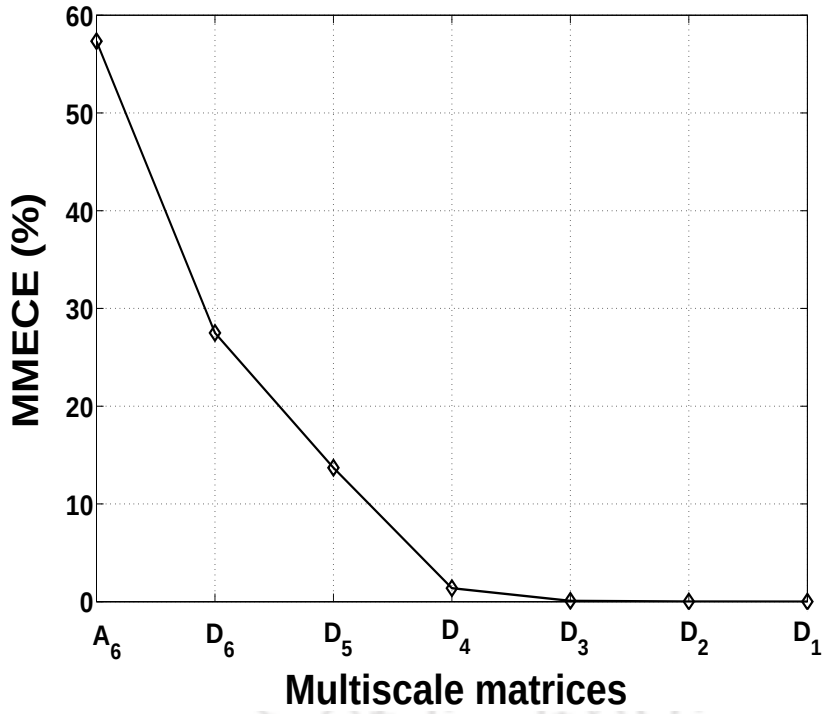

Figure 4.4: Energy contribution of multiscale multivariate matrices in terms of MMECE for 12 lead ECG. Data set is taken from CSE multilead measurement library and wavelet decomposition using six level Daubechies 9/7 biorthogonal wavelet filters is used.

shows the relative energy contribution by multiscale matrices. The matrices $\mathbf{A_6}$, $\mathbf{D_6}$, $\mathbf{D_5}$ and $\mathbf{D_4}$ contribute most of the energy whereas $\mathbf{D_3}$, $\mathbf{D_2}$ and $\mathbf{D_1}$ contain small amount of energy. It is observed, MMECE in multivariate analysis (Fig.4.4) and ECE in single lead analysis (Fig.4.3), follow similar

TH-1102_06610204

energy distribution. Higher order subband matrices contain vital clinical signal components which contribute more energies. Lower energy content of lower order subband matrices may be due to non-clinical components. The wavelet subbands cD1, cD2 and cD3 are usually remained outside of normal ECG spectrum [159] for 6 level wavelet decomposition. These may be subjected to dimension reduction to eliminate redundancies.

4.2.2 Multiscale Correlations

It is expected to get higher correlations and more redundancies if multichannel ECG signals are wavelet transformed to multiscale levels. Redundancies can be evaluated using covariance or correlation analysis of matrices. In Fig.4.5, correlations between leads with scatter plots are shown at D_6 wavelet matrix. It is seen that there are higher mean for correlation values than that found in original data set.

Table 4.1: Mean and variance analysis of multiscale correlation matrices, CSE database, Dataset-M01-033

Matric	Original data set	A_6	D_6	D_5	D_4	D_3	D_2	D_1
Mean	0.6296	0.6361	0.6479	0.8020	0.8160	0.5344	0.3959	0.3684
Variance	0.0982	0.0850	0.0911	0.0352	0.0299	0.0933	0.0937	0.0951

In Table 4.1, mean and variance values for correlation coefficients are shown for multiscale matrices resulted from 6 level wavelet decomposition. The mean of correlation coefficients of multichannel data set is found as 0.6296 whereas for multiscale correlation matrices, the mean values are higher for higher order scales. For A_6, D_6, D_5 and D_4 matrices the mean values of correlation coefficients are 0.6361, 0.6479, 0.8020 and 0.8160 respectively. For lower order matrices the mean values are lower. If mean values and variances of multiscale matrices are observed, it is seen that the correlations are higher and it suggests that the redundancies may be higher. As a result, it will help efficient implementation of PCA.

In wavelet domain, covariances quantify the correlations between coefficients of different leads for a subband level. Covariance matrix gives all possible correlations between pairs of leads. In Table 4.2, mean values of covariances of different matrices are shown. The mean values are evaluated taking averages of mean of covariances from 10 data sets from CSE multilead measurement library [2], with six level wavelet decomposition. Higher mean values in $\mathbf{D_5}$, $\mathbf{D_6}$ and $\mathbf{A_6}$ indicate presence of

TH-1102_06610204

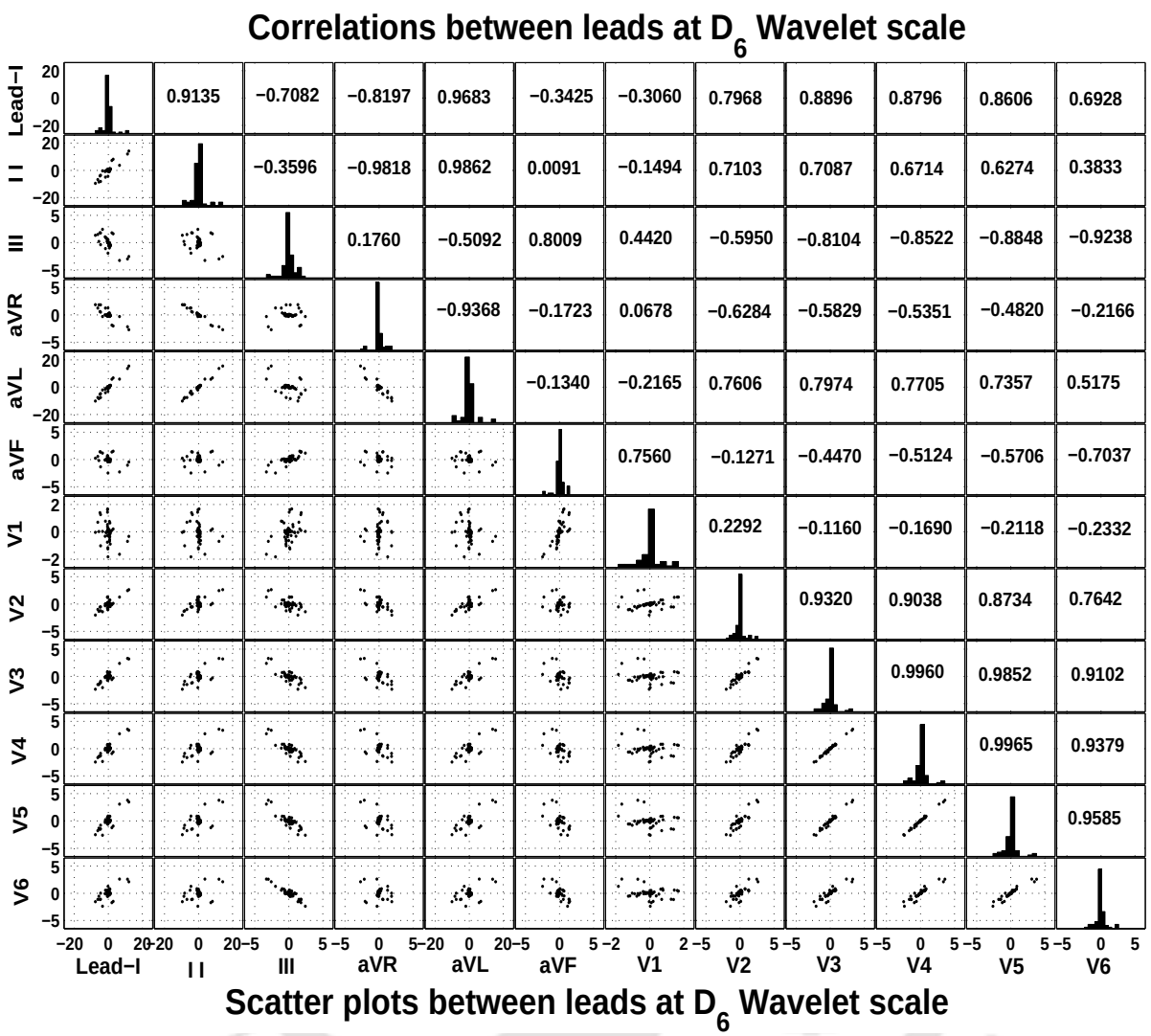

Figure 4.5: Scatter plots and correlation coefficients between leads at D_6 wavelet scale. Signals in different ECG leads are scatter plotted. The diagonal plots show the distribution of individual lead. Database used is CSE multilead measurement library, data set M01-033.

higher redundancies in these matrices. This may be due to the presence of components of MECG, such as P-waves, T-waves and part of QRS complexes. QRS-complex constitutes with Q-wave, R-wave and S-wave. The duration of Q-wave is expected to be $<$40 ms. The amplitude may be 25% of the amplitude of the R-wave. For a six level wavelet decomposition, the constituents of QRS-complex may spread over $\mathbf{D_4}$, $\mathbf{D_5}$ and $\mathbf{D_6}$ [159]. Other lower order subband matrices, $\mathbf{D_1}$, $\mathbf{D_2}$ and $\mathbf{D_3}$, show low mean values of covariances. These subbands fall normally outside the normal ECG spectrum for

Table 4.2: Mean value of covariances at multiscale matrices of data set M01-001 to M01-010, from CSE multilead measurement library.

Data set	$\mathbf{D_1}$	$\mathbf{D_2}$	$\mathbf{D_3}$	$\mathbf{D_4}$	$\mathbf{D_5}$	$\mathbf{D_6}$	$\mathbf{A_6}$
M01-001	0.0001	0.0004	0.002	0.031	0.366	0.844	1.563
M01-002	0.0001	0.0015	0.018	0.181	0.576	0.976	1.471
M01-003	0.0002	0.0013	0.012	0.073	0.224	0.260	1.036
M01-004	0.0001	0.0003	0.003	0.061	0.258	0.430	0.316
M01-005	0.0001	0.0004	0.008	0.071	0.257	0.320	0.335
M01-006	0.0001	0.0003	0.003	0.053	0.114	0.157	0.667
M01-007	0.0000	0.0004	0.007	0.131	0.326	0.566	0.420
M01-008	0.0000	0.0003	0.006	0.093	0.274	0.259	0.545
M01-009	0.0002	0.0005	0.004	0.034	0.116	0.299	0.555
M01-010	0.0000	0.0001	0.001	0.006	0.199	0.829	2.068
Average	0.0001	0.0005	0.006	0.073	0.271	0.494	0.898

a six level wavelet decomposition. Also, uncorrelated noise dominates these subbands.

Based on above investigations of correlations between leads and relative subband energies at wavelet scales for multichannel ECG signals, we propose multiscale principal component analysis as a feasible method. Fig.4.6 shows the block diagram of the proposed multiscale PCA for multichannel ECG signals. Signals of different leads are subjected to amplitude normalization and mean removal. In wavelet transform block signals are wavelet transformed using 9/7 biorthogonal wavelet filters. The coefficients are arranged in different subbands and multiscale matrices are formed at block shown as multiscale subband matrices. These matrices represent the transformed data at different wavelet scales. For a six level wavelet decomposition there is a single matrix at approximation level as A_6 and there are six matrices at detail scales as D_6, D_5, D_4, D_3, D_2, D_2 and D_1. PCA is applied on multiscale matrices at multiscale principal analysis block with proper selection of eigenvalues. The output of this block is PCA transformed data at different scales. Next to this, subband signals are reconstructed to form reconstructed subband matrices. At inverse wavelet transform block reconstruction of ECG signals are performed from recovered wavelet coefficients. The block shown in dotted line is optional. It can be used to perform quality control MSPCA.

At each wavelet scale, PCA based processing of subband data may be developed using wavelet subband matrices, A_L and D_j. Due to Multiresolution Decomposition (MRD), diagnostically important PQRST morphologies appear at different scales. To get advantage of multivariate nature and

TH-1102_06610204

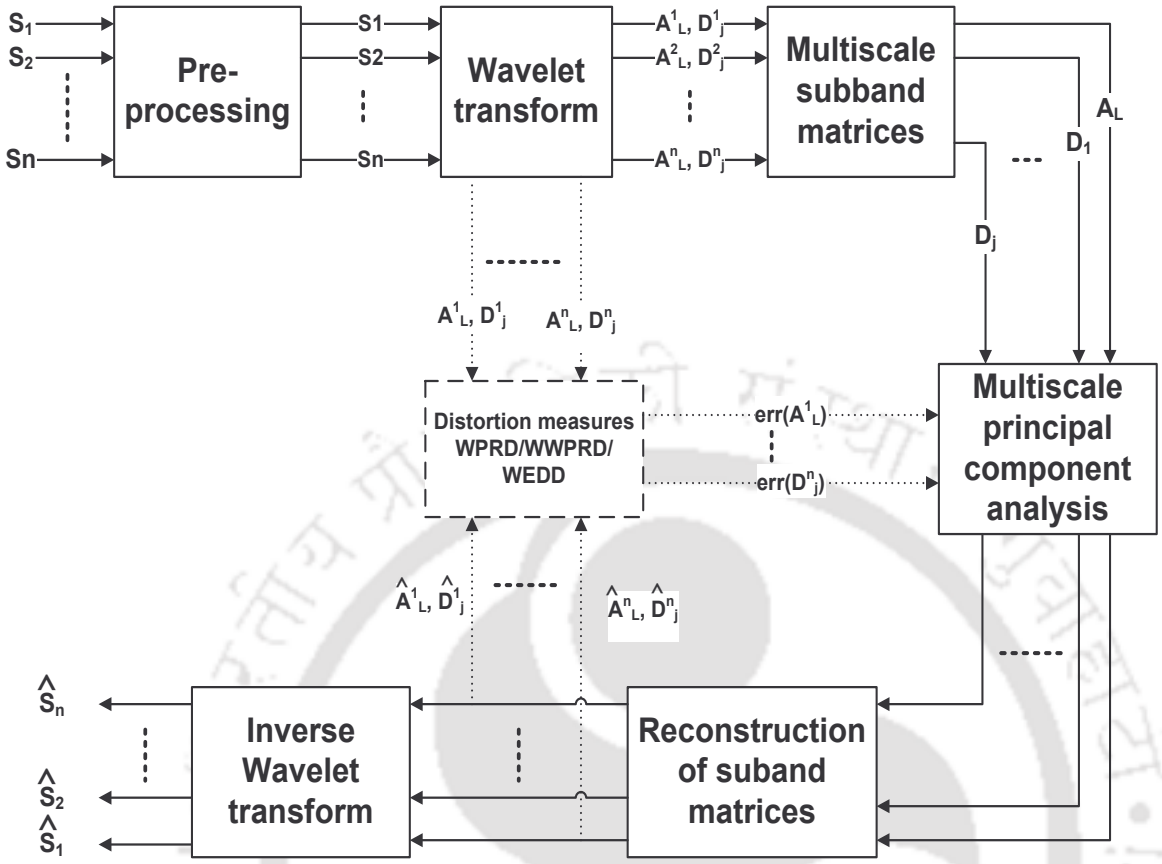

Figure 4.6: Block diagram of the proposed MSPCA. The block and lines shown with dotted line is optional and not implemented in this work. These may be incorporated to get quality control MSPCA for data reduction.

.

multiscale nature of ECG signal, it is necessary to develop a wavelet weighted multiscale PCA. This may lead to preserve the diagnostic components at selective subbands. Covariance gives the spareness of the wavelet coefficients at a particular scale. Evaluation of covariance matrices from mean removed data help find the correlations of data between dimensions (channels) of data. For approximation subband and details subband matrices, the covariance matrices from mean removed multiscale multivariate matrices are evaluated as

$$\mathbf{C_{A_L}} = \frac{1}{(n-1)}([\mathbf{A_L}][\mathbf{A_L}]^T) \tag{4.6}$$

$$\mathbf{C_{D_j}} = \frac{1}{(n-1)}([\mathbf{D_j}][\mathbf{D_j}]^T) \tag{4.7}$$

TH-1102_06610204

where n is the number of ECG channels.

These square symmetric covariance matrices exploit all the possible correlations at different wavelet scales between coefficients of all channels. The diagonal terms are variances of coefficients and off diagonal terms are correlation between coefficients of all possible pairs of channels at a particular wavelet scale. The main objective is to minimize redundancy measured by covariance and to maximize the signal measured by variance [161]. Higher covariance values indicate higher redundancies. To solve this, eigen-decomposition of above covariance matrices can be performed. If covariance matrix is diagonalized, eigenvectors and eigenvalues at different scales can be obtained.

The eigenvalue decomposition of these covariance matrices results

$$\mathbf{C_{A_L}V_{A_L}} = \mathbf{V_{A_L}\Lambda_{A_L}} \tag{4.8}$$

$$\mathbf{C_{D_j}V_{D_j}} = \mathbf{V_{D_j}\Lambda_{D_j}} \tag{4.9}$$

where $\mathbf{V_{A_L}}$, $\mathbf{V_{D_j}}$ and $\mathbf{\Lambda_{A_L}}$, $\mathbf{\Lambda_{D_j}}$ are the eignevectors and eigenvalues for matrices of approximation and details subband matrices respectively. Eigenvector matrices $\mathbf{V_{A_L}}$ and $\mathbf{V_{D_j}}$ diagonalize the covariance matrix $\mathbf{C_{A_L}}$ and matrices $\mathbf{C_{D_j}}$ as

$$\mathbf{V_{A_L}C_{A_L}V_{A_L}^{-1}} = \mathbf{\Lambda_{A_L}} \tag{4.10}$$

$$\mathbf{V_{D_j}C_{D_j}V_{D_j}^{-1}} = \mathbf{\Lambda_{D_j}} \tag{4.11}$$

$\mathbf{\Lambda_{A_L}}$ and $\mathbf{\Lambda_{D_j}}$ are the diagonal matrices with eigenvalues as diagonal elements. Eigenvectors and eigenvalues appear in pairs. Eigenvalues are arranged in descending order and accordingly the corresponding eigenvectors. The eigenvectors with corresponding higher eigenvalues produce the principal components. Thus these orthonormal eigenvectors represent the signals in the direction of maximum variances. The reduction of dimension depends on the number of eigenvalues selected. Ordered eigenvalues in approximation and details subband matrices are

$$\lambda_{A_{L_1}}, \lambda_{A_{L_2}}, \cdots, \lambda_{A_{L_n}} \tag{4.12}$$

$$\lambda_{D_{j_1}}, \lambda_{D_{j_2}}, \cdots, \lambda_{D_{j_n}} \tag{4.13}$$

The eigenvectors selected based on significant eigenvalues for multivariate data set will help form

TH-1102_06610204

feature vector's matrices F_{A_L} and F_{D_j} for approximation and details scales respectively. F_{A_L} and F_{D_j} are constructed by selected significant eigenvectors from all eigenvectors and forming a matrix with eigenvectors in the column.

The feature vector matrices play important role for data reduction. In conventional PCA, eigenvalues are arranged in descending order and accordingly the corresponding eigenvectors. Similarly. in MSPCA the new data set can be derived out of feature vectors and original mean removed data sets as

$$\mathbf{R_{A_L}} = \mathbf{A_L} \times F_{A_L} \tag{4.14}$$

$$\mathbf{R_{D_j}} = \mathbf{D_j} \times F_{D_j} \tag{4.15}$$

where $\mathbf{R_{A_L}}$ is dimension reduced data set for approximation and $\mathbf{R_{D_j}}$ is dimension reduced data set for details subbands. To get the reconstructed subband matrices from the dimension reduced data set, following matrix operation is performed as

$$\widehat{\mathbf{A_L}} = \mathbf{R_{A_L}} \times F_{A_L}^T \tag{4.16}$$

$$\widehat{\mathbf{D_j}} = \mathbf{R_{D_j}} \times F_{D_j}^T \tag{4.17}$$

where $\widehat{\mathbf{A_L}}$ is the reconstructed approximation subband matrix and $\widehat{\mathbf{D_j}}$ are the reconstructed details subband matrices. To get back the reconstructed signal matrix, $\mathbf{S}$, inverse wavelet transform is performed.

4.2.3 Selection of Principal Components

Eigen-decompositions of covariance matrices produce the eigenvalues at different wavelet scales. The selection of eigenvalues after arranging it in descending order is an important part in PCA analysis. There are many methods suggested in literature for the selection of eigenvalues for dimension reduction. Generally, to select the subset of principal components (PCs), cumulative percentage of total variation of variances from 70% to 90% [124] is taken as practice. The selected eigenvectors form the feature vectors which represent the principal components (PCs) [162]. The data reduction depends on the number of PCs retained for further processing.

4.2.3.1 Selection of PC based on Wavelet Subband Weights

Most of the energy of ECG signal remain in higher order Wavelet subbands and hence the relative energies measured in energy contribution efficiency (ECE) is found higher in these higher order subbands [159], [102], [71]. Due to multi-resolution decomposition, the QRS-complex, the P-and the T-waves are remained in higher order subbands and it is clinically essential to preserve these diagnostic features. So, there is a need to assign weights to MSPCA at different wavelet subband matrices as they contain the signal components.

The choice of number of significant eigenvalues decides the number of PCs. The eigenvalues at approximation subband matrix are $\lambda_{A_{L_1}}, \lambda_{A_{L_2}}, \cdots, \lambda_{A_{Ln}}$ and at details subband matrices are $\lambda_{D_{j_1}}, \lambda_{D_{j_2}}, \cdots, \lambda_{D_{jn}}$.

It is proposed to assign weights to select number of PC at wavelet subband matrices as

$$W_{A_L} = \frac{\sum_{i=1}^{n} \lambda_{A_{L_i}}}{\sum_{i=1}^{n} \lambda_{A_{L_i}} + \sum_{j=1}^{L} \sum_{i=1}^{n} \lambda_{D_{j_i}}} \tag{4.18}$$

$$W_{D_j} = \frac{\sum_{i=1}^{n} \lambda_{D_{j_i}}}{\sum_{i=1}^{n} \lambda_{A_{L_i}} + \sum_{j=1}^{L} \sum_{i=1}^{n} \lambda_{D_{j_i}}} \tag{4.19}$$

where W_{A_L} and W_{D_j} are the weights for approximation subband matrix and details subband matrices respectively. In Equation (4.18) and Equation (4.19), weights for approximation and details subband matrices are derived from energy features. An eigenvalue for a subband matrix is given a unity gain if it is greater than proposed weight else it is set equal to zero. Eigen values in a matrix are selected if their values get unity gain. So, these weights for subband matrices decide the number of principal components. Thus the dimensions to be reduced are decided based on these weights. From Multiresolution Analysis (MRA) of ECG [159], [102], [71], it is seen that subbands $D1$, $D2$ and $D3$ may contain redundant signal with lower ECE values. Higher order subbands contain higher signal energies. To preserve the diagnostic components lying in higher order subbands, the PCA is applied at the lower order subband matrices with proposed weights to select number of PCs.

4.2.3.2 Selection of PC based on Fractional Energy

The eigenvectors with corresponding higher eigenvalues produce the principal components. Thus these orthonormal eigenvectors represent the signals in the direction of maximum variances. The

TH-1102_06610204

reduction of dimension depends on the number of eigenvalues selected. As ordered eigenvalues in approximation and details matrices are $\lambda_{A_{L_1}}, \lambda_{A_{L_2}}, \cdots, \lambda_{A_{L_n}}$ and $\lambda_{D_{j_1}}, \lambda_{D_{j_2}}, \cdots, \lambda_{D_{j_n}}$, cumulative sum of energies by all multiscale matrices can be written as

$$S_\sigma = \sum_{i=1}^{n} [\lambda_{A_{L_i}}] + \sum_{j=1}^{L} \sum_{i=1}^{n} [\lambda_{D_{j_i}}] \tag{4.20}$$

The Average Fractional Energy Contribution (AFEC) of the eigenvalues at approximation and details subband matrices are defined as

$$\eta_{A_L} = \frac{\sum_{i=1}^{n} \lambda_{A_{L_i}}}{S_\sigma} \Big/ n \tag{4.21}$$

$$\eta_{D_j} = \frac{\sum_{i=1}^{n} \lambda_{D_{j_i}}}{S_\sigma} \Big/ n \tag{4.22}$$

where η_{A_L} and η_{D_j} are AFEC by eigenvalues of L^{th} approximation and j^{th} detail subband matrices respectively. The selection of principal components are based on AFEC by individual eigenvalues as

$$\lambda_{A_{L_i}} = 1 \; ; \quad if \quad \lambda_{A_{L_i}} > \eta_{A_L} \tag{4.23}$$

$$= 0 \; ; \quad else \tag{4.24}$$

$$\lambda_{D_{j_i}} = 1 \; ; \quad if \quad \lambda_{D_{j_i}} > \eta_{D_j}; \; \forall \; j \tag{4.25}$$

$$= 0 \; ; \quad else \tag{4.26}$$

In this work, it is proposed to select eigenvalues which are greater than AFEC. This will decide the number of principal components (PC). After PCA operation at wavelet scales, the transformed coefficients are uniform quantized and Huffman encoded [83], [163], [164] for multichannel compression.

4.3 Proposed MSPCA based Compression Method

The proposed compression method based on MSPCA has four major steps. First, the covariance matrices are estimated from multiscale matrices. In the second step, the covariance matrices are subjected to eigenvalue decomposition. Third, the eigenvalues are selected based on a threshold derived from fractional energy contribution of eigenvalue. The covariance matrices ($\mathbf{C_{A_L}}$ and $\mathbf{C_{D_j}}$) from mean removed multiscale multivariate matrices are evaluated using Equation 4.6 and Equation 4.7. The eigenvalue decomposition of these covariance matrices by Equation 4.8 and Equation

4.9 results eignevectors matrices $\mathbf{V_{A_L}}$, $\mathbf{V_{D_j}}$ and eigenvalues for matrices, $\mathbf{\Lambda_{A_L}}$, $\mathbf{\Lambda_{D_j}}$ for approximation and details subband matrices respectively. Eigenvector matrices $\mathbf{V_{A_L}}$ and $\mathbf{V_{D_j}}$ diagonalize the covariance matrix $\mathbf{C_{A_L}}$ and matrices $\mathbf{C_{D_j}}$ as $\mathbf{V_{A_L}C_{A_L}V_{A_L}^{-1}} = \mathbf{\Lambda_{A_L}}$ and $\mathbf{V_{D_j}C_{D_j}V_{D_j}^{-1}} = \mathbf{\Lambda_{D_j}}$. Thus we get diagonal matrices, $\mathbf{\Lambda_{A_L}}$ and $\mathbf{\Lambda_{D_j}}$ with eigenvalues as diagonal elements. Eigenvectors and eigenvalues appear in pairs. Eigenvalues are arranged in descending order and accordingly the corresponding eigenvectors. With selected PCs, PCA operation gives dimension reduced data set. Finally, in fourth step, PCA coefficients are uniform quantized and Huffman encoded to achieve multichannel compression.

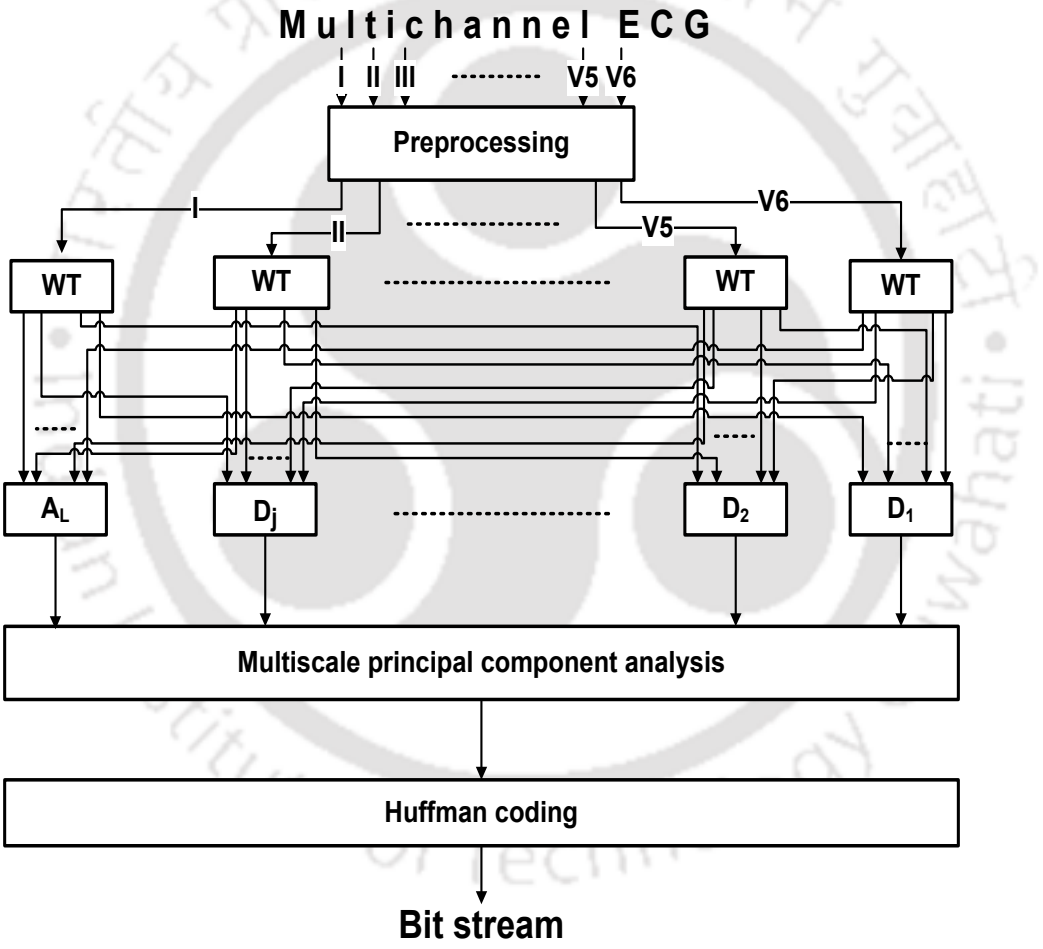

Figure 4.7: Block diagram of proposed compression method.

In Fig.4.7, the proposed compression method based on MSPCA and Huffman coding is shown. After preprocessing the multichannel ECG signals, each channel is wavelet transformed (WT) applying

TH-1102_06610204

same dyadic analysis filter bank. Re-arranging subbands of all channels, wavelet subband matrices, A_L and D_j, are formed. MSPCA analysis on these matrices are carried out. The selection of PC is based on the method proposed in Section 4.2.3.2. Number of PC decides the dimension reduction which results the reduction in samples. The PCA coefficients are uniform quantized and Huffman coded Huffman encoded [83], [163], [164]. This gives the compressed bit stream.

For reconstruction of the original signals, Huffman encoded PCA coefficients are decoded using Huffman decoder. To find the PCA coefficients for signal reconstruction a PCA reconstruction operation is performed. This gives the wavelet coefficients which represent the original signals. These wavelet coefficients are passed through the same wavelet reconstruction filter.

4.4 Results and Discussion

The multichannel ECG data from CSE multilead measurement library [2] is taken for experiment. From each channel data, 4096 samples are selected as a block. Data blocks are subjected to amplitude normalization and mean removal. Data matrix is formed with samples in rows and channels in columns. So, a matrix with dimensions $[4096 \times 12]$ of multichannel ECG is created. To create the subband matrices, the wavelet decomposition using Daubechies 9/7 biorthogonal wavelet filters up to six levels are used for each column data. The coefficients after wavelet decomposition are arranged to form seven subband matrices.

4.4.1 Results for Multiscale PCA

Table 4.3: Covariance values for all lead signal at scale D_1, CSE database, Dataset-M01-033

Leads	I	II	III	aVR	aVL	aVF	V1	V2	V3	V4	V5	V6
I	0.714	0.325	-0.394	-0.010	0.584	0.002	0.008	0.019	0.037	0.037	0.054	0.020
II	0.325	0.749	0.107	-0.180	0.656	0.021	0.021	0.032	0.036	0.034	0.044	0.074
III	-0.394	0.107	0.356	-0.078	-0.137	0.009	0.004	0.001	-0.011	-0.012	-0.021	0.018
aVR	-0.010	-0.180	-0.078	0.051	-0.122	-0.006	-0.005	-0.007	-0.006	-0.005	-0.006	-0.019
aVL	0.584	0.656	-0.137	-0.122	0.734	0.015	0.018	0.031	0.043	0.042	0.058	0.058
aVF	0.002	0.021	0.009	-0.006	0.015	0.017	0.021	0.011	0.006	0.005	0.005	0.002
V1	0.008	0.021	0.004	-0.005	0.018	0.021	0.047	0.025	0.016	0.013	0.012	0.007
V2	0.019	0.032	0.001	-0.007	0.031	0.011	0.025	0.027	0.019	0.016	0.014	0.006
V3	0.037	0.036	-0.011	-0.006	0.043	0.006	0.016	0.019	0.022	0.017	0.016	0.007
V4	0.037	0.034	-0.012	-0.005	0.042	0.005	0.013	0.016	0.017	0.022	0.018	0.008
V5	0.054	0.044	-0.021	-0.006	0.057	0.005	0.012	0.014	0.016	0.018	0.025	0.009
V6	0.020	0.074	0.018	-0.019	0.058	0.002	0.007	0.006	0.007	0.008	0.009	0.325

In Fig.4.8, subband coefficients of different leads collected in subband matrix D_1 are plotted in

TH-1102_06610204

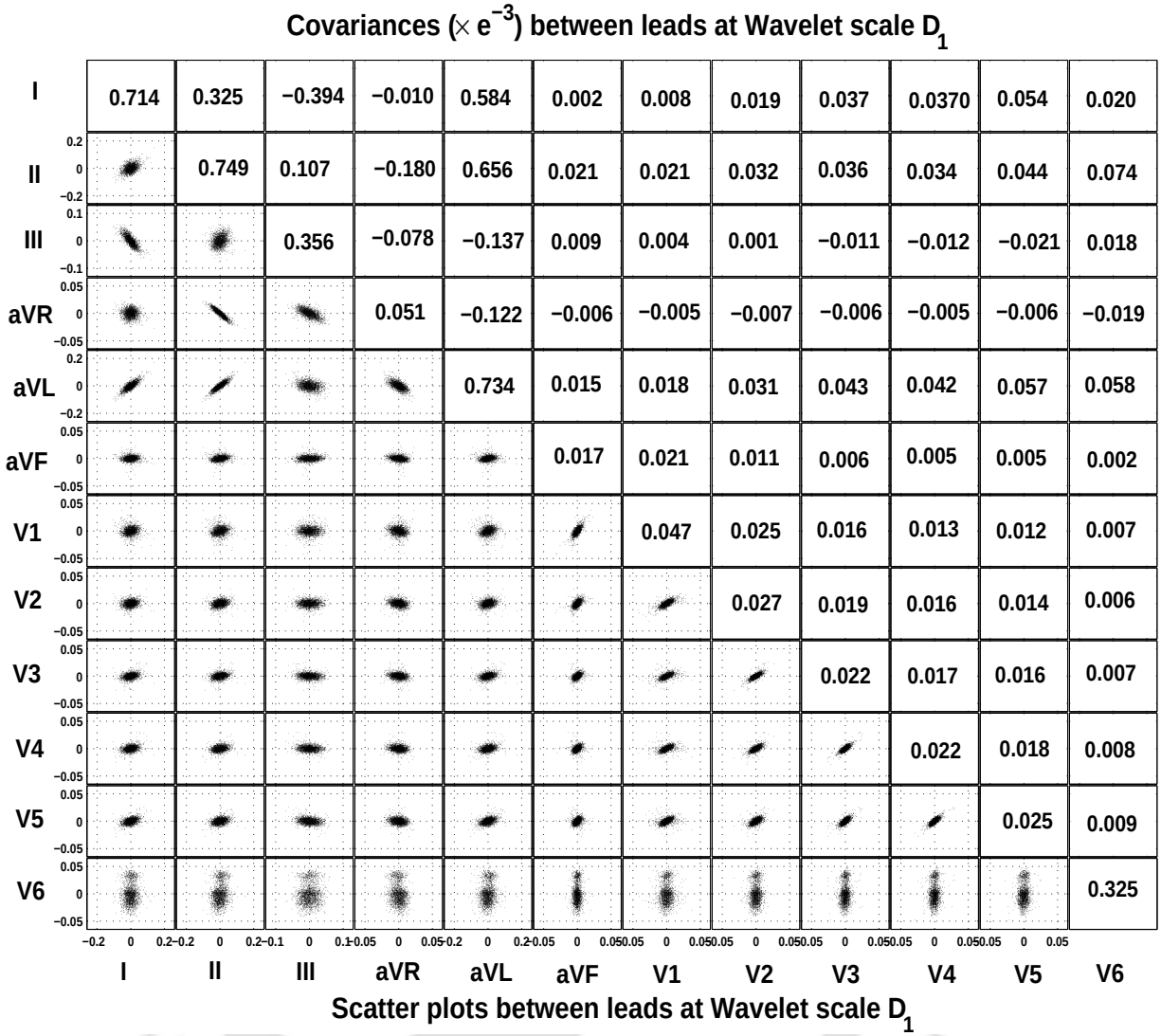

Figure 4.8: Scatter matrix plot for multichannel subband matrix D_1. Database used CSE multilead measurement library, data set M01-033 with 6 level wavelet decomposition.

.

scatter plot matrix format. It shows the redundancy between different channels at D_1 wavelet scale. The diagonal elements represent variances of the ECG leads at D_1 wavelet scale. Lower triangular elements show the scatter plots between signals of different leads at wavelet scale D_1. The upper triangular elements show the covariance values between data of different leads at the lowest wavelet scale. Covariances quantify the linear relation between variables. Higher numerical values of covariances like 0.584 (between lead-I and lead-aVL), 0.656 (between lead-II and lead-aVL), 0.325 (between lead-I and lead-II) and -0.394 (between lead-I and lead-III) imply linear relations between variables.

TH-1102_06610204

Low covariances such as between lead-I and lead-aVF (0.002), lead-III and lead-V1 (0.004), lead-aVR and lead-V1 (0.005), lead-aVF and lead-V3 (0.006) and lead-V1 and lead-V6 (0.007) in Fig.4.8 indicate weak linear relations between variables. Like-wise for other subband matrices the covariance values and scatter plot matrices are examined in the experiments. The values indicate possibility of data reduction. Also, the scatter plot matrices from D_1 to D_6 and A_6 give us the idea about the linear relation between variables and amount of redundancies present between variables at different wavelet scales. Further to analyze the multiscale covariance matrices for inter-channel redundancies, means and variances are evaluated and they are shown in Table 4.4.

Table 4.4: Mean and variance analysis of multiscale covariance matrices, CSE database, Dataset-M01-033

Matric	D_1	D_2	D_3	D_4	D_5	D_6	A_6
Mean	.000044	0.0002	0.0030	0.0808	0.6844	0.9425	1.4752
Variance	0.0482	0.0392	0.0400	0.0649	0.0452	0.0442	0.0448
$\frac{Mean}{Variance}$	0.0009	0.0050	0.0753	1.2437	15.1519	21.3406	32.9053

The mean correlation value, 0.000044, is lowest at lowest order wavelet scale and it increases gradually to the highest order scale as 1.4752. The ratios between the mean value and the variance value at higher scale matrices are higher and at lower order scale these values are lower. Since this is evaluated on covariance matrices, it indicates that the higher order wavelet scale have more redundant signal information compared to the lower order scales. Thus, more dimensions can be reduced in these scales. But, clinically important diagnostic components are present at higher order scales. Multichannel multiscale matrices and their eigen-analysis reveal that the sum of eigenvalues is higher for matrices comprising higher order wavelet scales. The sum follows the order as $A_6 > D_6 > D_5 > D_4 > D_3 > D_2 > D_1$. This is due to more signal energy in higher order scales.

In Table 4.5, ordered eigenvalues for all multiscale wavelet matrices are shown. It is observed that matrices which are formed taking lower order subband coefficients contribute less compared to the other higher order subband matrices. The magnitudes of first eigenvalues of multiscale matrices A_6, D_6, D_5, D_4, D_3, D_2 and D_1 are 72.6252, 34.7043, 17.9600, 0.0764, 0.0085 and 0.0019 respectively. So, higher order wavelet matrices essentially important in terms of clinical information. Since lower order matrices have less contribution, there is possibility to reduce more dimensions without losing significant information. Though higher order matrices exhibit higher correlation between leads, it may

Table 4.5: Eigenvalues of multiscale wavelet matrices

Eigenvalues at different scale, CSE database, Dataset-M01-033						
A_6	D_6	D_5	D_4	D_3	D_2	D_1
72.6252	34.7043	17.9600	1.7425	0.0764	0.0085	0.0019
6.3740	3.0118	0.8564	0.1383	0.0196	0.0049	0.0008
1.2290	0.7181	0.3518	0.0267	0.0166	0.0008	0.0003
0.1269	0.1006	0.0249	0.0142	0.0041	0.0005	$9.38e^{-005}$
0.0129	0.0072	0.0082	0.0032	0.0005	0.0002	$2.95e^{-005}$
0.0073	0.0021	0.0018	0.0008	0.0004	$5.37e^{-005}$	$8.74e^{-006}$
0.0052	0.0004	0.0003	0.0002	0.0003	$2.48e^{-005}$	$5.94e^{-006}$
0.0012	0.0002	0.0001	0.0002	$3.83e^{-005}$	$1.15e^{-005}$	$4.42e^{-006}$
0.0004	$4.32e^{-005}$	$1.44e^{-005}$	$1.21e^{-005}$	$9.06e^{-006}$	$5.47e^{-006}$	$3.83e^{-006}$
$3.30e^{-005}$	$1.12e^{-005}$	$7.04e^{-006}$	$3.60e^{-006}$	$3.37e^{-006}$	$2.93e^{-006}$	$1.79e^{-006}$
$9.57e^{-006}$	$8.31e^{-007}$	$1.32e^{-006}$	$1.62e^{-006}$	$2.07e^{-006}$	$1.66e^{-006}$	$1.19e^{-006}$
$8.48e^{-007}$	$4.39e^{-007}$	$3.09e^{-007}$	$2.13e^{-007}$	$2.51e^{-007}$	$2.28e^{-007}$	$1.62e^{-007}$

not be correct to reduce dimensions due to more clinical information content. This is required to ensure that the most significant clinical information to be retained in the signal.

In Fig.4.9, eigenvalues are plotted against the PC number (in log scale) for three lower order subband matrices, D_1, D_2 and D_3. These eigenvalues are ordered similar to that of conventional PCA. It is evident from the figure that the significant information lies only with a few number of PCs. So, the selection of number of PCs in an optimum way can preserve the clinical components and hence the data reduction may be achieved with required signal fidelity. Thus the selection of subset of PCs may play an important rule. As proposed in Section 4.2.3.1, equation (4.18) and (4.19), can provide weights to select the number of PCs. Accordingly, subset of PC are derived for data reduction.

In Fig.4.10, original and reconstructed signals are shown from standard MECG signal from CSE multilead measurement library, dataset-M01-033. In panel (a) and (b) original and reconstructed signals of Lead-I are plotted. The reconstructed signal shows all the clinical components retained with essential diagnostic information. In panel (c) and (d), Lead-III signals are plotted and reconstruction shows an acceptable quality. Similarly, panels (e) and (f) and panels (g) and (h) show Lead-V1 and Lead-aVL signals respectively. The reconstructed signals show minimum distortion with all clinical components present. In panel (d), at 'QRS' complex the signal is slightly smoothed out. This may be due to the noise present in the original data set and the algorithm also shows the denoising effect. This is due to the removal of eigen vectors with lower energy. Though the dataset is a pathological

TH-1102_06610204

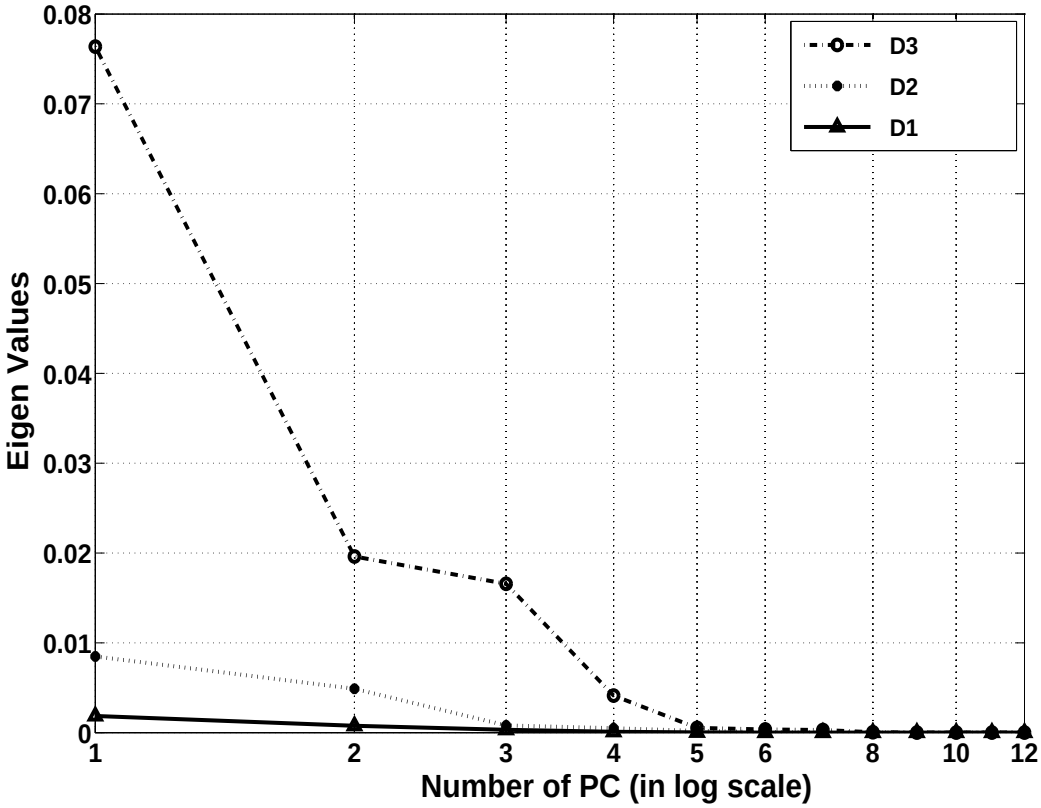

Figure 4.9: Eigenvalues plotted against the number of principal components for three wavelet subband matrices D_1, D_2 and D_3. Database used is CSE multilead measurement library, data set M01-033 with 6 level wavelet decomposition.

.

one and PQRST morphologies show a slight variation from an ideal ECG, still the proposed MSPCA preserve all the diagnostically essential components. The critical and vital clinical information are retained in reduced data set by using the proposed MSPCA.

4.4.1.1 Evaluation of Signal Distortion

To measure distortion on clinical or diagnostic information in processed ECG signal, error measures are used for evaluation of quality of processed ECG signal. Percentage root mean square difference (PRD) is widely used because of its simplicity [93, 138]. In wavelet based method, Wavelet Weighted PRD (WWPRD) is defined [109]. In [71], a Wavelet Energy based Diagnostic Distortion (WEDD) measure is proposed.

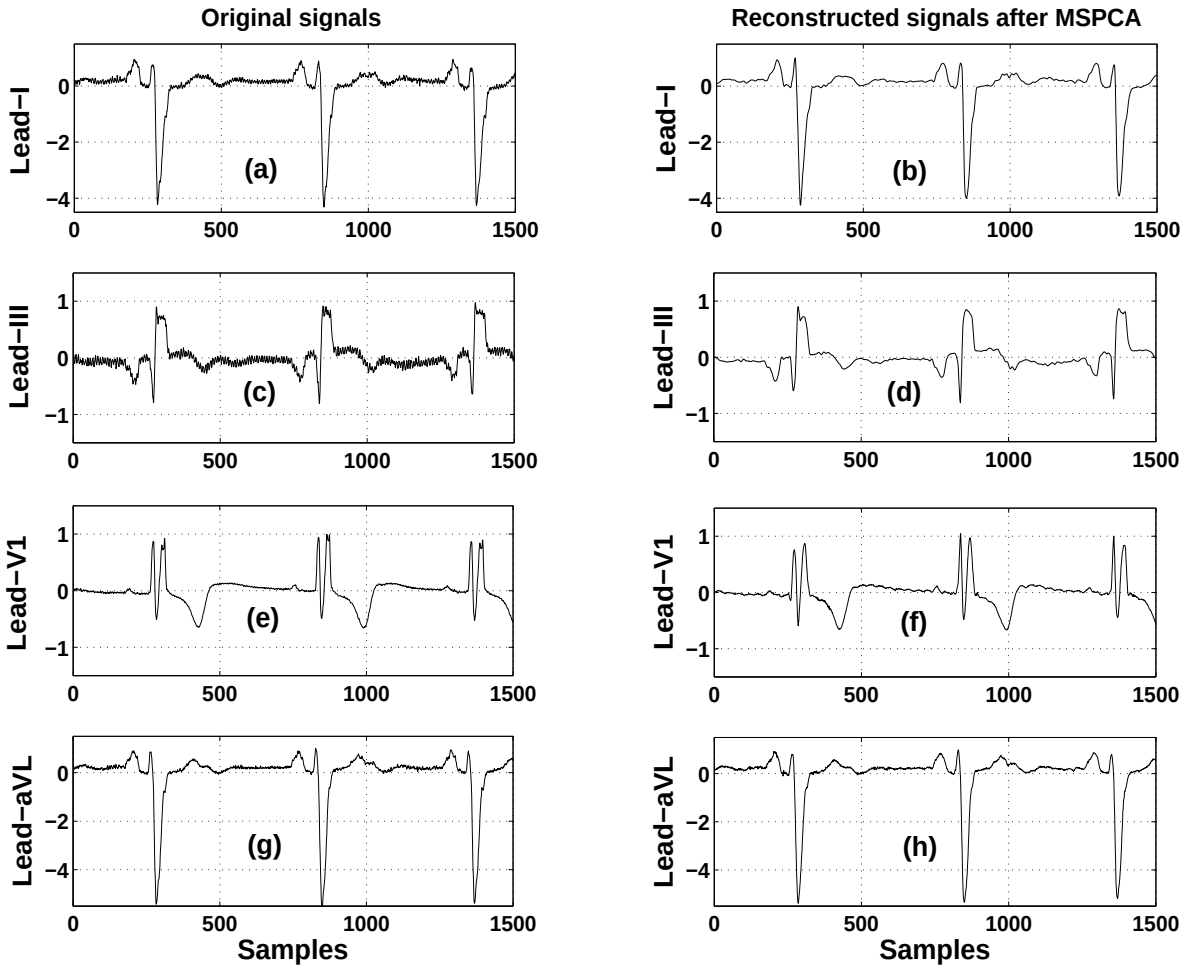

Figure 4.10: Reconstructed signals after applying proposed wavelet subband weighted MSPCA. To retain diagonstic component intact in the processed signal, only 3 lower order subbands are considered for MSPCA. In panel (a) and (b) Lead-I, (c) and (d) Lead-III, (e) and (f) Lead-V1 and (g) and (h) Lead-aVL original and reconstructed signals are shown. Database used is CSE multilead measurement library, data set M01-033 with 6 level wavelet decomposition.

.

Table-4.6, shows distortion measures PRD, WWPRD and WEDD for the proposed MSPCA based data reduction method for multichannel ECG signals. In Table below, values of these error measures are also compared with the error values obtained for conventional PCA based method. WEDD values are the lowest compared to other two error measures. The lowest PRD is observed as 2.743 for lead-aVL which has WEDD value as 1.667 and WWPRD value as 7.928. The lowest WWPRD value is 4.467 for lead-V3. The lowest WEDD value is 1.667 for lead-aVL. These quantitative results are

TH-1102_06610204

Table 4.6: Distortion Measures in terms of PRD, WWPRD and WEDD, CSE multilead measurement library, Dataset-M01-033

Proposed MSPCA												
Measures	Lead-I	II	III	aVR	aVL	aVF	V1	V2	V3	V4	V5	V6
PRD	8.97	6.09	18.47	9.45	2.74	16.33	9.12	10.46	3.70	10.01	10.15	14.61
WWPRD	24.10	20.22	27.56	33.18	7.93	26.00	16.25	12.94	4.47	14.74	15.53	33.53
WEDD	2.35	1.94	5.27	3.01	1.67	3.94	3.88	4.70	2.54	3.26	3.12	4.41
Conventional PCA												
Measures	Lead-I	II	III	aVR	aVL	aVF	V1	V2	V3	V4	V5	V6
PRD	4.39	7.94	10.43	13.15	14.16	131.43	108.99	86.67	161.73	0.48	1.28	1.28
WWPRD	4.85	9.34	11.74	15.17	16.28	126.97	108.10	79.97	152.91	0.52	1.35	1.19
WEDD	4.35	7.79	10.87	13.14	13.83	121.80	101.53	82.14	156.79	0.46	1.23	1.21

compared with qualitative plots in Fig.4.10 for lead-I, lead-III, lead-V1 and lead-aVL. For conventional PCA, lead-aVF, V1, V2 and V3 show the highest PRD, WWPRD and WEDD. This is due to the large distortion introduced by the conventional PCA processing. It is observed that the proposed MSPCA yield signals containing all the relevant clinical features.

To compare qualitative performance of conventional PCA and proposed MSPCA, reconstructed signals of lead-aVF, lead-V2, lead-V1 and lead-aVL are plotted with their original signals. Loss of diagnostic information are noticed at the points marked 1 through 4 in Fig.4.11. In panel (e) and (h)of Fig. 4.11, 'T-wave' and 'ST' segments are disturbed whereas at panel (f) and (g) 'QRS' complexes are distorted. Such type of distortions are not desirable in clinical ECG. Also the PRD and WEDD values for these signals are higher.

It is found that an ECG signal in wavelet domain shows a few properties such as (a) energy contribution and (b) diagnostic components present in different subbands. These help multiscale formation of MECG for data reduction. The j^{th} subband coefficients of MECG signal are collected at j^{th} level to form $(j+1)$ subband matrices. The nature of wavelet coefficients for different channels collected in a subband matrix are similar in respect to the frequency content and energy contribution patterns. By applying the proposed PC selection method, dimensions are reduced in three lower order subband matrices. Other matrices are subjected to MSPCA without dimension reduction. Lower order subbands contain higher number of coefficients and also the redundant information is higher for an ECG signal. The data reduction (DR) ratio is calculated as total number samples after MSPCA to total number of samples in original signals. The average PRD (APRD) taking into account of all the channels is 10.01% with over-all data reduction of 50.37%. A low WEDD value such as 1.67 for lead-aVL

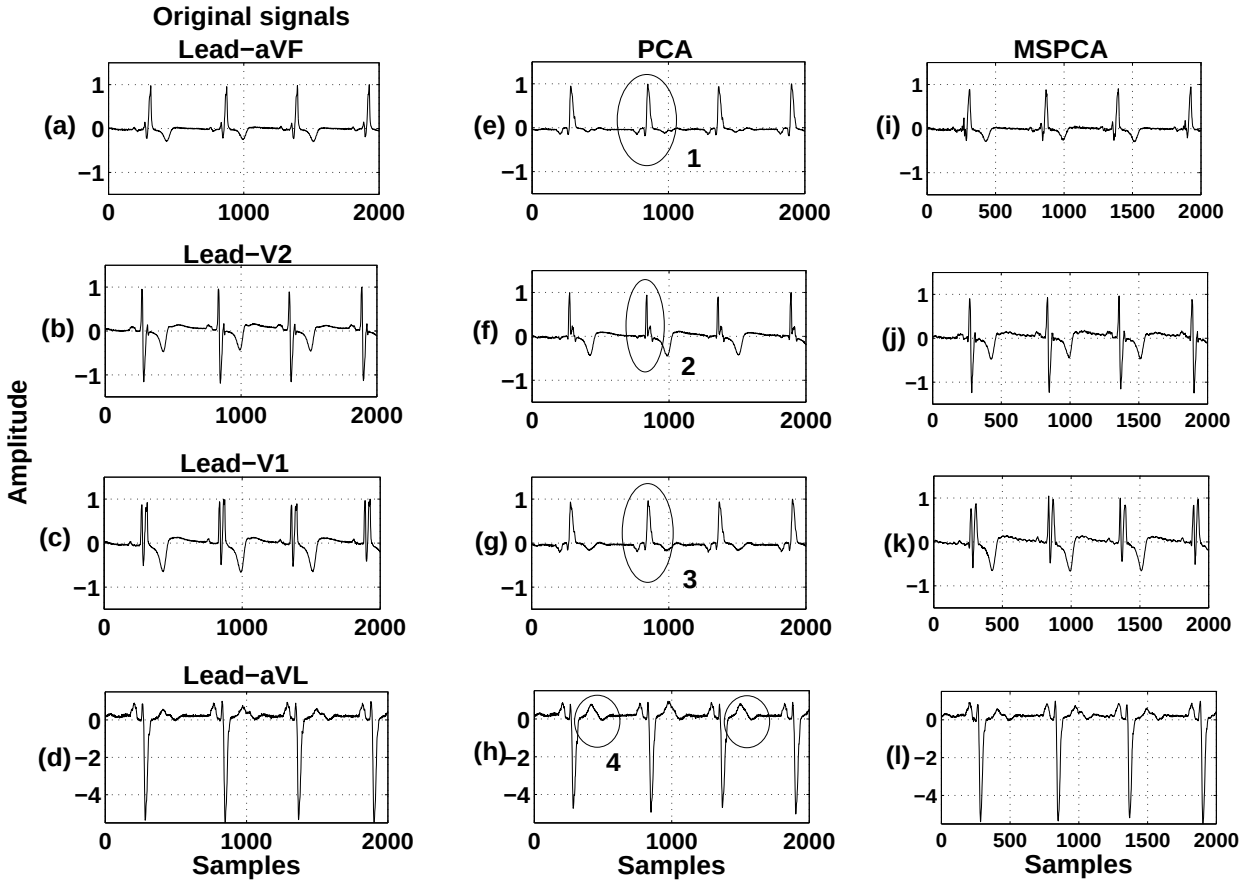

Figure 4.11: Reconstructed signals after applying conventional PCA and proposed MSPCA. In conventional PCA from original 12 dimensions 8 dimensions are considered. In panel (a), (e) and (i) Lead-aVF; (b), (f) and (j) Lead-V2; (c), (g) and (k) Lead-V1 and (d),(h) and (l) Lead-aVL original, reconstructed using conventional PCA and using proposed MSPCA signals are shown. Database used is CSE multilead measurement library, data set M01-033 with 6 level wavelet decomposition.

.

shows a better performance of proposed MSPCA on multichannel ECG signals.

4.4.2 Results for MSPCA based Compression Method

Multichannel ECG signals from standard ECG database, CSE mutlilead measurement library [2], are subjected to amplitude normalization and mean removal. Amplitude normalization factors for each lead are stored which are required during reconstruction of signals. For this work, the data set 3 of CSE multilead measurement library [2] is considered. 4096 samples from each channel, are taken as a block, from data set M01-014. Wavelet decomposition up to six levels using Daubechies 9/7

TH-1102_06610204

biorthogonal wavelet filters is used for each signal and same has been applied for reconstruction filters also. The wavelet decomposition and arrangement of coefficients resulted in seven subband matrices. Each column in a subband matrix corresponds to subband of one channel. PCA is performed on these multiscale multivariate matrices. Higher order subbands have higher energies. These subbands have important clinical components. In earlier work, [146], to avoid distortion in clinical components, the higher order subbands are not subjected to any compression. The matrices, $\mathbf{D_4}$, $\mathbf{D_5}$, $\mathbf{D_6}$ and $\mathbf{A_6}$ are PCA transformed considering all eigenvectors. To avoid the loss of clinical components present in low frequency subbands, no dimension reduction is carried out in these matrices. Only lower order wavelet subband matrices, $\mathbf{D_1}$, $\mathbf{D_2}$ and $\mathbf{D_3}$, are dimension reduced and compressed. PCA transformed coefficients are uniformly quantized and Huffman encoded [83], [163], [164] for compression. To reconstruct the signals, Huffman decoding, de-quantization and PCA reconstruction is performed. The wavelet coefficients are passed through the same wavelet reconstruction filter and de-normalized to get the multichannel signals. In Table 4.7, selected number of PC based on above proposed method is shown. The average number of PC obtained from 10 data sets are as expected with the correlation values (Table 4.2). Due to higher correlation values in $\mathbf{D_5}$, $\mathbf{D_6}$ and

Table 4.7: Number of PC selected using proposed method. Data sets are taken from CSE multilead measurement library.

Number of PC selected at different matrices							
Data set	$\mathbf{D_1}$	$\mathbf{D_2}$	$\mathbf{D_3}$	$\mathbf{D_4}$	$\mathbf{D_5}$	$\mathbf{D_6}$	$\mathbf{A_6}$
M01-001	8	8	7	5	4	4	5
M01-002	7	7	5	4	3	3	4
M01-003	7	7	6	5	4	5	5
M01-004	6	6	5	4	3	2	5
M01-005	9	9	8	6	5	4	6
M01-006	8	8	6	5	5	6	4
M01-007	8	6	6	4	3	5	5
M01-008	6	5	5	3	3	3	4
M01-009	5	5	5	5	5	4	4
M01-010	7	7	7	6	4	4	3
Average	7.1	6.8	6.0	4.7	3.9	4.0	4.5

$\mathbf{A_6}$, less number of PC can effectively capture the information content. In $\mathbf{D_1}$, $\mathbf{D_2}$ and $\mathbf{D_3}$, MMECE is very less (Fig. 4.4) and correlation is very low (Table 4.2). This suggests, the number of PC selected due to uncorrelated signal present in the matrices. Thus, to capture energies due to corre-

lated signals appearing in these matrices, the number of PC should be selected as $(M - N)$, where M is the total number of eigenvalues (it is equal to number of channels) and N is the number of eigenvalues selected from above method. In Fig.4.12, original and reconstructed signals of lead-I, lead-aVL and lead-V5 of data set M01-014 from CSE multilead measurement library are shown. PC selected using proposed method are 5, 4 and 4 for $\mathbf{D_1}$, $\mathbf{D_2}$ and $\mathbf{D_3}$ respectively. The MSPCA operation gives reduction of samples $1.45 : 1$ before coding stage. The presence of clinically relevant

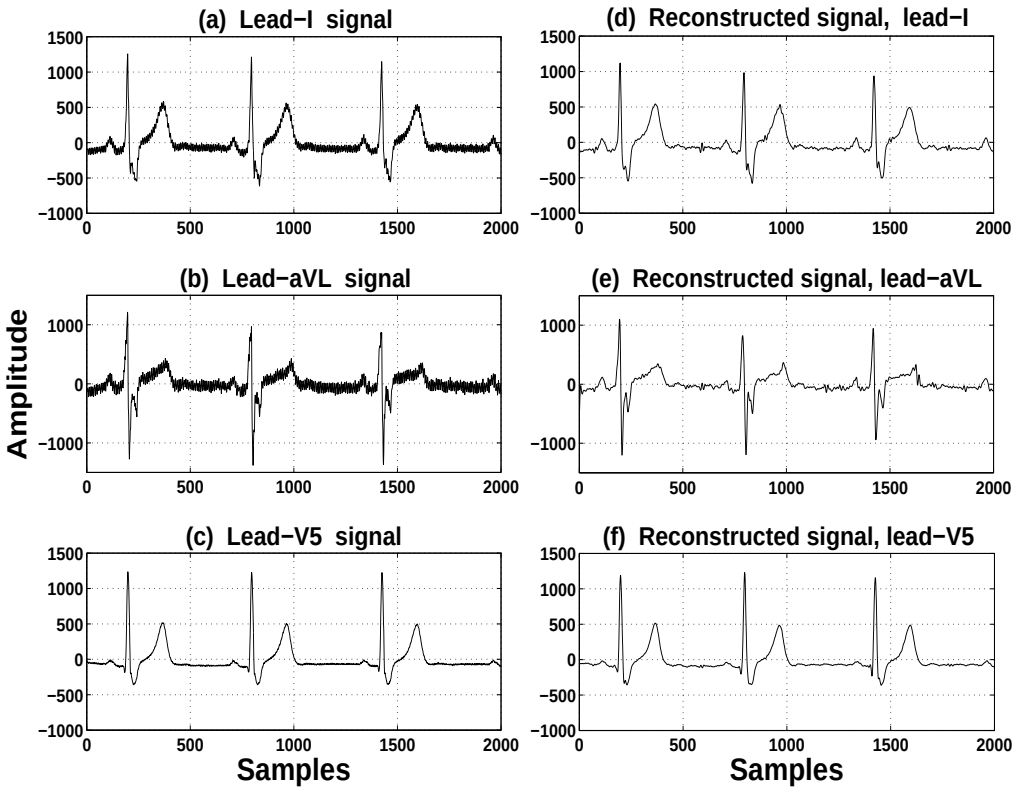

Figure 4.12: Original signals (a), (b) and (c) and reconstructed signals (d), (e) and (f) of lead-I, lead-aVL and lead-V5 respectively. MECG data set M01-014 is taken from CSE multilead measurement library and wavelet decomposition using six level Daubechies 9/7 biorthogonal wavelet filters is used.

diagnostic components, P-wave, QRS-complex and T-wave in the reconstructed signals, proves satisfactory performance of the proposed method. Also, the dimension reduction at lower order wavelet subbands shows a positive denoising effect. This result is produced with 8 bit quantization of PCA coefficients. Performance at different quantization bits with compression ratio (CR) and average PRD (APRD) are evaluated. Fig.4.13, shows the variation of CR with quantization bits and APRD with CR. In Fig.4.13(a), the CR is exponentially decreasing with increase in number of quantization bits. APRD

TH-1102_06610204

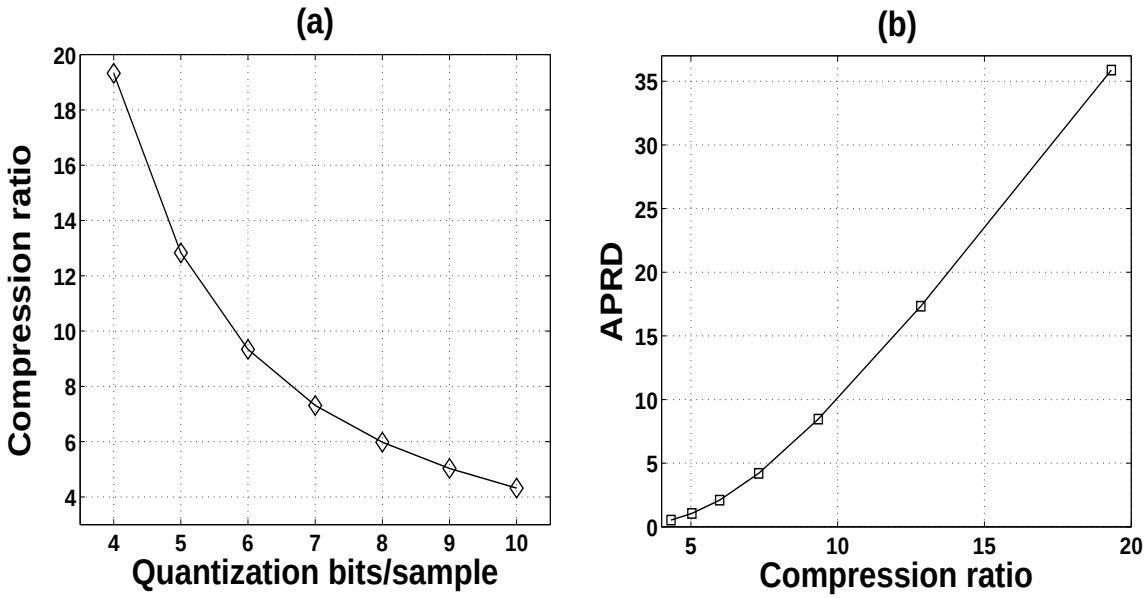

Figure 4.13: Compression ratio, quantization (bits/sample) and average PRD (a) compression ratio versus quantization bits/sample and (b) PRD versus compression ratio. MECG data set M01-014 is taken from CSE multilead measurement library and wavelet decomposition using six level Daubechies 9/7 biorthogonal wavelet filters is used.

is increasing with the increase of CR. For 4, 6, 8 and 10 bits quantization, the CRs are 19.32:1, 9.34:1, 5.98:1 and 4.32:1 respectively. Average PRD of the coder at different CR are shown in Fig.4.13(b). For CRs 19.32:1, 9.34:1, 5.98:1 and 4.32:1, the APRDs are 35.89, 8.46, 2.09 and 0.52 respectively. So, there are optimum limits among quantization bits, CR and APRD which can give better performance. The overall performance of the proposed method is evaluated by quantifying the distortion

Table 4.8: Distortion measures in terms of PRD and WEDD, CSE multilead measurement library, Dataset-M01-014

	Leads											
Metrics	I	II	III	aVR	aVL	aVF	V1	V2	V3	V4	V5	V6
PRD	18.76	20.74	12.51	12.85	35.80	8.09	9.82	11.74	14.08	10.33	7.63	6.82
WEDD	8.26	5.87	6.28	5.54	27.18	9.23	9.57	8.34	10.97	6.38	4.27	4.19

metric in terms of PRD [93, 138] and WEDD [71] for signals in each ECG lead. In Table 4.8, PRD and WEDD values are shown for all 12 ECG leads after decompression and wavelet reconstruction. Most of the leads show low WEDD values. The WEDD values of 4.19 (lead-V6), 4.27 (lead-V5) and 6.38 (lead-V4), 5.54 (lead-aVR), 6.28 (lead-III), 5.87 (lead-II) fall under excellent and very good category [71]. The high PRD and WEDD values for lead-aVL, may be due to higher noise level present

in the original signal (Fig. 4.12(a) and Fig. 4.12(b)) which is removed by MSPCA operation.

Mean Opinion Score's (MOS's) are evaluated as subjective quality measure of the reconstructed signals. The evaluators (10 in numbers) are researchers working in signal processing areas. It represents the true quality of the reconstructed signal [137] by reviewing the diagnostic features of the original and compressed signal. In this work, semi-blind MOS is evaluated for the quality of the diagnostic features such as P-wave, PR-segment, PR-interval, QRS-complex, ST-segment and T-wave for every tested signal. The observer provides an evaluation of the similarity between the original and the compressed signal features. The quality ratings are 1 (bad), 2 (almost tolerable), 3 (tolerable), 4 (good) and 5 (excellent) [137] for each signal under evaluation. All such scores are recorded. The average rank of each ECG signal is determined. This average rating is known as mean opinion score (MOS) for the signal.

For an l^{th} ECG segment or clinical feature, MOS is defined as

$$MOS(l) = \frac{1}{N_c} \sum_{c=1}^{N_c} R(c) \tag{4.27}$$

where N_c is the number of cardiologist and $R(c)$ is the quality rating for the l^{th} segment or clinical feature.

For a signal under evaluation, the MOS is defined as the average of all MOS ratings of ECG segments or clinical features

$$MOS = \frac{1}{N_f} \sum_{f=1}^{N_f} MOS(l) \tag{4.28}$$

where N_f is the number of ECG segments or clinical features and $MOS(l)$ is the MOS rating of the segment.

Finally, for a semi-blind test, gold standard diagnostic error measures, MOS errors, for ECG segments and compressed signal are given as

$$MOS_e(l) = \frac{5 - MOS(l)}{5} \times 100 \tag{4.29}$$

$$MOS_e = \frac{5 - MOS}{5} \times 100 \tag{4.30}$$

where $MOS_e(l)$ and MOS_e are the MOS errors (by percentages) for an ECG segment and overall ECG signal respectively.

TH-1102_06610204

Table 4.9: Mean opinion score error (in $\%$) for reconstructed signals

MOS error for ECG segments			
Segments	Lead-I	Lead-aVL	Lead-V5
P-wave	02.22	11.11	01.11
PR-segment	13.33	13.33	06.67
PR-interval	11.11	11.12	12.22
QRS-complex	14.44	12.22	05.56
ST-segment	06.67	15.00	03.33
T-wave	02.21	10.00	04.44
MOS error for ECG signals			
Overall signal	08.33	12.13	05.56

In Table 4.9 , MOS errors for ECG segments or diagnostic features and MOS error for overall reconstructed signals are shown for lead-I, lead-aVL and lead-V5 signals (Fig.4.12). For an ECG segment the lowest MOS error ($MOS_e(l)$) is 1.11 for P-wave of lead-V signal followed by 2.22 and 2.11 for P-wave and T-wave of lead-I signal respectively. Also, lead-V5 signal gives the lowest overall MOS error (MOS_e). This lead also shows lower PRD and WEDD values (Table 4.8). Based on MOS error criteria the reconstructed all ECG segments and signals falls under very good category [137].

Table 4.10: CR and PRD: Comparision with existing methods

Measures	Proposed	Zigel [138]	Miaou [93]	Cetin [115]	Ershad [165]	Manikandan [102]
PRD	2.09%	8%	7.3%	6.19%	8.13	6.33%
CR	5.98:1	30:1	27.1:1	6.17:1	28:1	12:1
No. of channels	12	1	2	8	2	1

The proposed compression method is compared with existing ECG data compression method in Table 4.10. The APRD of 2.09 with CR of 5.98:1 for proposed method with 12-lead ECG is the lowest compared to the other methods. Miaou et at. have obtained [93], Compressed Data Rate (CDR) of 146 b/s with APRD of 7.3% (ECG sampling rate 360 Hz and 11 bit resolution). It gives CR, 27.1:1. An enhanced set partitioning in hierarchical trees (ESPHIT) algorithm by Ershad [165], for multichannel ECG compression gives CR, 28:1 with PRD, 8.13. Linear transform such as KLT and DCT is applied by Cetin et al. [115] to decorrelate and code the signals with CR=6.17 and APRD=6.19%. A compression ratio 30:1 with a PRD value below 8% and Weighted Diagnostic Distortion (WDD) below 4% is reported by Zigel et al. [138]. A wavelet threshold based compression for target distortion level (TDL) and target data rate (TDR) by Manikandan et al. [102] gives APRD of 6.33% with compression fac-

tors 12, 8 and 4 using data from the MIT-BIH Arrhythmia (mita), the Creighton University Ventricular Tachyarrhythmia (cuvt) and the MIT-BIH Supraventricular Arrhythmia (mitsva) databases respectively. Using proposed method, Dimension Reduction (DR) using MSPCA gives Sample Reduction Ratio (SRR) of 1.45:1 and entropy coding stage gives compression ratio $5.98:1$.

4.4.3 Evaluation of MSPCA based Compression Method under Noise Conditions

For proposed MSPCA based compression method for multichannel ECG signals, a few more experiments are carried out after addition of Gaussian noise, Baseline Wander and Power line interference. The qualitative and quantitative results are shown below-

Addition of white Gaussian noise

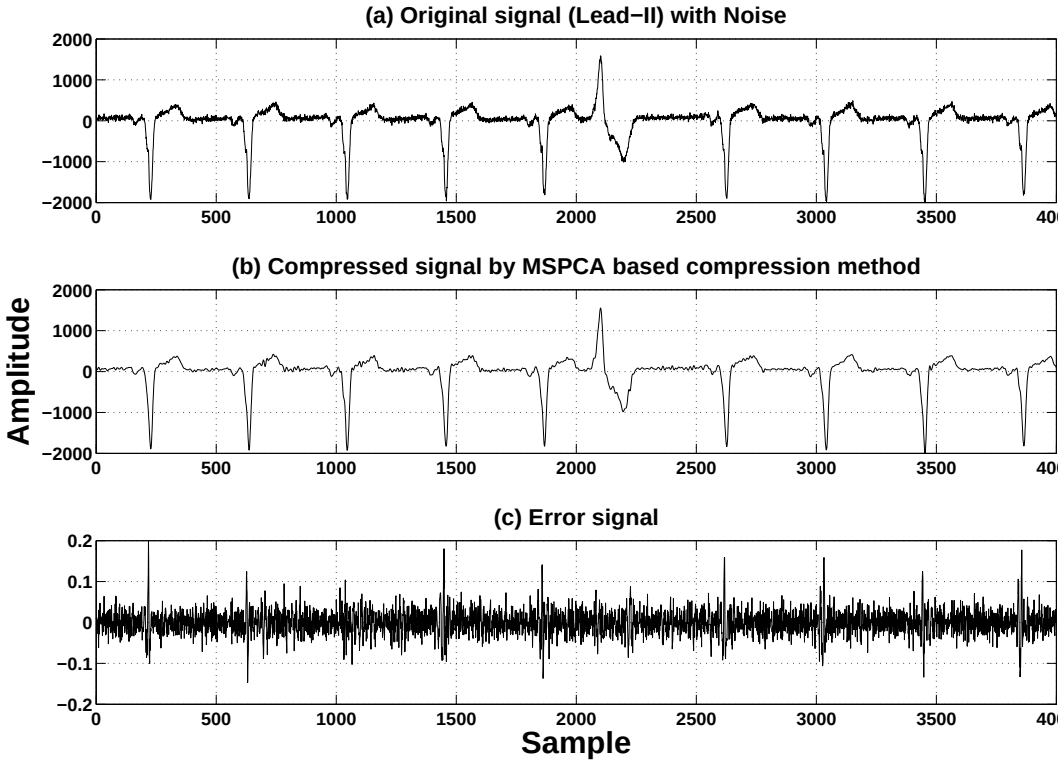

Figure 4.14: Compression of Lead-II signal by MSPCA based compression method when corrupted with Gaussian noise (Input SNR 9.01 dB), (a) Original lead-II signal with noise, (b) Compressed lead-II ECG signal by MSPCA based compression (c) Error signal.

In Figure 4.14, Gaussian noise is added in Lead-II signal and subjected to the proposed MSPCA

TH-1102_06610204

based compression method. The compressed signal shows the presence of all the clinical components like P-wave, QRS-complex and T-wave as they are found in original signal. The input SNR is measured at 9.01 dB. The algorithm shows denoising effect which may be due to the dimension reduction at wavelet scales. The quantitative measurement of signal quality is evaluated using PRD, WWPRD and WEDD. The WWPRD value is found 36.09% whereas WEDD value is 3.47%. This WEDD value falls under excellent category. The PRD value is 0.008%.

In Figure 4.15, lead-II signal is corrupted with higher noise level at input SNR (-23.10 dB). The

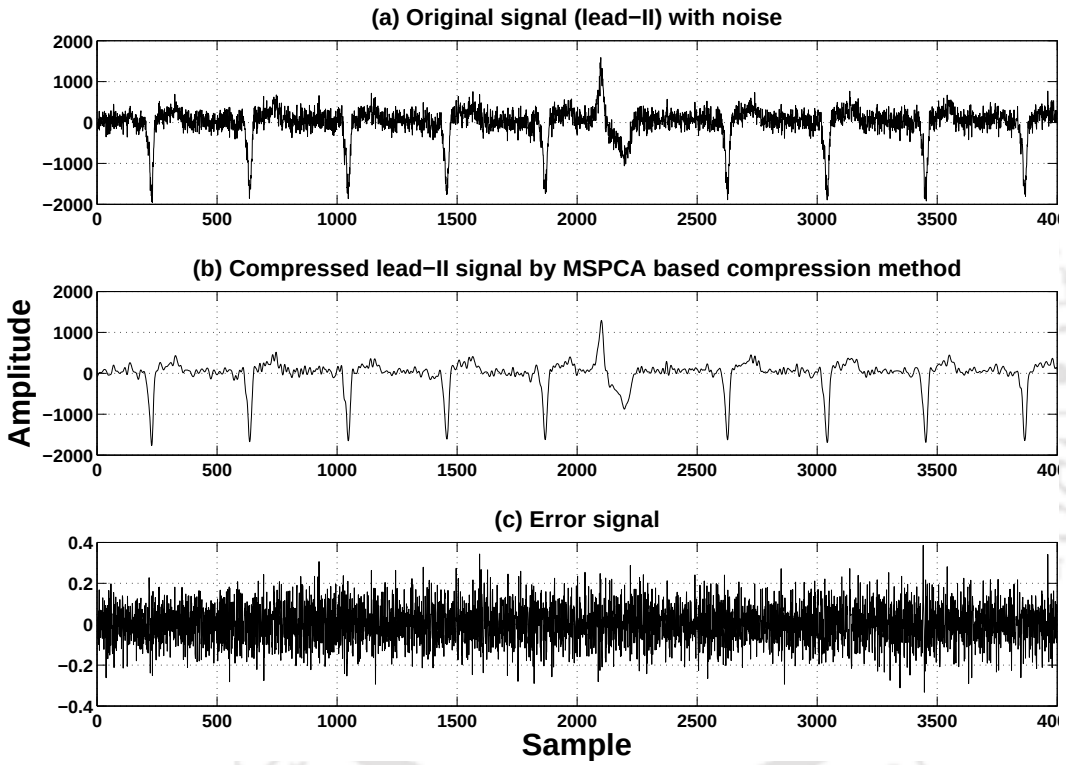

Figure 4.15: Compression of Lead-II signal by MSPCA based compression method when corrupted with Gaussian noise (Input SNR -23.10 dB), (a) Original lead-II signal with noise, (b) Compressed lead-II ECG signal by MSPCA based compression (c) Error signal.

output of the MSPCA based compression method shows a successful recovery of the signal. The PRD, WWPRD and WEDD values are found as 0.03%, 68.47% and 23.69% respectively. The proposed method also shows the denoising effected which may be due to the PCA operation at wavelet scales. The output signal is not as smooth as earlier cases. Also, the WEDD value is higher, 23.69%. This may be due to the removal of higher noise level from the signal.

Addition of white Gaussian noise and Base line Wander

In Figure 4.16, Gaussian noise and base line wander is added to the lead-II signal. The input SNR

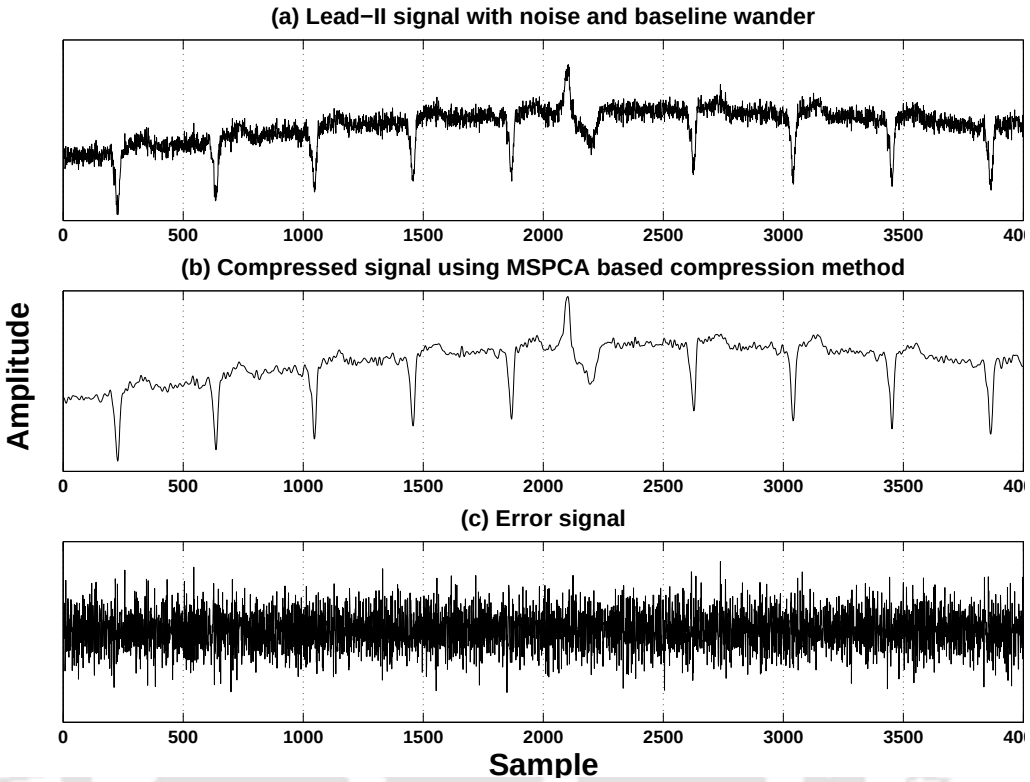

Figure 4.16: Compression of Lead-II signal by MSPCA based compression method when corrupted with Gaussian noise and Base line wander (Input SNR -21.83 dB), (a) Original lead-II signal with noise and Base line wander, (b) Compressed lead-II ECG signal by MSPCA based compression (c) Error signal.

value is -21.83. Then the corrupted signal is subjected to MSCPA based compression method. The reconstructed signal shows a positive denoising effect and successful recovery of the original signal. The output SNR value is 58.5 dB. Though the reconstructed signal shows the presence of all the clinical components like P-wave, T-wave and QRS-complex, it fails to provide smooth output signal. It may be due to the higher noise level at input (input SNR is at -21.83 dB). So, the reconstructed signal is not smooth. Also, the WEDD value is found to be too high (91.99%). The compression ratio is 10.49. The WWPRD value is 86.20%.

Addition of white Gaussian noise, Base line Wander and Power line noise

TH-1102_06610204

In Figure 4.17, the input signal (lead-II) is corrupted with Gaussian noise, base line wander and power line noise. The corrupted signal is subjected to MSPCA based dimension reduction and then

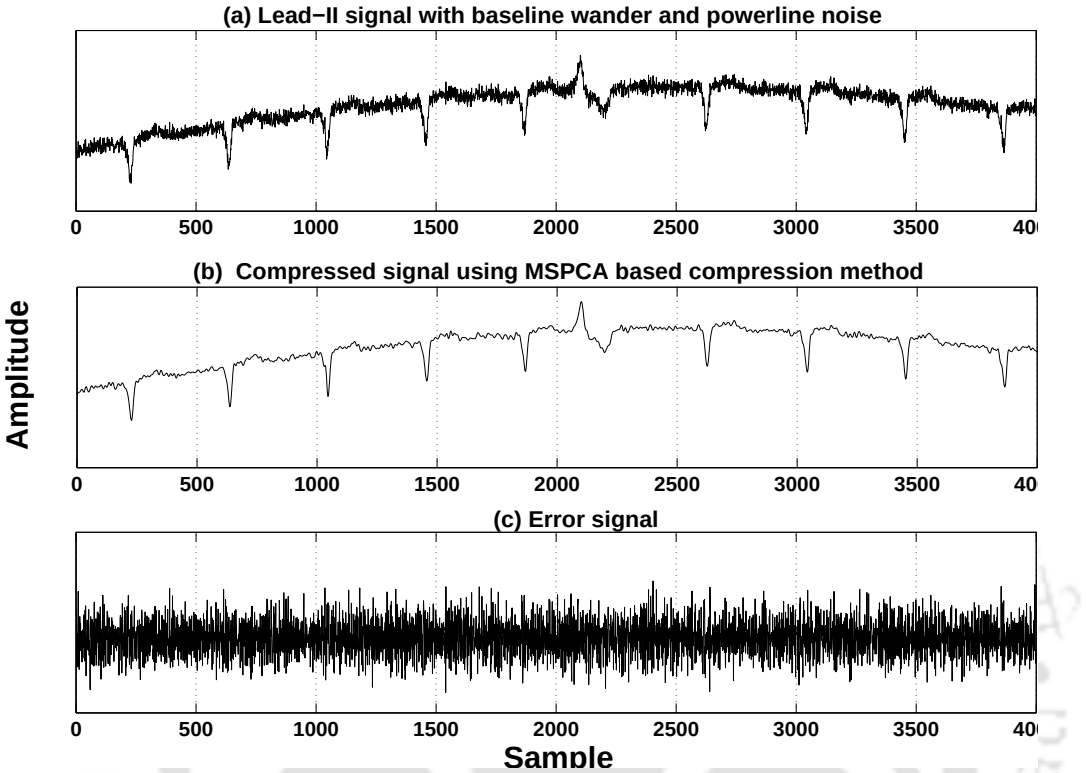

Figure 4.17: Compression of Lead-II signal by MSPCA based compression method when corrupted with Gaussian noise and Base line wander and Power line interference, (a) Original lead-II signal with Gaussian noise, Base line wander and Power line interference (b) Compressed lead-II ECG signal by MSPCA based compression (c) Error signal.

compression. The reconstructed signal is not smooth. But it contains the entire clinical component as present in the original signal. Due to higher noise content, the WEDD value is found to be higher as earlier case.

4.5 Summary

In this Chapter, the correlations between channels and the multiscale properties of wavelet transform are used for improvement in dimension reduction and hence samples reduction of multichannel ECG signals without distortion of clinical information. Signals are decomposed into subbands using wavelet transform. Coefficients are arranged in subband matrices. In different wavelet scales, higher

correlations are observed between standard 12 leads ECG signal. Also, relative energy contribution of subband matrices are evaluated in terms of MMECE. The proposed MSPCA is applied on subbands matrices. Two novel PC selection method based on subband weights and fractional energy are also proposed. Qualitative and quantitative performance are compared with methods existing in literatures. A sample reduction of 50.37% with APRD value of 10.01% is obtained for the proposed MSPCA based method using PC selection method proposed in Section 4.2.3.1. The reconstructed signals of all the leads show preservation of diagnostic features.

Multiscale PCA based compression method for multichannel ECG signals is demonstrated without distorting the clinical information. A novel PC selection method proposed in Section 4.2.3.2 is used for compression scheme. MSPCA coefficient at a few certain scales are uniformly quantized and Huffman encoded for multichannel compression. Quantitatively, the performance is compared with existing compression method. The reconstructed signals of all the leads show preservation of diagnostic features and a very good MOS rating. Using proposed scheme, dimension reduction using MSPCA gives sample reduction ratio of 1.45:1 and entropy coding stage gives compression ratio $5.98:1$ with PRD value 2.09% and the lowest WEDD value of 4.19%

TH-1102_06610204

Indian Institute of Technology Guwahati

5

Clinical Entropy and Multiscale Distortion

Contents

TH-1102_06610204

Conventional multivariate signal analysis tool such as principal component analysis (PCA) [124] can be employed to process multichannel electrocardiogram signals (MECG). By selecting suitable number of PCs, the dimensions can be reduced with minimal loss. In an ECG signal, the clinical components such as P-wave, QRS-complex and T-wave appear at different frequency bands and these clinical information are captured by the eigenvalues. The quantification and subsequent preservation of clinical information in multichannel ECG signals are challenging tasks.

In Chapter 4, MSPCA analysis and MSPCA based compression of multichannel electrocardiogram signals are presented. It is shown that the principal components selected in both the methods play major role to capture the clinical information. To retain diagnostic features of ECG signals, proper selection of PC is the most essential task. It will be meaningful to investigate the correlation between the principal components and the clinical information in the signal. In this Chapter, we introduce Clinical Entropy (Centropy) which is more relevant to clinical information present in a physiological signal such as electrocardiogram. In Section 5.1, PCA based Clinical Entropy and MSPCA based Clinical Entropy are discussed. Section 5.1.3 proposes a multiscale signal distortion measure for MSPCA based application. Results are discussed in Section 5.2.

5.1 Clinical Entropy

In this Section, an information theoretic approach for principal component analysis (PCA) of multichannel ECG signals is proposed. Clinical information (clinical entropy) is evaluated from the inverse of the diagonal eigenvalue matrix. Centropy based method can select the optimum number of PC's and shows improved performance compared to the conventional PCA. The proposed method exhibits superior signal quality with higher cross correlation (CC), lower percentage root mean square difference (PRD) and lower root mean square error (RMSE) values.

5.1.1 PCA based Clinical Entropy

Conventional PCA can be applied to multichannel ECG signals by forming appropriate multivariate matrix. The multivariate $N \times n$, signal matrix, **S**, is constructed with n number of channels as column and N number of samples in each channel. Each element, s_{ij}, represents the i^{th} sample of the j^{th} channel. The square symmetric covariance matrix, $\mathbf{C_s}$, is evaluated as $\mathbf{C_s} = \frac{1}{(n-1)}([\mathbf{S}][\mathbf{S}]^T)$.

It exploits all the possible signal correlations between the channels. The main objective is to minimize redundancy measured by covariance and to maximize the signal measured by variance. Eigen decomposition of square symmetric covariance matrix gives eigenvalue, $\mathbf{\Lambda_s}$, and eigenvector, $\mathbf{V_s}$, matrices. Orthogonal eigenvector matrix, $\mathbf{V_s}$, diagonalizes the covariance matrix, $\mathbf{C_s}$, as

$$\mathbf{V_s C_s V_s^{-1}} = \mathbf{\Lambda_s} \tag{5.1}$$

$\mathbf{\Lambda_s}$ is the diagonal matrix where the diagonal elements, λ_i ($i = 1, 2, \cdots, n$), are the eigenvalues. The eigenvectors with higher eigenvalues are the principal components. These orthogonal eigenvectors represent the signals in the direction of maximum variances. In conventional PCA [124], the threshold, T_s, for the selection of PC is defined as

$$T_s = \frac{\sum_{i=1}^{p} \lambda_i}{\sum_{i=1}^{n} \lambda_i} \times 100 \tag{5.2}$$

where λ_i is the i^{th} eigenvalue, n is the total number of eigenvalues, p is the number of eigenvalues selected. Generally, to select the subset of PC, cumulative percentage of total variation of variances [124] is taken. Thus, with lower value of T_s more dimension reduction is possible. Careful implementation of PCA is required for retention of clinical information in Multichannel ECG signals. Higher eigenvalues are resulted from significant energy contributed by P-wave, QRS-complex and T-wave. The noise and other signal components are captured by lower eigenvalues. Proper selection of eigenvalues can ensure retention of clinical information. Fig.5.1 shows lead-I ECG signal and corresponding reconstructed signal after elimination of selected principal components. There are 12 PCs. Based upon the magnitudes, the eigenvalues are arranged in descending order and corresponding PCs are named as PC1 to PC12. Fig.5.1(b) shows the reconstructed signal without PC1. It is observed that the low frequency content of the signal with clinical components, P-wave, T-wave and some part of QRS-complex, are distorted. Fig.5.1(c) shows the reconstructed signal without PC1 and PC2. It is observed that, in addition to P-wave and T-wave, the QRS-complex is significantly affected. After removal of five PCs (PC1 to PC5), the ECG signal is completely distorted as shown in Fig.5.1(d). This result shows the clinical significance of PCs with higher eigenvalues. The clinical information captured by eigenvalues has motivated us to apply information theoretic approach. In this work, Centropy is proposed for selection of appropriate number of eigenvalues. For evaluation

TH-1102_06610204

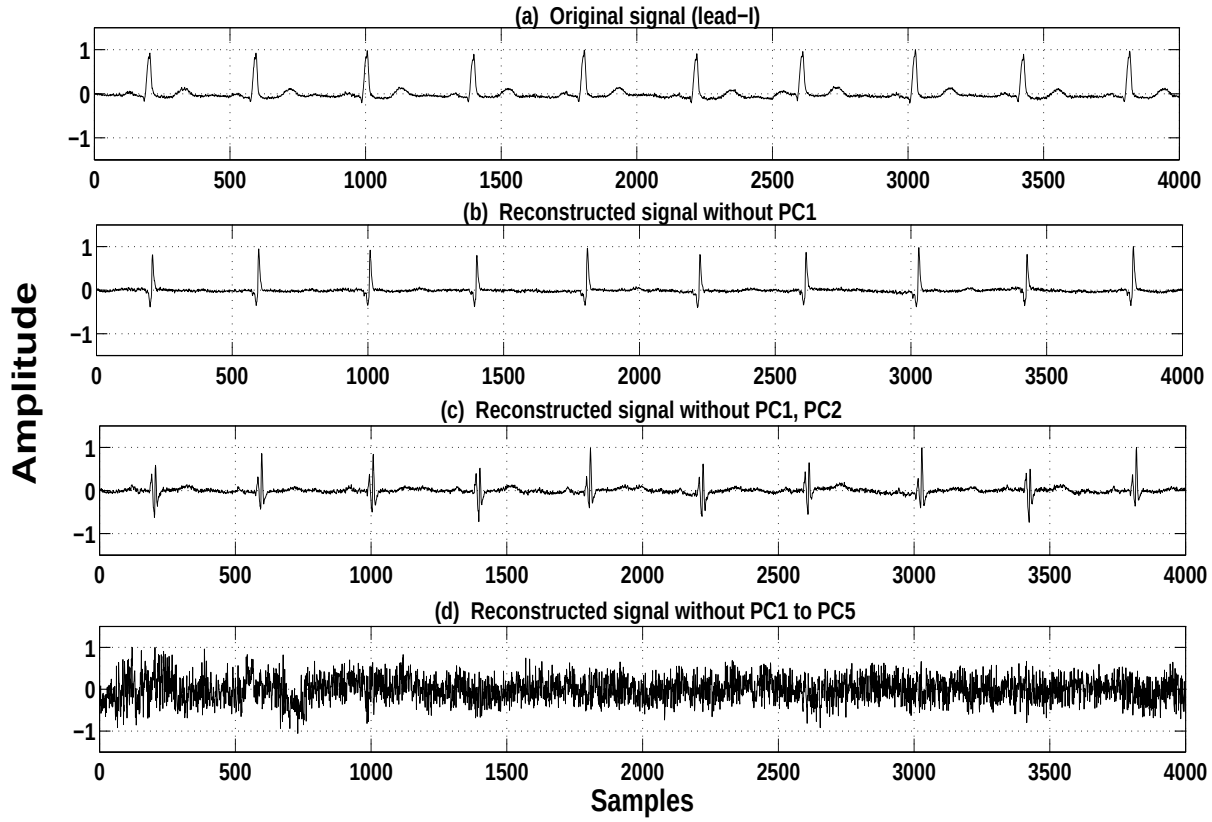

Figure 5.1: (a) ECG signal of lead-I, reconstructed signals (b) without PC1 with the highest eigenvalue, (c) without PC1 and PC2, (d) without PC1, PC2 and PC5. The dataset-M01-004 is taken from CSE multilead measurement library.

of Centropy, first, the diagonal eigenvalue matrix ($\mathbf{\Lambda_s}$) is inverted. The probability of each diagonal element ($\lambda_i^{'}$) of this inverse matrix is defined as

$$P_i = \frac{\lambda_i^{'}}{\sum_{i=1}^{n} \lambda_i^{'}} \tag{5.3}$$

where $\lambda_i^{'}$ is the reciprocal of i^{th} eigenvalue. Higher eigenvalues will result in lower probability values. The self-information contributed by the i^{th} eigenvalue can be given as

$$I_i = -\log(P_i) \tag{5.4}$$

Hence, the entropy information [146] contributed by i^{th} eigenvalue is given as $H_i = -P_i \log(P_i)$ and it is termed as Clinical Entropy (Centropy). It is expected that the eigenvalue with lower probability will have higher self-information and higher entropy. In this work, the selection of number of PCs is

based on total cumulative entropy. The Centropy based threshold, (T_H), is defined as

$$T_H = \frac{\sum_{i=1}^{p'} H_i}{\sum_{i=1}^{n} H_i} \times 100 \tag{5.5}$$

For conventional PCA, probability of i^{th} eigenvalue can be defined as the ratio between the i^{th} eigenvalue and the sum of all eigenvalues. Thus, the self-information and the entropy of i^{th} eigenvalue for conventional PCA can be estimated using this probability value.

5.1.2 Multiscale PCA based Clinical Entropy

In this section, multiscale Clinical Entropy Centropy) is proposed for multiscale principal component analysis (MSPCA) for multichannel electrocardiogram signals. An information theoretic approach is proposed to define Centropy based on eigenvalues at wavelet subband matrices. Centropy gives the optimum number of principal component (PC) for dimension reduction. Centropy based MSPCA method is expected to show improved performance compared to the conventional PCA.

The covariance matrices from mean removed multiscale multivariate matrices ($\mathbf{A_L}$ and $\mathbf{D_j}$) are evaluated as discussed in earlier using Equation 4.6 and Equation 4.7. Covariance matrices extract all the possible signal correlations between the channels at wavelet scales. The main objective is to minimize redundancy measured by covariance and to maximize the signal measured by variance. The eigenvalue decomposition by Equation 4.8 and Equation 4.9 of these covariance matrices gives eignevectors and eigenvalues, $\mathbf{V_{A_L}}$, $\mathbf{V_{D_j}}$ and $\mathbf{\Lambda_{A_L}}$, $\mathbf{\Lambda_{D_j}}$ for the matrices of approximation and details subband respectively. Eigenvector matrices $\mathbf{V_{A_L}}$ and $\mathbf{V_{D_j}}$ diagonalize the covariance matrix $\mathbf{C_{A_L}}$ and matrices $\mathbf{C_{D_j}}$. The $\mathbf{\Lambda_{A_L}}$ and $\mathbf{\Lambda_{D_j}}$ are the diagonal matrices with eigenvalues as diagonal elements. Eigenvectors and eigenvalues appear in pairs. Eigenvalues are arranged in descending order and accordingly the corresponding eigenvectors. The eigenvectors with corresponding higher eigenvalues produce the principal components. Thus these orthonormal eigenvectors represent the signals in the direction of maximum variances. The reduction of dimension depends on the number of eigenvalues selected. Ordered eigenvalues in approximation and details subband matrices are

$$\lambda_{A_{L_1}}, \lambda_{A_{L_2}}, \cdots, \lambda_{A_{L_n}} \tag{5.6}$$

$$\lambda_{D_{j_1}}, \lambda_{D_{j_2}}, \cdots, \lambda_{D_{j_n}} \tag{5.7}$$

TH-1102_06610204

Generally, to select the subset of PC, cumulative percentage of total variation of variances [124] is considered. In conventional PCA, the threshold, T_{A_L} and T_{D_j}, for the approximation and details for the selection of PC are defined as

$$T_{A_L} = \frac{\sum_{i=1}^{p} \lambda_{A_{Li}}}{\sum_{i=1}^{n} \lambda_{A_{Li}}} \times 100 \tag{5.8}$$

$$T_{D_j} = \frac{\sum_{i=1}^{p} \lambda_{D_{ji}}}{\sum_{i=1}^{n} \lambda_{D_{ji}}} \times 100 \tag{5.9}$$

where $\lambda_{A_{Li}}$ and $\lambda_{D_{ji}}$ are the i^{th} eigenvalues, n is the total number of eigenvalues, p is the number of eigenvalues selected. Lower values of T_{A_L} and T_{D_j}, more dimension reduction is possible. But for retention of clinical information in multichannel ECG signals, the selection of PCs needs careful attention. Significant energy contributed by P-wave, QRS-complex and T-wave is captured by higher eigenvalues. Hence, for proper selection of eigenvalues to ensure the retention of clinical information, Centropy is proposed. For evaluation of Centropy, first, the diagonal eigenvalue matrices $\mathbf{\Lambda_{A_L}}$ and $\mathbf{\Lambda_{D_j}}$ are inverted. The probability of each diagonal element of ($\lambda'_{A_{Li}}$) and ($\lambda'_{D_{ji}}$) of these inverse matrices are defined as

$$P_{A_{Li}} = \frac{\lambda'_{A_{Li}}}{\sum_{i=1}^{n} \lambda'_{A_{Li}}} \tag{5.10}$$

$$P_{D_{ji}} = \frac{\lambda'_{D_{ji}}}{\sum_{i=1}^{n} \lambda'_{D_{ji}}} \tag{5.11}$$

where ($\lambda'_{A_{Li}}$) and ($\lambda'_{D_{ji}}$) are the reciprocal of i^{th} eigenvalues. Thus, higher eigenvalues will result in lower probability values. The self-information contributed by the i^{th} eigenvalue can be given as

$$I_{A_{Li}} = -\log(P_{A_{Li}}) \tag{5.12}$$

$$I_{D_{ji}} = -\log(P_{D_{ji}}) \tag{5.13}$$

Hence, the entropy information [146] by i^{th} eigenvalues are expressed as $H_{A_{Li}} = -P_{A_{Li}} \log P_{A_{Li}}$ and $H_{D_{ji}} = -P_{D_{ji}} \log P_{D_{ji}}$. They are termed as Clinical Entropy (Centropy). Higher entropy do have higher self-information and hence lower probability. Based on this, the selection of number of PCs for

approximation and details are proposed as

$$T_{H_L} = \frac{\sum_{i=1}^{p'} H_{A_{Li}}}{\sum_{i=1}^{n} H_{A_{Li}}} \times 100 \quad (5.14)$$

$$T_{H_{Dj}} = \frac{\sum_{i=1}^{p'} H_{D_{ji}}}{\sum_{i=1}^{n} H_{D_{ji}}} \times 100 \quad (5.15)$$

The thresholds, T_{H_L} and $T_{H_{Dj}}$ are based on Centropy due to p' number of selected eigenvalues. Higher threshold value is set due to higher cumulative entropy value. Thus, it retain more information. So, the selection of number of PC, based on clinical information content is more meaningful. These reduced number of PCs, can help expressing data with new dimensions to retain clinical content.

5.1.3 Multiscale Distortion Measure

In this Subsection, a distortion measure for multichannel electrocardiogram (MECG) is introduced for evaluation of signals processed with multiscale principal component analysis (MSPCA). After reconstruction of MSPCA processed multichannel signals, proposed Multiscale Multivariate Distortion (MMD) is calculated for matrices at different wavelet scales. The Multiscale Distortion (MD) is evaluated based on average of MMDs.

Distortion of processed ECG signal should be evaluated to check the clinical or diagnostic information. Diagnostic fidelity of ECG signal is evaluated through numerical error measure such as PRD [102], WWPRD [109] and (WEDD) [71]. For multichannel ECG signal, after multiscale PCA analysis it is essential to check the distortion introduced due to dimension reduction. So, it is proposed to evaluate multiscale multivariate distortion (MMD) for approximation and details as

$$\varepsilon_{AL} = \frac{\| A_L - \widehat{A_L} \|}{\| A_L - \overline{A_L} \|} \times 100 \quad (5.16)$$

$$\varepsilon_j = \frac{\| D_j - \widehat{D_j} \|}{\| D_j - \overline{D_j} \|} \times 100 \quad (5.17)$$

where $\mathbf{A_L}$ is the multivariate matrix at L^{th} decomposition level, $\mathbf{D_j}$ is the multivariate matrix at j^{th} level, $\widehat{\mathbf{A_L}}$ and $\widehat{\mathbf{D_j}}$ are reconstructed matrices and $\overline{A_L}$ and $\overline{D_j}$ are the corresponding mean value of original matrices. This distortion measure, captures the error at wavelet subband levels or scales.

TH-1102_06610204

The deviation in signal energy from original due to dimension reduction using MSPCA is well reflected in the proposed method.

Thus, the multiscale distortion (MD) is proposed and defined as

$$MD = \frac{1}{L+1}\left[\varepsilon_{AL} + \sum_{j=1}^{L}\varepsilon_j\right] \tag{5.18}$$

This error measure represent the distortion introduced due multiscale operation on signals. A proper weight can be assigned to each MMD in above expression to reflect the actual and more accurate MD.

5.2 Results and Discussions

Multichannel signals from CSE multilead measurement library [2] datasets M01-040 and M01-004 are used to form multivariate data matrix, $\mathbf{S}$. In this matrix there are 12 columns which correspond to 12 channels of data. Each column consists of 4096 samples. First, mean removal, amplitude normalization and base-line wander removal for each channel data are carried-out. The matrix, S, is subjected to covariance analysis. For the proposed Centropy based PCA, self-information and entropy information of eigenvalues are evaluated using the inverse of the diagonal eigenvalue matrix.

It is shown in Fig.5.1 that the elimination of number of principal components may distort the original signal. The PC1 which is associated with the highest eigenvalue is removed in Fig.5.1(b). The low frequency content of the signal with clinical components, P-wave, T-wave and some part of QRS-complex, are distorted. Similar results are seen in Fig.5.1(c) (removing PC1 and PC2) and Fig.5.1(d) (removing PC1 to PC5). This result shows the clinical significance of PCs with higher eigenvalues. Fig.5.2, shows the RMSE and CC values for reconstructed signals after removal of PCs. The results for Lead-II, lead-aVF and lead-V2 signals are shown in the figure. From Fig.5.2(a), it is observed that the RMSE values increase with removal of more number of PCs. Similarly, it is observed that the CC values decrease with removal of more number of PCs as shown in Fig.5.2(b). The above results (Fig.5.1 and Fig.5.2) prove that the clinical significance of PCs is higher for those with higher eigenvalues.

Fig.5.3 shows, the scree (eigenvalue), the conventional PCA based entropy and Centropy values.

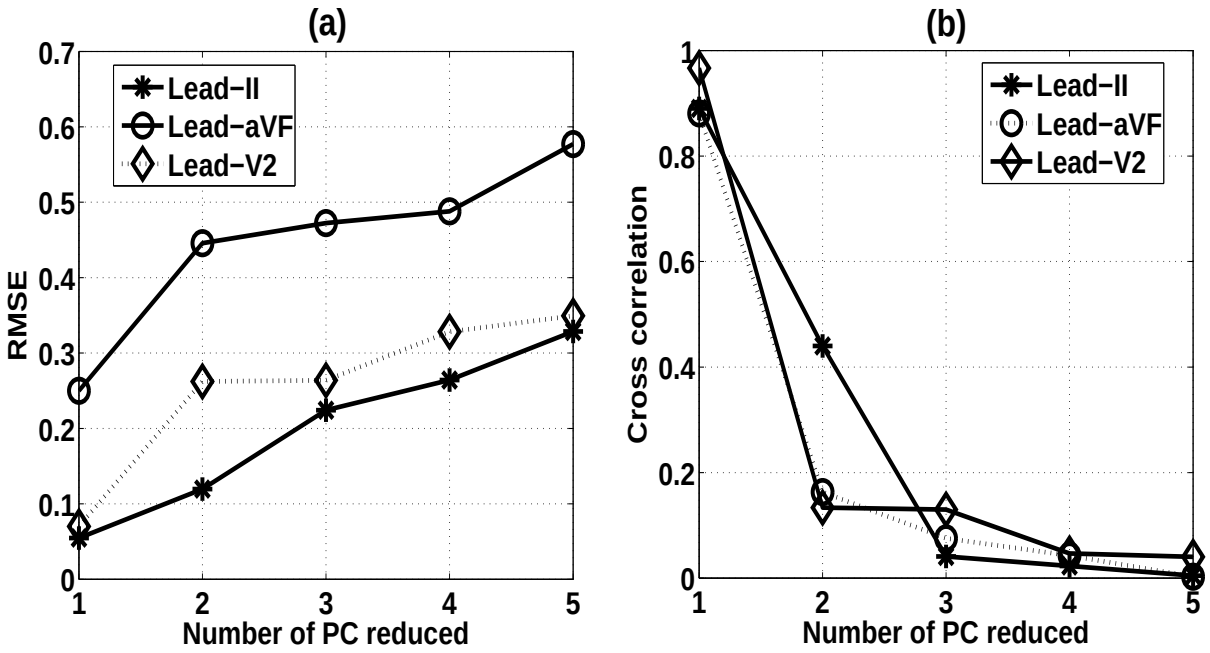

Figure 5.2: RMSE and cross correlation plots; (a) RMSE with reduction of PCs and (b) CC with reduction of PCs for signals of lead-II, lead-aVF and lead-V2 respectively. The dataset-M01-004 is taken from CSE multilead measurement library.

The x-axis represents the principal component number (eigenvalue number). Higher eigenvalues are associated with the significant clinical information such as P-wave, QRS-complex and T-wave in an ECG signal. From the results shown in Fig.5.3, it is observed that the Centropy values are higher for higher eigenvalues. Hence, higher values of Centropy represent significant clinical information in an ECG signal. This justifies the assumption that the Centropy can quantify the clinical information. On contrary, the conventional PCA based entropy values are lower for higher eigenvalues as shown in Fig.5.3.

Fig.5.4 shows segments of ECG signals from three channels and corresponding results for Centropy based PCA and conventional PCA. The original signals from lead-III, V4 and V5 are shown in Fig 5.4(a), (d) and (g) respectively. The reconstructed signals for Centropy based PCA and from conventional PCA are shown in Fig 5.4(b), (e), (h) and Fig 5.4(c), (f) and (i) respectively. For retaining 99% of the total variance, the number of PC required is 6 in case of Centropy based PCA whereas for conventional PCA, the number of PCs is 3. It is observed that the segment of reconstructed signal in Fig.5.4(c) which is marked as ‘R’ is distorted compared to the same segment in the original signal

TH-1102_06610204

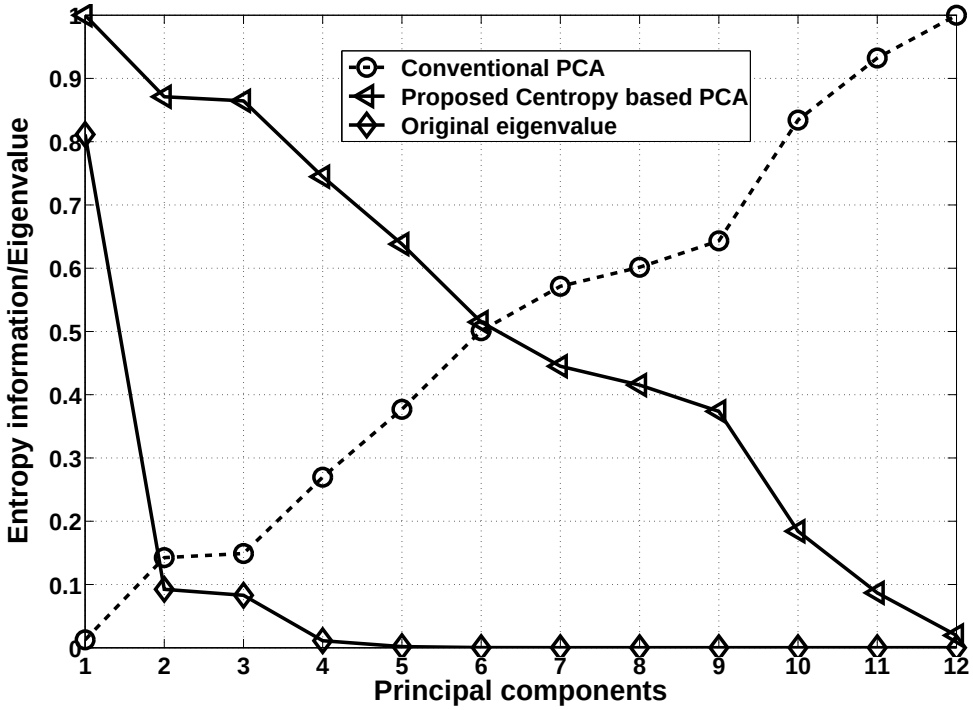

Figure 5.3: Scree and Centropy plots for Conventional and Centropy PCA. CSE multilead measurement library, dataset-M01-040 is used.

shown in Fig.5.4(a). The reconstructed signal in Fig.5.4(b) shows no perceivable distortion compared to the original signal. The clinical information like P-wave, QRS-complex and T-wave are well preserved with sufficient clinical fidelity. Similar results are observed with the other two signals. These results show that the Centropy based PCA method performs better compared to the conventional PCA based method from the point of view of preservation of clinical information. The performances

Table 5.1: Distortion measures: PRD (in %), RMSE (in %) and CC for proposed method and conventional PCA

Metric/leads	I	II	III	aVR	aVL	aVF	V1	V2	V3	V4	V5	V6
PRD-Proposed	0.56	0.35	0.06	0.47	0.49	0.75	1.62	1.34	1.43	3.67	2.21	3.72
PRD-Conventional	11.79	4.33	14.38	6.12	3.13	8.93	11.43	15.29	18.79	21.62	19.86	11.70
RMSE-Proposed	0.07	0.09	0.04	0.10	0.09	0.48	0.70	0.29	0.32	0.61	0.38	0.67
RMSE-Conventional	1.58	1.08	8.96	1.31	0.59	5.70	4.96	3.33	4.16	3.62	3.39	2.12
CC-Proposed	1.000	1.000	1.0000	1.000	1.000	1.000	0.999	0.999	0.999	0.999	0.999	0.999
CC-Conventional	0.996	0.999	0.990	0.998	0.999	0.996	0.995	0.990	0.987	0.977	0.980	0.993

of Centropy based PCA and conventional PCA are quantitatively evaluated using distortion metrics, PRD, RMSE and CC for all 12 channel data. The results are shown in Table-5.1. It is observed that the PRD and the RMSE values are lower for all the channels in case of the proposed Centropy

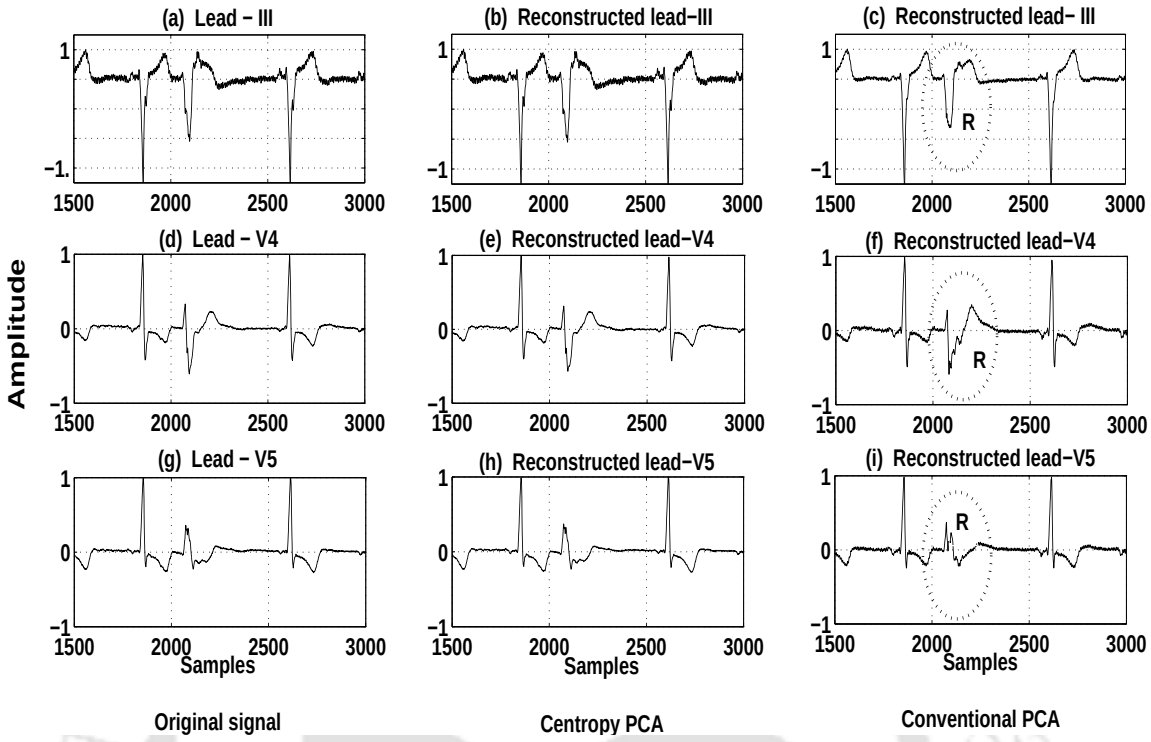

Figure 5.4: Original signals and reconstructed signals using proposed Centropy method and conventional PCA. In panels (a) and (d) original signals of lead-V4 and V5; (b) and (e) reconstructed signals using proposed Centropy PCA and, (c) and (f) reconstructed signals using conventional PCA. The dataset-M01-040 is taken from CSE multilead measurement library.

based PCA method compared to the conventional PCA based method. The CC values are higher in case of Centropy based PCA method for all the channels. Lower PRD and RMSE values and higher CC values prove that the reconstructed signal quality is better in case of the Centropy based PCA method. These results prove that the proposed Centropy based PCA method is superior to the conventional PCA based method. In Fig. 5.5, the reconstructed signals after Centropy based PCA and Centropy based MSPCA are compared. The lead-III signal from same dataset M01-040 is processed with proposed Centropy based PCA method and Centropy based MSPCA methods. It is observed that signal in Fig. 5.5(c) is better reconstructed. It shows a denoising effect and the signal do have all the clinical components. Redundant information are reduced. The threshold to select the number of PC is depends on cumulative percentage of information to be retained in the processed signal. In this, the threshold at 80% of information for PC selection is taken. For D_1, D_2 and D_3 matrices, the number of PC selected by this method are 8, 7 and 7 respectively. However, Centropy based

TH-1102_06610204

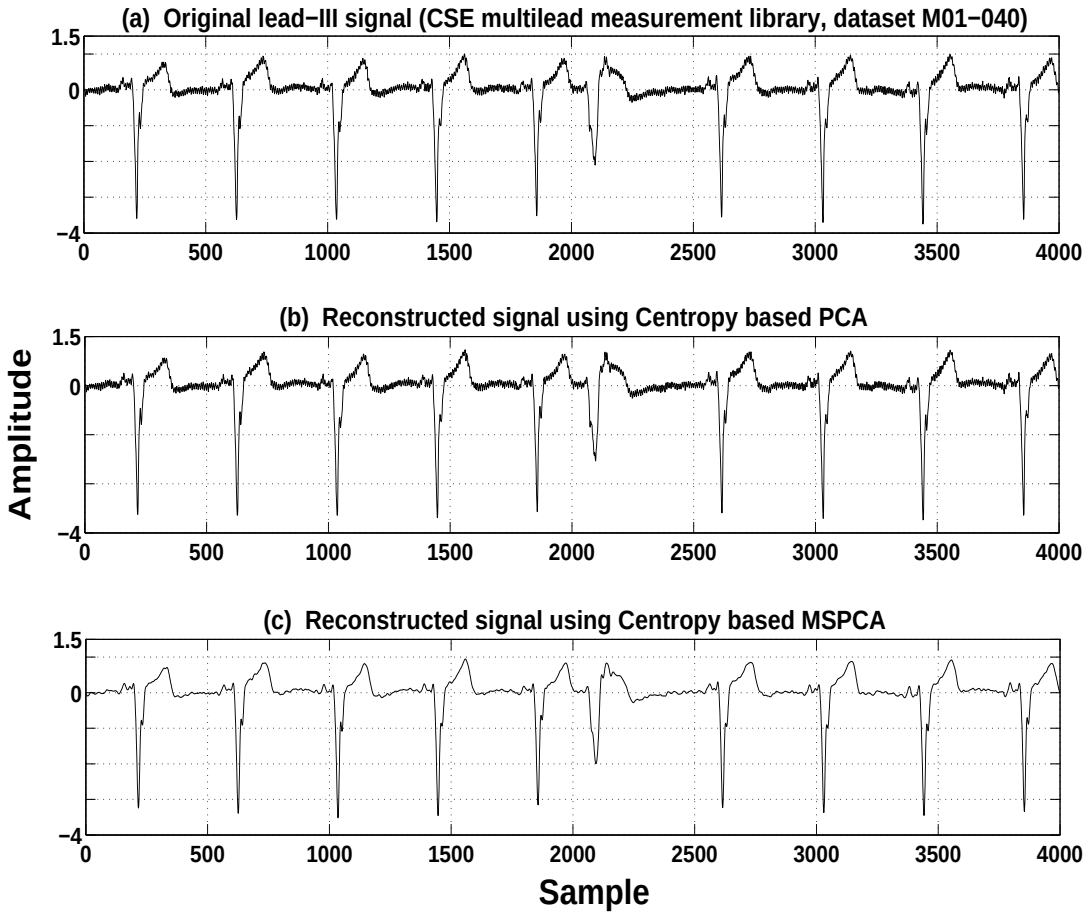

Figure 5.5: Original signal and reconstructed signals using proposed Centropy based PCA and MSPCA method. In panels (a) Original lead-III signal, (b) and (c) reconstructed signals using proposed Centropy based PCA and Centropy based MSPCA respectively. The dataset-M01-040 is taken from CSE multilead measurement library.

PCA method does not show denoising effect. That is, it removes less redundant information. For Centropy based MSPCA mehtod, the PRD, WWPRD and WEDD values for lead-III signal are 11.725, 29.124 and 5.274 respectively. The lower PRD for Centropy based method (Table-5.1) is due to the non-removal of redundant information. It does not show denoising effect in reconstructed signal as found in case of Centropy based MSCPA method.

Subjective quality of reconstructed signal is evaluated using Mean Opinion Scores (MOSs) as described in Section 4.4.2. In Table 5.2, MOS scores for ECG segments and reconstructed signals are shown for Centropy based PCA and MSPCA methods. The results are shown for Lead-III signals from data set M-01-040. The MOS for segments and signal (MOS value is 26.85%) are found to be

Table 5.2: Mean Opinion Score errors (in $\%$) for reconstructed signals processed by Centropy based PCA and MSPCA. Lead-III signal from Data set M-01-040 is shown.

MOS error for ECG segments		
Segments	Centropy based PCA	Centropy based MSPCA
P-wave	31.11	11.11
PR-segment	26.67	11.12
PR-interval	22.22	11.01
QRS-complex	23.33	08.89
ST-segment	32.22	10.00
T-wave	25.55	08.89
MOS errors for ECG signal		
Overall signal	26.85	10.18

higher for Centropy based PCA method. The Centropy based MSPCA method shows better MOS ratings for ECG segments and signal (MOS value is 10.18%). As per the quality group [71] of the processed signal, the overall signal quality falls under very good category. A few reconstructed ECG segments (QRS-complex, ST-segment and T-wave) fall in excellent groups.

In Figure 5.6, first three beats of an ECG signal is distorted with random Gaussian noise and is processed with Centropy based MSPCA method. The clinical component like T-wave is more effected (Figure 5.6(b)). The proposed Centropy captures clinical information. The Centropy based MSPCA method recovers these noisy beats. That is even in noisy ECG data environment, Centropy represents the clinical information and helps selecting PC's that carry information related to ECG beats. Similarly, in Figure 5.7, noise is introduced in isoelectric region. The method based on MSPCA not only clean these region but equally preserve the clinical information existing in other regions.

5.2.1 Evaluation of Multiscale Distortion

Multichannel ECG (MECG) signals from standard ECG database, CSE multilead measurement library, data set-M01-021, are considered. These are subjected to amplitude normalization and mean removal. From each channel data, 4096 samples are chosen as a block. Wavelet decomposition using Daubechies 9/7 biorthogonal wavelet filters up to six levels are used for each channel data and same has been applied for reconstruction filters also. The seven multiscale matrices, A_L, and D_j, are processed with MSPCA. It is seen that the relative energy of wavelet subbands in terms of energy contribution efficiency (ECE) is higher in higher order subbands. Thus, the main clinical components

TH-1102_06610204

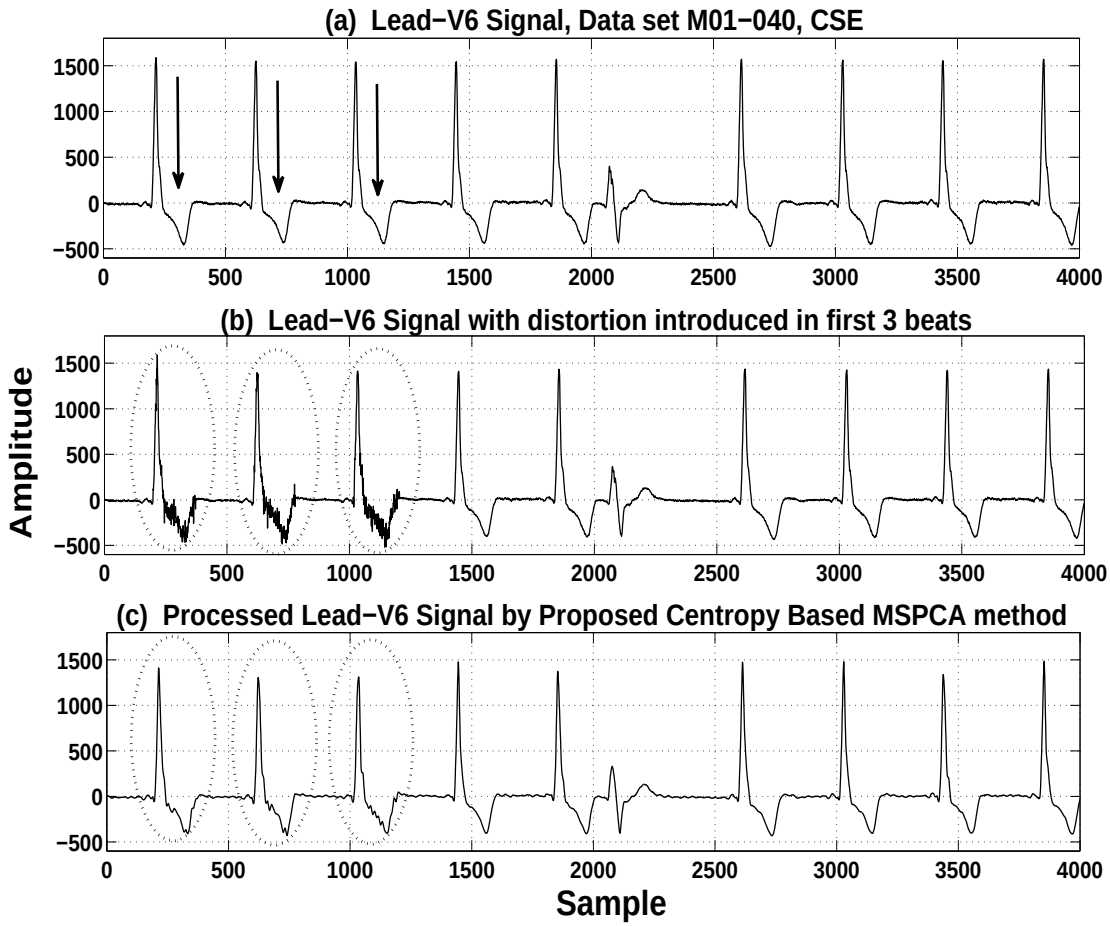

Figure 5.6: Original Lead-V6 signal, beats distorted signal and processed signal using Centropy based MSPCA method. In panels (a) Original Lead-V6 signal, (b) Signal with distortion introduced in first three beats by random Gaussian noise (c) reconstructed signals using proposed Centropy based MSPCA. The dataset-M01-040 is taken from CSE multilead measurement library.

of an ECG signal remain in higher order subbands whereas lower order subbands are less significant. This implies the dimension reduction (DR) may be possible at lower order subband matrices without losing 'PQRST' morphologies. So, D_1, D_2 and D_3 are treated with reduced dimensions and distortion measures are evaluated for validation of this method.

In Fig. 5.8, original and reconstructed lead-II ECG signal is shown after MSPCA operation. With more dimension reduction in multiscale matrices such as D_1, D_2 & D_3, more deviation of reconstructed signal from the original is noticed. This deviation is nicely captured by proposed MMD metrics. Also, the average distortion which is proposed as MD reflect the mismatch between signals. In panel Fig. 5.8(b), the reconstructed signal with DR=2 is shown which gives lower MMD values

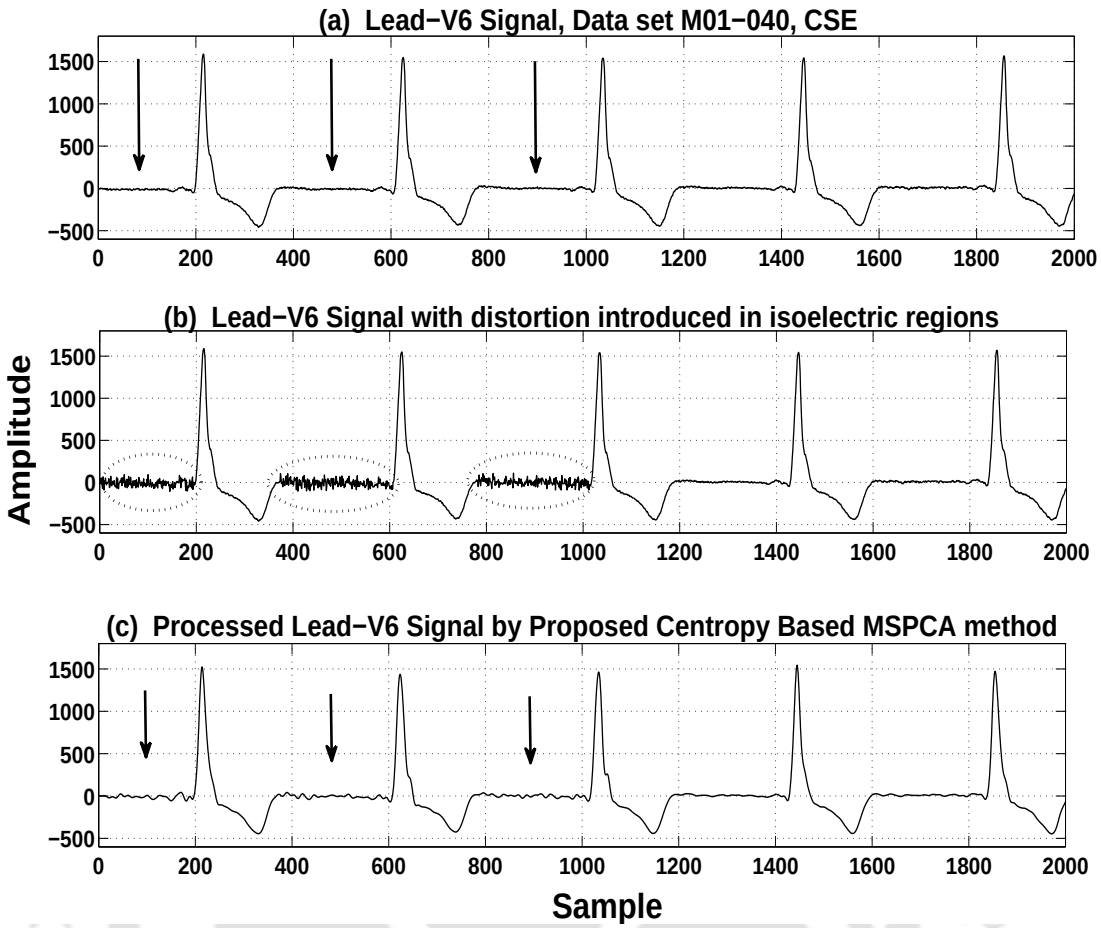

Figure 5.7: Original Lead-V6 signal, distorted signal and processed signal using Centropy based MSPCA method. In panels (a) Original Lead-V6 signal, (b) Signal with distortion introduced in isoelectric region by random Gaussian noise (c) reconstructed signals using proposed Centropy based MSPCA. The dataset-M01-040 is taken from CSE multilead measurement library.

as $\varepsilon_1 = 26.89$, $\varepsilon_2 = 19.13$, $\varepsilon_3 = 50.65$ and $MD = 15.63$. The signal is close to original and reflect all diagnostic components P-wave, QRS-complex and T-wave with sufficient fidelity. In panel Fig. 5.8(c), reconstructed signal with DR=5 shows a denoising effect. It gives MMD values $\varepsilon_1 = 39.01$, $\varepsilon_2 = 46.80$, $\varepsilon_3 = 72.88$ and $MD = 24.98$. In panel Fig. 5.8(d), where DR=10 signal distortion is noticed. Distortion metrics are found as $\varepsilon_1 = 97.73$, $\varepsilon_2 = 90.02$, $\varepsilon_3 = 90.63$ and $MD = 47.12$.

In Table 5.3, multichannel signal distortion measures in terms of proposed MMD and MD are shown. In MSPCA based processing without reducing dimensions at multiscale matrices the quantitative values of proposed distortion measures give satisfactory results. For no reduction in dimensions at all multiscale matrices MMD values are $\varepsilon_{A6} = 2.44$, $\varepsilon_6 = 2.57$, $\varepsilon_5 = 2.03$, $\varepsilon_4 = 1.40$, $\varepsilon_3 = 1.60$,

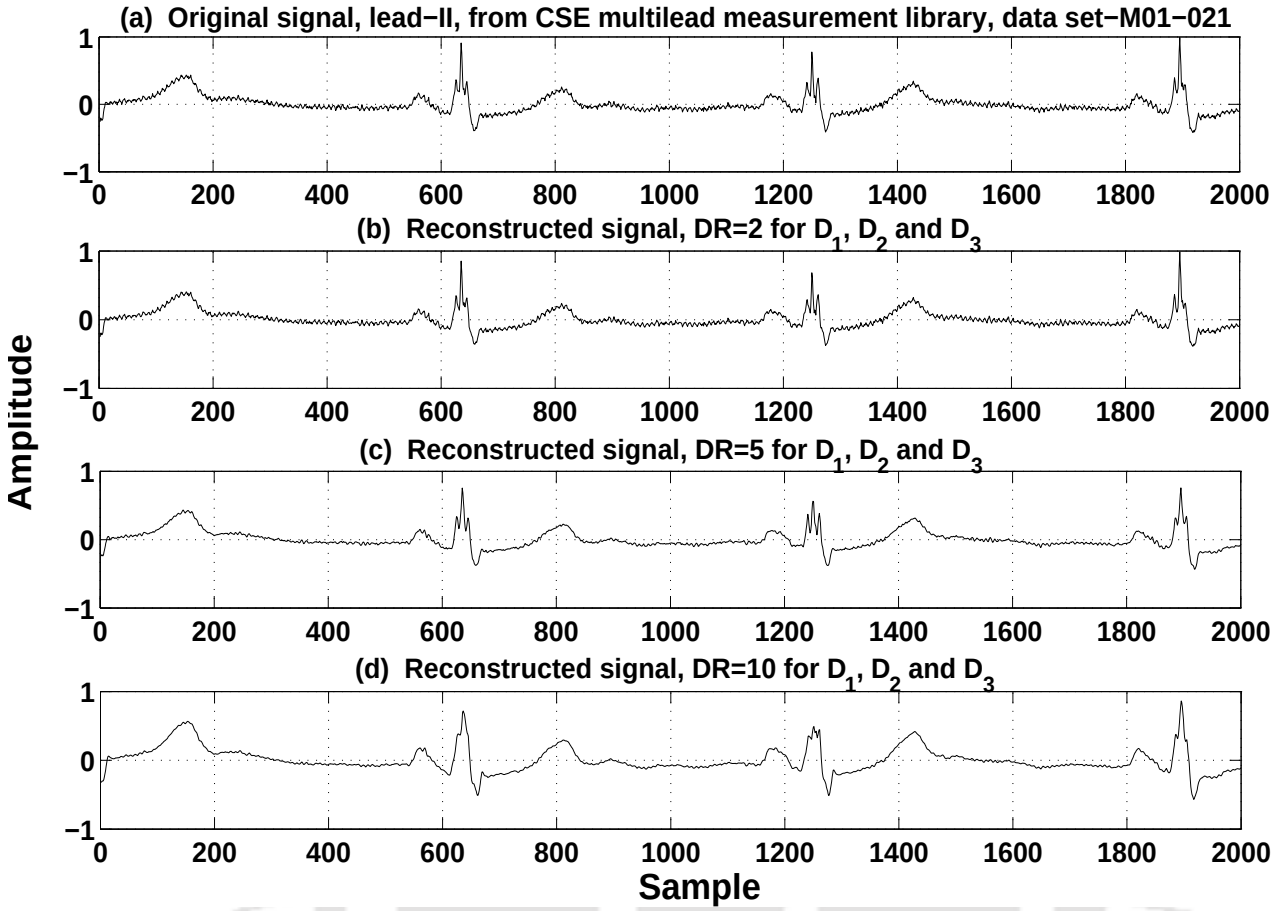

Figure 5.8: Original and reconstructed signal using MSPCA: (a) Original signal, (b) Reconstructed signal after MSPCA with DR=2 for D_1, D_2 & D_3 with corresponding MMDs $\varepsilon_1 = 26.89$, $\varepsilon_2 = 19.13$, $\varepsilon_3 = 50.65$ and $MD = 15.63$, (c) Reconstructed signal after MSPCA with DR=5 for D_1, D_2 & D_3 with corresponding MMDs $\varepsilon_1 = 39.01$, $\varepsilon_2 = 46.80$, $\varepsilon_3 = 72.88$ and $MD = 24.98$ and (d) Reconstructed signal after MSPCA with DR=10 for D_1, D_2 & D_3 with corresponding MMDs $\varepsilon_1 = 97.73$, $\varepsilon_2 = 90.02$, $\varepsilon_3 = 90.63$ and $MD = 47.12$. CSE multilead measurement library, data set-M01-021.

$\varepsilon_2 = 1.44$, $\varepsilon_1 = 1.03$ and MD is 1.79. For dimension reduction (DR) from 1 to 11 for matrices D_1=D_2=D_3, proposed distortion metrics are shown in table. It is noticed that the quantitative values of MMDs and MD are increasing with increasing number of DR. This indicates the correct trend. That is, if we reduce more dimensions less number of eigen-values are retaining in MSPCA processing. So, it captures the less energy of original signal and loss in signal energy will be more.

For the same data set-M01-040, the proposed multiscale distortion metrics are evaluated. If the threshold is decided at 80% of information, the selection of PC for matrices D_1, D_2 and D_3 are 8, 7

Table 5.3: Multiscale multivariate distortion (MMD) and multiscale distortion (MD), Database used is CSE multilead measurement library, data set-M01-021

Multiscale multivariate distortion when dimension reduction in subband matrices D_1=D_2=D_3												
MMD	**DR=1**	**DR=2**	**DR=3**	**DR=4**	**DR=5**	**DR=6**	**DR=7**	**DR=8**	**DR=9**	**DR=10**	**DR=11**	**No DR**
$\varepsilon_{A6}(A_6)$	3.71	3.17	2.95	3.44	3.82	5.77	6.57	8.73	0.50	11.05	11.76	2.44
$\varepsilon_6(D_6)$	4.19	3.50	3.16	3.76	4.34	4.68	5.60	7.54	10.46	14.24	15.48	2.57
$\varepsilon_5(D_5)$	4.21	3.38	3.06	3.67	4.25	5.08	6.01	7.15	10.35	12.85	13.83	2.03
$\varepsilon_4(D_4)$	3.58	2.67	2.41	2.83	3.22	7.03	8.40	11.33	13.59	13.30	14.24	1.40
$\varepsilon_3(D_3)$	34.50	50.65	64.64	72.88	73.41	78.28	78.27	81.12	81.80	90.63	93.85	1.60
$\varepsilon_2(D_2)$	13.69	19.13	23.36	46.19	46.80	75.94	80.35	86.64	86.61	90.02	93.94	1.44
$\varepsilon_1(D_1)$	22.77	26.89	36.60	36.78	39.01	65.15	79.30	89.27	96.14	97.73	97.61	1.03
Multiscale distortion when dimension reduction in D_1=D_2=D_3												
MD	12.38	15.63	19.45	24.22	24.98	34.56	37.78	41.68	44.21	47.12	48.67	1.79

and 7 respectively. The MMD values for D_1, D_2, D_3 D_4, D_5, D_6 and A_6, are 79.92, 45.48, 63.89, 2.14, 2.08, 1.93, and 2.07. The overall distortion is measure in terms of MD. for above data set, MD value is found as 0.5268. The distortion values are higher in the matrices where dimensions are reduced. Low distortion values are found where no dimensions are reduced. This reflects the ability of this method for true representation of distortion introduced.

5.3 Summary

In this Chapter, novel Centropy based PCA and MSPCA are proposed for multichannel electrocardiogram signals. It is seen that the Centropy quantifies the clinical information. For preservation of signal fidelity in terms of clinical information, threshold based on Centropy can be successfully used for selection of principal components. The evaluation of measures such as PRD, RMSE and CC show that Centropy based PCA perform superior to conventional PCA. The Centropy based MSPCA method efficiently removes the redundant information. At wavelet scales Centropy better quantifies the clinical information. It captures the signal energy while filtered the unwanted signals. The MOS evaluation shows that the processed signal falls under very good category.

Secondly, a novel distortion measure for wavelet based processing for multichannel ECG is proposed. After MSPCA processing of multichannel ECG, MMD is evaluated for multiscale matrices. MD is evaluated taking average of all MMDs. It is seen that the MMD and MD are well correlated with the distortion introduced by reducing the number of significant eigen values. There is a need to add weights to multiscale MMDs to get a proper MD measure.

TH-1102_06610204

TH-1102_06610204

6

Conclusions

Contents

TH-1102_06610204

In this thesis, a few schemes for multiscale processing of multichannel Electrocardiogram signals are investigated. For preprocessing of signals, two novel denoising methods are proposed and performances are compared with existing gold standard denoising methods. For multichannel electrocardiogram data compression, Multiscale PCA is introduced and dimension reduced PCA coefficients are Huffman encoded. Also, a novel Clinical Entropy (Centropy) based method for PCA and Multiscale PCA is investigated. The compressed signals after multiscale PCA applications are subjected to error analysis. A Multiscale Distortion Measure is introduced.

In **Chapter 1** and **2**, introduction to single channel and multichannel electrocardiogram signals and various processing methods are discussed. In **Chapter 1**, the significance of clinical components of ECG signals are discussed. Also, its processing in time, frequency and time-frequency domain are reviewed from existing published literatures. In **Chapter 2**, a related reviews of wavelet transform based ECG signal processing is given. To extract information in depth which may not be readily available in time domain signals, the signal transformation tools are used. Wavelet transformed based noise elimination and compression for single and multi-lead signals are discussed along with PCA based processing. It is felt that the wavelet and PCA may be combined to process multichannel signals.

In **Chapter 3**, two novel denoising methods are proposed. In the first method (M1), HOS and ECE based, four denoising factors are introduced for filtering of ECG signal. Best performance is observed with DF_{jM1} which is based on HOS and ECE of wavelet subband signal. Kurtosis employed in this work, discriminate signal and noise. It is observed that the spikes or sudden change in signal frequency along with noise gives a higher value of Kurtosis. Taking advantage of this property of Kurtosis, DF_{jM1} is scaled by ECE of MECG signal. Since it is established that the ECE value in higher level wavelet subband coefficients are more than lower ones, most of the energy of ECG signal remain in higher sub-bands such as cA6, cD6, cD5 and cD4. So, lower subbands, cD1, cD2 and cD3, are chosen for thresholding.

The second method (M2), introduces a novel denoising method based on relative energy contribution of wavelet subbands and Kurtosis based Gaussian noise estimator for filtering of ECG signal. Estimated noise variance in wavelet subband is computed with a new approach which includes Gaussianity measure in term of Kurtosis instead of conventional statistical approach. Lower order

subbands are expected to have relatively higher noise energy compared to the signal energy. The proposed method gives higher threshold values for lower order subbands. It is the combination of three individual factors, α_j, β_j and γ_j. Combined denoising factor gives improved results. The method is tested with spatially nonhomogeneous functions, Blocks, Bumps, HeaviSine and Doppler with noise. The performance of the proposed thresholding method evaluated using synthetic ECG signal after adding noise and the recorded signal from database. Also, it is compared with the existing classical thresholding method such as soft thresholding, hard threshoding and SURE. Results show that the performance of the proposed method is better compared to the existing methods. The proposed denoising method not only filters ECG signal effectively but also can help retain the clinical information in the signal.

The lowest PRD value of 3.4736 is found for lead-V4 for the first denoising method (M1) whereas for second method (M2) lead-V2 shows the lowest PRD value of 9.523. Similarly, the lowest WWPRD and WEDD values 5.1903 (lead-V4) and 1.8718 (lead-aVL) are found for the first method. The second method yields the lowest WWPRD and WEDD for lead-V3 (17.743) and lead-V2 (4.00) respectively. WEDD measure is more robust and it is claimed to represent the quality of the diagnostic features in a processed ECG signal [71]. As per this metric the filtered signals of all the leads by 'M1', fall under 'excellent' category whereas 'M2' gives excellent category signal only for leads Lead-II. Remaining filtered multichannel signals by means of 'M2' fall under 'very good' or 'good' categories. It may be due to higher thresholds for 'M2' filtering method which removes more wavelet coefficients giving higher WEDD values.

In **Chapter 4**, the correlations between channels and the multiscale properties of wavelet transform are used for improvement in dimension reduction and hence samples reduction of multichannel ECG signals without distortion of clinical information. Signals are decomposed into subbands using wavelet transform. Coefficients are arranged in subband matrices. In different wavelet scales, higher correlations are observed between standard 12 leads ECG signal. The proposed MSPCA is applied on these subbands matrices. A new PC selection method based on subband weights is also proposed. Qualitative and quantitative performance are compared with methods existing in literatures. A data reduction of 50.37% samples with APRD value of 10.01% is obtained for the proposed method. The reconstructed signals of all the leads show preservation of diagnostic features.

TH-1102_06610204

Subsequently, Multiscale PCA in wavelet domain is used for compression of multichannel ECG signals without distorting the clinical information. A new PC selection method based on energy (AFEC) is also proposed. MSPCA coefficient at a few certain scales are uniformly quantized and Huffman encoded for multichannel compression. Quantitatively, the performance is compared with existing compression method. The reconstructed signals of all the leads show preservation of diagnostic features and a very good MOS rating. The proposed scheme based on MSPCA gives sample reduction ratio of 1.45:1 and Entropy coding stage gives compression ratio $5.98:1$ with PRD value 2.09% and the lowest WEDD value of 4.19%. Based on MOS error criteria the reconstructed all ECG segments and signals (Table 4.9) falls under very good category [71, 137].

In **Chapter 5**, novel clinical entropy based PCA and MSPCA are proposed for multichannel electrocardiogram signals. It is seen that the Centropy quantifies the clinical information. For preservation of signal fidelity in terms of clinical information, threshold based on Centropy can be successfully used for selection of principal components. The evaluation of measures such as PRD, RMSE and CC show that Centropy based PCA perform superior to conventional PCA. The Centropy based MSPCA method efficiently removes the redundant information. At wavelet scales Centropy better quantifies the clinical information. It captures the signal energy while filtered the unwanted signals. Subjective quality of reconstructed signal is evaluated using Mean Opinion Scores (MOSs). MOS scores for ECG segments and reconstructed signals are evaluated for Centropy based PCA and MSPCA methods. The MOS value, 26.85%, is found for Centropy based PCA method whereas Centropy based MSPCA method shows better MOS value, 10.18%. As per the quality group [71] of the processed signal, the overall signal quality falls under very good category.

Secondly, after MSPCA processing of multichannel ECG, Multiscale Multivariate Distortion (MMD) is evaluated for multiscale matrices. Multiscale Distortion (MD) is evaluated taking average of all MMDs. It is seen that the MMD and MD are well correlated with the distortion introduced by reducing the number of significant Eigenvalues. There is a need to add weights to multiscale MMDs to get a proper MD metric. This may help find more meaningful distortion metric representing distortion on diagnostically important clinical components.

The major contributions of the work reported in this thesis includes,

(i) Denoising using Higher Order Statistics in wavelet Subbands.

(ii) Denoising based on Estimated Noise Variance based on Kurtosis, Multiscale Energy and Number of Samples.

(iii) Multiscale principal component analysis for multichannel ECG and compression of multichannel ECG data.

(iv) Clinical Entropy based PCA and MSPCA analysis for ECG Signals.

(v) Multiscale Distortion measure for multichannel ECG signals.

The other contributions are,

(i) Multiscale multivariate energy contribution efficiency for multichannel ECG.

(ii) Denoising multichannel ECG using multiscale principal component analysis.

(iii) Quality controlled denoising of multichannel ECG signals using multiscale principal component analysis.

6.1 Scope for the Future Work

- Multiscale PCA can be used for noise elimination from multichannel data. There is a scope to use it for quality controlled denoising of the signals. So, the proposed MSPCA based method may be tested with other physiological signals like Electroencephalogram (EEG), Electromyogram (EMG) etc.
- The Multiscale PCA can be used for extraction of speech signal from its multichannel recording.
- The proposed Multiscale PCA can be used for diagnostic decision purpose. This can to be developed with sufficient pathological data.
- The problem of fetal ECG separation from mother ECG using multilead recording can be investigated using proposed MSPCA based processing.

TH-1102_06610204

- MSPCA based processing of multichannel ECG can be exploited for cardiac mapping applications.
- The proposed method can be used for applications like body surface potential mapping and body surface area networks.
- The PCA and MSPCA based Centropy (Clinical Entropy) can be applied to other biomedical signals.

भारतीय प्रौद्योगिकी संस्थान गुवाहाटी • Indian Institute of Technology Guwahati •

References

[1] S. A. Jones, *ECG Success: Exercises in ECG Interpretation*. F. A. Davis Company, Philadelphia, Copyright 2008.

[2] J. L. Willems, “CSE multilead atlas, measurement results - data set 3, common standards for quantitative electrocardiography,” *Commission of the European Communities, Medical and Public Health Research, Leuven*, vol. Ref. Nr. CSE 88-04-15, 15th. April 1988.

[3] L. Schamroth, *An Introduction to Electro Cardiology*. Blackwell Science, London.

[4] F. Morris, J. Edhouse, W. J. Brady, and J. Camm, Eds., *ABC of clinical electrocardiography*. BMJ Books, BMA House, Tavistock Square, London WC1H 9JR, 2003.

[5] W. Tompkins, *Biomedical Digital Signal Processing*. New Jersey: Prentice-Hall, 1993.

[6] A. C. Guyton and J. E. Hall, *Textbook Of Medical Physiology*, 11th ed. Elsevier Inc., 2006.

[7] M. Kania, M. Fereniec, and R. Maniewski, “Wavelet denoising for multi-lead high resolution ECG signals,” *Measurement Science Review*, vol. Volume 7, Section 2, No. 4, pp. 30–33, 2007.

[8] P. Laguna, R. Jane, and P. Caminal, “Automatic detection of wave boundaries in mulilead ECG signalsl validation with the CSE database,” *Computer and Biomedical Research, Academic Press, Inc.*, vol. 27, pp. 45–60, 1994.

[9] S. Mehta and N. Lingayat, “Development of SVM based classification techniques for the delineation of wave components in 12-lead electrocardiogram,” *Biomedical Signal Processing and Control, Elsevier*, vol. 3, pp. 341–349, 2008.

[10] M. Shen, L. Wang, K. Zhu, and J. Zhu, “Multi-lead ECG classification based on independent component analysis and support vector machine,” vol. 3, pp. 960 –964, oct. 2010.

[11] W. Ye, S. Li, X. Wu, and J. Ye, “Detection of multilead ECG character points and assessment based on a reference database,” pp. 3895 –3898, jan. 2005.

[12] F. Castells, P. Laguna, L. Sornmo, A. Bollmann, and J. Roig, “Principal component analysis in ECG signal processing,” *EURASIP Journal on Advances in Signal Processing, Hindawi Publishing Corporation*, vol. doi:10.1155/2007/74580, p. 21, 2007.

[13] M. P. S. Chawla, “A comparative analysis of principal component and independent component techniques for electrocardiograms,” *Neural Comput and Applic, Springer-Verlag London Limited*, vol. 18, pp. 539 – 556, 2009.

[14] P. Langley, E. J. Bowers, and A. Murray, “Principal component analysis as a tool for analyzing beat-to-beat changes in ECG features: Application to ECG-derived respiration,” *IEEE Transactions on biomedical engineering,*, vol. 57 (4), pp. 821 – 829, 2010.

[15] L. Sornmo and P. Laguna, *Bioelectrical Signal Processing in Cardiac and Neurological Applications*. Elsevier Academic Press, 2005.

[16] H. Tam and J. G. Webster, “Minimizing electrode motion artifact by skin abrasion,” *IEEE Trans. Biomed. Eng*, vol. 24, pp. 134–139, 1977.

[17] D. P. Burbank and J. G. Webster, “Reducing skin potential motion artifact by skin abrasion,” *Med. Biol. Eng. Comput*, vol. 16, pp. 31–38, 1978.

[18] J. C. Huhta and J. G. Webster, “60-hz interference in electrocardiography,” *IEEE Trans. Biomed. Eng*, vol. 43, pp. 91–101, 1973.

[19] R. Sameni, C. J. Mohammad B. Shamsollahi, and G. D. Clifford, “A nonlinear bayesian filtering framework for ECG denoising,” *IEEE Trans. Biomed. Eng.*, vol. Vol. 54, No. 12, pp. 2172 – 2185, December 2007.

[20] I. I. Christov and I. K. Daskalov, “Filtering of electromyogram artefacts from the electrocardiogram,” *Med. Eng. Phys*, vol. 21, p. 731736, 1999.

[21] S. Leanderson, P. Laguna, and L. Sornmo, “Estimation of respiration frequency using spatial information from the VCG,” *Med. Eng. Physics*, vol. 25, pp. 501–507, 2003.

[22] N. V. Thakor and Y.-S. Zhu, “Applications of adaptive filtering to ECG analysis: Noise cancellation and arrhythmia detection,” *IEEE Trans. on Biomedical Engineering*, vol. 38(8), pp. 785–794, August 1991.

[23] A. Lallouani, M. Gabrea, and C. Gargour, “Wavelet based speech enhancement using two different threshold-based denoising algorithms,” in *CCECE 2004- CCGEI 2004, Niagara Falls, Maylmai 2004*, copyright 2004 IEEE.

[24] Y. Wu, R. M. Rangayyan, Y. Zhou, and S.-C. Ng, “Filtering electrocardiographic signals using an unbiased and normalized adaptive noise reduction system,” *Medical Engineering and Physics, Elsevier*, vol. vol.31, pp. 17–26, 2009.

[25] R. M. Rangayyan, *Biomedical signal analysis: A case-study approach*. New York, NY: IEEE and Wiley, 2002.

[26] W. B, G. JR, M. JM, W. CS, and e. a. Hearn RH, “Adaptive noise cancelling: principles and applications,” *Proc IEEE 1975*, vol. Vol. 63, No. 12, pp. 1692 – 1716, 1975.

[27] I. Daubechies, Ed., *Nonlinear Wavelet Methods for Recovery of Signals, Densities, and Spectra from Indirect and Noisy Data*, vol. Vol 47, Different Perspectives on Wavelets, Proceeding of Symposia in Applied Mathematics. Providence, R.I.: Amer. Math. Soc., 1993, nonlinear Wavelet Methods for Recovery of Signals, Densities, and Spectra from Indirect and Noisy Data.

[28] D. L. Donoho, “De-noising by soft thresholding,” *IEEE Trans. Inform. Theory*, vol. 41, pp. 613 – 627, May 1995.

[29] D. L. Donoho and I. M. Johnstone, “Adapting to unknown smoothness via wavelet shrinkage,” *J. Amer. Statist. Assoc.*, vol. 90, pp. 1200 –1224, Dec. 1995.

[30] J. Gao, H. Sultan, J. Hu, and W.-W. Tung, “Denoising nonlinear time series by adaptive filtering and wavelet shrinkage: A comparison,” *IEEE SIGNAL PROCESSING LETTERS*, vol. vol. 17, no. 3, March 2010.

[31] C. M. Kortman, “Redundancy reduction-a practical method of data compression,” *Proceedings of the IEEE*, vol. 55 (3), pp. 253–263, March 1967.

[32] J. R. C. et al., “AZTEC: A preprocessing program for real-time ECG rhythm analysis,” *IEEE Trans. Biomed. Eng.*, vol. 15, p. 128129, 1968.

[33] W. C. Mueller, “Arrhythmia detection program for an ambulatory ECG monitor,” *Biomed. Sci. Instrument,*, vol. 14, p. 8185, 1978.

[34] J. P. Abenstein and W. J. Tompkins, “New data reduction algorithm for real-time ECG analysis,” *IEEE Trans. Biomed. Eng*, vol. 29, p. 4348, 1982.

[35] M. Ishijima, S.-B. Shin, G. H. Hostetter, and J. Sklansky, “Scan-along polygonal approximation for data compression of electrocardiograms,” *IEEE Trans. Biomed. Eng.*, vol. 30, pp. 723–729, 1983.

[36] S. M. S. Jalaleddine and et. al., “ECG data compression techniques - a unified approach,” *IEEE Transactions on Biomedical Engineering*, vol. 37, No. 4, pp. 329 – 343, 1990.

[37] S. C. Tai, “Slope-a real-time ECG data compressor,” *Medical and Biological Engineering and Computing*, vol. 29 (2), pp. 175–179, March 1991.

[38] ——, “ECG data compression by corner detection,” *Medical and Biological Engineering and Computing*, vol. 30 (6), pp. 584–590, March 1992.

[39] X. Huang, M. English, and R. Vincent, “Fast ECG data compression algorithms suitable for microprocessor systems,” *Journal of Biomedical Engineering*, vol. 14 (1), pp. 64–68, January 1992.

[40] H. I. Shahein and H. M. Abbas, “ECG data compression via cubic-splines and scan-along polygonal approximation,” *Signal Processing*, vol. 35 (3), pp. 269–283, February 1994.

[41] V. Kumar, S. Saxena, V. Giri, and D. Singh, “Improved modified AZTEC technique for ECG data compression: Effect of length of parabolic filter on reconstructed signal,” *Computers and Electrical Engineering*, vol. 31, (4-5), pp. 334–344, June-July 2005.

[42] N. Ahmed, P. J. Milne, and S. G. Hams, “Electrocardiographic data compression via orthogonal transforms,” *IEEE Transactions on Biomedical Engineering*, vol. 22 (6), pp. 484–487, Nov. 1975.

[43] M. Womble, J. Halliday, S. Mitter, M. Lancaster, and J. Triebwasser, “Data compression for storing and transmitting ECG’s/VCG’s,” *Proceedings of the IEEE*, vol. 65 (5), pp. 702–706, May 1977.

[44] W. S. Kuklinski, “Fast walsh transform data-compression algorithm; ECG applications,” *Medical and Biological Engineering and Computing*, vol. vol. 21, pp. 465–472, 1983.

[45] E. Berti, F. Chiaraluce, N. Evans, and J. McKee, “ECG data compression using double logarithmic quantisation of walsh spectrum,” *Electronics Letters*, vol. 31 (13), pp. 1025–1026, June 1995.

[46] B. R. S. Reddy and I. S. N. Murthy, “ECG data compression using fourier descriptors,” *IEEE Transactions on Biomedical Engineering*, vol. 33 (4), pp. 428–434, April 1986.

[47] H. A. M. Al-Nashash, “ECG data compression using adaptive fourier coefficients estimation,” *Medical Engineering and Physics*, vol. 16 (1), pp. 62–66, January 1994.

[48] S. C. Tai, “Six-band sub-band coder on ECG waveforms,” *Medical and Biological Engineering and Computing*, vol. 30, pp. 187–192, 1992.

[49] M. Aydin, A. Cetin, and H. Koymen, “ECG data compression by sub-band coding,” *IET Electronics Letters*, vol. 27 (4), pp. 359–360, Feb. 1991.

[50] J. H. Husy and T. Gjerde, “Computationally efficient subband coding of ECG signals,” *Medical Engineering and Physics*, vol. 18 (2), pp. 132–142, March 1996.

[51] M. Blanco-Velasco, F. Cruz-Roldn, F. Lpez-Ferreras, ngel Bravo-Santos, and D. Martnez-Muoz, “A low computational complexity algorithm for ecg signal compression,” *Medical Engineering and Physics*, vol. 26 (7), pp. 553–568, Sept. 2004.

[52] B.-V. M., C.-R. F., G.-L. J. I., and K. Barner, “ECG compression with retrieved quality guaranteed,” *IET Electronics Letters*, vol. 40 (23), pp. 1466–1467, Nov. 2004.

[53] W. Philips and G. De Jonghe, “Data compression of ECG’s by high-degree polynomial approximation,” *IEEE Transactions on Biomedical Engineering*, vol. 39 (4), pp. 330–337, Apr. 1992.

[54] ——, “Data compression of ecg’s by high-degree polynomial approximation,” *Biomedical Engineering, IEEE Transactions on*, vol. 39, no. 4, pp. 330 –337, april 1992.

[55] A. A. Colomer and A. A. Colomer, “Adaptive ECG data compression using discrete legendre transform,” *Digital Signal Processing*, vol. 7 (4), pp. 222–228, Oct. 1997.

[56] W. Philips, “ECG data compression with time-warped polynomials,” *IEEE Transactions on Biomedical Engineering*, vol. 40 (11), pp. 1095–1101, Nov 1993.

[57] L. V. Batista, E. U. K. Melcher, and L. C. Carvalho, “Compression of ECG signals by optimized quantization of discrete cosine transform coefficients,” *Medical Engineering and Physics*, vol. 23 (2), pp. 127–134, March 2001.

[58] R. Borsali, A. Nait-Ali, and J. Lemoine, “ECG compression using an ensemble polynomial modeling: Comparison with the dct based technique,” *Cardiovascular Engineering: An International Journal Neurosci Methods*, vol. 4 (3), pp. 237–244, Sept. 2004.

[59] V. A. Allen and J. Belina, “ECG data compression using the discrete cosine transform,” *Computers in Cardiology, IEEE Computer Society Press, Silverspring, MD*, pp. 687–690, Oct. 1992.

[60] B. Madhukar and I. S. N. Murthy, “ECG data compression by modeling,” *Computers and Biomedical Research*, vol. 26 (3), pp. 310–317, June 1993.

[61] P. Chazal, M. O’Dwyer, and R. B. Reilly., “Automatic classifcation of heart-beats using ECG morphology and heartbeat interval features,” *IEEE Trans. on Biomedical Engineering*, vol. 51(7), pp. 1196–1206, July 2004.

[62] N. V. Thakor, J. G. Webster, and W. J. Tompkins, “Design, implementation, and evaluation of a microcomputer-based portable arrhythmia monitor,” *Medical and Biological Engineering and Computing*, vol. 22(2), pp. 151–159, March 1984.

[63] ——, “Estimation of QRS-complex power spectra for design of a QRS filter,” *IEEE Trans. on Biomedical Engineering*, vol. 31(11), pp. 702–706, November 1984.

[64] G. M. Friesen, T. C. Jannett, M. A. Jadallah, S. L. Yates, S. R. Quint, and H. T. Nagle, “A comparision of the noise sensitivity of nine qrs detection algorithms,” *IEEE Trans. on Biomedical Engineering*, vol. 37(1), pp. 85–98, Jan. 1990.

[65] B.-U. Kohler, C. Hennig, and R. Orglmeister, “The principles of software QRS detection,” *IEEE Engineering in Medicine and Biology*, pp. 42–57, Jan.-Feb. 2002.

[66] H. C. Bazett, “An analysis of the time relations of electrocardiograms,” *Heart*, vol. 7, pp. 353–370, 1920.

[67] P. J and T. W., “A real-time QRS detection algorithm,” *IEEE Trans Eng Biomed Eng.*, vol. 32(3), p. 230236, 1985.

[68] P. S. Hamilton and W. J. Tompkins, “Quantitative investigation of QRS detection rules using the MIT/BIH arrhythmia database,” *IEEE Trans. on Biomedical Engineering*, vol. 33(12), pp. 1157–1165, Dec. 1986.

[69] D. S. B. et al., “A new QRS detection algorithm based on the hilbert transform,” *Comput. Cardiol.*, vol. 27, p. 379382, 2000.

[70] Stamkopoulos, T., K. Diamantaras, N. Maglaveras, and M. Strintzis, “ECG analysis using nonlinear pca neural networks for ischemia detection,” *Signal Processing, IEEE Transactions on*, vol. 46, no. 11, pp. 3058 –3067, nov 1998.

[71] M.S.Manikandan and S. Dandapat, “Wavelet energy based diagnostic distortion measure for ECG,” *Journal of Biomedical Signal Processing and Control, Elsevier*, vol. 2, pp. 80 – 96, 2007.

[72] K. Nagarajan, E. Kresch, S. Rao, and Y. Kresh, “Constrained ECG compression using best adapted wavelet packet bases,” *IEEE Signal Processing Letters*, vol. 3 (10), pp. 273–275, Oct 1996.

[73] J. Chen and S. Itoh, “A wavelet transform-based ECG compression method guaranteeing desired signal quality,” *IEEE Trans. Biomed. Eng.*, vol. 45, no. 12, pp. 1414 – 1419, Dec. 1998.

[74] M. Sabah, A. Al-Shrouf, and M. Abo-Zahhad, “ECG data compression using optimum non-orthogonal wavelet transform,” *Med. Eng. Phys*, vol. 22, p. 3946, 2000.

[75] R. Istepanian and A. Petrosian, “Optimal zonal wavelet-based ECG data compression for a mobile telecardiology system,” *IEEE Transactions on Information Technology in Biomedicine*, vol. 4 (3), pp. 200–211, Sept. 2000.

[76] R. Istepanian, L. Hadjileontiadis, and S. Panas, “ECG data compression using wavelets and higher order statistics methods,” *IEEE Transactions on Information Technology in Biomedicine*, vol. 5 (2), pp. 108–115, Jun 2001.

[77] B. Rajoub, “An efficient coding algorithm for the compression of ECG signals using the wavelet transform,” *IEEE Transactions on Biomedical Engineering*, vol. 49 (4), pp. 355–362, Apr. 2002.

[78] M. Abo-Zahhad and B. A. Rajoub, “An effective coding technique for the compression of one-dimensional signals using wavelet transforms,” *Medical Engineering and Physics*, vol. 24 (3), pp. 185–199, April 2002.

[79] R. Benzid, F. Marir, A. Boussaad, M. Benyoucef, and D. Arar, “Fixed percentage of wavelet coefficients to be zeroed for ECG compression,,” *IET Electronics Letters*, vol. 39 (11), pp. 830–831, May 2003.

[80] B. Kim, S. Yoo, and M. Lee, “Wavelet-based low-delay ECG compression algorithm for continuous ECG transmission,” *IEEE Transactions on Information Technology in Biomedicine*, vol. 10 (1), pp. 77–83, Jan. 2006.

[81] C. T. Ku, H. S. Wang, K. C. Hung, and Y.-S. Hung, “A novel ECG data compression method based on nonrecursive discrete periodized wavelet transform,” *IEEE Transactions on Biomedical Engineering*, vol. 53 (12), pp. 2577–2583, Dec. 2006.

[82] C. T. Ku, K. C. Hung, H. S. Wang, and Hung, “High efficient ECG compression based on reversible round-off non-recursive 1-D discrete periodized wavelet transform,” *Medical Engineering and Physics*, vol. 29 (10), pp. 1149–1166, Dec. 2007.

[83] M.S.Manikandan and S. Dandapat, “Wavelet threshold based ECG compression using USZZQ and huffman coding of DSM,” *Journal of Biomedical Signal Processing and Control, Elsevier*, vol. 1, no.4, pp. 261 – 270, 2006.

[84] M. Blanco-Velasco, F. Cruz-Roldan, J. Godino-Llorente, and K. Barner, “Wavelet packets feasibility study for the design of an ECG compressor,” *IEEE Transactions on Biomedical Engineering*, vol. 54 (4), pp. 766–769, April 2007.

[85] R. Benzid, F. Marir, and N. Bouguechal, “Electrocardiogram compression method based on the adaptive wavelet coefficients quantization combined to a modified two-role encoder,” *IEEE Signal Process. Lett.*, vol. 14 (6), pp. 373–376, 2007.

[86] M. Hilton, “Wavelet and wavelet packet compression of electrocardiograms,” *IEEE Transactions on Biomedical Engineering*, vol. 44 (5), pp. 394–402, May 1997.

[87] Z. Lu, D. Y. Kim, and W. Pearlman, “Wavelet compression of ECG signals by the set partitioning in hierarchical trees algorithm,” *IEEE Transactions on Biomedical Engineering*, vol. 47 (7), pp. 849–856, Jul 2000.

[88] S.-G. Miaou and C.-L. Lin, “A quality-on-demand algorithm for wavelet-based compression of electrocardiogram signals,,” *IEEE Transactions on Biomedical Engineering*, vol. 49 (3), pp. 233–239, Mar 2002.

[89] W. Hwang, C. Chine, and K. Li, “Scalable medical data compression and transmission using wavelet transform for telemedicine applications,” *IEEE Transactions on Information Technology in Biomedicine*, vol. 7 (1), pp. 54–63, ,2003.

[90] G. Tohumoglu and K. Erbil Sezgin, “ECG signal compression by multi-iteration ezw coding for different wavelets and thresholds,” *Computers in Biology and Medicine*, vol. 37 (2), pp. 173–182, February 2007.

[91] K. Anant, F. Dowla, and G. Rodrigue, “Vector quantization of ECG wavelet coefficients,” *IEEE Signal Processing Letters*, vol. 2 (7), pp. 129–131,, Jul 1995.

[92] S.-G. Miaou and H.-L. Yen, “Quality driven gold washing adaptive vector quantization and its application to ECG data compression,” *IEEE Transactions on Biomedical Engineering*, vol. 47 (2), pp. 209–218, Feb 2000.

[93] S. Miaou, H. L. Yen, and C. L. Lin, "Wavelet-based ECG compression using dynamic vector quantization with tree code vectors in single codebook," *IEEE Trans. Biomed. Eng.*, vol. 49 (7), pp. 671 – 680, July 2002.

[94] S.-G. Miaou and S.-N. Chao, "Wavelet-based lossy-to-lossless ECG compression in a unified vector quantization framework," *IEEE Transactions on Biomedical Engineering*, vol. 52 (3), pp. 539–543, March 2005.

[95] X. Wang and J. Meng, "A 2-d ecg compression algorithm based on wavelet transform and vector quantization,," *Digital signal Processing*, 2007.

[96] B. Bradie, "Wavelet packet-based compression of single lead ECG," *IEEE Transactions on Biomedical Engineering*, vol. 43 (5), pp. 493–501, May 1996.

[97] A. G. Ramakrishnan and S. Saha, "ECG coding by wavelet-based linear prediction," *IEEE Trans. Biomed. Eng.*, vol. vol. 44, no. 12, Dec. 1997.

[98] A. Al-Shrouf, M. Abo-Zahhad, and S. M. Ahmed, "A novel compression algorithm for electrocardiogram signals based on the linear prediction of the wavelet coefficients," *Digital Signal Processing*, vol. 13 (4), pp. 604–622, October 2003.

[99] A. A., S. Olmos, R. Istepanian, and J. Garcia, "Enhanced real-time ECG coder for packetized telecardiology applications," *IEEE Transactions on Information Technology in Biomedicine*, vol. 10 (2), pp. 229–236, April 2006.

[100] J. Crowe, N. Gibson, M. Woolfson, and M. Somekh, "Wavelet transform as a potential tool for ECG analysis and compression," *Journal of Biomedical Engineering*, vol. 14 (3), pp. 268–272, May 1992.

[101] N. Thakor, Y. Sun, H. Rix, and P. Caminal, "Multiwave: A waveletbased ECG data compression algorithm," *IEICE Transaction on Information and Systems*, vol. E76-D (12), p. 14621469, 1993.

[102] M. S. Manikandan and S. Dandapat, "Wavelet threshold based TDL and TDR algorithms for real-time ECG signal compression," *Journal of Biomedical Signal Processing and Control, Elsevier*, vol. 3, pp. 44 – 46, 2008.

[103] C.-T. Ku, K.-C. Hung, T.-C. Wu, and H.-S. Wang, "Wavelet-based ECG data compression system with linear quality control scheme," *Biomedical Engineering, IEEE Transactions on*, vol. 57 (6), pp. 1399 – 1409, June 2010.

[104] H. Kim, R. Yazicioglu, P. Merken, C. Van Hoof, and H.-J. Yoo, "ECG signal compression and classification algorithm with quad level vector for ecg holter system," *Information Technology in Biomedicine, IEEE Transactions on*, vol. 14 (1), pp. 93 – 100, Jan. 2010.

[105] L. J. Hadjileontiadis and S. M. Panas, "Separation of discontinuous adventitious sound from vesicular sounds using a wavelet based filter," *IEEE Trans. Biomed. Eng.*, vol. 44, no. 12, Dec 1997.

[106] A. Cohen and J. Kovacevic, "Wavelets: the mathematical background," *Proceedings of the IEEE*, vol. 84, no. 4, pp. 514 –522, apr 1996.

[107] M. M. Shaker, "EEG waves classifier using wavelet transform and fourier transform," *International Journal of Biomedical and Medical Sciences*, vol. 1,2, pp. 85 – 90, 2006.

[108] A. Graps, "Intrduction to wavelets," *IEEE Computer Siciety (Original paper published by IEEE Computer Siciety, 1995)*, vol. 2 (2), 2003.

[109] A. S. Al-Fahoum, "Quality assessment of ECG compression techniques using a wavelet-based diagonstic measure," *IEEE Trans. on Information Technology in Biomedicine*, vol. 10, no.1, pp. 182 –191, Jan.2006.

[110] J. S. Walker, *A primer on WAVELETS and their Scientific Applications*, C. P. LLC, Ed. Chapman and Hall/CRC, copyright 1999.

[111] A. Alesanco, S. Olmos, R. Istepanian, and J. Garcia, “A novel real-time multilead ECG compression and denoising method based on wavelet transform,” *Computer in Cardiology*, vol. 30, pp. 593–596, copyright 2003 IEEE.

[112] G. Fu, A. Hojjat, and A. Colchester, “Wavelet noise reduction based on energy features,” *Springer-Verlag Berlin Heidelberg, LNCS 5112*, vol. ICIAR 2008, pp. 75–84, 2008.

[113] C.-F. Ho, B.-K. Ling, T.-L. Wong, A.-P. Chan, and P.-S. Tam, “Fuzzy multiwavelet denoising on ECG signal,” *Electronics Letters*, vol. 39, no. 16, pp. 1163 – 1164, aug. 2003.

[114] X.-L. Yang and J.-T. Tang, “Hilbert-huang transform and wavelet transform for ECG detection,” pp. 1 –4, oct. 2008.

[115] A. Cetin, H. Koymen, and M. Aydin, “Multichannel ECG data compression by multirate signal processing and transform domain coding techniques,” *Biomedical Engineering, IEEE Transactions on*, vol. 40, no. 5, pp. 495 –499, may 1993.

[116] A. Cohen and Y. Zigel, “Compression of multichannel ECG through multichannel long-term prediction,” *Engineering in Medicine and Biology Magazine, IEEE*, vol. 17, no. 1, pp. 109 –115, jan.-feb. 1998.

[117] S.-G. Miaou and H.-L. Yen, “Multichannel ECG compression using multichannel adaptive vector quantization,” *Biomedical Engineering, IEEE Transactions on*, vol. 48, no. 10, pp. 1203 –1207, oct. 2001.

[118] L. N. Sharma, S. Dandapat, and A. Mahanta, “Multiscale principal component analysis to denoise multichannel ECG signals,” in *2010 5th Cairo International Biomedical Engineering Conference, CIBEC 2010, pp.17 - 20, Cairo, Egypt*, Dec. 2010.

[119] M. Kotas, “Application of projection pursuit based robust principal component analysis to ECG enhancement,” *Biomedical Signal Processing and Control, Elsevier*, vol. 1 (4), pp. 289–298, 2006.

[120] B. He and R. Cohen, “Body surface laplacian ECG mapping,” *Biomedical Engineering, IEEE Transactions on*, vol. 39, no. 11, pp. 1179 –1191, nov. 1992.

[121] D. Finlay, C. Nugent, M. Donnelly, P. McCullagh, and N. Black, “Optimal electrocardiographic lead systems: Practical scenarios in smart clothing and wearable health systems,” *Information Technology in Biomedicine, IEEE Transactions on*, vol. 12, no. 4, pp. 433 –441, july 2008.

[122] K. Pearson, “On lines and planes of closest fit to systems of points in space .” *Philosophical Magazine*, vol. Series 6, 2(11), pp. 559 – 572, 1901.

[123] H. Hotelling, “Analysis of a complex of statistical variables into principal components,” *Journal of Educational Psychology*, vol. 24(6 and 7), pp. pp.417 – 441 and pp.498 – 520, 1933.

[124] I. T. Joliffe, *Principal Component Analysis*, second edition ed. Springer, New York, NY, USA, 2002.

[125] N. P. and M. J. F., “Monitoring batch processes using multiway principal component analysis,” *The American Institute of Chemical Engineering Journal*, vol. 40 (8), p. 1361 1375, 1994.

[126] D. D. and M. T. J., “Nonlinear principal component analysis-based on principal curves and neural networks,” *Computers and Chemical Engineering*, vol. 20, p. 65 78, 1996.

[127] B. R. Bakshi, P. Bansal, and M. N. Nounou, “Multiscale rectification of random errors without fundamental process models,” *Computers and Chemical Engineering, Elsevier*, vol. 21, pp. S1167 – S1172, 20 May 1997.

[128] B. R. Bakshi, “Multiscale PCA with application to MSPC monitoring,” *AIChE Journal*, vol. vol. 44, no. 7, pp. 1596 – 1610, July 1998.

[129] ——, “Multiscale analysis and modeling using wavelets,” *Journal of Chemometrics*, vol. vol.13, pp. 415 – 434, 1999.

[130] M. E. Tipping and C. M. Bishop, “Probabilistic principal component analysis,” *Journal of the Royal Statistical Society. Series B (Statistical Methodology)*, vol. 61(3), pp. 611 – 622, 1999.

TH-1102_06610204

[131] R. C. and L. J.A., "Multivariate and multiscale monitoring of wastewater treatment operation," *Wat. Res., Elsevier*, vol. 35 (14), p. 3402 3410, 2001.

[132] G. Kerschen and J.-C. Golinval, "Non-linear generalization of principal component analysis: from a global to a local approach," *Journal of Sound and vibration*, vol. 254(5), pp. 867 – 876, 2002.

[133] M. Misra, H. H. Yue, S. J. Qin, and C. Ling, "Multivariate process monitoring and fault diagnosis by multi-scale PCA," *Computers and Chemical Engineering, Elsevier*, vol. 26, p. 1281 1293, 2002.

[134] D. S. Lee, J. M. Park, and P. A. Vanrolleghem, "Adaptive multiscale principal component analysis for on-line monitoring of a sequencing batch reactor," *Journal of Biotechnology, Elsevier*, vol. 116, p. 195 210, 2005.

[135] R. Sameni, C. Jutten, and M. Shamsollahi, "Multichannel electrocardiogram decomposition using periodic component analysis," *Biomedical Engineering, IEEE Transactions on*, vol. 55, no. 8, pp. 1935 –1940, aug. 2008.

[136] V. Monasterio, P. Laguna, and J. Martinez, "Multilead analysis of T-Wave alternans in the ECG using principal component analysis," *Biomedical Engineering, IEEE Transactions on*, vol. 56, no. 7, pp. 1880 –1890, july 2009.

[137] Y. Zigel, A. Cohen, and A. Katz, "The weighted diagnostic distortion (WDD) measure for ECG signal compression," *IEEE Trans. Biomed. Eng.*, vol. 47, no.11, pp. 1422 –1430, Nov. 2000.

[138] ——, "ECG signal compression using analysis by synthesis coding," *IEEE Trans.Biomed.Eng.*, vol. 47, no.10, pp. 308 – 316, Oct. 2000.

[139] J. M. Mendel, "Tutorials on higher-order statistics (spectra) in signal processing and system theory: Theoretical results and some applications," *Proceedings of the IEEE*, vol. 79, No. 3, p. 278305, March 1991.

[140] D. DiPietroPaolo, H. P. Muller, and S. N. E. G. Nolte, "Noise reduction in magnetocardiography by singular value decomposition and independent components analysis," *Med Bio Eng Compu (2006), International Federation for Medical and Biological Engineering*, vol. 44, pp. 489 – 499, 2006.

[141] R. J. Brychta, R. Shiavi, D. Robertson, and A. Diedrich, "Spike detection in human muscle sympathetic nerve activity using the kurtosis of stationary wavelet transform coefficients," *Journal Neurosci Methods*, vol. 160(2), pp. 359 – 367, March 15, 2007.

[142] H. Hong and M. Liang, "K-hybrid: A kurtosis-based hybrid thresholding method for mechanical signal denoising," *Transactions of the ASME*, vol. 129, pp. 458 – 470, August 2007.

[143] Z. M. N. et al., "Peak-valley segmentation algorithm for kurtosis analysis and classification of fatigue time series data," *European Journal of Scientific Research, ISSN 1450-216X*, vol. 29, No.1, pp. 113 –125, 2009.

[144] J. J. G. de la Rosaa and A. M. Munoz, "Higher-order cumulants and spectral kurtosis for early detection of subterranean termites," *Journal of Mechanical Systems and Signal Processing*, vol. 22, pp. 279 – 294, 2008.

[145] S. Dandapat and G. C. Ray, "Spike detection in biomedical signals using midprediction filter," *Medical and Biological Engg. and Computing, Springer Berlin / Heidelberg*, vol. 35, No. 4, pp. 354 – 360, July 1997.

[146] M.S.Manikandan and S. Dandapat, "Multiscale entropy-based weighted distortion measure for ECG coding," *IEEE Signal Processing Letters*, vol. 15, 2008.

[147] ——, "Effective quality-controlled SPIHT-based ECG coding strategy under noise environments," *Electronics Letters*, vol. 44, no.20, Sept. 2008.

[148] I. M. Johnstone and B. W. Silverman, "Wavelet threshold estimators for data with correlated noise," *Journal of the Royal Statistical Society. Series B (Methodological)*, vol. Vol. 59, No. 2, pp. 319–351, 1997.

[149] H.-C. Huang and N. Cressie, “Deterministic/stochastic wavelet decomposition for recovery of signal from noisy data,” *Technometrics, American Statistical Association and American Society for Quality*, vol. Vol. 42, No. 3, pp. 262–276, Aug. 2000.

[150] L. T. DeCarlo, “On the meaning and use of kurtosis,” *Psychological Methods, American Psychological Association, Inc*, vol. Vol. 2, No. 3, pp. 292–307, 1997.

[151] P. J. Rousseeuw and C. Croux, “Alternatives to the median absolute deviation,” *Journal of the American Statistical Association*, vol. 88 (424), pp. 1273 – 1283, Dec., 1993.

[152] F. R. Hampel, “The influence curve and its role in robust estimation,” *Journal of the American Statistical Association*, vol. 69 (346), pp. 383 – 393, Jun. 1974.

[153] W. H. Swallow and F. Kianifard, “Using robust scale estimates in detecting multiple outliers in linear regression,” *Biometrics, International Biometric Society*, vol. 52 (2), pp. 545–556, June 1996.

[154] P. McSharry and G. Clifford. (Retrieved December 2010) ECGSYN - a realistic ecg waveform generator. contributed to PhysioNet. [Online]. Available: http://www.physionet.org/physiotools/ecgsyn/

[155] C. Rao, “The use and interpretation of principal component analysis in applied research,” *Sankhya, The Indian Journal of Statistics, Series A*, vol. 26 (4), pp. 329 – 358, 1964.

[156] S. Wold, N. Kettaneh, and K. Tjessem, “Hierarchical multiblock PLS and PC model for easier model interpretation and as an alternative to variable selection,” *Journal Chemometrics*, vol. 10, 463, 1996.

[157] H. H. Yue and M. Tomoyasu, “Weighted principal component analysis and its applications to improve fdc performance,” Atlantis, Paradise Island, Bahamas, Dec.14 - 17, 2004.

[158] A. C. Davison and S. Sardy, “The partial scatterplot matrix,” *Journal of Computational and Graphical Statistics, Published by: American Statistical Association, Institute of Mathematical Statistics, and Interface Foundation of America*, vol. 9 (4), pp. 750 – 758, Dec. 2000.

[159] L. N. Sharma, S. Dandapat, and A. Mahanta, “ECG signal denoising using higher order statistics in wavelet subbands,” *Biomed. Signal Process. Control, Elsevier*, vol. vol 5, pp. 214 – 222, 2010.

[160] ——, “Kurtosis-based noise estimation and multiscale energy to denoise ECG signal,” *Signal, Image and Video Processing, Springer*, vol. DOI: 10.1007/s11760-011-0227-7, copyright Springer-Verlag London Limited, 2011.

[161] J. Shlens, “A tutorial on principal component analysis,” *Systems Neurobiology Laboratory, Salk Insitute for Biological Studies and Institute for Nonlinear Science, University of California*, Dec. 10, 2005.

[162] L. I. Smith, “A tutorial on principal components analysis,” February 26, 2002.

[163] R. Gray and D. Neuhoff, “Quantization,” *IEEE Trans. Inf. Theory*, vol. 44 (6), p. 23252383, 1998.

[164] K. Sayood, *Introduction to Data Compression*. Elsevier, CA, 2003.

[165] E. Sharifahmadian, “Wavelet compression of multichannel ECG data by enhanced set partitioning in hierarchical trees algorithm,” in *Proceedings of the 28th IEEE EMBS Annual International Conference*, New York City, USA, Aug 30-Sept 3 2006, pp. 5238 – 5243.

TH-1102_06610204

भारतीय प्रौद्योगिकी संस्थान गुवाहाटी • Indian Institute of Technology Guwahati •

LIST OF PUBLICATIONS

Refereed Journals:

1. L. N. Sharma, S. Dandapat, A. Mahanta, "Multichannel ECG data compression based on multiscale principal component analysis", *IEEE Trans. on Information Technology in Biomedicine*, Published on line 19 April, 2012.
2. L.N. Sharma, S. Dandapat, A. Mahanta, "Multiscale PCA based quality controlled denoising of multichannel ECG signals," *International Journal of Information and Electronics Engineering (IJIEE)*, Published by: International Association of Computer Science and Information Technology Press (IACSIT), ISSN: 2010-3719, vol. 2, no. 2, pp.107-111, 2012.
3. L.N. Sharma, S. Dandapat, A. Mahanta, "Kurtosis-based noise estimation and multiscale energy to denoise ECG signal", *Signal, Image and Video Processing, Springer*, ©Springer-Verlag London Limited 2011, DOI: 10.1007/s11760-011-0227-7.
4. L.N. Sharma, S. Dandapat, A. Mahanta, "ECG signal denoising using higher order statistics in Wavelet subbands," *Biomed. Signal Process. Control, Elsevier*, vol 5, pp.214 - 222, 2010.

Article in Book:

1. L.N. Sharma, S. Dandapat, A. Mahanta, "Multiscale distortion measure for multichannel electrocardiogram signals," *Biomedical Engineering*, Narosa Publishing House Pvt. Ltd., Delhi, India, pp. 102 - 107, Copyright 2011.

Manuscripts under Review

1. L. N. Sharma, S. Dandapat, A. Mahanta, "Subband weighted multiscale principal component analysis for multichannel ECG signals", *Signal, Image and Video Processing, Springer*, 2012.

Refereed Conferences:

1. L. N. Sharma, S. Dandapat, A. Mahanta, "Multiscale distortion measure for multichannel electrocardiogram signals," *2011 International Conference on Biomedical Engineering (ICBME 2011)*, Manipal Institute of Technology, Manipal, India, Dec 10-12., 2011.

TH-1102_06610204

2. L. N. Sharma, S. Dandapat, A. Mahanta, “Guaranteeing Target Quality Denoising of Multichannel ECG Signals using MSPCA”, *2011 International Conference on Computer and Computational Intelligence (ICCCI 2011)*, Bangkok, Thailand, 2-4 Dec., 2011 (**Won Best Paper Award**).

3. L.N. Sharma, S. Dandapat, A. Mahanta, “Multiscale principal component analysis to denoise multichannel ECG signals,” *2010 5th Cairo International Biomedical Engineering Conference, CIBEC 2010*, pp.17 - 20, Cairo, Egypt, Dec. 2010.

4. L.N. Sharma, S. Dandapat, A. Mahanta, “Multiscale entropy based multiscale principal component analysis for multichannel ECG data reduction,” *Proceedings of the IEEE/EMBS Region 8 International Conference on Information Technology Applications in Biomedicine, ITAB 2010*, Corfu, Greece, Nov. 2010.

5. L. N. Sharma, S. Dandapat, A. Mahanta, “Multiscale Wavelet energies and relative energy based denoising of ECG Signal”, *1st. IEEE International Conference on Communication Control and Computing Tecgnologies (IEEE ICCCCT 2010)*, Syed Ammal Engineering College, Ramanathapuram and St.Xavier’s Catholic College of Engineering, Kanyakumari., Tamilnadu, 7-9 Oct., 2010.

6. L. N. Sharma, S. Dandapat, A. Mahanta, “Kurtosis based Multichannel ECG Signal Denoising and Diagnostic Distortion Measures”, *IEEE TENCON 2009*, Singapore, November 23 - 26, 2009.

7. L. N. Sarma, S. R. Nirmala, M. S. Manikandan and S. Dandapat, “Compression of multi-lead ECG signals and retinal images using 2-D wavelet transform and SPIHT coding scheme for mobile telemedicine,” *in Proc. workshop on Image and Signal Processing (WISP 2007),* pp. 18-27, Dec. 2007.

8. L. N. Sharma, M. Sabarimalai Manikandan and S. Dandapat, “Modern ECG Instrumentation and Compression Techniques”, *Seminar on Bioelectronics*, Tezpur University, 27th. March 2007.

TH-1102_06610204